

**PHOTORESPONSIVE LIQUID CRYSTALLINE AZOBENZENE
POLYESTERS: DESIGN, SYNTHESIS AND SELF
ORGANIZATION STUDY**

**THESIS SUBMITTED TO THE
SAVITRIBAI PHULE PUNE UNIVERSITY**

**FOR THE DEGREE OF
DOCTOR OF PHILOSOPHY**

(IN CHEMISTRY)

**BY
CHINMAY G. NARDELE**

RESEARCH SUPERVISOR

DR. S. K. ASHA

**POLYMER SCIENCE AND ENGINEERING DIVISION
CSIR-NATIONAL CHEMICAL LABORATORY
PUNE-411008**

DECEMBER 2014

Dedicated to


My Family and Friends

For their endless love and support



DECLARATION

I hereby declare that the thesis entitled “**Photoresponsive Liquid Crystalline Azobenzene Polyesters: Design, Synthesis and Self Organization Study**” submitted for the award of degree of *Doctor of Philosophy* in Chemistry to the Savitribai Phule Pune University has been carried out by me. This work was carried out at the Polymer Science and Engineering Division of CSIR-National Chemical Laboratory, Pune under the supervision of Dr. S. K. Asha. I also affirm that this work is original and has not been submitted in part or full, for any other degree or diploma to this or any other University or Institution.



Chinmay G. Nardele

December 2014

CSIR-National Chemical Laboratory
Pune- 411 008



**Polymer Science & Engineering Division
CSIR-National Chemical Laboratory
Council of Scientific & Industrial Research
Dr. Homi Bhabha Road
Pune-411008, India**

Dr. S. K. Asha
Scientist

Tel: 91-20-25902062; Fax: 91-20-25902615
E-mail: sk.asha@ncl.res.in

CERTIFICATE

This is to certify that the work presented in the thesis entitled **“Photoresponsive Liquid Crystalline Azobenzene Polyesters: Design, Synthesis and Self Organization Study”** has been carried out by **Mr. Chinmay G. Nardele** under my supervision at Polymer Science and Engineering Division of CSIR-National Chemical Laboratory, Pune and the same has not been submitted elsewhere for any other degree. Such materials as obtained from other sources have been duly acknowledged in the thesis.

Dr. S. K. Asha

(Research Supervisor)

Polymer Science and Engineering Division

CSIR-National Chemical Laboratory

Pune 411008

December 2014

ACKNOWLEDGEMENTS

*First and foremost, I would like to express my sincere gratitude to my research supervisor **Dr. S. K. Asha** for her endless support during my Ph.D. study and research, for her patience, inspiration, care, encouragement and immense knowledge. Her guidance helped me in all ways of up and down time of my research and writing of this thesis. She was always there for me in throughout my Ph.D. life from putting my first reaction to the entire tough journey of my research. I am thanking the god almighty for giving me such a wonderful and humble personality as my mentor. She has given me full freedom in my research and I could not imagine have a better mentor than her.... Thank you Madam for everything I have achieved during this Ph.D. life,,,,,*

*I would like to offer my sincere thank to **Dr. M. Jayakannan** for his fruitful advices, support and constant encouragement. His immense knowledge about the polymer chemistry helped lot during my Ph.D. His passion and enthusiasm to do scientific research always motivated me. He used to nourish my mind with plenty of ideas and has filled my research life with positive energy by saying “do it man”,,,, His door is always open for me for any discussions,, My sincere gratitude to you Sir for your valuable guidance,,,, friendly and energetic approach.*

It is my immense pleasure to say gratitude to Dr. S. Sivaram, the legend of polymer science and a good teacher who taught me the fundamentals of polymer science and I am proud to say he is my teacher.

My sincere thanks also go to Dr. Prakash Wadagoankar and Prof. V. G. Anand for their encouragement, valuable suggestion and insightful evaluation.

My Sincere thanks to Prof. S. Ramakrishnan (IISc Bangalore) whose deep knowledge in transesterification chemistry helped me to improve my research work.

I extend sincere thanks to the current Director of CSIR-NCL Dr. Sourav Pal, Dr. A. J. Varma (Head of Polymer Science and Engineering Division), Dr. M. G. Kulkarni (former Head of Polymer Science and Engineering Division), Dr. K. Krishnamoorthy, Dr. J. Nithyanandhan, Dr. Rahul Banerjee, Dr. Sayam Sen Gupta, Dr. Ashish Lele, Dr. Kumar Vanka, Dr. Ramesh C., Dr. K. Guruswamy, for their kind help and valuable

suggestions. My sincere gratitude to Dr. K. Vijayamohanan, Dr. Satish Ogale, Dr. P. A. Joy for their advice and help

I also acknowledge the financial support of CSIR, New Delhi and CSIR-NCL for providing the best infrastructure for a fruitful research.

I take this opportunity to thanks Dr. K. Sreekumar and Mr. Vishal for the collaborative work and valuable suggestion during the impedance spectroscopy measurement. I also thanks to Prof. V. A. Raghunathan and Mrs. Vasudha K. N. (RRI Bangalore) and Mr. Neeraj Maheshwari (IISER, Pune) for their help in XRD measurement. I extend thanks to Mrs. Deppa Dhoble, Mrs. Anuya Nisal, Mr. Saroj Kumar Jha and Mrs. Poorvi Purohit for their kind help in giving training for the instrument facility. I wish to thank Mr. Shamal K. Menon for helping in GPC measurements. I am highly thankful to Mrs. B. Santhakumari, Mr. Gholap, Mr. Ketan and Miss. Shravya for helping me lot in various characterization of my samples.

I would like to thank Meenu, Shyam and Appu for bringing a cheerful environment during this period. I would like to thank Sharanya, Vaishali vaihini, Swati vaihini and Deepika bhabhi for giving a homely atmosphere. I would like thank my all seniors and colleagues who have offered unconditional support and help during my Ph. D study. My lab seniors Dr. Deepak Vishnu, Dr. Anilkumar, Dr. Jinish, Dr. Rekha, Dr. Balamurugan, Dr. Mahima, and Dr. Kaushal for their valuable advice and help in lab practices which I greatly acknowledge. I can never forget the assist and helpful advices from my seniors Dr. Abasaheb, Dr. Satish, Dr. Manmath, Dr. Korbad B., Dr. Sachin Patil, Dr. Nagesh Khupse, Dr. Bharat, G., Dr. Ankush, Dr. Praksah S., Dr. Kedar R., Dr. Deepak J., Dr. Abhijeet P., Dr. Abhijeet K., Dr. Ganesh, Dr. Dhanraj, Dr. Pankaj D., Dr. Malvi, Mangesh, Eknath, Deepak C., Gopi, Shankar.

I would like to special thanks to all my labmates and friends from CSIR-NCL and IISER Pune: Nagesh, Ghanashyam, Shekhar, Dr. Nisha, Senthil, Prajitha, Saibal, Swapnil, Sandeep, Sarabojot, Srivishakh, Bavitha, Jeena, Anil, Nitin, Vinay, Alok, Charu, Harish, Akshitha, Vikas, Smita, Pramod, Ananthraj, Bapu, Moumita, Bhagyashree, Narsimha, Rajendra, Nilesh, Sonashree, Tamiz, Mehak and Maitreyee. I want to thanks my beloved friends Digambar, Kiran, Pradeep, Vinayak, Tukaram, Hemant, Ram, Atul, Majid, Bhausahab, Maroti, Manoj, Govind, Manik, Satej, Manik Sil, Jijil, Manjunath,

Rajashree, Neeta, Dnyaneshwar, Valmik, Arun, Satish B., Raja Ambal, Jayashree Madam, Milkha singh (Dr. Gobinda), Vinita, Leena, Nisha, Dr. Beena, Siddu and Yogesh. I would like to thank my roommates Subhadeep, Dr. Jithendra, Jagadish, and Raja Perumal. I would like to thanks my GJ hostel friends Arjit, Tamas, Chandan, Sharat, Chakadola, Dr. Edwin, Souman, Bikash, Krunal, Subha, Pravat, Manoj Sharma, Prabhu, Mohanraj, Sanjay N., Krishanu, Dhanya, Nalini S. Munmun, Sushama, Subhdeep, Indravadan, Shivakumar, Hemendar Chand, Prakash Chandra, Achintya, Arpan, Anjan, Mrinmoy, Chaithanya kiran, Venu, Arul, Lenin, Rajesh, etc. and all the past and present GJ hostilities. My special thanks to my best companion Pradeep, Kiran, Shekhar, Nagesh, Digu and Dhanu for their friendship and support which made my life easier here. A special thanks to all the members of D WING (24 hrs active) for giving such a fantastic environment which alert me to keep on working. Thanks to NCL for giving such a nice infrastructure and facilities in PAML.

Finally, I would like to thanks my beloved parents, my sisters and brother in laws, uncle and aunty for their support throughout my Ph.D study. A special thanks to my chiller party: Diksha, Deepika, Anushka, piyu, Swapnil and Om,,, I would like to gratitude my brothers Balaji, Basu and sisters Baby tai, Meena, Rekha, Rani and Shilpa for with me in all the difficult time.

This journey will be incomplete without your presence, your blessing and I don't have words to express my gratitude to you,,, Thanking you the god almighty for giving me a chance to be here with a calm and beautiful life and for everything that you have bring to me and I believe that you will be always with me in this whole journey. As always, it is impossible to mention everybody who had an impact on this work although there are those whose spiritual support is even more important.

- Chinmay Nardele

Table of Contents		
Abbreviations		
Abstract		
Chapter 1		1-38
Introduction and Literature Survey		
1.1	Introduction to liquid crystals	2
1.2	Classification of liquid crystals	2
1.3	Liquid crystalline polymers (LCPs)	5
1.4	Classification of liquid crystalline polymers	8
1.5	Liquid crystalline polyesters	10
1.6	Transesterification reaction	12
1.7	Structural chemistry of azobenzene	13
1.8	Photochemistry of azobenzene chromophore	15
1.8.1	Mechanism of photoisomerization	16
1.9	Azo LC polymers: photoresponsive properties and application	17
1.9.1	Photodeformation and photomechanical effects	20
1.9.2	Tunable diffraction gratings	23
1.9.3	Optical data storage	26
1.10	Methods employed for the mesophase investigation	29
1.10.1	Differential scanning calorimetry (DSC)	29
1.10.2	Polarized light microscope (PLM)	29
1.10.3	X-ray diffraction	30
1.11	Aim of the thesis	30
1.12	References	33
Chapter 2		39-82
Twin Liquid Crystals and Segmented Thermotropic Polyesters containing Azobenzene - Effect of Spacer length on LC Properties		
2.1	Introduction	40
2.2	Experimental	42
2.2.1	Materials	42
2.2.2	Instrumentation	42

2.2.3	Synthesis and characterization	44
2.3	Results and discussion	52
2.3.1	Photophysical properties	60
2.3.2	Thermal mesophase characteristics of twin molecules	63
2.3.3	Thermal mesophase characteristics of azobenzene copolymers	72
2.4	Summary	80
2.5	References	81
Chapter 3		83-130
Thermo and Photoresponsive Ionic Conductivity probed in Main Chain Liquid Crystalline Azobenzene Polyesters		
3.1	Introduction	84
3.2	Experimental section	87
3.3.1	Materials	87
3.3.2	Instrumentation	87
3.3.3	Synthesis and characterization	89
3.4	Results and discussion	93
3.4.1	Thermal mesophase characteristics	101
3.4.2	Polarized light microscopy (PLM)	106
3.4.3	Wide angle X-ray diffraction (WXRd)	107
3.4.4	Ionic conductivity and phase transitions	114
3.4.5	Photoresponsive ionic conductivity	122
3.5	Summary	127
3.6	References	128
Chapter 4		131-170
Liquid Crystalline Triped and Tetraped Azobenzene Molecules		
4.1	Introduction	132
4.2	Experimental section	135
4.2.1	Materials	135
4.2.2	Instrumentation	135
4.2.3	Synthesis of triped and tetraped bromo intermediates	136
4.2.4	Synthesis of triped and tetraped molecules	138
4.2.5	Synthesis of model compound	140
4.3	Results and discussion	141

4.3.1	Synthesis and characterization	141
4.3.2	Mesophase characteristics of triped and tetraped molecules	147
4.3.3	Isothermal photoswitching in the LC state	157
4.4	Summary	161
4.5	References	168
Chapter 5		171-200
Photoresponsive Smectic Liquid Crystalline Hyperbranched Azo Polymers		
5.1	Introduction	172
5.2	Experimental section	174
5.2.1	Materials	174
5.2.2	Instrumentation	174
5.2.3	Synthesis of HB polymers: melt polycondensation	175
5.3	Results and discussion	177
5.3.1	Synthesis and characterization of HB-polymers	177
5.3.2	Mesophase characteristics of hyperbranched polymers	184
5.3.3	Isothermal photoswitching in the LC state	191
5.3.4	Photoswitching in spin coated thin films	193
5.4	Summary	197
5.5	References	198
Chapter 6		201-205
Conclusions		
Publication /Symposia		
Erratum		

List of Abbreviations

Abbreviations	Expansion
ATR	Attenuated total reflectance
CHCl ₃	Chloroform
CDCl ₃	Deuterated chloroform
CH ₃ CN	Acetonitrile
CD	Compact disc
CTE	Coefficient of thermal expansion
DCM	Dichloromethane
DMAc	N,N-Dimethylacetamide
DMF	N,N-Dimethylformamide
DMSO-d ₆	Deuterated dimethyl sulfoxide
DMS	Dimethyl sebacate
DEG	Diethylene glycol
DSC	Differential scanning calorimetry
DVD	Digital versatile disc
DFT	Density functional theory
dL	Deciliter
EtOAc	Ethyl acetate
FT-IR	Fourier transform infrared
GPC	Gel permeation chromatography
g	Gram
HCl	Hydrochloric acid

H ₂ SO ₄	Sulfuric acid
HEG	Hexaethylene glycol
HPLC	High-performance liquid chromatography
HRMS	High resolution mass spectrometry
ΔH	Change in enthalpy
HBP _s	Hyperbranched polymers
ITO	Indium tin oxide
KJ	Kilojoule
K ₂ CO ₃	Potassium carbonate
KI	Potassium iodide
LC	Liquid crystal
LCP _s	Liquid crystalline polymers
LCE _s	Liquid crystalline elastomers
LPL	Linearly polarized light
LiCF ₃ SO ₃	Lithium triflate
MALDI-TOF	Matrix-assisted laser desorption ionization-time of flight
MCLCP _s	Main chain liquid crystalline polymers
mg	Milligram
mL	Millilitre
μL	Microliter
mmol	Millimole
MHz	Megahertz
M _n	Number average molecular weight
M _w	Weight average molecular weight

NMR	Nuclear magnetic resonance
N ₂	Nitrogen
nm	Nanometer
Nm	Nematic
η_{inh}	Inherent viscosity
OD	Optical density
PDI	Polydispersity index
ppm	Part per million
PLM	Polarized light microscope
PEO	poly(ethylene oxide)
PPTA	p-phenylene terephthalamides
PBA	Polybenzamide
RI	Refractive index
SEM	Scanning electron microscope
SEC	Size exclusion chromatography
SCLCPs	Side chain liquid crystalline polymers
SMT	Surface mount technology
SiO ₂	Silicon dioxide
Sm	Smectic
ΔS	Change in entropy
TEG	Tetraethylene glycol
THF	Tetrahydrofuran
TFA	Trifluoroacetic acid
(Ti(Obu) ₄)	Titanium tetrabutoxide

TGA	Thermogravimetric analysis
T _m	Melting temperature
T _g	Glass transition temperature
T _{cl}	Clearing temperature
T _c	Crystallization temperature
T _D	Decomposition temperature
UV	Ultraviolet
VTXRD	Variable temperature X-ray diffraction
WXRD	Wide angle X-ray diffraction

PREFACE

The azobenzene is a well known mesogen as well as photoresponsive chromophore which has found a variety of application in optical displays, optical shutters, molecular switches, photocontrollable coatings, photomechanical systems etc. It can undergo reversible conformational change from a rod (trans form) to bent shape (cis form) upon alternate UV-Vis irradiation, enabling the manipulation of the physical and chemical properties of materials with external stimuli, which forms the basis of stimuli responsive systems.

Liquid crystalline polymers (LCPs) combines both properties of polymers and liquid crystals and are considered as suitable materials for a variety of application such as optoelectronics, optics, photonics, holographic, display technology, telecommunication etc. However, LCPs containing azobenzene (main chain or side chain) have gained considerable attention because of their large photoinduced anisotropy and photochemical phase transition. The photoinduced change in the LC orientation of azobenzene LCPs can modulate physical properties of materials such as birefringence, refractive index, modulus viscosity, conductivity, volume, electric and magnetic susceptibility which make them suitable candidate for photonic application.

The objective of the present work is to design and synthesize multifunctional monomers that could be directly used in a melt polycondensation polymerization route. Twin azobenzene having the structure azobenzene-spacer-azobenzene, where the central spacer is oligooxyethylene of varying length is a versatile design for the synthesis of main chain azo polyesters via the melt polycondensation approach. Main chain liquid crystalline polymers incorporating the photoresponsive azobenzene as well as the oligo(ethylene oxide) segments that supports ionic conduction is expected to serve as good thermo as well as photoresponsive ionic conducting materials upon complexation with lithium salt. Triped and tetraped liquid crystalline molecules incorporating the azobenzene moiety was also designed using a phloroglucinol core connected to three or four azobenzene moieties via a pentyl or decyl alkyl spacer segment. These triped and tetraped molecules with terminal methyl carboxylic ester groups were used as the B₃ and B₄ monomers respectively for the synthesis of hyperbranched polymers with tetraethylene glycol as the A₂ type co monomer. The

azo containing B_3 and B_4 monomer design is a simple and robust one enabling melt polymerization without degradation of the azo chromophore for the synthesis of liquid crystalline hyperbranched polymers (LCHBPs).

The systematic study of the thermotropic liquid crystalline properties of the newly synthesized monomers and their polymers was conducted using differential scanning calorimetry (DSC), polarized light microscopy (PLM) combined with variable temperature X-ray diffraction analysis (VT-XRD). Additionally, the study of change in the LC orientation of mesogen in LCPs can modulate interesting properties such as photoswitching response, birefringence, conductivity etc. By keeping the above objectives in mind, the following specific work was selected for the present thesis:

1. Synthesis of a series of azotwin monomers and main chain LC random copolymers incorporating photoresponsive azobenzene chromophore by a facile melt polycondensation approach.
2. Development of novel thermo and photoresponsive ion conductive main chain liquid crystalline azobenzene polyester as solid polymer electrolyte (SPE).
3. Design and synthesis of liquid crystalline triped and tetraped multifunctional molecules containing azobenzene for synthesis of azo hyperbranched polymers.
4. Synthesis and characterization of photoresponsive liquid crystalline hyperbranched azo polymers: using A_2B_3 and A_2B_4 type monomers by using the melt polycondensation approach.

This thesis has been structured into six chapters. Chapter 1 gives brief introduction to liquid crystals and a review of the structure property relationship in the design of various monomers and polymers. A general introduction about the azobenzene chromophore, photoisomerization mechanism and photoresponsive properties of LC polymers is also discussed with relevant literature examples. Previous studies of azo LC polymers on various issues related to synthesis, mesophase type, transition temperature etc. in different architectures such as main chain polymers (MCLCPs), side chain polymers (SCLCPs) and hyperbranched polymers (HBLCPs) is compared.

Chapter 2 describes the synthesis of a homologous series of phenyl and naphthyl twin azobenzene (**PnP** and **NpnNp**) monomers as well as segmented copolyesters based on them. The twin monomers had the structure azobenzene-oligooxyethylene - azobenzene where the ethyleneoxy length was varied from 2 to 6 units. A representative general structure of phenyl and naphthyl twinazobenzene is shown in Figure 1.

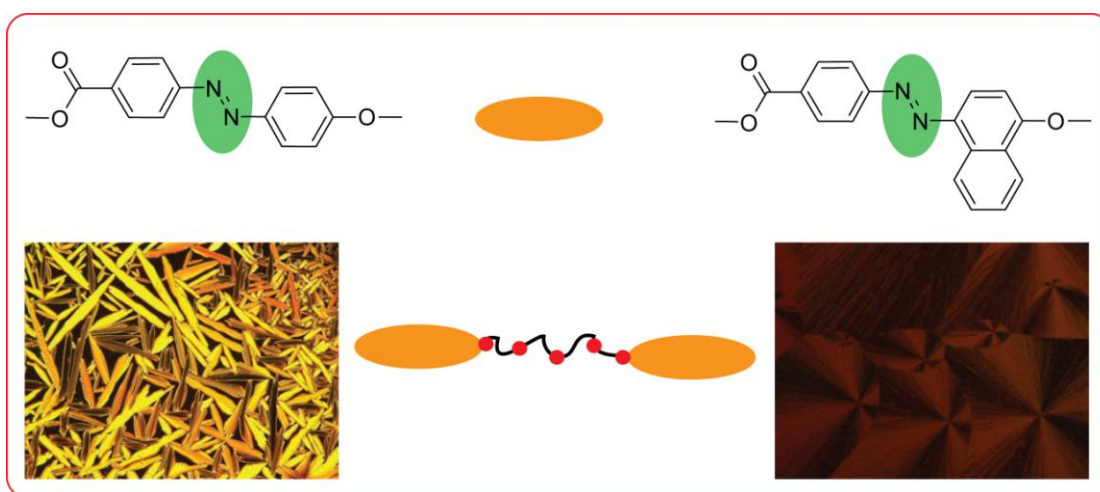


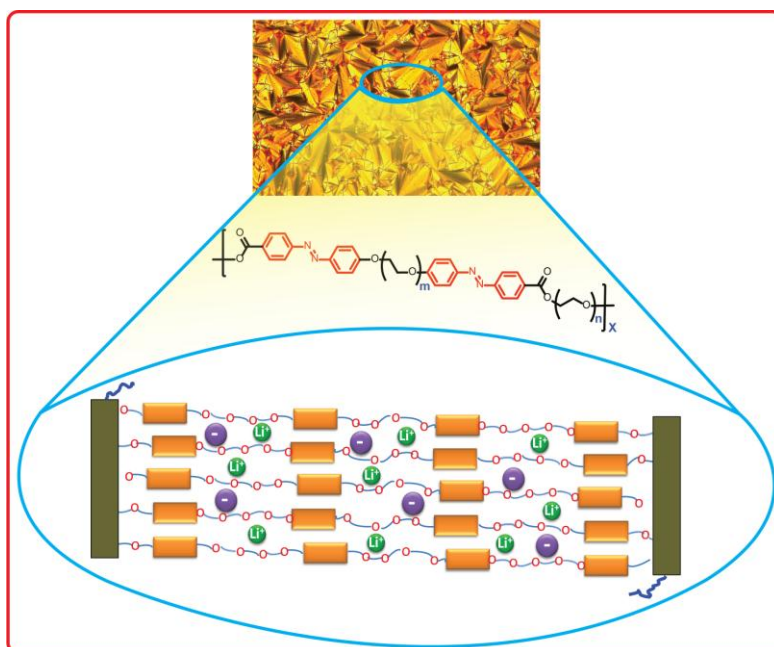
Figure 1 Structure of phenyl and naphthyl twin azo monomers.

One non-LC short spacer twin (**P2P**) and one LC long spacer twin (**P6P**) were incorporated as part of a main chain polyester composed of fully aliphatic segments of sebacate and di or tetraethylene glycol (DEG/TEG) units by melt polycondensation.

The thermotropic liquid crystalline (LC) properties of twin monomers as well as copolyesters were investigated using differential scanning calorimetry (DSC), polarized light microscopy (PLM) combined with variable temperature X-ray diffraction (VT-XRD) analysis. The analysis of two azotwin series and their main chain copolyesters showed that they were dependent on the length of the oligooxyethylene linkers as well as the nature of the azo chromophore (phenylazo vs. naphthylazo). In case of phenylazo twin a very low incorporation (5 mole %) of “rigid phenylazo twin” into a non-mesogenic polymer helped to induce mesogenicity in the copolymer. While, naphthylazo twin failed to induce mesogenicity even after 30 mole % incorporation. Although the phenyl twin molecules exhibited smectic LC phases, their incorporation in the copolymer at low mol % resulted mostly in nematic LC

phase. Overall, the observation of mesogenicity is a complex phenomenon especially in random copolymers and both the “rigid” and the “flexible” spacer would be expected to have almost equal contribution in deciding the final outcome.

Chapter 3 illustrates the design, synthesis, and characterization of three series of main chain thermotropic liquid crystalline azobenzene polymers. The polymers were synthesized using azobenzene twin molecules as the AA monomer and diols like diethylene glycol (DEG), tetraethylene glycol (TEG) and hexaethylene glycol (HEG) as the BB comonomer. The twin azobenzene units had the structure Phenylazobenzene - oligooxyethylene spacer – Phenylazobenzene (**PnP**), where the spacer length ‘n’ was chosen from 2, 4 and 6 oxyethylene units. The terminal azobenzene unit was suitably functionalized with $-\text{C}(\text{O})\text{OMe}$ units to facilitate transesterification with diols to form polyesters. The twin molecular design reduced the melting temperature and also improved the solubility as well as miscibility in the molten reaction medium thereby enabling melt polycondensation. The combination of polar oligooxyethylene unit with non-polar rigid aromatic azo chromophore produced stable smectic mesophases in all the polymers and most of the polymers showed higher ordered smectic mesophase transition.



One of the polymers was chosen to prepare composite polymer electrolyte with lithium triflate (LiCF_3SO_3) and ionic conductivity was measured with the help of

a. c. impedance spectroscopy. The polymer/0.3 Li salt complex exhibited a maximum ionic conductivity in the range of 10^{-5} S cm^{-1} at room temperature (25 °C), which increased to 10^{-4} S cm^{-1} above 65 °C. Reversible optical modulation of ionic conductivity was observed upon irradiation of the polymer/0.3 Li salt complex with alternate UV and visible irradiation.

Chapter 4 presents the design and synthesis of triped and tetraped liquid crystalline molecules containing azobenzene moiety. The design consists of a phloroglucinol core connected to three or four azobenzene moieties via a pentyl or decyl alkyl spacer segment. These tri and tetraped molecules were suitably end functionalized with methyl carboxylic ester functionality for enabling transesterification reaction. Thus, they could be used as the B₃ and B₄ type monomers respectively for the synthesis of hyperbranched azo polymers with appropriate A₂ comonomer. The structure-property dependence on the mesophase characteristics of the multipod molecules was analyzed using various instrumentation techniques like differential scanning calorimetry (DSC), polarized light microscopy (PLM) and variable temperature X-ray diffraction (VT-XRD).

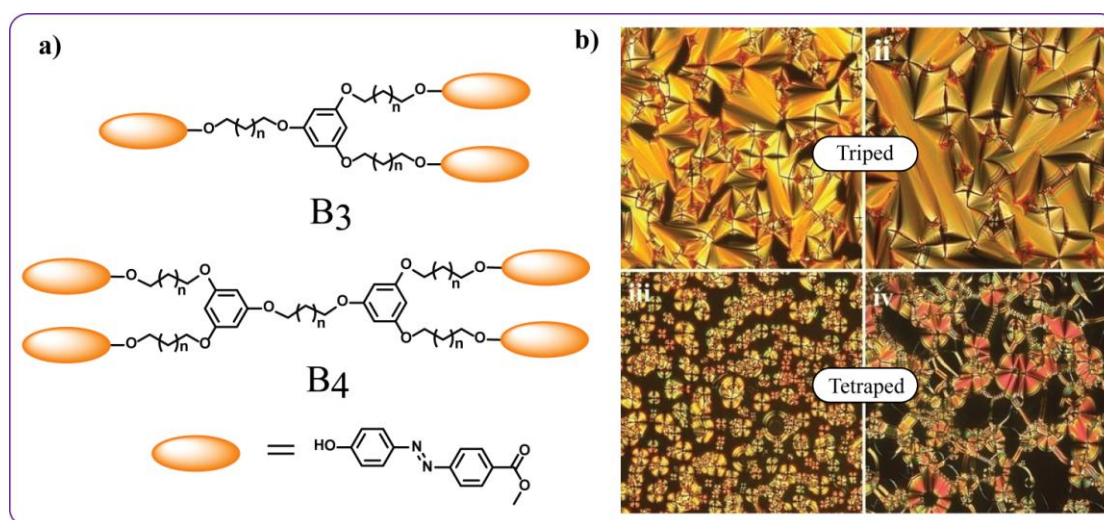
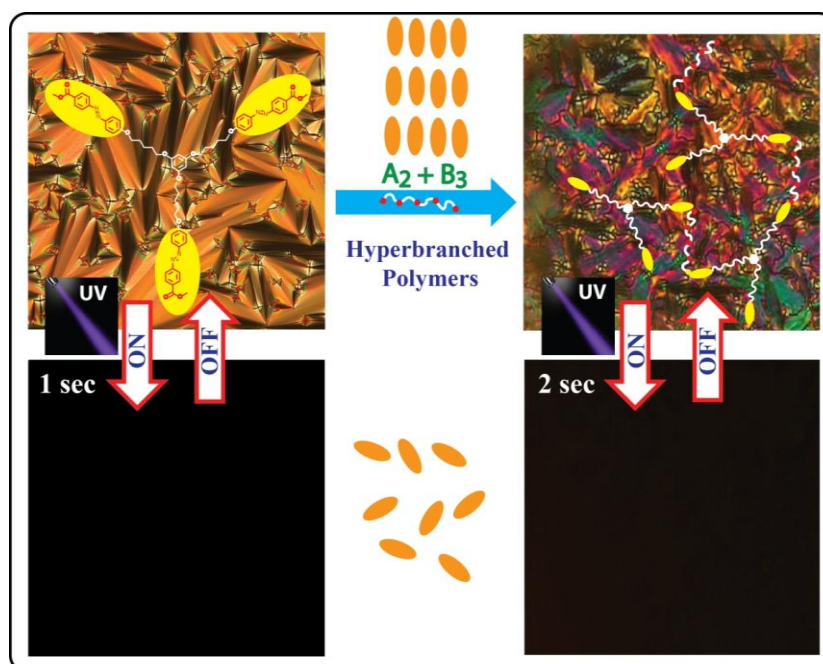


Figure 2 a) azo triped and tetraped molecules b) Crossed polarized optical micrographs of **T4star5-** i) 140 °C (20X-Sm), ii) RT-25 °C (20X-SmF/H) and **T4star10-** iii) 126 °C (20X-Sm), iv) RT-25 °C (20X-SmF/H).

Interestingly all multipod molecules exhibited thermotropic LC phases. A tendency towards higher ordered LC phases was observed with increased branching. For instance, the tripeds with five or ten alkyl spacer showed only SmA phases whereas tetrapod (dimeric) structures showed higher ordered Smectic phases. All multipod molecules exhibited faster reversible isothermal photoswitching from Smectic-Isotropic (S-I) phase upon UV irradiation in the LC phase.

Chapter 5 discusses the synthesis, characterization and studies on the thermotropic liquid crystalline properties of hyperbranched polymers (HBPs) containing azobenzene moiety. The tripod and tetrapod molecules with methyl carboxylic ester groups were used as B_3 and B_4 monomers respectively for the synthesis of hyperbranched polymers with tetraethylene glycol as the A_2 type comonomer. The polymerization was conducted via melt polycondensation route during which gelation was efficiently suppressed to obtain soluble hyperbranched polymers with moderate molecular weight.



The mesophase behavior was studied using differential scanning calorimetry (DSC), polarizing light microscopy (PLM) combined with variable temperature X-ray diffraction (VT-XRD). The hyperbranched polymers exhibited thermotropic liquid crystalline behavior. More importantly, in case of HB polymers lamellar organization

Thesis Abstract

was observed even in as-solvent precipitated powder sample, which indicated higher extent of microphase segregation. These HB polymers also showed reversible Smectic-Isotropic isothermal phase transition achieved in ~ 2 sec UV irradiation. Overall, the azo incorporated B₃ and B₄ monomer design described here is a simple and robust one enabling melt polycondensation polymerization without degradation of azobenzene monomer. These hyperbranched azo containing chromophore could be promising LC material due to their fast reversible switching response in LC state.

The last chapter summarizes the overall outcome of research work carried out in the present Ph. D. thesis.

Chapter 1

Introduction and Literature Survey

1.1 Introduction to Liquid Crystals

The liquid crystalline state is an intermediate state of matter which is between that of a liquid and crystal. It must possess a degree of molecular order which is intermediate to that of three dimensionally ordered solid and completely disordered isotropic liquid.¹ It exhibits some typical properties of liquid like fluidity, formation and coalescence of droplets and inability to support shear as well as some crystalline properties like anisotropy in optical, electrical, and magnetic properties, periodic arrangement of molecules in one spatial direction etc.

1.2 Classification of liquid crystals

Liquid crystals are generally classified into three classes based on their formation

1) *Thermotropic liquid crystal*

In this class LC phase formation mainly depends on temperature factor. Several thermotropic LC molecules exhibit a variety of phases as the temperature changes. The LC phase which is stable at a temperature above melting point is termed as enantiotropic. The liquid crystalline phase that is stable only at temperature below the melting point and can be obtained only with decreasing temperature is called monotropic.

2) *Lyotropic liquid crystal*

In this class LC phases arise from the interaction of solvent. The important factors responsible for lyotropic LC formation are concentration of the solution, solvent strength and temperature. In general, the amphiphilic molecules show lyotropic LC organization upon addition of solvent.

3) *Amphotropic liquid crystal*

This LC class of molecules has the ability to form thermotropic as well as lyotropic liquid crystalline phases. For instance alkali salts having long chain aliphatic acids can exhibit both thermotropic as well as lyotropic LC phases.

Depending on the type of ordering in mesogens, the thermotropic liquid crystals are further classified into four major categories namely nematic, smectic, cholesteric and discotic liquid crystals.

1.2.1 Nematic

One of the most common LC phases is the nematic phase. This LC phase is distinguished by long-range orientational order i. e. the long axes of the molecules tend to align along a preferred direction with no positional order. Therefore, the molecules are free to flow and positions of the centers of mass are randomly distributed as in a liquid, but a certain amount of short-range order may exist as in ordinary liquids. Most of the nematic LCs are uniaxial materials. The typical textures of nematic phases are shown in Figure-1.1.

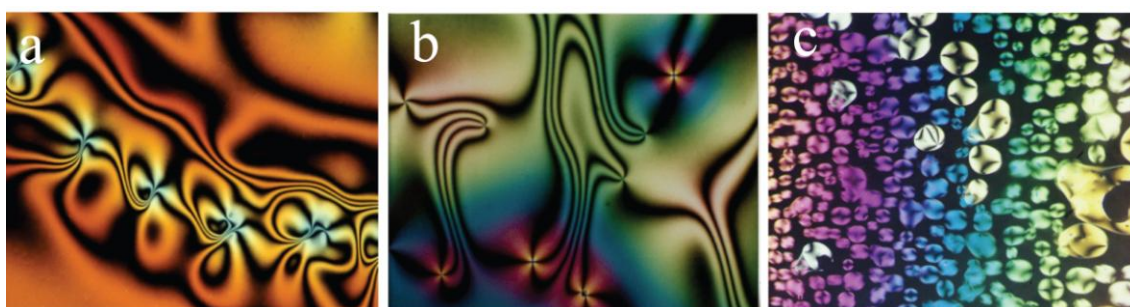


Figure 1.1 a) Schlieren texture of nematic LC b) Schlieren texture of a nematic film with surface point defects (boojums and c) Nematic droplets (^{a,b}Photos courtesy of Dr. Oleg Lavrentovich, ^cSource:<http://education.mrsec.wisc.edu/courses/colorsymp/park/images/nematic1.jpg> g).

1.2.2 Smectic

In case of smectic mesophase the molecules are arranged in layers and exhibit some correlations in their position in addition to the orientational ordering. In this class layered structural organization is the common characteristic due to which a large movement in any direction other than tangential to the surface is quite difficult. As a consequence, smectic phases are relatively viscous and solid like. Some typical textures of smectic phases reported in literature are shown in Figure 1.2. This phase is commonly observed in rod-shaped molecules i. e. calamitics.

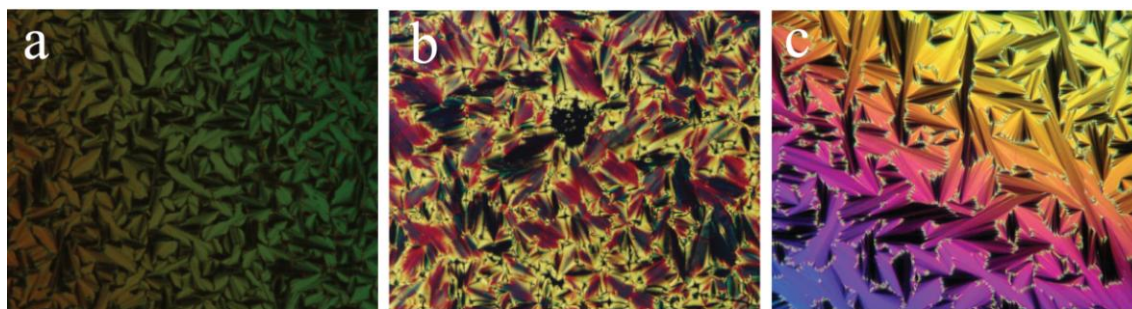


Figure 1.2 a) Broken fan-like structures of SmA phase b) Focal conic structures of SmA phase c) broken fan-like structures of SmC mesophase. (Adapted from ^b<http://education.mrsec.wisc.edu/courses/colorsymp/park/index.html> and ^c<http://chemistry.about.com/od/growingcrystals/ig/Crystal-Photo-Gallery/Liquid-Crystals.-MuZ.htm>).

1.2.3 Cholesteric (Chiral nematic liquid crystal)

The cholesteric liquid crystal phase is typically composed of nematic mesogenic molecules containing a chiral centre, which brings intermolecular forces that favor arrangements of molecules at a slight angle with respect to one another. This phase consists of local nematic layers, which are continuously twisted with respect to each other giving rise to helical superstructure with a twist axis perpendicular to local director. Some typical textures of cholesteric phases are shown in Figure 1.3, having finger print, polygonal texture etc.



Figure 1.3 a) Texture of cholesteric phase b) Finger print texture of cholesteric liquid crystal c) Polygonal texture in cholesteric phase. (Adapted from source <http://dept.kent.edu/spie/liquidcrystals/textures2.html>).

1.2.4 Discotic phases

In 1977 Chandrasekhar *et al.* found that not only rod-like molecules, but also compounds with disc-like molecular shapes formed liquid crystalline phases.² A common requirement for observing discotic LC phase is disc-like molecules substituted at periphery with flexible chains of at least five carbon atoms and four or more lateral substituents normally alkoxy or ester groups. Typical discotic LC texture exhibited by triphenyleneimidazole core is shown in Figure 1.4.³ The molecular dynamics simulation study on hexabenzocoronene showed that both core-core and side chain interactions were accountable for the discotic LC phase formation (Figure 1.4b).⁴ Amongst the various new LC material design, discotic liquid crystals are currently viewed as a new generation of organic semiconductors because they exhibit one-dimensional charge transport that is fairly sensitive to the structural defects and large orbital overlap compared to rod-shaped LC molecules (calamitics).⁵

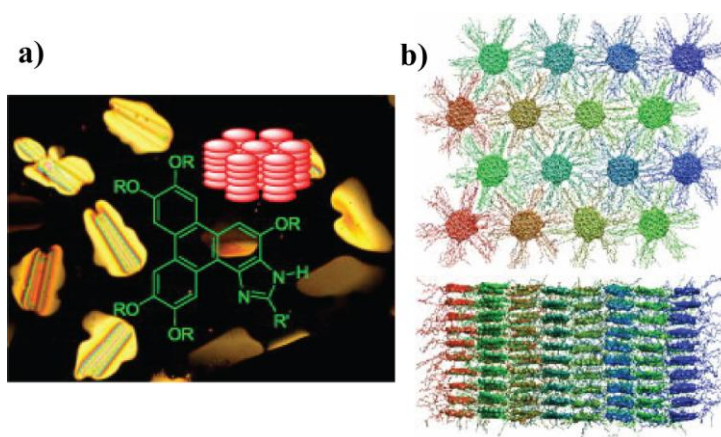


Figure 1.4 a) Texture of discotic phase with chemical structure of discotic moiety³ b) MD simulation results: snapshot of the hexabenzocoronene system with the C12 side chains. Aromatic cores are highlighted. Both top and side views are shown. $T = 400$ K, $P = 0.1$ MPa.⁴

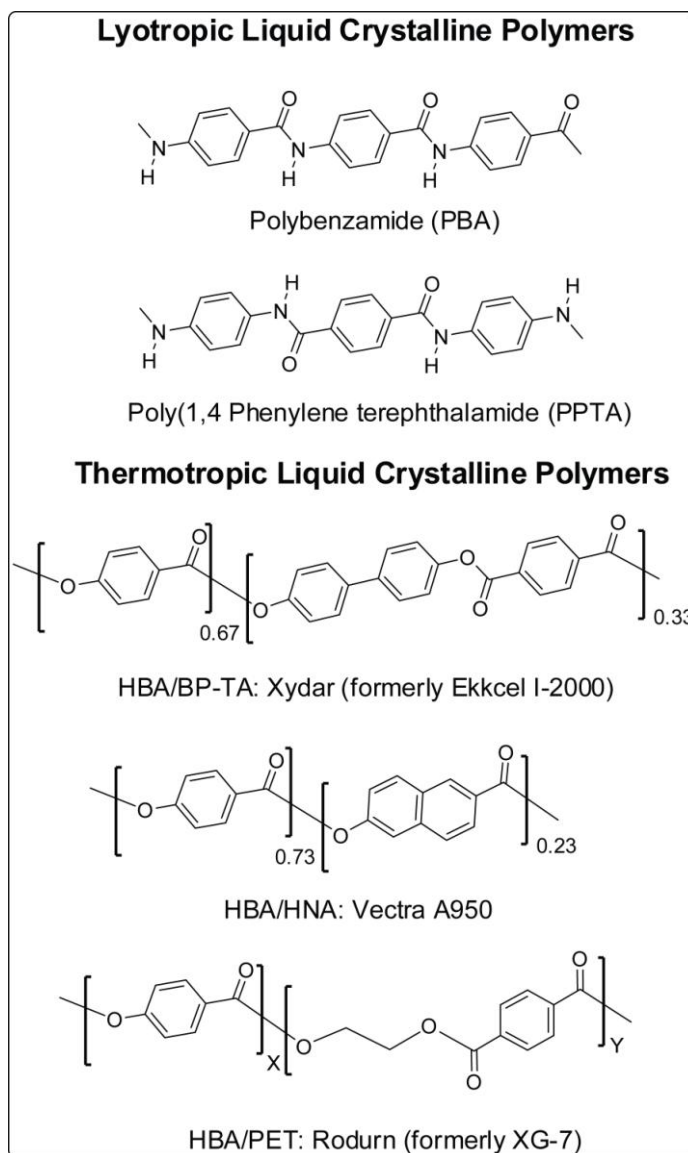
1.3 Liquid crystalline polymers (LCPs)

Polymers are high performance materials endowed with film forming nature, high processability, easy fabrication, high corrosion resistance and low manufacturing cost. Liquid crystalline polymers (LCPs) possess both properties of polymers and liquid crystals and are considered as functional materials for a variety of applications such as optics, optoelectronics, photonics, holographic display technology,

telecommunication and areas of modern engineering.⁶ So far, the synthesis of several thousands of liquid crystalline macromolecules or polymers have been accomplished. These polymers show specific features of structural designs; they contain flexible and rigid (mesogenic) fragments shaped as rods and disks, connected to each other in different ways. Based on fundamental requirements of rigidity and flexibility balance of the molecular design, various LC architecture containing mesogenic groups in main chains (main chain LC polymers) and side chain (side chain LC polymers or comb shaped LC polymers) have been reported.^{7 b-6} In addition to purely linear or side/comb LC structures, designs incorporating mesogenic groups both in main chain as well as side chain are also known.⁸ More complex LC polymers incorporated with alternating rod and disk-like groups have been synthesized.⁹

The versatility of chemical design of LC polymers has widened the scope of these materials by the synthesis of complex structures like binary and ternary copolymers, preparation of LC networks,¹⁰ as well as LC block¹¹ and graft copolymers¹² in which mesogenic groups are used as at least one of the components. Recently researchers found that liquid crystalline hyperbranched polymers possessed specific properties of branched molecules such as absence of entanglements and high concentration of end groups, making them promising materials for the preparation of LC materials having low viscosity.¹³ In all LC polymers described until now, the mesogenic groups were attached covalently to polymer backbone. In recent years, LC polymers based on specific non covalent interactions, such as hydrogen bonding, charge transfer,¹⁴ ionic interactions¹⁵ or coordination complexation,¹⁶ have received considerable attention due to their simple fabrication, interesting properties and potential applications.^{15,17} LCPs can be made by polymerizing single mesogenic unit, but these polymers often have melting temperature higher than their degradation temperature. Thus, these polymers cannot be melt processed using conventional techniques. So usually they are processed from solution phase (lyotropic LCPs). Typical example of this class is terephthalamide (PPTA) and polybenzamide (PBA), with PPTA being more commonly known as Kevlar (structures are shown in Scheme 1.1). To create thermotropic LCPs, the polymer should have low melting transition compared to the degradation temperature. From this point of view, thermoplastic LC polyesters offer great potential for the combination of ease of processability with

superior mechanical properties of strength and stiffness. Further, using copolymerization approach one can easily tune the mesophase properties such as type of mesophase, mesophase transition temperature etc.



Scheme 1.1 Liquid crystalline polymer structures: includes both lyotropic as well as thermotropic LC polymers.

The structures of some of the already commercialized thermotropic liquid crystalline copolyesters are shown in Scheme 1.1. These polymers have extraordinary properties such as high strength and modulus, excellent creep resistance, high dielectric constant, high impact resistance, excellent chemical resistance and low coefficient of thermal

expansion (CTE).

1.4 Classification of liquid crystalline polymers

Based on the position of a mesogenic group on the LC polymer, they are classified in to three major categories.

1.4.1 Main chain liquid crystalline polymers (MCLCPs)

In this class of LC polymers, the mesogen are covalently connected with flexible spacer in a head to tail fashion throughout the polymer backbone. A variety of flexible spacers such as polymethylene, poly(ethylene oxide), polysiloxane etc. are incorporated in the main chain backbone to fine tune LC properties of polymers. The general template for the design of MCLCPs is shown in Figure 1.5.

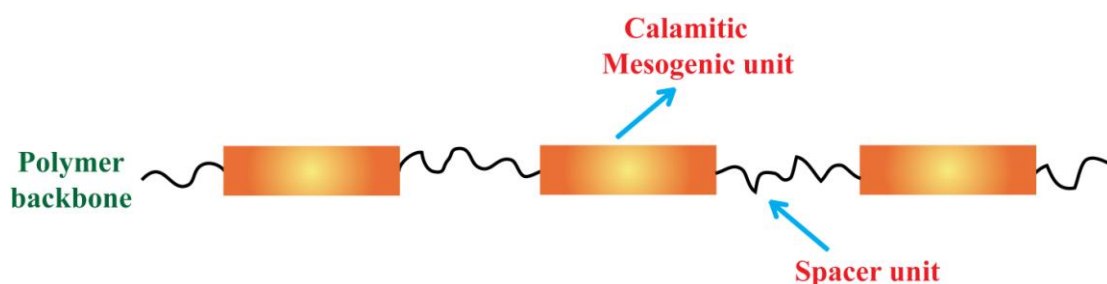


Figure 1.5 General template for the design of main chain LC polymers (MCLCPs).

The basic structure of MCLCPs consists of benzene rings interlinked at para positions. However such rod-like molecules tend to be infusible and intractable crystalline solids. For instance, the melting transition of 610 and 600 °C were measured by DSC for poly(p-hydroxy benzoic acid) and poly(p-phenylene terephthalate), respectively.¹⁸ Therefore, the aim of thermotropic MCLCPs design is to lower the melting point to a melt processable range without destroying the LC formation. There are a few ways to achieve this by destroying the perfect regularity of para linked aromatic benzene rings, by (i) Introduction of disruptors (flexible spacer or rigid kinks) in linear polymer chains, (ii) substitution on aromatic rings and (iii) copolymerization.¹⁸⁻¹⁹ Usually at least two of these combinations are required to achieve melt processability and high mechanical strength in the final LC polymer.

1.4.2 Side chain liquid crystalline polymers (SCLCPs)

Side chain LCPs emerged as an area of enormous practical importance due to their exceptional optical properties which are useful in electro-optical devices.²⁰ In these types of polymers the mesogenic groups are linked with suitable flexible spacer to an existing polymer backbone. The spacer length has a profound effect on the temperature and type of phase transitions.²¹ Usually short spacers tend to lead to nematic phases, whereas longer spacers lead to smectic mesophases. The general templates for the design of SCLCPs are shown in Figure 1.6.

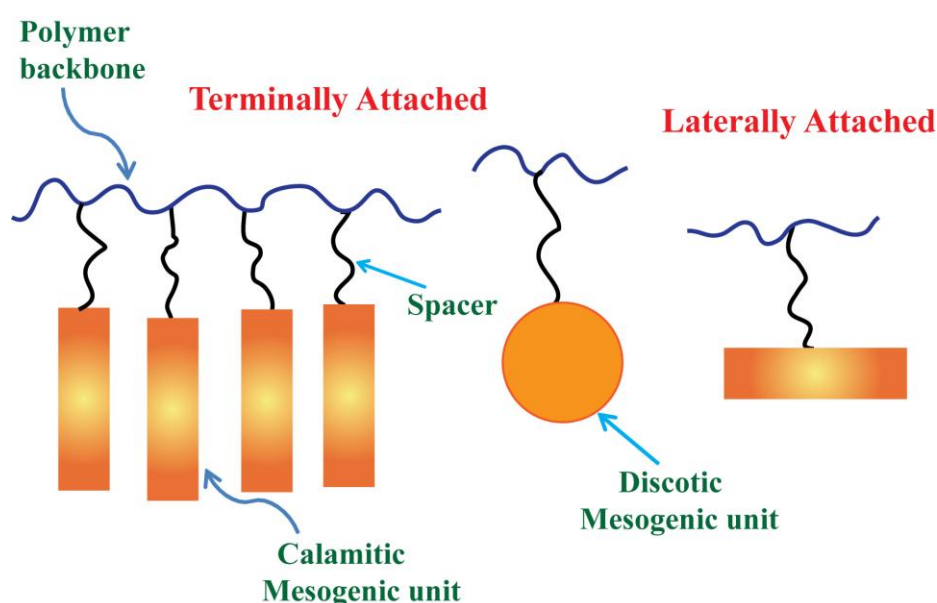


Figure 1.6 General templates for the design of side chain LC polymers.

Polymers with mesogenic side chains are usually thermotropic and the mesogenic group maintains a degree of orientation freedom depending on the coupling strength to the polymer backbone.

1.4.3 Combined liquid crystalline polymers (CLCPs)

The combination of chemical features of MCLCPs as well as SCLCPs can result in a new hybrid class of LC polymers called combined liquid crystalline polymers. It is expected that combined liquid crystalline polymers may have more complex behavior compared to conventional MCLCPs or SCLCPs. It might lead to various supramolecular mesoscopic structures. In this type of LCPs, mesogenic groups are incorporated as part of main as well as side chain which are separated by suitable

flexible spacer. The general templates for the synthesis of combined LCPs are shown in Figure 1.7. The first example of this class of LCPs was reported by Ringsdorf *et al.* using combination of azobenzene and biphenyl mesogen.²² Recently, there are several reports available on combined LCPs.²³

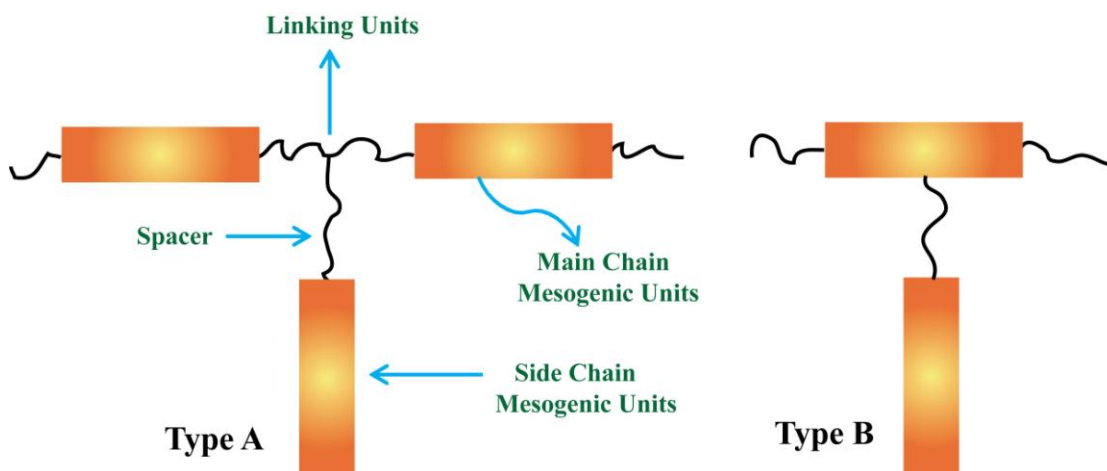


Figure 1.7 Common templates for the design of combined LC polymers.

1.5 Liquid crystalline polyesters

Liquid crystalline polyesters are considered as one of the most intriguing materials in the area of engineering thermoplastic due to their extraordinary properties like superior mechanical properties, moldability, heat resistance, accuracy of dimensions etc.²⁴ The history of thermoplastic polyesters goes back to 1929 with the pioneering contribution of Carothers. In 1932, the first thermoplastic processable polyester was invented and it was synthesized from adipic acid and ethylene glycol. Polyesters attracted industrial interest in 1942, with the synthesis of high melting point products based on terephthalic acid. Recently, these type of LC polyesters are used in precision electronic parts suitable for surface mount technology (SMT).²⁵

In general, polyesters are mostly condensation polymers which can be synthesized by melt condensation or by the solution route. Usually, condensation polymerization methods use high temperature, high vacuum and metal catalyst. The solvent-free melt polymerization processes are often preferred in engineering thermoplastics because of the direct utilization of the raw materials for processing into the desired products. The typical methods and corresponding starting materials which

are employed for the synthesis of polyesters are illustrated below.

1.5.1 Polyesters from hydroxycarboxylic acids

The hydroxycarboxylic acids are AB type of monomers having both reacting functionality as part of the same monomer. The polycondensation of these AB type monomers results in the formation of polyesters. The aliphatic hydroxycarboxylic acids could be polymerized into high molecular weight polyesters by the melt polycondensation. However, these polymerizations frequently come across with the formation of unwanted cyclic ester (lactones) as a side product. The polycondensation of aromatic hydroxycarboxylic acids e. g. 4-hydroxybenzoic acid and 2,6-dihydroxynaphthalenecarboxylic acid, which are very useful starting materials for the synthesis of thermotropic liquid-crystalline polyesters have gained importance in recent years.

1.5.2 Polyesters from dicarboxylic acid and diols

Dicarboxylic acids and diols (A-A and B-B monomers) are usually polymerized with melt polycondensation route. However, it sometimes results in low molecular weight polyesters. More importantly, the thermal stability of the starting materials at high temperature is also necessary during condensation reaction. Another choice is solution polycondensation if the reactants and polyesters are well soluble in a common solvent system. Typically polymerization of dicarboxylic acids and diols are driven to high molecular weight polyesters by removal of water molecule as side product which is often a slow process. In such circumstance the suitable functional derivative of dicarboxylic acid and diols are used instead of the direct condensation.

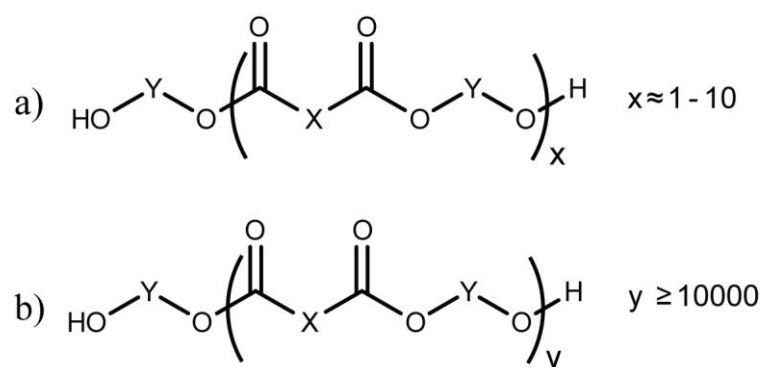
1.5.3 Polyesters from dicarboxylic acid derivatives and diols

The polycondensation reaction between dicarboxylic acid derivatives (e. g. dimethyl ester) and diol can be carried out in melt condition at a significantly lower temperature compared to the corresponding free acid. In this type of starting materials, in presence of acidic or basic catalysts transesterification occurs with the elimination of the readily volatile alcohol as by product. As a substitute of diesters of carboxylic acid one can carry out polycondensation of their dicarboxylic acid

chlorides with appropriate diols to obtain final polyesters. For instance, high melting polyesters could be made from terephthaloyl dichloride and bisphenols.²⁶

1.6 Transesterification reaction

Thermoplastic polyesters are commonly synthesized by transesterification reaction between dicarboxylic acid and dihydric alcohols in a two step process. In the first step a polyester precondensate (M_n 100-2000, depending upon the molar ratio of starting compounds) with formula shown in Scheme 1.2-a is formed. The precondensate later reacts in the second step (polycondensation) with elimination of dihydric alcohol to form high molecular weight polyester ($M_n > 10000$) having formula shown in Scheme 1.2-b. Transesterification and esterification are equilibrium reactions that are often accelerated in presence of acidic or basic catalyst. For example, by strong acid (P-toulenesulfonic acid), metal oxide (antimony oxide), Lewis acid (titanium tetra-



Scheme 1.2 *Transesterification reaction a) first step formation of polyester precondensate ($M_n = 100-2000$) and b) second step elimination of dihydric alcohol to form high molecular weight polyesters ($M_n > 10000$).*

butoxide, tin acetates, tin octoates) and weak acid salts of alkali metals or alkaline earth metals (acetates or benzoates). The other way of shifting the reaction equilibrium continuously towards polyester precondensate is by removing the more volatile side products like alcohol or water. It is often carried out under solvent-free melt polymerization conditions. Copolymerization approach would give an opportunity to tune various properties of resultant polyesters such as dyeability, elasticity, pilling behaviour, shrinkage, hydrophilicity and flame resistance etc. by using appropriate comonomer combinations.

1.7 Structural chemistry of azobenzene

Azobenzene, with two phenyl rings separated by an azo ($-N=N-$) linkage, serves as the parent structure for a wide class of aromatic azo compounds. Most of the molecules have planar geometry with respect to the nitrogen atom in the trans form. The $-N=N-$ bond length was found to be 1.22-1.25 Å in case of aliphatic azo compounds while aromatic azo compounds showed slightly longer bonds of 1.24-1.26 Å. The azo chromophores have great importance in both research areas - fundamental and applied. The strong electronic absorption can be tailored via ring substitution from the UV to visible red regions, which allows the chemical fine-tuning of color. The rigid rod shape of the molecule is well suited for the spontaneous organization of liquid crystalline (LC) phases, and hence polymers doped or functionalized with azobenzene leads to a variety of self organized polymeric LC structures which form common LC media for various application. One of the most exciting properties of these chromophores is the readily induced and reversible isomerization about the azo linkage between the trans and cis geometric isomers. This light-induced interconversion for the azobenzene incorporated materials allow systems to be used as photoswitches, carrying out rapid and reversible control over a variety of chemical, mechanical, electronic and optical properties.²⁷

Azobenzenes can be classified into three spectroscopic classes, azobenzene-type molecules, aminoazobenzene-type molecules and pseudo-stilbenes.²⁸ The examples from each class of azomolecules and their absorption spectra is shown in Figure 1.8. Many azobenzene derivatives exhibit absorption spectra similar to unsubstituted azobenzene prototypes. These molecules exhibit a low intensity $n-\pi^*$ band in the visible region and a much stronger $\pi-\pi^*$ band in the UV region. Although the $n-\pi^*$ is symmetry-forbidden for the trans azobenzene (C_{2h}), vibrational coupling and some extent of non-planarity however make it observable in most of the cases.²⁹ Putting substituents on the azobenzene rings may induce minor or major spectroscopic changes. The substitution particularly at ortho- or para- positions leads to a new class of compounds called aminoazobenzenes. In these molecules, the $n-\pi^*$ and $\pi-\pi^*$ bands are much closer. In fact, the $n-\pi^*$ band may be completely buried under the $\pi-\pi^*$ band. These azobenzenes are sensitive to solvent polarity, for instance the absorption band shifts to lower wavelength in non-polar solvents and shifts to

higher wavelength in polar solvents. Substitution at the 4 and 4' position of azobenzene with an electron donor and an electron acceptor (such as an amino and a nitro, $-\text{NO}_2$ group) leads to strongly asymmetric electron distribution (often called as a “push-pull” system). This shifts the $\pi-\pi^*$ absorption towards higher wavelength (lower energy) and past the $n-\pi^*$ absorption. Due to the inverted ordering of the absorption bands, the third spectroscopic class are called as the pseudo-stilbenes (analogous to stilbene, phenyl-C=C-phenyl). These compounds are very sensitive to local environment.

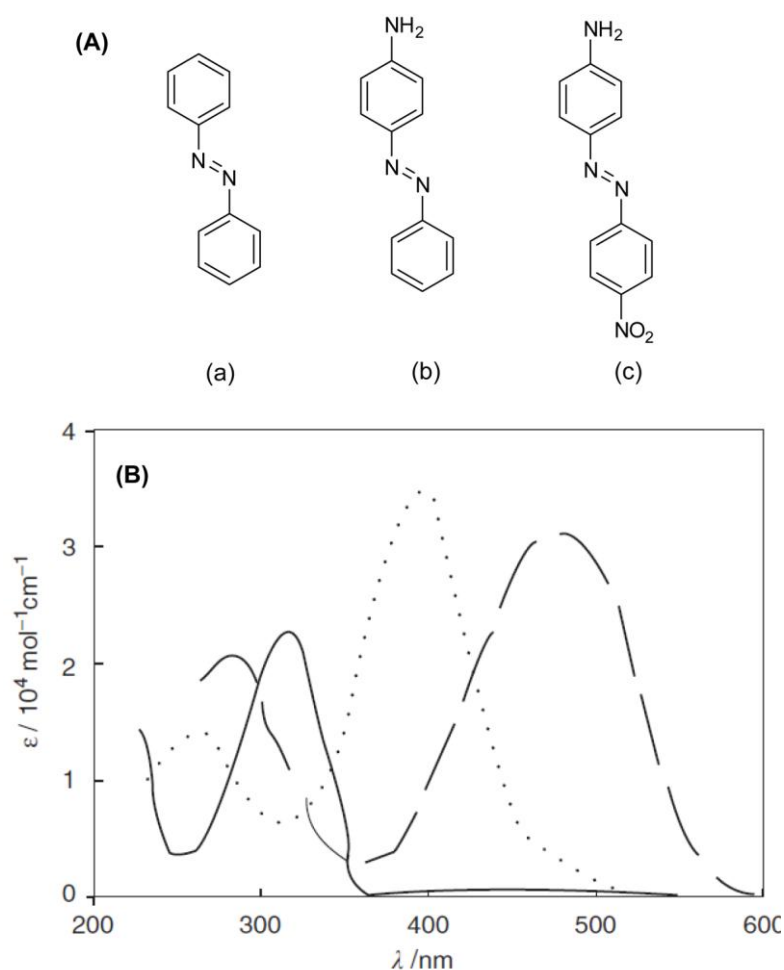


Figure 1.8 (A) Examples of azo molecules classified as (a) azobenzene, (b) aminoazobenzene and (c) pseudo-stilbenes. (B) Typical absorption spectra of trans azobenzenes. The azobenzene-type molecules (solid line) have a strong absorption in the UV region and a low intensity band in the visible region. The aminoazobenzene (dotted line) and pseudo-stilbenes (dashed line) have strong absorption in the visible region.³⁰

The azobenzenes are sensitive to packing and aggregation, mostly in condensed phases (liquids and solids). The π - π stacking gives rise to shift in the absorption spectrum. If the azo dipoles have a parallel (head-to-head) arrangement, they are called J-aggregates, and is characterized by red shift in the absorption spectrum (bathochromic) compared to the isolated chromophore. If the dipoles are antiparallel (head-to-tail), they are called H-aggregates which lead to a blue shift in the absorption spectrum (hypsochromic). Fluorescence is observed in aminoazobenzene and many pseudo-stilbenes but not in case of azobenzenes.

1.8 Photochemistry of Azobenzene chromophore

Azobenzenes, well-known by their nitrogen-nitrogen double bond, undergo clean and reversible conformational changes upon photon absorption, which is schematically shown in Figure 1.9. This process called photoisomerization, enables the manipulation of the physical and chemical properties of azobenzene containing materials with external stimuli. Photoisomerization proceeds with a large structural change as reflected in the dipole moment and change in geometry.

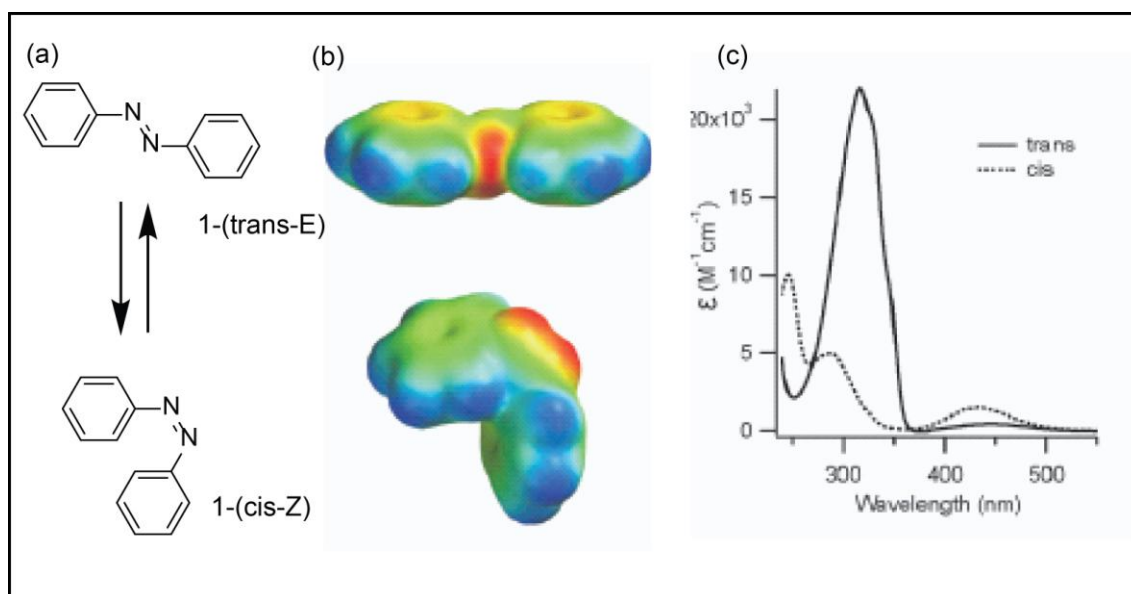


Figure 1.9 (a) Structures of trans and cis isomers of azobenzene, (b) space filling models of trans and cis isomers colored by electrostatic potential (red-negative to blue-positive) and (c) Electronic absorption spectra of the trans and cis isomers of azobenzene dissolved in ethanol. (*Chem. Soc. Rev.* **2011**, 40, 4422-4437).

The process involves a decrease in the distance between para carbons in azobenzene from about 9.0 Å in trans form to 5.5 Å in the cis form.³¹ For the planar trans isomer, the dipole moment is zero, whereas for the bent nonplanar cis isomer, it is 3 Debye. The typical absorption spectra of azobenzenes consist of three major bands. The lowest energy transition occurs at approximately 430-440 nm and is assigned to the $n-\pi^*$ transition. The second transition occurs in the UV region around 320 nm and is assigned to the $\pi-\pi^*$ transition for trans azobenzene (for cis azobenzene the $\pi-\pi^*$ band occurs around 280 nm). The peak maximum of this band is sensitive to the polarity and also to the presence of substituents. The third energy transition around 230-240 nm is considered to arise from the $\pi-\pi^*$ transition in the phenyl rings.³²

1.8.1 Mechanism of photoisomerization

It has been well accepted that the photoisomerization of azobenzene depends upon the excitation wavelength. The trans-cis isomerization prefers an inversion mechanism under $n-\pi^*$ excitation, whereas the rotational mechanism drives under the $\pi-\pi^*$ excitation similar to the isomerization of stilbene.³³

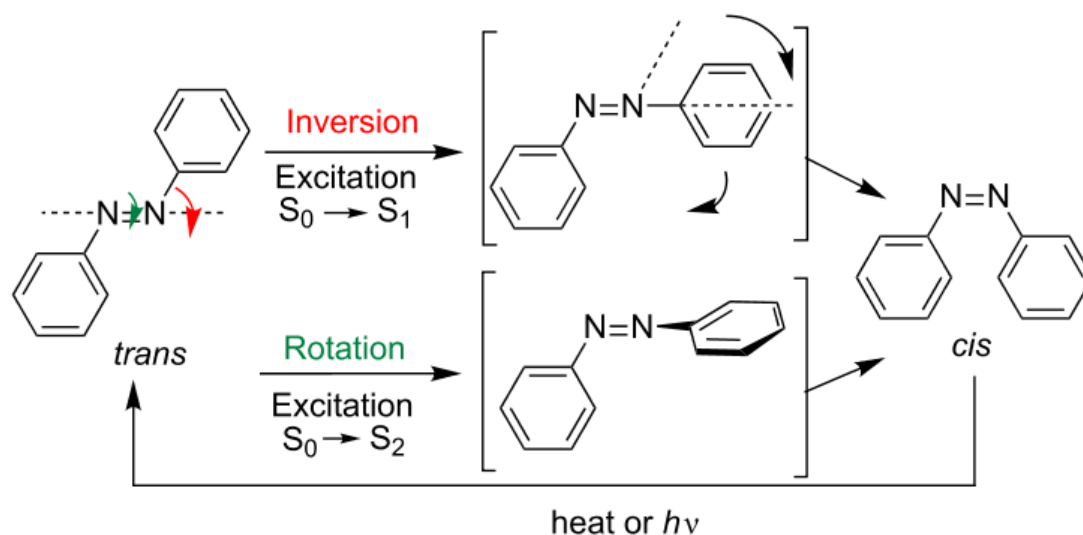


Figure 1.10 Mechanism of azobenzene isomerization via rotation or inversion pathway.³⁴

The mechanism of azobenzene isomerization has undergone considerable debate. Isomerization takes place either through a rotation about the $-N=N-$ bond, with rupture

of the π bond, or through an inversion, with a semilinear and hybridized transition state, where the π bond remains intact (Figure 1.10). The thermal relaxation is well agreed to be via rotation, while for the photochemical isomerization, both mechanisms appear feasible.³⁵ More recent experiment strongly support the inversion mechanism for instance based on matrix and molecular constraints to the azobenzene isomerization.³⁶ Moreover, studies using picosecond raman and femtosecond fluorescence showed intact double bond (N=N) in the excited state, confirming the inversion mechanism.³⁷ In contrast, Ho *et al.* found evidence that the pathway was compound specific; a nitro substituted azobenzene photoisomerizes via the rotation pathway.³⁸ Additionally, ab initio and density functional theory calculations showed that both pathways are energetically accessible, although inversion mechanism is preferred.³⁹ Thus, both mechanisms can exist competing with each other depending on the particular chromophore and environment. The inversion is the dominant pathway for most azobenzenes. This also support the fact that the azo is able to isomerize easily in rigid matrices, such as glassy polymers, since the inversion mechanism has a much smaller free volume requisite than rotation.⁴⁰

1.9 Azo LC Polymers: Photoresponsive Properties and Application

The LCPs containing azo group possesses the unique features of ordinary LC materials such as self-organization, long-range ordered fluidity, molecular cooperative motions, a large birefringence, anisotropy in various physical properties and orientational control by external stimuli at surfaces and interfaces. But the photoresponsive properties of azo (e. g. photoisomerization) also exerts great influence on the LC features. For instance photochemical phase transition, photoinduced alignment and photo-triggered molecular cooperative motion (Figure 1.11) can be obtained upon photoirradiation by choosing appropriate light, to make soft materials with light-controllable properties.⁴¹

In general, a rod-like trans azo molecule isomerizes into its bent shaped cis isomer upon unpolarized UV light irradiation. By choosing light of suitable wavelength and intensity several intriguing phenomenon could be observed as shown in Figure 1.11. The photochemical phase transition between ordered LC phase to a completely disordered isotropic phase could be observed because of rod shaped trans azo form can exhibit mesophase where as the bent cis azo destabilizes LC phase at

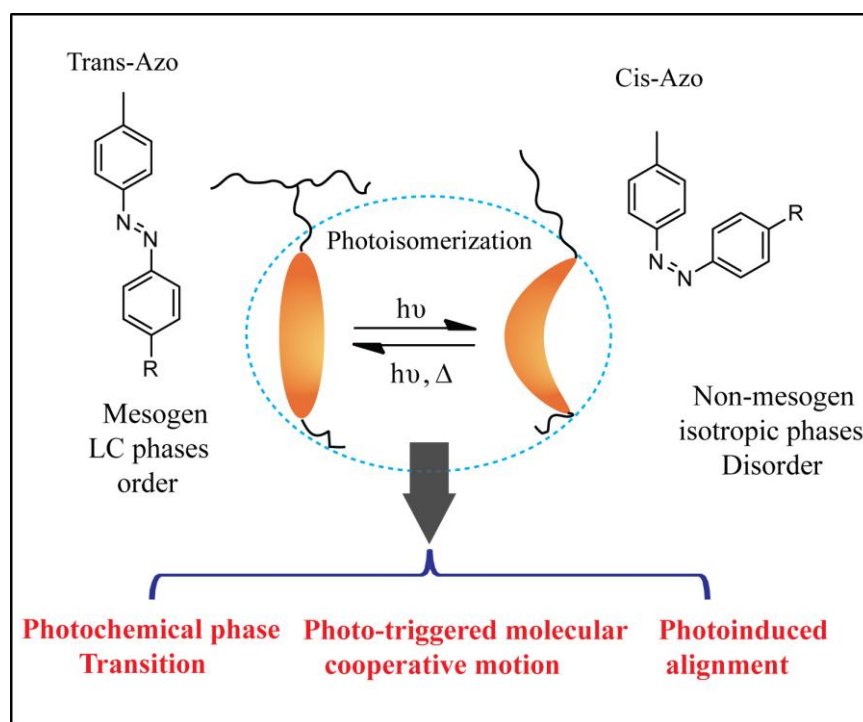


Figure 1.11 Scheme of photoresponsive properties of azo-containing LCPs. Due to the reversible photoisomerization, outstanding photoresponsive performances such as photochemical phase transition, photo-triggered molecular cooperative motion and photo induced alignment are observed.⁴¹ (adapted from *J. Mater. Chem. C*, **2014**, 2, 3047-3054).

any temperature. The photoinduced molecular cooperative motion between azo molecules and other photoinactive mesogens is one of the most remarkable properties in LC copolymers and polymer blends.⁴² Another very interesting property is the photoinduced alignment of azo molecules with their transition moments almost perpendicular to the polarization direction of the incident light using plane polarized light (LPL), which is known as the Weigert effect.⁴³

The photoinduced change in the LC orientation of azo LCPs can result in a variety of interesting physical performances such as change in refractive index, birefringence, modulus, viscosity, conductivity, volume, electric and magnetic susceptibility, which make them suitable for photonic applications.⁴¹ The photoinduced change in birefringence of azo containing LCPs is interesting because it can be caused by the photoalignment of light responsive mesogens. Initial work in this

area was performed on the LPL-induced change in the alignment of Azo embedded polymers.⁴⁴ For enhancing the stability of the photoinduced anisotropy, amorphous polymers covalently attached to Azo moieties were specially designed.⁴⁵ However, the birefringence with an amorphous state was too small to satisfy the prerequisite of photonic application. In contrast, the azo containing LC material showed large photoinduced birefringence upon changing the LC orientation directions.

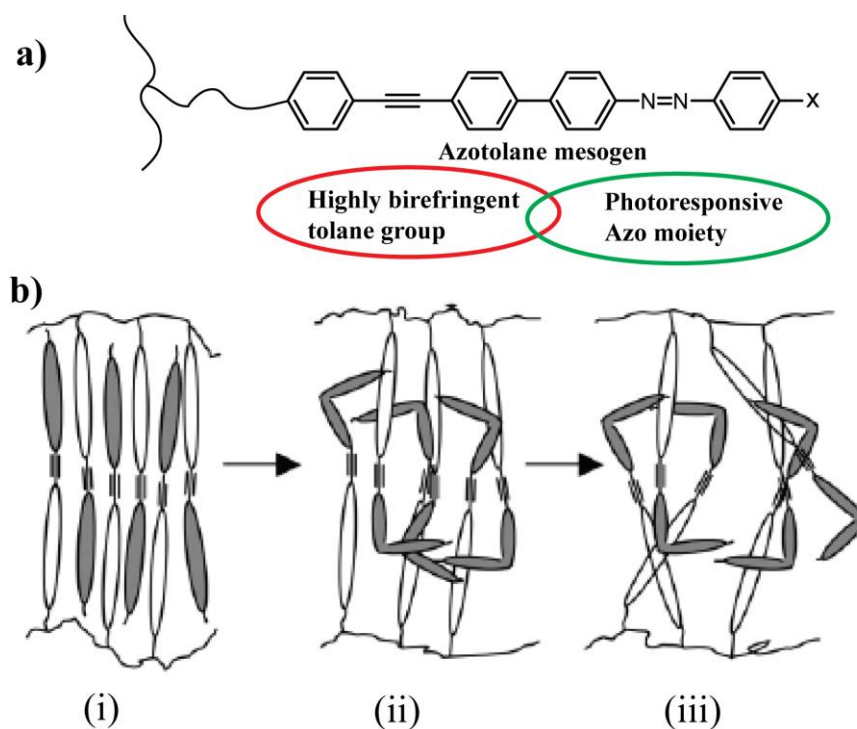


Figure 1.12 a) Chemical structure of LCPs containing azotolane mesogen for photoinducing a large change in birefringence b) Schematic of phase transitions in azotolane mesogen upon exposure to s-polarized pump beam. (Adapted from *Adv. Mater.* **2006**, *18*, 523-527).

It is well accounted that a tolane moiety is one of the common core structures for the design of highly birefringent LC molecules due to its longer molecular conjugation length. The LC random copolymer containing both tolane and azo moieties in the side chain showed large change in the birefringence. However photoresponse was not high due to low content of azo moiety. To increase the photosensitivity and a larger birefringence, a new concept of molecular design was

projected, in which a tolane moiety was directly attached onto azo molecule to prepare azotolane mesogen, which is shown in Figure 1.12.⁴⁶ A large birefringence could be obtained even at the telecommunication wavelength (1550 nm) due to photoinduced phase transition, from the azotolane containing polymer. Based on these phenomena the azo LC materials are intriguingly used in a variety of applications for instance photomechanical actuators, optical storage, tunable diffraction gratings etc.

1.9.1 Photodeformation and photomechanical effects

The basis of smart materials is their ability to respond to very minor changes in the surrounding environment, such as temperature, light, P_H , magnetic or electric field, ionic factors, and biological molecules. The responses are expressed as changes in shape, surface characteristics, solubility, and formation of complex molecular self assembly, sol-gel transition etc.⁴⁷

Liquid crystalline elastomers (LCEs) have exceptional combinations of the anisotropic features of the LC phases and the rubber elasticity of the polymer networks. Due to LC properties of mesogens the LCEs can be aligned and the alignment of mesogens can be coupled with polymer network structures. This coupled effect gives rise to many exciting properties in LCEs. LCEs have emerged as motivating topics recently because large deformations could be achieved by external stimuli such as electric fields, change in temperature and light. These features make LCEs as promising raw materials for artificial muscles and actuators.⁴⁸ The LCEs are typically lightly cross-linked polymer networks. The cross-linking density has a great influence on the macroscopic properties as well as phase structures.⁴⁹ The segmental motion of polymer chains decreases with an increase in the cross-linking density and as a consequence the overall mobility of mesogens in the vicinity of a cross link is suppressed.

The concept of LCEs was first proposed by de Gennes (1975), and the first example of a LCE was prepared by Finkelmann *et al.*⁵⁰ Since then a variety of LCEs with various LC phases, such as nematic,⁵¹ smectic,⁵² cholesteric^{52c} and discotic⁵³ have been prepared by the polymerization of various monomers containing more than one polymerizable group. LCEs could also be prepared by block copolymerization and supramolecular interaction such as hydrogen bonding.⁵⁴ Li *et al.* proposed a muscle like material with a lamellar organization based on a nematic triblock

copolymer.^{48a} The light responsive LCEs are more fascinating because light as a stimulus allows noncontact activation at ambient temperature.⁵⁵ In fact, Finkelmann and coworkers were able to induce a contraction by 20 % in an azobenzene LCE upon UV light irradiation due to trans-cis photoisomerization of the azobenzene moiety.⁵⁶ Terentjev *et al.* incorporated a wide variety of azobenzene derivatives in to LCEs as photoresponsive handle and studied their deformation behavior upon exposure to UV light.⁵⁷ Li and co-workers synthesized monodomain nematic side-on elastomers containing azobenzene by photopolymerization.^{48d} Photopolymerization was performed with aligned nematic azobenzene monomers in conventional LC cells. Thin films of these LCEs showed fast photochemical contraction of up to 18 % upon UV light exposure and a slow thermal back relaxation in the dark which is shown in Figure 1.13.

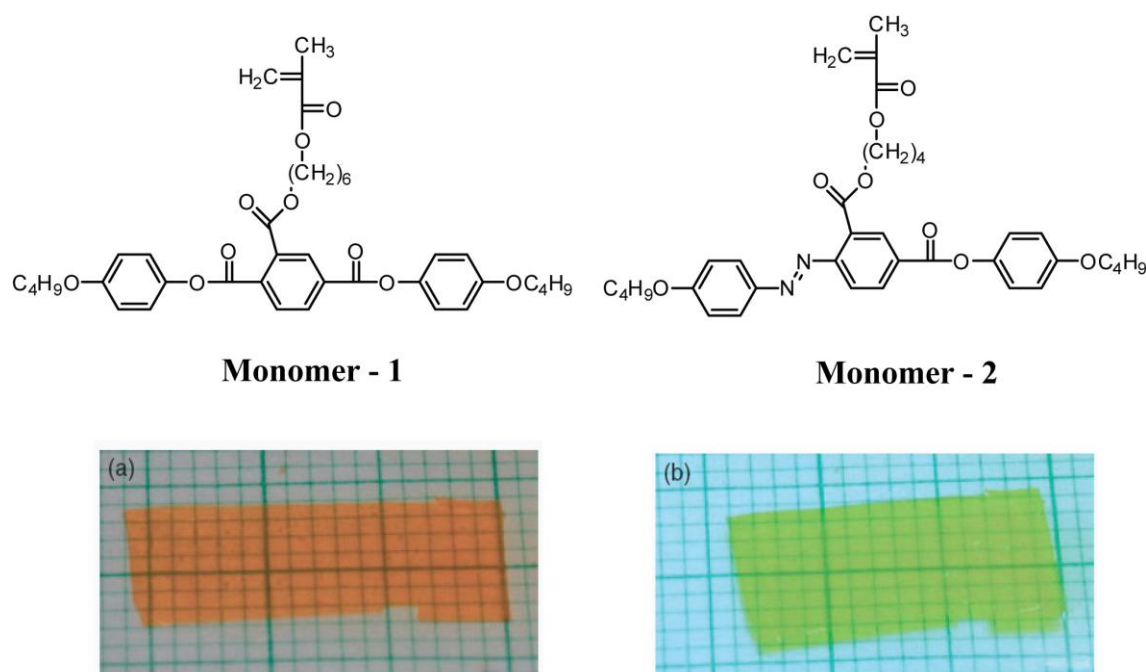


Figure 1.13 Side on-liquid crystalline monomer structures and photographs of photodeformation of azobenzene side on LCE (a) before irradiation and (b) under UV irradiation. (Adapted from *Adv. Mater.* **2003**, *15*, 569-572).

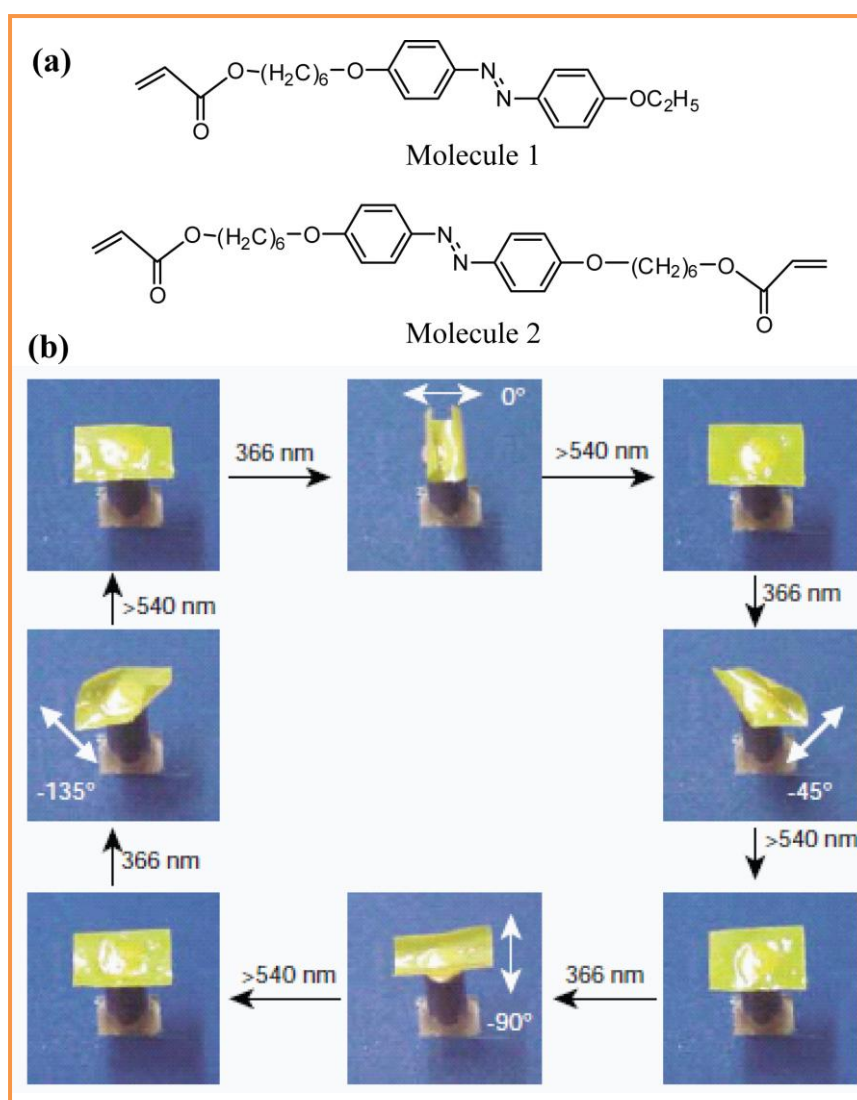


Figure 1.14 Precise control of the bending direction of a film by linearly polarized light (a) chemical structure of the liquid crystal monomer (molecule 1) and crosslinker (molecule 2) used for the preparation of the film. (b) Photographic frames of the film bending in different directions in response to irradiation by linearly polarized light of different angles of polarization (white arrows) at 366 nm, and being flattened again by visible light longer than 540 nm. (Adapted from *Nature* **2003**, 425, 145-145).

The above examples demonstrated two-dimensional movements of LCE films, whereas many examples of three-dimensional photoinduced movements of LCEs have also been reported. Ikeda and coworkers reported for the first time photoinduced

anisotropic bending and unbending behavior of LC gels.⁵⁸ In comparison to two dimensional expansion or contraction, the bending/unbending - a full three dimensional movement, could be more valuable for a variety of real manipulation application. Recently, Ikeda *et al.* were also able to control the direction of photoinduced bending in a single polydomain LCE, so that LCE film could be bent repeatedly and precisely along any chosen direction (Figure 1.14). The film bent toward the irradiation source in a direction parallel to the polarization of the light.⁵⁹

1.9.2 Tunable diffraction gratings

The tunable diffraction gratings refer to gratings whose features can be reversibly altered by an external stimulus. This tunable material has potential features that offer a new way of application in such devices as fibre-optic switches and dynamically variable focal-length lenses.⁶⁰ The reversible and rapid trans to cis photoisomerization of azobenzene and its derivatives make polymers and liquid crystal bearing this chromophore a proper medium for recording a diffraction grating for light. A diffraction grating basically is an optical component with periodical change of refractive index. A uniform grating pattern is formed due to change in refractive index in the reactive region by exposing a film of the polymer or LC azobenzene to an interference pattern generated by two coherent recording laser beams, which falls on it after passing through a photomask.³⁰ The various phenomena in the reactive regions are related to the photoisomerization of azobenzene which is responsible for the index modulation. First, the simple conversion of trans-azobenzene to cis-azobenzene can result in index change, because two isomers do not have same index. In this event, the extent of index modulation is very small. Second, the photochemical orientation (alignment) of azobenzene moieties can change the refractive index. In this case, linearly polarized light (LPL) is required to induce orientation of azobenzene in the direction perpendicular to the polarization. Third, in case of liquid crystalline azobenzenes, photochemically induced phase transition like the nematic to isotropic transition, can also give rise to an index change.⁶¹

The Figure 1.15 schematically illustrates the three types such as mechanically, electrically and optically tunable gratings. For mechanically tunable diffraction gratings, the diffraction angle can be reversibly altered upon an elastic deformation of the material leading to a change in the refractive index and the diffraction efficiency

can be tuned. For an electrically tunable diffraction gratings, the application of electrical field operates through a change in the refractive index because of the electric field-induced LC orientation, which allows for switching of the diffraction efficiency between the on and off state (i. e. between high and low efficiency).

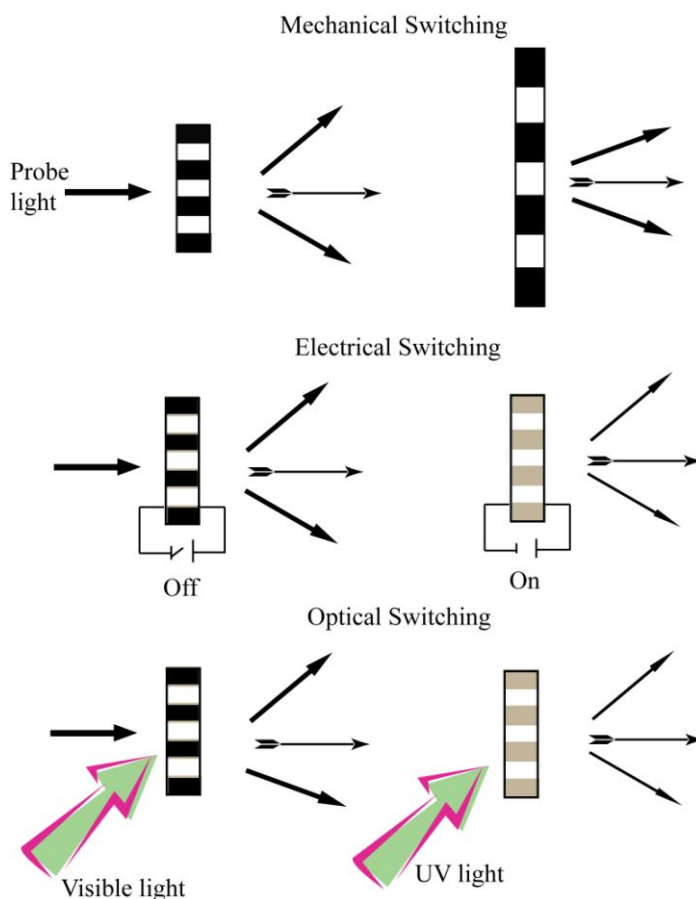


Figure 1.15 Schematic diagram of mechanically, electrically and optically switchable diffraction gratings. (Adapted from Yue Zhao; Tomiki Ikeda, *Smart Light-Responsive Materials: Azobenzene-Containing Polymers and Liquid Crystals*. John Wiley & Sons, Inc.: 2009).

In case of optical tunable diffraction grating, the switching among on and off state could be achieved by exposing the grating to light of two different wavelengths. In case of azobenzene incorporated polymers and LC materials, it is possible to perform trans to cis and reverse cis to trans isomerization of azobenzene moieties at two different wavelength, to generate a reversible change in index modulation of the grating.

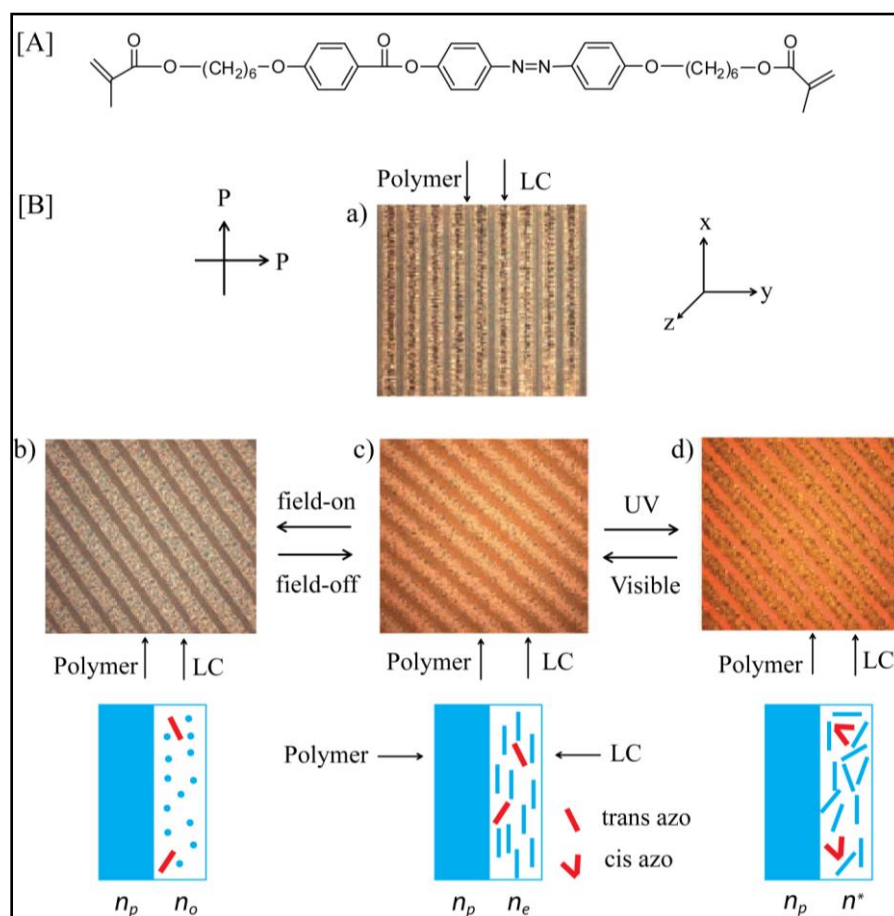


Figure 1.16 [A] Liquid crystalline azobenzene dimethacrylate monomer [B] Polarizing optical micrographs showing an electrically and optically switchable diffraction grating prepared with an azobenzene polymer stabilized nematic liquid crystal **a)** The grating with fringes parallel to one of the crossed polarizers (P), with LC molecules being oriented in the rubbing direction ; **b)** the same grating rotated by an angle of about 45° ; **c)** the grating after (b) subjected to an alternating current (AC) field (1000 Hz, 40 V peak to peak), the LC molecules being oriented in the field direction (z-axis) ; **d)** the grating after (b) exposed to UV light ($\lambda = 365 \text{ nm}$, 20 mWcm^{-2}), resulting in the nematic-to-isotropic phase transition. The graphic illustrates the different orientation states of LC molecules and corresponding refractive index modulation of the grating for probe light propagating along the z-axis and polarized along the x-axis. (Adapted from Tong et al. *Adv. Mater.* **2005**, *17*, 370-374).

Based on the above principle Tong *et al.* demonstrated, both electric field and optical switching of diffraction gratings based on azo-polymer stabilized liquid crystal (Azo-PSLC), which is shown in Figure 1.16-B.⁶² The diffraction grating was obtained by using a homogenous mixture composed of a dimethacrylate azobenzene monomer that was inherently liquid crystalline, a photoinitiator and LC media (Figure 1.16-A). Using this combined LC media, it was possible to achieve reversible electrical and optical switching of index modulation. This combined electrical and optical switching capability may be helpful for such device application as, for example electrically controllable UV-visible image conversion.

1.9.3 Optical data storage

Emerging development in digital technologies has required the use and storage of large amounts of data. Recently, different technologies are being used for the data storage, even though optical data storage has had a great impact on daily life. Compact disc (CD), digital versatile disc (DVD) and Blue ray-disc are common modes of use. A promising way to increase the storage capacity is holographic storage.⁶³ Using this method it is possible to record information in a photosensitive media by recording an optical interference pattern. Several polymeric materials such as photopolymers and photorefractive polymers⁶⁴ have been proposed for these applications and in particular azobenzene based polymers have been extensively explored.^{63c,65}

In case of azobenzene incorporated materials the diffraction efficiency depends on photoinduced change in refractive index. In an isotropic material, the change in refractive index by photoirradiation is rather small and the efficiency is not high. In addition, the material is theoretically polarization inactive. On the other hand, anisotropic material could show large birefringence. By controlling their molecular alignment by photoirradiation, a large change in refractive index and high diffraction efficiency can be obtained. Furthermore, an anisotropic material shows polarization activity.^{65a} Therefore, Liquid crystals (LCs) containing azobenzene materials are promising material for holographic storage because their optical anisotropy and fluidity and their molecular alignment can be cooperatively varied by external stimuli. In the early stage, the azobenzene containing LC systems have been developed to facilitate two-dimensional image storage and 3D image in Raman-Nath holograms.⁶⁶

Recently, holographic recording in thick polymer film has been explored, for developing holographic memory with high-density information storage.^{65b,67}

Initially Wendroff *et al.* demonstrated how the photoinduced orientation was amenable to holography in the polymer film.^{66a,68}

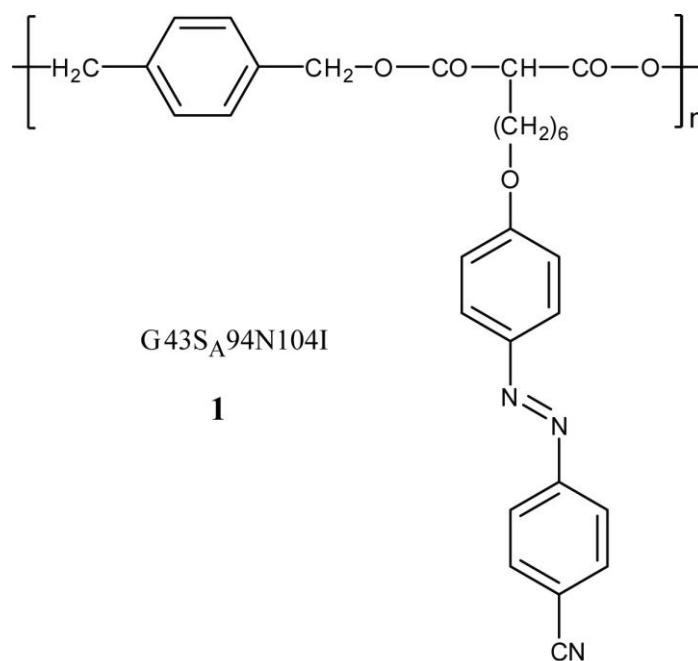


Figure 1.17 Chemical structure and phase transition of side chain azo LC-polymer, which was used for the first time in holographic application. (*G*-glassy, *S_A*-Smectic-*A* phase, *N*-nematic and *I*-isotropic phase transition).^{66a}

The first liquid crystalline polymer used was a side chain LC polymer **1**. Whose chemical structure and phase transitions are shown in Figure 1.17. Very stable gratings with diffraction efficiencies up to 4 % were obtained and erasing also could be done by heating the sample just above the isotropization temperature. Initially, the anticipated mechanism appeared puzzling because the reorientation was clearly obtained through trans to cis isomerization, but the subsequent cis-trans isomerisation occurring without irradiation, did not affect the final outcome. After more detailed studies on photo orientation, the proposed mechanism was believed to involve a change in the orientational order induced by the change in shape of the mesogen from trans to cis.⁶⁹ After that a variety of LC side chain homopolymers containing

azobenzene was prepared and studied in thick films for optical holographic data storage. One major problem was the high absorption of chromophores, films with large amount of azobenzene had a large absorption and the recording light could not penetrate more than few micrometers through the film making these materials inappropriate for large volume storage application. To circumvent this problem, dilution of azobenzene content by various strategies of random copolymerization with either mesogenic or non-mesogenic co-monomer was employed.⁷⁰ Bieringer and coworkers, attained large birefringence values under illumination of polarized light using side chain copolymer incorporated with azobenzene mesogenic chromophore and mesogenic side groups.⁷¹ Recently, Ishiguro *et al.* demonstrated the formation of stable holographic gratings in thick polymer films prepared from the copolymer having azobenzene chromophore and tolane moiety in the side chain.⁷²

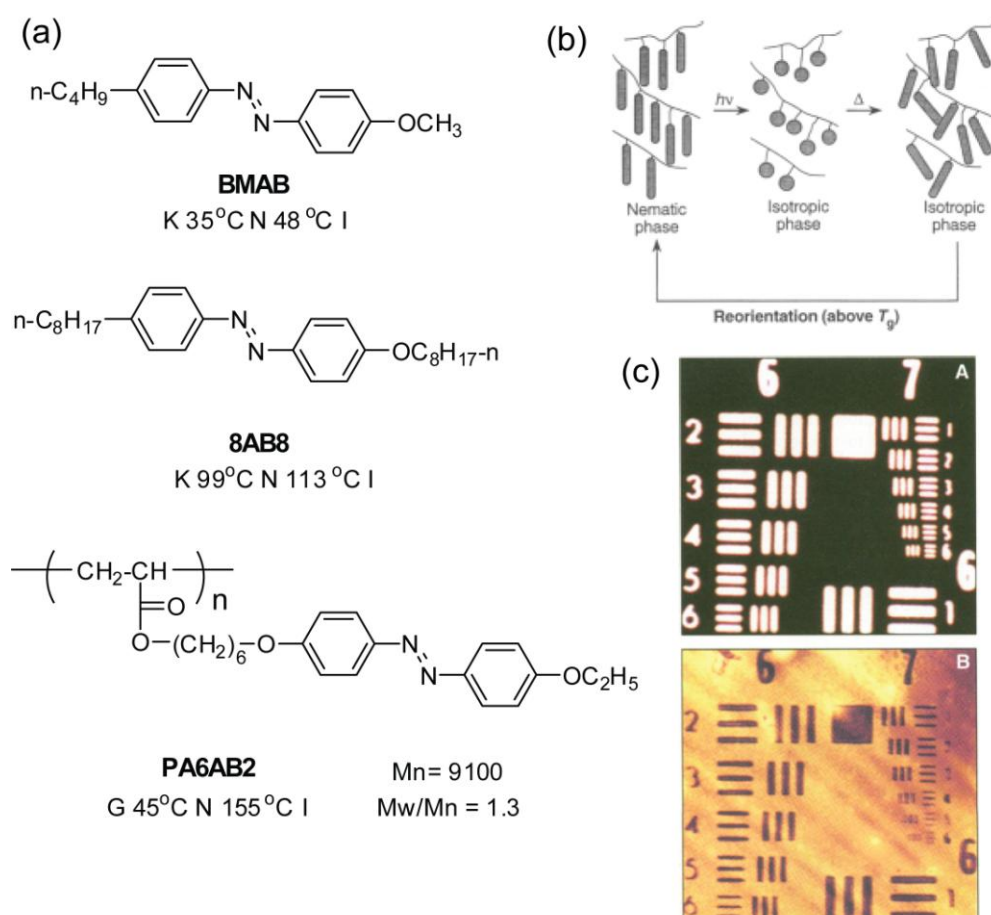


Figure 1.18 (a) Structures and phase transitions of three azobenzene liquid crystal (abbreviations: K- crystal, N- nematic, I- isotropic and G- glassy) (b) Orientation of transazobenzene mesogens after the trans-cis-trans cycles and (c) Stored image in a

*polymeric NLC. The thin film of PA6AB2 was covered with photomask - A and irradiated with a single pulse of the YAG laser, the third harmonic at 355 nm, at 23 °C (below the T_g). The image storage for 8 months is shown in B. (Adapted from Ikeda et al. Science **1995**, 268, 1873-1875).*

Based on the photochemical and isothermal phase transition in LCPs, Ikeda and coworkers reported optical switching and image storage in azobenzene liquid-crystal films.⁴⁰ They observed that polymeric azobenzene LC films had two advantages compared to low molecular weight LC molecules; first advantage was the much wider nematic LC phase in the LC polymer making available a wide temperature range for optical switching. Secondly, they had a glass transition, so that they could function as image storage materials when they were operated below the glass transition temperature as shown in Figure-1.18. Additionally, the image could be erased just by increasing the temperature above the glass transition temperature (T_g) of polymer.

1.10 Methods employed for the mesophase investigation

1.10.1 Differential scanning calorimetry (DSC)

DSC is a popular and suitable technique for determining thermal behavior of materials. The heat flow rate difference between a substance and a reference is measured as a function of temperature, while the sample is subjected to a controlled temperature program.⁷³ Transition temperature, enthalpy values and transition entropy values can be easily calculated by this method.

1.10.2 Polarized light microscope (PLM)

Polarized light microscope (PLM) is a very useful technique for a preliminary characterization of the mesophase. It provides a determination of both phase transition temperatures and types of phases. In PLM, a picture of thin layer of liquid crystal is observed by the microscope under linearly polarized light. The features of the picture, usually termed as “texture” by Fridel, are caused by the existence of defects and mesophases (nematic, smectic and cholesteric) which are identified based on the texture.⁷⁴

Nematic LCPs generally shows threaded texture or schlieren texture. Semi-

rigid or side chain nematic LCPs usually show similar texture to lower mass LC compound, but not all the aromatic LC polyesters show these typical texture. Smectic LCPs show numerous kinds of textures - schlieren, fan shaped, batonnets and mosaic etc. Cholesteric LCPs also shows several types of texture - polygonal, fingerprint, grandjean textures etc.

1.10.3 X-ray diffraction

X-ray diffraction technique gives the information about modes of the packing of molecules and the types of order present in the mesophase.⁷⁵ X-ray diffraction studies can be performed on either oriented or unoriented samples. Unoriented samples are easier to prepare, but oriented samples are more informative for structural analysis. In the case of liquid crystalline polymers (LCPs), a combination of these methods are often needed to identify the mesophase type because of their broad molecular weight distribution, high viscosities and features of polycrystalline and amorphous material.

1.11 Aim of the thesis

From the previous literature discussion, it can be well understood that the azobenzene containing liquid crystalline materials have potential application in photonics, optics, electrical/electronic and automotive industries. Therefore, fine tuning of mesophase types and mesophase transition temperature of azobenzene based liquid crystalline material is very relevant to material science in order to generate suitable materials for various applications. Liquid crystalline polymers (LCPs) have certain advantages over a low molecular weight LC compound such as high mechanical strength at high temperature, extreme chemical resistance, easy processability, inherent flame retardancy, and good weatherability.⁷⁶ However, it is more challenging to control LC self organization of a liquid crystalline polymer compared to their low molecular weight analogous. In case of LCPs, the monomer design and choice of polymerization method also plays an important role to achieve liquid crystalline properties without sacrificing fundamental properties of the polymer backbone. The monomer design should be easy to synthesize and be scalable for large-scale production. Thermotropic main chain liquid crystalline polyesters have unique features of both liquid crystalline and thermoplastic nature. In general, main chain azo LC polyesters are mostly synthesized by solution route. Solution polymerization has been the method of

polymerization for the most reported azobenzene polymers mainly because of the low degradation temperature which precluded a melt polycondensation route. The melt polycondensation route has the advantage that it is devoid of solvent and also helps to build the molecular weight. It is applicable for the synthesis of a variety of polymeric architecture such as main chain LCPs, hyperbranched LCPs etc. The branched LC architecture incorporating azobenzene chromophores is found to be promising for the preparation of LC materials with lower viscosity due to their fast switching response in devices.

The objective of this thesis is to design and develop new multifunctional monomers that could be directly used in a melt polycondensation reaction. Twin azobenzene having the structure azobenzene-spacer-azobenzene, where the spacer was oligoxyethylene of varying length is a versatile design for the synthesis of main chain azo polyester through the melt polycondensation approach. Main chain liquid crystalline polyesters containing azobenzene and oligo(ethylene)oxide segments that could support ionic conduction is expected to serve as good thermo and photoresponsive ion conductive materials upon complexation with lithium salt. These poly/Li composites have potential as solid polymer electrolyte (SPE) in Li-ion batteries. Tri and tetrapod polymerizable multifunctional monomer design incorporating azobenzene was also designed for the synthesis of hyperbranched polyesters. In these multipods, the terminal azobenzene chromophores were suitably functionalized with methyl carboxylic ester which could be used as B₃ and B₄ type monomers for the synthesis of photoresponsive hyperbranched polyesters (HBPs).

The important highlights of the thesis are:

- 1) Two homologous series of azotwin monomer containing oligoxyethylene spacer was designed, which could be directly used as AA type monomer for the synthesis of segmented main chain liquid crystalline azo polyesters.
- 2) Development of novel thermo and photoresponsive ion conductive main chain liquid crystalline azobenzene polyester as a solid polymer electrolyte (SPE) for the lithium ion-batteries.
- 3) Design and synthesis of multifunctional monomers incorporating azobenzene chromophore (i. e. triped and tetrapod) for the synthesis of photoresponsive hyperbranched polymers.

- 4) Synthesis of photoresponsive hyperbranched polymers using ($A_2 + B_3$) and ($A_2 + B_4$) type monomers through melt polycondensation approach.
- 5) A comparative study of the LC phases of the triped and tetraped monomers and HB polymers as to the effect of variation of spacer length in each of these classes of materials as well as effect of branching on the LC characteristics of triped vs tetraped and monomers vs hyperbranched polymers was undertaken.

The current chapter gives a brief introduction to the various properties and systems incorporating azobenzene that are reported in literature. The second chapter deals with the synthesis of two homologous series of azotwin monomers. A series of random azo copolyesters were synthesized via melt polycondensation approach using the azo twin molecules. The control over mesophase fine tuning was achieved by varying spacer length of the azotwin monomers. The melt polycondensation approach was found to be a clean and environment friendly polymerization method for the synthesis of main chain azo polyesters. In the third chapter, alternating main chain azo copolyesters were synthesized using azotwin (AA monomer) and oligoethylene glycol (BB monomer) via melt polycondensation approach. Polymer composites of Li salt were prepared using these LC polymers in which Li^+ was stabilized in the polymer matrixes through an ion-dipole interaction which served as a better solid ion conductive media. The fourth chapter describes the design and synthesis of polymerizable multipod monomers containing azobenzene. All monomers exhibited LC behavior and the effect of branching and spacer length dependence on the LC characteristics of these triped as well as tetraped monomer were explored. The fifth chapter comprises the synthesis of photoresponsive hyperbranched polymers using multifunctional monomer ($A_2 + B_3$ and $A_2 + B_4$ type) through melt polycondensation approach and their detailed structural and thermal characterization. The multipod monomers and HB-polymers exhibited fast reversible isothermal photoswitching from Smectic to Isotropic (S-I) phase upon UV irradiation in the LC phase. Finally, the overall conclusion of the thesis is summarized in chapter six.

1.12 References

- (1) (a) John W. Goodby; Peter J. Collings; Takashi Kato; Carsten Tschierske; Helen Gleeson; Peter Raynes *Handbook of Liquid Crystals*; Wiley, 2014 (b) Chandrasekhar, S. *Rep. Prog. Phys.* **1976**, *39*, 613.
- (2) Chandrasekhar S; Sadashiva B. K.; Suresh K. A. *Pramana* **1977**, *9*, 471-480.
- (3) Kumar, S.; Gupta, S. K. *Tetrahedron Lett.* **2011**, *52*, 5363-5367.
- (4) Andrienko, D.; Marcon, V.; Kremer, K. *J. Chem. Phys.* **2006**, *125*, 124902-124901-124902-124909.
- (5) Sergeyev, S.; Pisula, W.; Geerts, Y. H. *Chem. Soc. Rev.* **2007**, *36*, 1902-1929.
- (6) (a) Ikeda, T. *J. Mater. Chem.* **2003**, *13*, 2037-2057 (b) Collyer, A. A. *Liquid Crystal Polymers: From Structure to Application*; Elsevier: London, 1992 (c) Shibaev, V. P. *Polymers as Electrooptical and Photooptical Active Media*; Springer: Berlin-Heidelberg, 1996 (d) D. Acierno; A. A. Collyer *Rheology and Processing of Liquid Crystal Polymers*; Chapman and Hall: Glasgow, 1996 (e) Yu, H. *Prog. Poly. Sci.* **2014**, *39*, 781-815.
- (7) Finkelmann, H.; Happ, M.; Portugal, M.; Ringsdorf, H. *Makromol. Chem.* **1978**, *179*, 2541-2544.
- (8) (a) Piao, X. L.; Kim, J.-S.; Yun, Y.-K.; Jin, J.-I.; Hong, S.-K. *Macromolecules* **1997**, *30*, 2294-2299 (b) Huang, W.; Han, C. D. *Macromolecules* **2006**, *39*, 4735-4745 (c) Xie, H.-L.; Jie, C.-K.; Yu, Z.-Q.; Liu, X.-B.; Zhang, H.-L.; Shen, Z.; Chen, E.-Q.; Zhou, Q.-F. *J. Am. Chem. Soc.* **2010**, *132*, 8071-8080.
- (9) Shibaev, V.; Bobrovsky, A.; Boiko, N. *Prog. Polym. Sci.* **2003**, *28*, 729-836.
- (10) Talroze, R. V.; Zubarev, E. R.; Kuptsov, S. A.; Merekalov, A. S.; Yuranova, T. I.; Plate, N. A.; Finkelmann, H. *React. Funct. Polym.* **1999**, *41*, 1-11.
- (11) (a) Tian, Y.; Watanabe, K.; Kong, X.; Abe, J.; Iyoda, T. *Macromolecules* **2002**, *35*, 3739-3747 (b) Yu, H.; Naka, Y.; Shishido, A.; Ikeda, T. *Macromolecules* **2008**, *41*, 7959-7966 (c) Osuji, C. O.; Chen, J. T.; Mao, G.; Ober, C. K.; Thomas, E. L. *Polymer* **2000**, *41*, 8897-8907 (d) He, X.; Sun, W.; Yan, D.; Xie, M.; Zhang, Y. *J. Polym. Sci., Part A: Polym. Chem.* **2008**, *46*, 4442-4450.

- (12) Prasad, P.; Mark, J.; Kandil, S.; Kafafi, Z.; Gomes, A.; Pinto, M. c.; Barbosa, C. In *Science and Technology of Polymers and Advanced Materials*; Springer US, 1998.
- (13) Marcos, M.; Martin-Rapun, R.; Omenat, A.; Serrano, J. L. *Chem. Soc. Rev.* **2007**, *36*, 1889-1901.
- (14) Kouwer, P. H. J.; Jager, W. F.; Mijs, W. J.; Picken, S. J. *Macromolecules* **2002**, *35*, 4322-4329.
- (15) Chen, Y.; Shen, Z.; Gehringer, L.; Frey, H.; Stiriba, S.-E. *Macromol. Rapid Commun.* **2006**, *27*, 69-75.
- (16) Hudson, S. A.; Maitlis, P. M. *Chem. Rev.* **1993**, *93*, 861-885.
- (17) (a) Felekis, T.; Tziveleka, L.; Tsiourvas, D.; Paleos, C. M. *Macromolecules* **2005**, *38*, 1705-1710 (b) Korhonen, J. T.; Verho, T.; Rannou, P.; Ikkala, O. *Macromolecules* **2010**, *43*, 1507-1514.
- (18) Jackson, W. J. *Br. Polym. J.* **1980**, *12*, 154-162.
- (19) Lenz, R. W. *Polym. J.* **1985**, *17*, 105-115.
- (20) Blumstein, A.; Coles, H. J.; Simon, R. In *Polymeric Liquid Crystals*; Springer US, 1985; Vol. 28.
- (21) Craig, A. A.; Imrie, C. T. *Macromolecules* **1995**, *28*, 3617-3624.
- (22) Reck, B.; Ringsdorf, H. *Makromol. Chem., Rapid Commun.* **1985**, *6*, 291-299.
- (23) (a) Zhou, M.; Han, C. D. *Macromolecules* **2005**, *38*, 9602-9609 (b) Xie, H.-L.; Wang, S.-J.; Zhong, G.-Q.; Liu, Y.-X.; Zhang, H.-L.; Chen, E.-Q. *Macromolecules* **2011**, *44*, 7600-7609 (c) Joo, S.-H.; Yun, Y.-K.; Jin, J.-I.; Kim, D.-C.; Zin, W.-C. *Macromolecules* **2000**, *33*, 6704-6712 (d) Ruan, J.-J.; Jin, S.; Ge, J. J.; Jeong, K.-U.; Graham, M. J.; Zhang, D.; Harris, F. W.; Lotz, B.; Cheng, S. Z. D. *Polymer* **2006**, *47*, 4182-4193.
- (24) (a) Inoue, T. *Plastics Age* **1995**, *41*, 132-140 (b) Inoue, T.; Yamanaka, T. In *Modern Polyesters: Chemistry and Technology of Polyesters and Copolyesters*; John Wiley & Sons, Ltd, 2004.
- (25) Inoue, T.; Yamanaka, T.; Kurematsu, T.; Nakamura, K. *Mol. Cryst. Liq. Cryst.*

1998, 318, 125-140.

(26) Honkhambe, P. N.; Biyani, M. V.; Bhairamadgi, N. S.; Wadgaonkar, P. P.; Salunkhe, M. M. *J. App. Poly. Sci.* **2010**, 117, 2545-2552.

(27) R. H. El Halabieh; Ozzy Mermut; Barrett, C. J. *Pure Appl. Chem* **2004**, 76, 1445-1465.

(28) Rau, H. *Photoisomerization of azobenzenes: In Rebek J, editor. Photochemistry and photophysics*; CRC Press, P. 119-141, 1990.

(29) Rau, H. *Berichte der Bunsen-Gesellschaft* **1968**, 72, 408-414.

(30) Zhao, Y.; Ikeda, T. *Smart Light-Responsive Materials: Azobenzene-Containing Polymers and Liquid Crystals*; John Wiley & Sons, Inc., Hoboken: New Jersey, 2009.

(31) Kumar, G. S.; Neckers, D. C. *Chem. Rev.* **1989**, 89, 1915-1925.

(32) Zollinger, H. *Azo and Diazo Chemistry, Aliphatic and Aromatic Compounds*; Interscience: New York, 1961.

(33) Rau, H. *J. Photochem.* **1984**, 26, 221-225.

(34) Merino, E.; Ribagorda, M. *Beilstein J. Org. Chem.* **2012**, 8, 1071-1090.

(35) Xie, S.; Natansohn, A.; Rochon, P. *Chem. Mater.* **1993**, 5, 403-411.

(36) (a) Liu, Z. F.; Morigaki, K.; Enomoto, T.; Hashimoto, K.; Fujishima, A. *J. Phy. Chem* **1992**, 96, 1875-1880 (b) Naito, T.; Horie, K.; Mita, I. *Macromolecules* **1991**, 24, 2907-2911 (c) Rau, H.; Lueddecke, E. *J. Am. Chem. Soc.* **1982**, 104, 1616-1620.

(37) Fujino, T.; Arzhantsev, S. Y.; Tahara, T. *J. Phys. Chem. A* **2001**, 105, 8123-8129.

(38) Ho, C.-H.; Yang, K.-N.; Lee, S.-N. *J. Poly. Sci., Part A: Poly. Chem.* **2001**, 39, 2296-2307.

(39) (a) Jursic, B. S. *Chem. Phys. Lett.* **1996**, 261, 13-17 (b) Angeli, C.; Cimiraglia, R.; Hofmann, H.-J. r. *Chem. Phys. Lett.* **1996**, 259, 276-282.

(40) Ikeda, T.; Tsutsumi, O. *Science* **1995**, 268, 1873-1875.

(41) Yu, H. *J. Mater. Chem. C* **2014**, 2, 3047-3054.

(42) Yu, H.; Asaoka, S.; Shishido, A.; Iyoda, T.; Ikeda, T. *Small* **2007**, 3, 768-771.

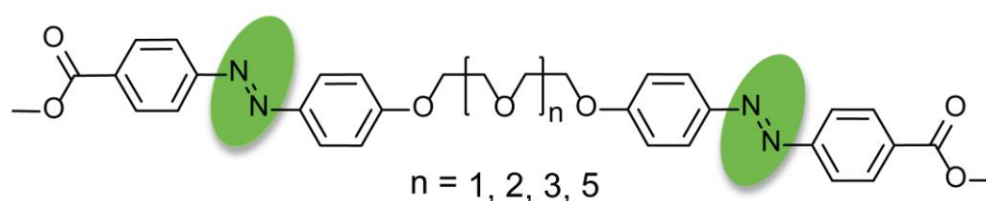
- (43) (a) Yu, H.; Iyoda, T.; Ikeda, T. *J. Am. Chem. Soc.* **2006**, *128*, 11010-11011 (b) Weigert, F. *Naturwissenschaften* **1921**, 583.
- (44) (a) Todorov, T.; Nikolova, L.; Tomova, N. *Appl. Opt.* **1984**, *23*, 4309-4312 (b) Todorov, T.; Nikolova, L.; Tomova, N. *Appl. Opt.* **1984**, *23*, 4588-4591.
- (45) Barrett, C.; Choudhury, B.; Natansohn, A.; Rochon, P. *Macromolecules* **1998**, *31*, 4845-4851.
- (46) (a) Okano, K.; Shishido, A.; Ikeda, T. *Adv. Mater.* **2006**, *18*, 523-527 (b) Okano, K.; Tsutsumi, O.; Shishido, A.; Ikeda, T. *J. Am. Chem. Soc.* **2006**, *128*, 15368-15369.
- (47) Kumar, A.; Srivastava, A.; Galaev, I. Y.; Mattiasson, B. *Prog. Polym. Sci* **2007**, *32*, 1205-1237.
- (48) (a) Li, M.-H.; Keller, P. *Phil. Trans. R. Soc. A* **2006**, *364*, 2763-2777 (b) Harris, K. D.; Cuypers, R.; Scheibe, P.; van Oosten, C. L.; Bastiaansen, C. W. M.; Lub, J.; Broer, D. J. *J. Mater. Chem.* **2005**, *15*, 5043-5048 (c) Wermter, H.; Finkelmann, H. *e-Polymers* **2001**, *013*, 1-13 (d) Li, M. H.; Keller, P.; Li, B.; Wang, X.; Brunet, M. *Adv. Mater.* **2003**, *15*, 569-572.
- (49) Küpfer, J.; Nishikawa, E.; Finkelmann, H. *Poly. Adv. Technol.* **1994**, *5*, 110-115.
- (50) Finkelmann, H.; Kock, H.-J.; Rehage, G. *Makromol.Chem., Rapid Commun.* **1981**, *2*, 317-322.
- (51) Tammer, M.; Li, J.; Komp, A.; Finkelmann, H.; Kremer, F. *Macromol. Chem. Phys.* **2005**, *206*, 709-714.
- (52) (a) Bispo, M.; Guillon, D.; Donnio, B.; Finkelmann, H. *Macromolecules* **2008**, *41*, 3098-3108 (b) Hiraoka, K.; Sagano, W.; Nose, T.; Finkelmann, H. *Macromolecules* **2005**, *38*, 7352-7357 (c) Gebhard, E.; Zentel, R. *Macromol. Chem. Rapid Commun.* **1998**, *19*, 341-344.
- (53) Disch, S.; Finkelmann, H.; Ringsdorf, H.; Schuhmacher, P. *Macromolecules* **1995**, *28*, 2424-2428.
- (54) (a) Cui, L.; Tong, X.; Yan, X.; Liu, G.; Zhao, Y. *Macromolecules* **2004**, *37*, 7097-7104 (b) Li, M. H.; Keller, P.; Yang, J.; Albouy, P. A. *Adv. Mater.* **2004**, *16*, 1922-1925.

- (55) Iqbal, D.; Samiullah, M. *Materials* **2013**, *6*, 116-142.
- (56) Finkelmann, H.; Nishikawa, E.; Pereira, G. G.; Warner, M. *Phys. Rev. Lett.* **2001**, *87*, 015501.
- (57) Hogan, P. M.; Tajbakhsh, A. R.; Terentjev, E. M. *Phys. Rev. E* **2002**, *65*, 041720.
- (58) Ikeda, T.; Nakano, M.; Yu, Y.; Tsutsumi, O.; Kanazawa, A. *Adv. Mater.* **2003**, *15*, 201-205.
- (59) Yu, Y.; Nakano, M.; Ikeda, T. *Nature* **2003**, *425*, 145-145.
- (60) Zhang, J.; Sponsler, M. B. *J. Am. Chem. Soc.* **1992**, *114*, 1506-1507.
- (61) Yoneyama, S.; Yamamoto, T.; Tsutsumi, O.; Kanazawa, A.; Shiono, T.; Ikeda, T. *Macromolecules* **2002**, *35*, 8751-8758.
- (62) Tong, X.; Wang, G.; Yavrian, A.; Galstian, T.; Zhao, Y. *Adv. Mater.* **2005**, *17*, 370-374.
- (63) (a) Matharu, A. S.; Jeeva, S.; Ramanujam, P. S. *Chem. Soc. Rev.* **2007**, *36*, 1868-1880 (b) Bruder, F.-K.; Hagen, R.; Rölle, T.; Weiser, M.-S.; Fäcke, T. *Angew. Chem. Int. Ed.* **2011**, *50*, 4552-4573 (c) Hvilsted, S.; Sanchez, C.; Alcalá, R. *J. Mater. Chem.* **2009**, *19*, 6641-6648.
- (64) (a) Cumpston, B. H.; Ananthavel, S. P.; Barlow, S.; Dyer, D. L.; Ehrlich, J. E.; Erskine, L. L.; Heikal, A. A.; Kuebler, S. M.; Lee, I. Y. S.; McCord-Maughon, D.; Qin, J.; Rockel, H.; Rumi, M.; Wu, X.-L.; Marder, S. R.; Perry, J. W. *Nature* **1999**, *398*, 51-54 (b) Strickler, J. H.; Webb, W. W. *Opt. Lett.* **1991**, *16*, 1780-1782.
- (65) (a) Shishido, A. *Polym. J.* **2010**, *42*, 525-533 (b) Häckel, M.; Kador, L.; Kropp, D.; Frenz, C.; Schmidt, H. W. *Adv. Func. Mater.* **2005**, *15*, 1722-1727.
- (66) (a) Eich, M.; Wendorff, J. H.; Reck, B.; Ringsdorf, H. *Makromol. Chem., Rapid Commun.* **1987**, *8*, 59-63 (b) Rasmussen, P. H.; Ramanujam, P. S.; Hvilsted, S. r.; Berg, R. H. *J. Am. Chem. Soc.* **1999**, *121*, 4738-4743 (c) Berg, R. H.; Hvilsted, S.; Ramanujam, P. S. *Nature* **1996**, *383*, 505-508.
- (67) Boyd, J. E.; Trentler, T. J.; Wahi, R. K.; Vega-Cantu, Y. I.; Colvin, V. L. *Appl. Opt.* **2000**, *39*, 2353-2358.

- (68) Eich, M.; Wendorff, J. H. *Makromol. Chem. Rapid Commun.* **1987**, *8*, 467-471.
- (69) (a) Anderle, K.; Birenheide, R.; Eich, M.; Wendorff, J. H. *Makromol. Chem., Rapid Commun.* **1989**, *10*, 477-483 (b) Eich, M.; Wendorff, J. *J. Opt. Soc. Am. B* **1990**, *7*, 1428-1436.
- (70) Bieringer, T.; Wuttke, R.; Haarer, D.; Geßner, U.; Rübner, J. *Macromol. Chem. Phys.* **1995**, *196*, 1375-1390.
- (71) Hagen, R.; Bieringer, T. *Adv. Mater.* **2001**, *13*, 1805-1810.
- (72) Ishiguro, M.; Sato, D.; Shishido, A.; Ikeda, T. *Langmuir* **2006**, *23*, 332-338.
- (73) Joseph D. Menczel; Prime, R. B. *Thermal Analysis of Polymers, Fundamentals and Applications*; Wiley, 2009.
- (74) Dierking, I. In *Textures of Liquid Crystals*; Wiley-VCH Verlag GmbH & Co. KGaA, 2004.
- (75) Seddon, J. M.; Demus, D.; Goodby, J.; Gray, G. W.; Spiess, H. W.; Vill, V. In *Handbook of Liquid Crystals Set*; Wiley-VCH Verlag GmbH, 2008.
- (76) (a) Chen, B.-K.; Tsay, S.-Y.; Chen, J.-Y. *Polymer* **2005**, *46*, 8624-8633 (b) Chen, L.; Ruan, C.; Yang, R.; Wang, Y.-Z. *Polym. Chem.* **2014**, *5*, 3737-3749.

Chapter 2

Twin Liquid Crystals and Segmented Thermotropic Polyesters containing Azobenzene - Effect of Spacer length on LC Properties



*In this chapter we present systematic studies on two homologous series of twin liquid crystalline (LC) molecules based on phenyl and naphthyl azobenzene (**PnP** and **NpnNp**) as well as segmented copolyesters based on them. The twin series had the structure azobenzene- oligoethoxyethylene - azobenzene where the ethyleneoxy length was varied from 2 to 6 units. The LC properties of the twin series depended on the chemical structure of the azo chromophore and also the length of the central oligoethoxyethylene segment. The **PnP** series exhibited smectic LC properties for $n > three$ oligoethoxyethylene units. On the other hand, **NpnNp** series exhibited spherulitic phases only for the shortest member **-Np2Np**. One non- LC short spacer twin (**P2P**) and one LC long spacer twin (**P6P**) were incorporated as part of a main chain polyester composed of fully aliphatic segments of sebacate and di or tetraethylene glycol (DEG/TEG) units by melt polycondensation. Non-LC **P2P** formed LC polymers even at low (5 mol %) incorporation in DEG based copolymers, whereas the LC-**P6P** could do so only at 30 mol % incorporation. The LC properties of the twin molecules as well as copolymers were studied using DSC, polarized light microscopy (PLM) along with variable temperature wide angle X-ray diffraction (VT-WXRD).*

2.1 Introduction

Azobenzene is a very attractive chromophore since it serves the dual role of mesogen as well as photoresponsive chromophore. The reversible and rapid trans to cis photoisomerization exerts a great impact on the properties of materials incorporating azobenzene, due to which it finds application in a variety of areas such as optical display,¹ optical data storage,² optical shutters,³ molecular switches,⁴ photocontrollable coatings,⁵ tunable diffraction gratings⁶ etc. Main chain polymers have unique combinations of thermoplastic nature as well as liquid crystalline properties. In general, main chain polymers are mostly synthesized by condensation polymerization which can be synthesized by melt condensation or solution route.⁷ Most of the reported azo main chain polymers have been synthesized by solution polymerization route mainly because of its low degradation temperatures which prohibited a melt condensation route. The melt polycondensation route has certain advantages like, it is devoid of solvent and also helps build molecular weight. However, it is applicable to monomers having low melting temperature (< 150 °C). Therefore, there is a need of versatile design of azo monomers having reasonably low melting temperature (< 200 °C), which could be directly used in melt polycondensation.

Twin molecules having the structure mesogen-spacer-mesogen or spacer-mesogen-spacer have long been considered as ideal representatives for “segmented main chain liquid crystal polymers” [-(flexible segment-rigid cores)_n]-.⁸ Although started out as model systems to understand the behavior of main chain liquid crystalline polymers, it was soon evident that these twin liquid crystals were interesting systems on their own. A vast majority of the studies comparing homologous twin systems and the related main chain polymers dealt with polymethylene chains as the flexible units.^{8a,9} The reason for this being the interesting “odd-even” oscillation observed in the isotropization temperatures and entropies as a function of the even or odd parity of the number of atoms in the methylene spacer length (Figure 2.1).¹⁰ On the other hand the poly(oxyethylene) units preferred a “gauche” conformation and the twins with poly(oxyethylene) central spacer generally did not show odd-even oscillation of the isotropic-LC transition entropy. In the design of our azobenzene twin molecules, the choice of oligooxyethylene as the central

spacer was very important since it served two purposes, firstly it reduced the melting transition of the resulting twin molecules so that melt polycondensation route could be adopted and secondly, it improved their solubility considerably.

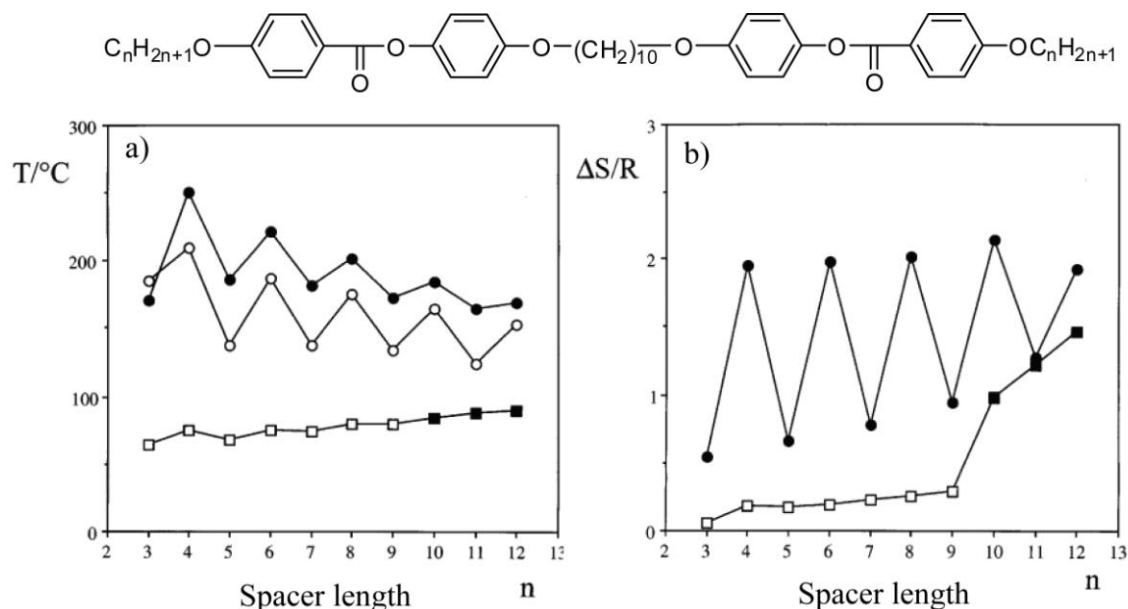


Figure 2.1 a) The dependence of the melting points (○) and nematic to isotropic transition (●) and b) entropy change associated with the nematic to isotropic transition (●) on the number of methylene unit in flexible spacer (n) for the α, ω bis(4,4'-cyanobiphenyloxy)alkanes.^{10b}

Another important feature was that the polar oligooxyethylene spacer units are usually incompatible with the rigid rod-like azobenzene mesogen resulting in segregation into separate domains leading to mesophase formation. Very few reports are available for azo based twin systems where the central spacer segment was based on oligooxyethylene $-(CH_2CH_2O)_n$.¹¹

Copolymerization is a versatile means to fine-tune the mesophase stability and sometimes the nature of the mesophase also. Segmented main chain copolymers can be synthesized starting from two premesogenic comonomers or one mesogenic and one non-mesogenic monomer. In this chapter, we describe the design and synthesis of two homologous series of twin azobenzene molecules having the structure azobenzene-oligooxyethylene-azobenzene where the ethyleneoxy length was varied from 2 to 6 units. The twin azobenzene molecules were incorporated in varying mole

ratios in a main chain polyester based on dimethyl sebacate and di or tetra ethylene glycol (DEG/TEG). This choice of the polyester scaffold for introducing the azobenzene moieties was also interesting as DEG and sebacate formed a semicrystalline polyester whereas TEG and sebacate resulted in a completely amorphous polymer. The issues that we addressed in this systematic study were the following (i) the effect of spacer length on the liquid crystalline properties of the two twin series (ii) the effect of the chromophore – phenylazo vs naphthylazo on the liquid crystalline properties of twin molecules having the same spacer length and (iii) the effect of copolymerization of mesogenic and non-mesogenic twin molecules with non-mesogenic co monomers. The detailed mesophase behavior of the twin molecules and copolyesters were investigated by differential scanning calorimetry (DSC), polarizing light microscopy (PLM) in combination with variable temperature wide angle X-ray diffraction studies (VT-WXRD).

2.2 Experimental

2.2.1 Materials

Di, tri, tetra and hexa ethylene glycol, dimethyl sebacate (DMS), titaniumtetrabutoxide ($\text{Ti}(\text{OBu})_4$), p-toulene sulphonyl chloride and α -naphthol were purchased from Aldrich Company Ltd. and were used as such. P-amino benzoic acid, phenol, sodium nitrite, potassium carbonate and potassium iodide were purchased from Merck Chemicals Ltd. Dimethyl formamide (DMF), chloroform (CHCl_3), tetrahydrofuran (THF), methanol and ethanol were purchased from Merck Chemicals Ltd. and were purified using standard procedures.¹²

2.2.2 Instrumentation

^1H and ^{13}C -NMR spectra were recorded on a Bruker-AVANCE 200 MHz spectrometer. Chemical shifts are reported in ppm at 25 °C using CDCl_3 or CDCl_3/TFA as solvent containing small amount of tetramethylsilane (TMS) as internal standard. The purity of the compounds was determined by elemental analysis as well as HRMS/MALDI-TOF in combination with size exclusion chromatography (SEC). Elemental analysis was done by ThermoFinnigan flash EA 1112 series CHNS analyser. The HRMS mass spectral analysis was done with HRMS-MSI (Auto concept) UK in EI mode. The MALDI-TOF analysis was done on Voyager-De-STR

MALDI-TOF (Applied Biosystems, Framingham, MA, USA) equipped with 337-nm pulsed nitrogen laser used for desorption and ionization. 1 μ M solution of sample was premixed with DHB (2,5 dihydroxy benzoic acid) matrix in CHCl_3 and mixed well before spotting on 96-well stainless steel MALDI plate by dried droplet method for MALDI analysis. For small molecules SEC was performed using polystyrene standards for the calibration in CHCl_3 as eluent. The flow rate of CHCl_3 was maintained as 1 μ L/min throughout the experiments and the sample solutions at concentrations 3-4 mg/mL were filtered through syringe filter and injected for recording the chromatograms at 30 $^\circ\text{C}$. The molecular weights of the polymers were determined by Gel Permeation Chromatography (GPC), which was performed using a Viscotek VE 1122 pump, Viscotek VE 3580 RI detector and Viscotek VE 3210 UV/vis detector in tetrahydrofuran (THF) using polystyrene as standards. Infrared spectra were recorded using Bruker FT-IR (ATR mode) spectrophotometer in the range of 4000-600 cm^{-1} . UV-Vis spectra were recorded using a Perkin Elmer Lambda-35 UV-Vis spectrometer. The thermal stability of all the model compounds and azo copolyesters were analyzed using PerkinElmer: STA 6000 thermogravimetric analyser (TGA) under nitrogen atmosphere from 40-800 $^\circ\text{C}$ at 10 $^\circ\text{C}$ /min. Differential Scanning Calorimetry (DSC) was performed using a TA Q10 model. About 2–3 mg of the samples were taken in aluminium pan, sealed and scanned at 10 $^\circ\text{C}$ /min. The instrument was calibrated with indium standards before measurements. The phase behaviour of the molecules were analyzed using LIECA DM2500P polarized optical microscope equipped with Linkam TMS 94 heating and cooling stage connected to a Linkam TMS 600 temperature programmer. The Transition from isotropic to liquid crystalline phase was monitored by the evolution of characteristic textures. WXRd was recorded by a Philips analytical diffractometer using Cu $K\alpha$ emission and the spectra were recorded in the range of (2θ) 3–50 $^\circ$ and analyzed using X'pert software. Powder X-ray diffraction of all the samples were carried out in a PANalytical X'pert Pro dual goniometer diffractometer. An X'celerator solid-state detector was employed in wide-angle experiments. The radiation used was Cu $K\alpha$ (1.54 A°) with a Ni filter and the data collection was carried out using a flat holder in Bragg-Brentano geometry. Care was taken to avoid sample displacement effects.

Variable temperature in-situ XRD experiments were carried out in an Anton-Paar XRK900 reactor.

2.2.3 Synthesis and Characterization

Synthesis of oligoethyleneoxy ditosylate

Diethylene glycol ditosylate: Diethylene glycol (2 g, 18.86 mmol), NaOH (1.89 g, 47.35 mmol), 10 mL water and 10 mL THF were taken in RB flask and cooled to 0 °C with magnetic stirring. p-toulene sulphonyl chloride (8.99 g, 47.35 mmol) dissolved in 10 mL THF was added dropwise to the above mixture maintaining the temperature at 0 °C. The solution was stirred at same temperature for 3 h and poured in to ice cold water. The solid white precipitate obtained was filtered, washed with water, and followed by hexane wash to remove excess of p-toulene sulphonyl chloride. The crude product was purified by column chromatography using hexane-ethyl acetate (v/v 65/35) mixture. Yield = 3.9 g (51 %) ¹H NMR (200 MHz CDCl₃): δ (ppm): 7.77 (4H, d, Ar), 7.32 (4H, d, Ar), 4.08 (4H, t, -SO₂-O-CH₂-CH₂-), 3.59 (4H, t, -O-CH₂-CH₂-), 2.43 (6H, s, H₃C-C₆H₄-). ¹³C NMR (CDCl₃) δ ppm: 21.59, 68.66, 68.96, 127.87, 129.85, 132.73, 144.93. FTIR (KBr) (cm⁻¹): 3564, 2925, 1925, 1738, 1495, 1453, 1359, 1246, 1175, 1137, 1096, 1019, 926, 817, 776, 665, 582, 555. HRMS m+1: 415.02.

Triethylene glycol ditosylate: Triethylene glycol ditosylate was prepared by using triethylene glycol (5 g, 20.0 mmol) and p-toulene sulphonyl chloride (7.03 g, 37 mmol). The crude oily product was purified by column chromatography using hexane-ethyl acetate (v/v 55/45) mixture. Yield = 7.0 g (77 %) ¹H NMR (200 MHz CDCl₃): δ (ppm): 7.78 (4H, d, Ar), 7.33 (4H, d, Ar), 4.12 (4H, t, -SO₂-O-CH₂-CH₂-), 3.65 (4H, t, -O-CH₂-CH₂-), 3.51 (4H, m, -OCH₂-CH₂O-CH₂-), 2.43 (6H, s, H₃C-C₆H₄-). ¹³C NMR (CDCl₃) δ ppm: 21.59, 68.67, 69.17, 70.62, 127.90, 129.81, 132.85, 144.84. FTIR (KBr) (cm⁻¹): 3564, 2925, 1925, 1738, 1495, 1453, 1359, 1246, 1175, 1137, 1096, 1019, 926, 817, 776, 665, 582, 555. HRMS m+1: 459.62.

Tetraethylene glycol ditosylate: Tetraethylene glycol ditosylate was prepared by using tetraethylene glycol (10 g, 51.54 mmol) and p-toulene sulphonyl chloride (24.48 g, 128.84 mmol). The crude oily product was purified by column chromatography

using hexane-ethyl acetate (v/v 40/60) mixture. Yield = 20.0 g (77 %) ^1H NMR (200 MHz CDCl_3): δ (ppm): 7.77 (4H, d, Ar), 7.32 (4H, d, Ar), 4.13 (4H, t, $-\text{SO}_2\text{-O-CH}_2\text{-CH}_2\text{-}$), 3.66 (4H, t, $-\text{O-CH}_2\text{-CH}_2\text{-}$), 3.54 (8H, m, $-\text{OCH}_2\text{-CH}_2\text{O-CH}_2\text{-}$), 2.42 (6H, s, $\text{H}_3\text{C-C}_6\text{H}_4\text{-}$). ^{13}C NMR (CDCl_3) δ ppm: 21.55, 61.61, 68.59, 69.18, 70.34, 70.54, 70.62, 70.62, 72.42, 127.89, 129.76, 132.84, 144.77. FTIR (KBr) (cm^{-1}): 3564, 2925, 1925, 1738, 1495, 1453, 1359, 1246, 1175, 1137, 1096, 1019, 926, 817, 776, 665, 582, 555. HRMS $m+1$: 502.31.

Hexaethylene glycol ditosylate : Hexaethylene glycol ditosylate was prepared by using hexaethylene glycol (3 g, 10.63 mmol) and p-toulene sulphonyl chloride (5.04 g, 26.52 mmol). The crude oily product was purified by column chromatography using hexane-ethyl acetate (v/v 10/90 up to 100 % ethyl acetate) mixture. Yield = 5 g (80 %) ^1H NMR (200 MHz CDCl_3): δ (ppm): 7.76 (4H, d, Ar), 7.32 (4H, d, Ar), 4.13 (4H, t, $-\text{SO}_2\text{-O-CH}_2\text{-CH}_2\text{-}$), 3.66 (4H, m, $-\text{OCH}_2\text{-CH}_2\text{O-CH}_2\text{-}$), 3.60 (8H, m, $-\text{OCH}_2\text{-CH}_2\text{O-CH}_2\text{-}$), 3.56 (8H, m, $-\text{OCH}_2\text{-CH}_2\text{O-CH}_2\text{-}$), 2.42 (6H, s, $\text{H}_3\text{C-C}_6\text{H}_4\text{-}$). ^{13}C NMR (CDCl_3) δ ppm: 21.52, 68.52, 69.17, 70.39, 70.58, 127.84, 129.73, 132.82, 144.72. FTIR (KBr) (cm^{-1}): 3564, 2925, 1925, 1738, 1495, 1453, 1359, 1246, 1175, 1137, 1096, 1019, 926, 817, 776, 665, 582, 555. HRMS $m+1$: 520.06.

Synthesis of Azo dye

Synthesis of 4-(4'-hydroxy-phenylazo)-benzoic acid methyl ester:

4-Amino methyl benzoate (14 g, 92.7 mmol) was dissolved in 10 % HCl (200 mL) and diazotized with aqueous sodium nitrite (7.67 g, 111.2 mmol) at 0 °C with stirring. The solution was further diluted with 400 mL cold water. Separately phenol (8.7 g, 92.7 mmol) was dissolved in 10 mL aqueous KOH (9.9 g, 176.1 mmol), which was added dropwise to the diazonium salt. After complete addition, the reaction mixture was stirred for additional 30 minutes and the orange colored precipitate was neutralized with KOH. The precipitate was filtered, thoroughly washed with water and dried in vacuum oven. The crude product was recrystallized from ethanol/water (80/20 v/v).

Yield = 9.1 g (38 %). mp = 223 °C. ^1H NMR (400 MHz CDCl_3 + few drops of DMSO- d_6): δ (ppm): 9.52 (s, 1 H, Ar-OH), 7.85 (d, 2 H, Ar) 7.55 - 7.60 (m, 4 H, Ar), 6.68 (d, 2 H, Ar), 3.65 (s, 3 H, $-\text{C}(\text{O})\text{OCH}_3$). FTIR (KBr) (cm^{-1}): 3357, 2923, 2854,

1688, 1588, 1498, 1462, 1428, 1398, 1268, 1219, 1188, 1106, 1002, 947, 846, 771, 725, 690. HRMS m: 256.08. HRMS m+1: 279.11. Elemental analysis calculated for $C_{14}H_{12}N_2O_3$: C, 65.62; H, 4.72; N, 10.93. Found: C, 65.32; H, 4.55; N, 10.97.

Synthesis of 4-(4'-hydroxy-naphthylazo)-benzoic acid methyl ester:

4-Amino methyl benzoate (2.0 g, 13.2 mmol) was dissolved in 10 % HCl (50 mL) and diazotized with aqueous sodium nitrite (0.91 g, 13.2 mmol in 5 mL H_2O) at 0 °C with stirring. The solution was further diluted with 100 mL cold water. Separately 1-naphthol (1.90 g, 13.2 mmol) was dissolved in aqueous 5 mL KOH (1.0 g, 25.4 mmol), which was added dropwise to the diazonium salt at 0-5 °C. After complete addition, the reaction mixture was stirred for additional 3 h. The dark brown colored precipitate was neutralized with KOH. The precipitate was filtered, thoroughly washed with water and dried in vacuum oven. The crude product was further purified by column chromatography in pet-ether/ethyl acetate (60/40 v/v).

Yield = 2.8 g (69 %). mp = 192 °C. 1H NMR (200 MHz DMSO- d_6): δ (ppm): 8.94 (d, 1 H, Ar) 7.91 - 8.36 (m, 5 H, Ar) 7.50 - 7.88 (m, 2 H, Ar) 7.20 (d, 1 H, Ar), 4.10 (s, 3 H, $-C(O)OCH_3$). FTIR (KBr) (cm^{-1}): 3428, 2928, 2848, 1681, 1576, 1508, 1466, 1428, 1395, 1286, 1247, 1191, 1140, 1095, 1019, 976, 937, 865, 817, 759, 696. HRMS m: 306.12. HRMS m+1: 307.12. Elemental analysis calculated for $C_{18}H_{14}N_2O_3$: C, 70.58; H, 4.61; N, 9.15. Found: C, 70.77; H, 4.40; N, 8.83.

Synthesis of azo model compounds

Synthesis of 4-(4'-methoxy-phenylazo)-benzoic acid methyl ester (P0):

4-(4'-hydroxy-phenylazo)-benzoic acid (1 g, 4 mmol), 0.5 mL sulphuric acid and 20 mL dry methanol were refluxed overnight. The reaction mixture was then poured into cold water, neutralized with base and the precipitate was filtered, washed with water and dried. The crude product was purified by column chromatography using hexane-ethyl acetate (v/v 95/5) mixture.

Yield = 0.9 g (86 %). mp = 169 °C. 1H NMR (200 MHz $CDCl_3$): δ (ppm): 8.18 (2H, d, Ar), 7.92 (4H, m, Ar), 7.02 (2H, d, Ar), 3.94 (3H, s, $-C(O)OCH_3$), 3.90 (3H, s, OCH_3). ^{13}C NMR ($CDCl_3$) δ ppm: 52.10, 55.57, 114.37, 122.34, 125.16, 130.55, 131.30, 147.19, 155.49, 162.76, 166.57. FTIR (KBr) (cm^{-1}): 3004, 2949, 2842, 1718, 1602, 1583, 1499, 1434, 1313, 1281, 1282, 1153, 1106, 1024, 959, 866, 840, 776,

698, 556. HRMS *m*: 270.29. HRMS *m*+1: 271.15. Elemental analysis calculated for C₁₅H₁₄N₂O₃: C, 66.66; H, 5.22; N, 10.36. Found: C, 66.32; H, 5.18; N, 9.97.

Synthesis of 4-(4'-methoxy-naphthalen-1-ylazo)-benzoic acid methyl ester (Np0)

A similar procedure as above was adopted using 4-(4'-hydroxy-naphthalen-1-ylazo)-benzoic acid. The crude product was purified by column chromatography using hexane-ethyl acetate (v/v 95/5) mixture.

Yield = 1 g (90 %). mp = 141 °C. ¹H NMR (200 MHz CDCl₃): δ (ppm): 8.99 (1H, d, Ar), 8.34 (1H, d, Ar), 8.23 (2H, m, Ar), 8.00 (3H, m, Ar), 7.72 (1H, d, Ar), 7.62 (1H, d, Ar), 6.93 (1H, d, Ar), 4.11 (3H, s, -C(O)OCH₃), 3.97 (3H, s, OCH₃) ¹³C NMR (CDCl₃) δ ppm: 52.28, 55.93, 103.78, 113.74, 122.17, 122.58, 123.02, 125.54, 125.88, 127.87, 130.61, 131.18, 132.88, 141.57, 155.59, 159.34, 166.65. FTIR (KBr) (cm⁻¹): 3053, 2953, 2843, 1717, 1602, 1579, 1468, 1433, 1392, 1247, 1192, 1095, 1014, 955, 922, 870, 815, 758. HRMS *m*: 320.12. Elemental analysis calculated for C₁₉H₁₆N₂O₃: C, 71.24; H, 5.03; N, 8.74. Found: C, 71.45; H, 5.16; N, 8.35.

Synthesis of phenyl azotwin chromophores

α,ω-bis(4-diethyleneoxyphenyl-4'-azophenyl)methylbenzoate (P2P)

4-(4-Hydroxy-phenyl-1-ylazo)benzoic acid methyl ester (0.3 g, 1.17 mmol), diethylene glycol ditosylate (0.4 g, 0.97 mmol), anhydrous potassium carbonate (0.29 g, 0.58 mmol), and catalytic amount of KI were dissolved in 10 mL of dry DMF. The mixture was stirred at 80 °C for 48 h under nitrogen. The resulting solution was cooled to room temperature, poured into water. The product was filtered, washed with water and dried.

Yield = 0.46 g (35 %) mp = 215 °C. ¹H NMR (200 MHz CDCl₃ + TFA): δ (ppm): 8.17 (4H, d, Ar), 7.95 (8H, m, Ar), 7.08 (4H, d, Ar), 4.35 (4H, t, -OCH₂-CH₂O), 4.10 (4H, m, -OCH₂-CH₂O-CH₂-), 3.99 (6H, s, -C(O)OCH₃). FTIR (KBr) (cm⁻¹): 3047, 2920, 2875, 1723, 1602, 1583, 1497, 1434, 1282, 1251, 1143, 1107, 1040, 1010, 928, 866, 840, 774, 697, 555. MALDI-TOF *m*+1: 582.

α,ω-bis(4-triethyleneoxyphenyl-4'-azophenyl)methylbenzoate (P3P) was synthesized using 4-(4-Hydroxy-phenyl-1-ylazo)benzoic acid methyl ester (0.5 g, 1.94 mmol) and triethylene glycol ditosylate (0.44 g, 0.97 mmol) under identical

conditions. The crude product was purified by column chromatography using CHCl₃-methanol (v/v 97/3) mixture.

Yield = 0.650 g (53 %) mp = 173 °C. ¹H NMR (200 MHz CDCl₃): δ (ppm): 8.17 (4H, d, Ar), 7.89 (8H, m, Ar), 7.01 (4H, d, Ar), 4.20 (4H, t, -OCH₂-CH₂O), 3.94 (6H, s, -C(O)OCH₃), 3.90 (4H, m, -OCH₂-CH₂O-CH₂-), 3.76 (4H, m, -OCH₂-CH₂O-CH₂-). ¹³C NMR (CDCl₃) δ ppm: 52.25, 67.74, 69.66, 70.94, 114.89, 122.35, 125.12, 130.55, 131.17, 147.04, 155.29, 161.83, 166.60. FTIR (KBr) (cm⁻¹): 3057, 2925, 2885, 1724, 1602, 1499, 1440, 1404, 1283, 1257, 1144, 1109, 1011, 923, 866, 841, 775, 697, 552. MALDI-TOF m+Na: 649. Elemental analysis calculated for C₃₄H₃₄N₄O₈: C, 65.17; H, 5.47; N, 8.94. Found: C, 64.71; H, 5.69; N, 9.23.

α,ω-bis(4-diethyleneoxyphenyl-4'-azophenyl)methylbenzoate (P4P) 4-(4-Hydroxy-phenyl-1-ylazo)benzoic acid methyl ester (0.3 g, 1.17 mmol), tetra ethylene glycol ditosylate (0.4 g, 0.97 mmol), anhydrous potassium carbonate (0.29 g, 0.58 mmol), a catalytic amount of KI were dissolved in 10 mL of dry DMF. The mixture was stirred at 80 °C for 48 h. under nitrogen. The resulting solution was cooled to room temperature, poured into water. The product was filtered, washed with water and dried. The crude product was purified by column chromatography using CHCl₃-methanol (v/v 96/4) mixture.

Yield = 0.265 g (34 %). mp = 140 °C. ¹H NMR (200 MHz CDCl₃): δ (ppm): 8.17 (4H, d, Ar), 7.89 (8H, m, Ar), 7.01 (4H, d, Ar), 4.20 (4H, t, -OCH₂-CH₂O), , 3.94 (6H, s, -C(O)OCH₃), 3.90 (4H, m, -OCH₂-CH₂O-CH₂-), 3.76 (4H, m, -OCH₂-CH₂O-CH₂-). ¹³C NMR (CDCl₃) δ ppm: 52.27, 67.74, 69.57, 70.67, 70.86, 114.86, 122.34, 125.12, 130.55, 131.14, 147.00, 155.26, 161.82, 166.60. FTIR (KBr) (cm⁻¹): 3017, 2932, 2866, 1721, 1602, 1499, 1437, 1407, 1285, 1257, 1191, 1145, 1108, 1060, 957, 867, 840, 774, 697, 553. MALDI-TOF m+Na: 693. Elemental analysis calculated for C₃₆H₃₈N₄O₉: C, 64.47; H, 5.71; N, 8.35; Found C, 64.61; H, 5.82; N, 8.82.

α,ω-bis(4-hexaethyleneoxyphenyl-4'-azophenyl)methylbenzoate (P6P) was synthesized using 4-(4-Hydroxy -phenyl-1-ylazo)benzoic acid methyl ester (0.4 g, 1.56 mmol), and hexaethylene glycol ditosylate (0.46 g, 0.78 mmol) under identical conditions. The crude product was purified by column chromatography using CHCl₃-methanol (v/v 95/5) mixture.

Yield = 0.400 g (51 %) mp = 119 °C. ¹H NMR (200 MHz CDCl₃): δ (ppm): 8.17 (4H, d, Ar), 7.89 (8H, m, Ar), 7.01 (4H, d, Ar), 4.20 (4H, t, -OCH₂-CH₂O), 3.94 (6H, s, -C(O)OCH₃), 3.90 (4H, m, -OCH₂-CH₂O-CH₂-), 3.76 (4H, m, -OCH₂-CH₂O-CH₂-). ¹³C NMR (CDCl₃) δ ppm: 52.25, 67.75, 69.55, 70.62, 70.88, 114.89, 122.33, 125.12, 130.56, 131.16, 147.00, 155.26, 161.85, 166.60. FTIR (KBr) (cm⁻¹): 3010, 2930, 2872, 1723, 1602, 1499, 1437, 1284, 1256, 1145, 1107, 1058, 957, 866, 839, 775, 697, 553. MALDI-TOF (m+1): 758. Elemental analysis calculated for C₄₀H₄₆N₄O₁₁: C, 63.31; H, 6.11; N, 7.38; Found C, 62.71; H, 5.98; N, 7.07.

Synthesis of naphthyl azotwinchromophores

Synthesis of α,ω -bis(4-diethyleneoxynaphthyl-4'-azophenyl)methylbenzoate (Np2Np): 4-(4-Hydroxy-naphthalen-1-ylazo) benzoic acid methyl ester (1 g, 3.26 mmol), anhydrous potassium carbonate (0.566 g, 4.10 mmol), catalytic amount of KI and diethylene glycol ditosylate (0.674 g, 1.62 mmol) were dissolved in 15 mL dry DMF. The mixture was refluxed at 80 °C for 48 h under nitrogen. The resulting solution was cooled to room temperature and poured into water. The product was filtered, washed with water, dried and purified by column chromatography using hexane-ethyl acetate mixture (v/v 70/30).

Yield = 0.700 g (31.53%) mp = 190 °C. ¹H NMR (200 MHz CDCl₃): δ (ppm): 8.93 (2H, d, Ar), 8.34 (2H, d, Ar), 8.19 (4H, d, Ar), 8.02 (6H, m, Ar), 7.66 (2H, t, Ar), 7.50 (2H, t, Ar), 6.90 (2H, d, Ar), 4.55 (4H, t, -OCH₂-CH₂O), 4.09 (6H, s, -C(O)OCH₃), 3.77 (4H, m, -OCH₂-CH₂O-CH₂-). ¹³C NMR (CDCl₃) δ ppm: 52.25, 68.11, 69.58, 70.81, 71.00, 104.57, 113.34, 122.59, 125.85, 127.74, 130.57, 131.02, 132.84, 141.68, 155.73, 158.22, 166.63. FTIR (KBr) (cm⁻¹): 3048, 2948, 2881, 1719, 1602, 1579, 1393, 1323, 1276, 1244, 1141, 1095, 961, 814, 763. MALDI-TOF m+1: 683.91. Elemental analysis calculated for C₄₀H₃₄N₄O₇: C, 70.37; H, 5.02; N, 8.21; Found C, 70.83; H, 4.75; N, 8.71.

α,ω -bis(4-tetraethyleneoxynaphthyl-4'-azophenyl)methylbenzoate (Np4Np) was synthesized using 4-(4-Hydroxy-naphthalen-1-ylazo) benzoic acid methyl ester (1 g,

3.26 mmol), and tetra ethylene glycol ditosylate (0.818 g, 1.62 mmol) under identical conditions.

Np4Np: Yield = 0.300g (12 %) mp = 139 °C. ¹H NMR (200 MHz CDCl₃): δ (ppm): 8.91 (2H, d, Ar), 8.31 (2H, d, Ar), 8.17 (4H, d, Ar), 7.91 (6H, m, Ar), 7.58 (4H, m, Ar), 6.80(2H, d, Ar), 4.30 (4H, t, -OCH₂-CH₂O), 3.95 (6H, s, -C(O)OCH₃), 4.01-3.70 (20H, m, -OCH₂-CH₂O, OCH₂-CH₂O-CH₂-). ¹³C NMR (CDCl₃) δ ppm: 52.25, 68.11, 69.58, 70.80, 71.00, 104.57, 113.34, 122.59, 125.85, 127.74, 130.56, 131.02, 132.83, 141.68, 155.72, 158.22, 166.63. FTIR (KBr) (cm⁻¹): 3047, 2944, 2871, 723, 1579, 1510, 1437, 1396, 1326, 1282, 1243, 1135, 1099, 1014, 949, 869, 761. MALDI-TOF m+1: 771.4. Elemental analysis calculated for C₃₆H₃₈N₄O₉: C, 68.56; H, 5.49; N, 7.27; Found C, 68.13; H, 5.75; N, 7.20.

α,ω-bis(4-hexaethyleneoxynaphthyl-4'-azophenyl)methylbenzoate (Np6Np) was synthesized using 4-(4-Hydroxy-naphthalen-1-ylazo) benzoic acid methyl ester (1 g, 3.26 mmol) and hexa ethylene glycol ditosylate (0.962 g, 1.63 mmol) under identical conditions.

Np6Np: Yield = 0.400 g (14.2 %) mp = 67 °C. ¹H NMR (200 MHz CDCl₃): δ (ppm): 8.91 (2H, d, Ar), 8.27 (2H, d, Ar), 8.17 (4H, d, Ar), 7.97 (6H, m, Ar), 7.63 (2H, t, Ar), 7.55 (2H, t, Ar), 6.87 (2H, d, Ar), 4.46 (4H, t, -OCH₂-CH₂O), 3.90 (6H, s, -C(O)OCH₃), 3.66-3.57 (20H, m, -OCH₂-CH₂O, OCH₂-CH₂O-CH₂-). ¹³C NMR (CDCl₃) δ ppm: 52.24, 68.12, 69.54, 70.54, 70.97, 104.59, 113.35, 122.57, 125.87, 127.76, 130.57, 132.83, 141.70, 155.74, 158.24, 166.62. FTIR (KBr) (cm⁻¹): 3050, 2941, 2870, 1718, 1577, 1510, 1433, 1394, 1320, 1277, 1244, 1189, 1096, 1037, 949, 859, 795, 761. MALDI-TOF m+1: 861. 2. Elemental analysis calculated for C₄₈H₅₀N₄O₁₁: C, 67.12; H, 5.87; N, 6.52; Found C, 66.32; H, 6.35; N, 6.01.

Synthesis of polymers: Melt Polycondensation

SDP2P-5%: Dimethyl sebacate (DMS) (0.412 g, 1.788 mmol (x mol)), **P2P** (0.0548 g, 0.094 mmol (1-x mol)), diethylene glycol (DEG) (0.200 g, 1.884 mmol) were taken in a test tube shaped polymerization apparatus (Figure 2.2) and melted by placing in oil bath at 100 °C with constant stirring in order to melt the solid. Once a homogenous

mixture was formed, the reaction mixture was cooled to room temperature and 1 mol % of titanium tetrabutoxide ($\text{Ti}(\text{O}i\text{Bu})_4$) was added as a catalyst. The polycondensation apparatus was made oxygen and moisture free by nitrogen purge. The polymerization tube was immersed in the oil bath at 150 °C and the polymerization was carried out with slow nitrogen purge for 4 h. The resultant viscous mass was further condensed by applying high vacuum (0.01 mm of Hg) at 150 °C for 2 h. The polymer was dissolved in THF, filtered to remove catalyst and precipitated in cold methanol to obtain the azo copolyester.

Yield = 0.350 g (48 %). ^1H NMR (200 MHz CDCl_3): δ (ppm): 8.17 (4H, d, Ar), 7.90 (8H, m, Ar), 7.04 (4H, d, Ar), 4.50 (4H, s, Ar- $\text{C}(\text{O})\text{-OCH}_2\text{-CH}_2\text{O}$), 4.23-3.67 (22H, oligooxyethylene region), 2.31 (4H, t, Alph- $\text{C}(\text{O})\text{-OCH}_2\text{-CH}_2$), 1.59 (4H, m, $-\text{C}(\text{O})\text{-O-CH}_2\text{-CH}_2\text{-R-CH}_2\text{-CH}_2\text{-C}(\text{O})\text{-O-}$), 1.28 (8H, m, $-\text{C}(\text{O})\text{-O-CH}_2\text{-CH}_2\text{-(CH}_2\text{)}_4\text{-CH}_2\text{-CH}_2\text{-C}(\text{O})\text{-O-}$).

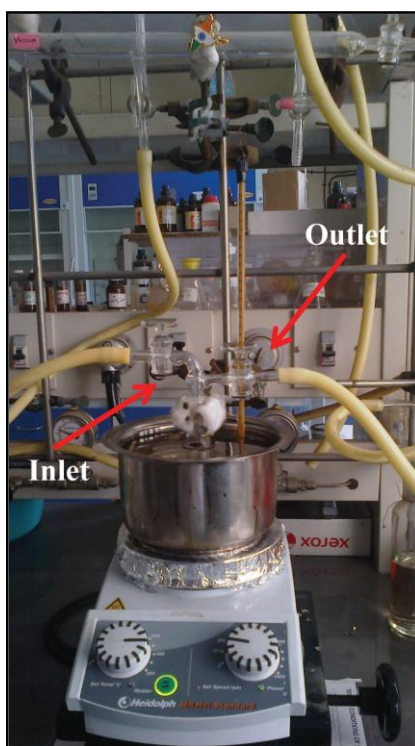


Figure 2.2 Polymerization set-up used for the synthesis of azo copolyesters via melt polycondensation approach.

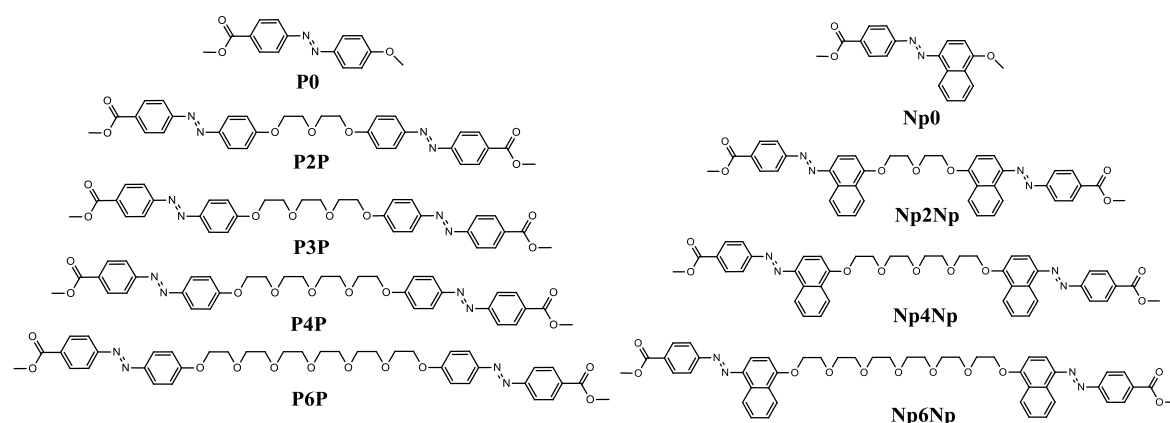
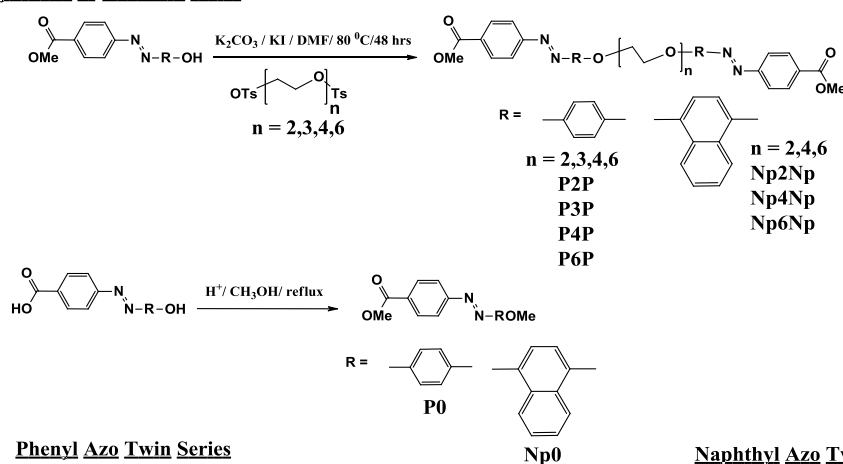
SDNpnNp-x: Dimethyl sebacate (DMS), naphthyl twin azobenzene (**NpnNp**) and diethylene glycol (DEG) were taken as monomers, adopting the same polymerization procedure as that of **SDP2P-5%**.

STPnP-x: Dimethyl sebacate (DMS), phenyl twin azobenzene (**PnP**) and tetraethylene glycol (TEG) were taken as monomers, adopting the same polymerization procedure as that of **SDP2P-5%**.

2.3 Results and Discussion

The synthesis of the twin azobenzenes along with **P0**, and **Np0** - model compounds without ethylene glycol units is given in Scheme 2.1. The detailed procedure for the synthesis of the azo dyes and their ester derivative is given in experimental section. The twin series having the structure - azo dye-(oligooxyethylene spacer)_n-azodye was synthesized by coupling the ditosylate of different oligooxyethylene with the azo dye esters.

Synthesis of AzoTwin series



Scheme 2.1 Synthesis of phenyl and naphthyl twin azobenzenes.

P0 and **Np0** were synthesized by refluxing the azodye in presence of acid in methanol as solvent. Normally introduction of ether linkage at phenolic position requires the reaction of alkyl halide in the presence of base. However in these push-pull azo

systems carrying out esterification for longer time resulted in the esterification of carboxyl group as well as introduction of ether linkage at the phenolic position.

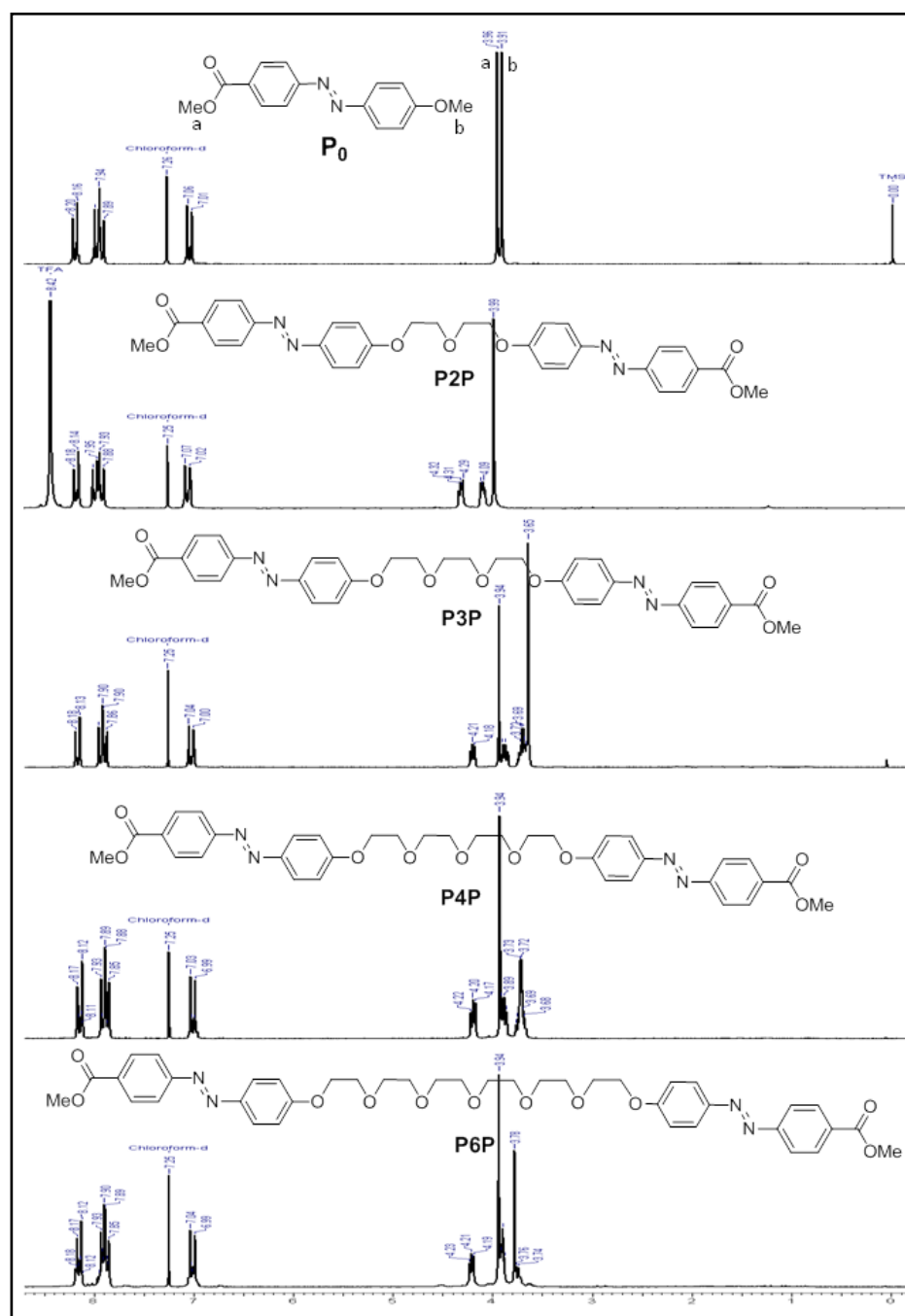


Figure 2.3 $^1\text{H-NMR}$ spectra of phenyl twin azobenzene in CDCl_3 solvent.

This was confirmed by the appearance of two $-\text{OCH}_3$ peaks corresponding to ester and ether linkage respectively in the ^1H NMR spectra (Figure 2.3 and 2.4). The structures of all the azo dye molecules are shown in Scheme 2.1. The structural

characterization of the azo twin series were done by ^1H NMR and ^{13}C NMR spectroscopy. Figure 2.3 and 2.4 shows ^1H -NMR spectra for the phenyl and naphthyl twinazobenzene respectively. The purity of all molecules were confirmed by size exclusion chromatography (SEC), high resolution mass spectroscopy or matrix assisted laser desorption ionization–time of flight (MALDI-TOF) analysis along with elemental analysis.

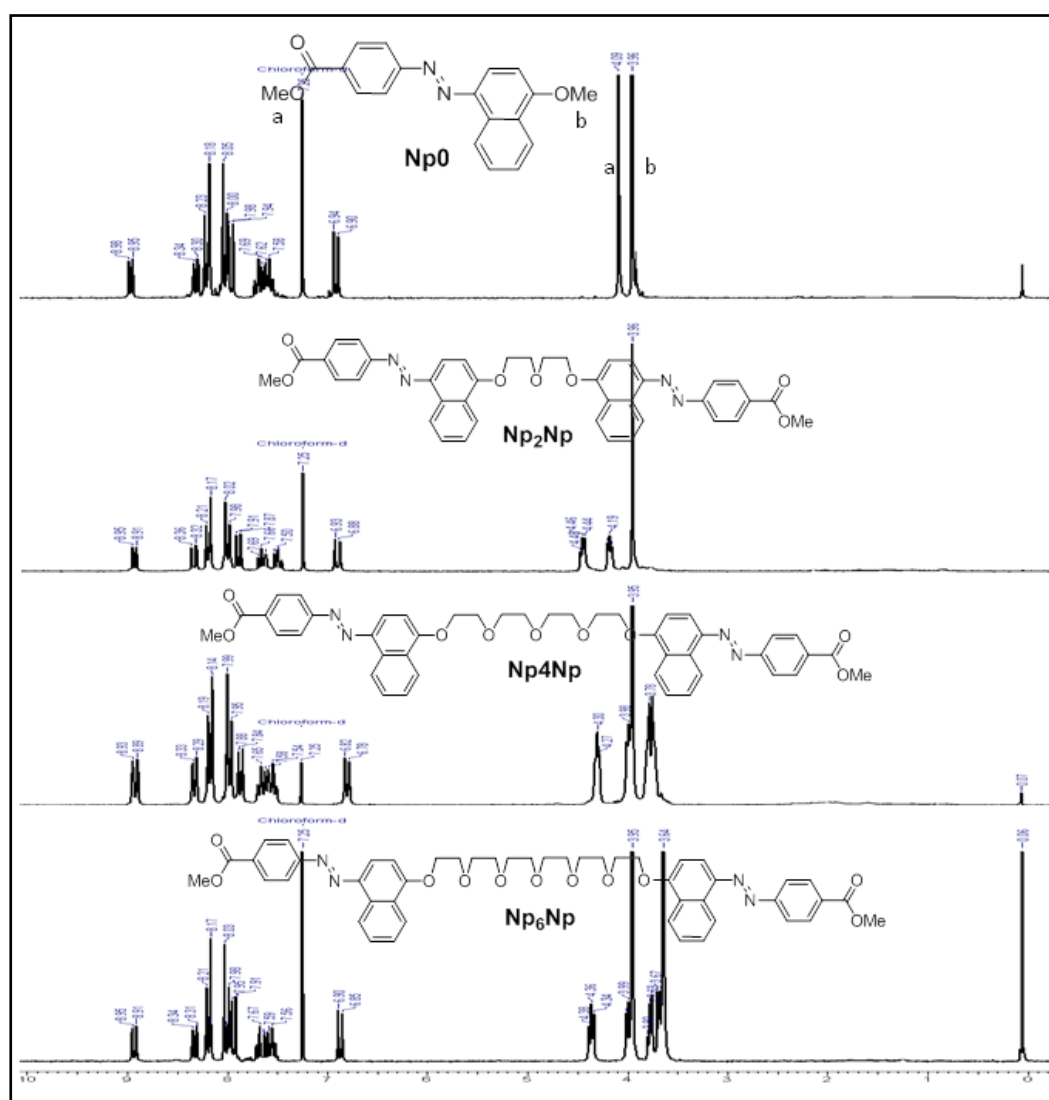
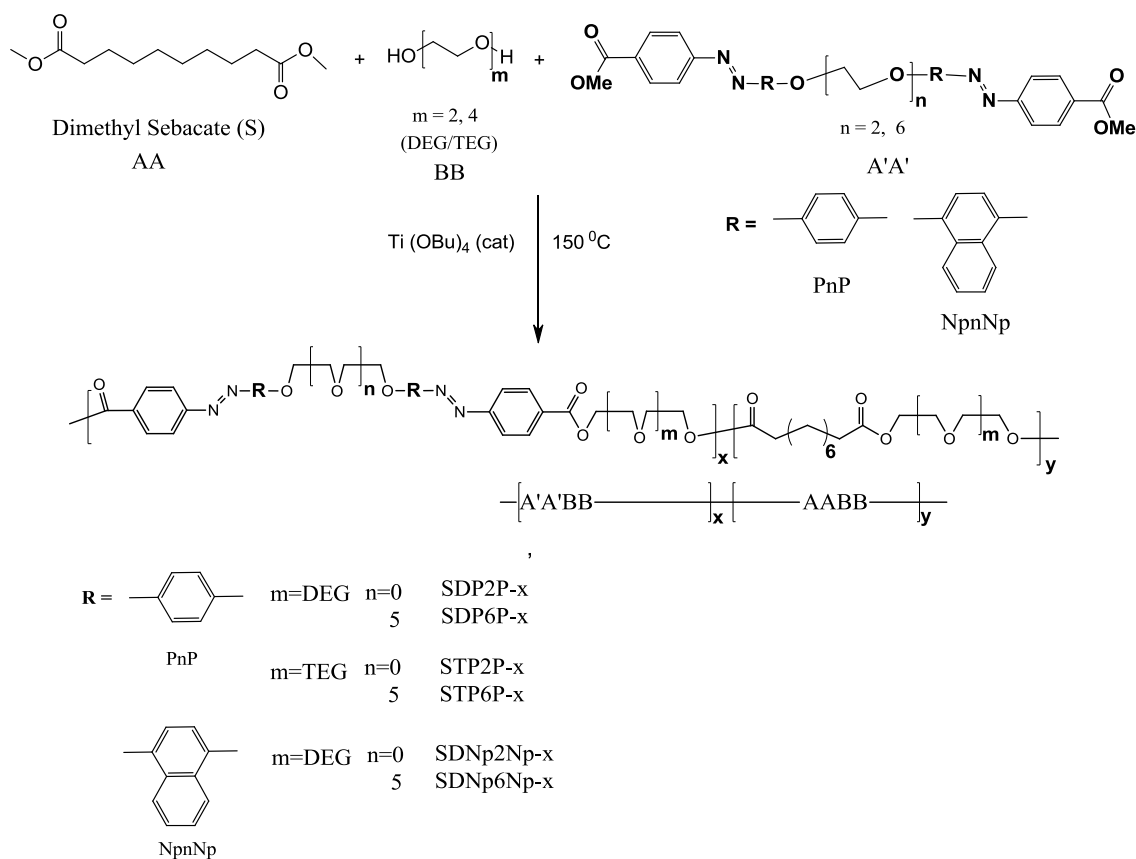


Figure 2.4 ^1H -NMR spectra of naphthyl twin azobenzene in CDCl_3 solvent.

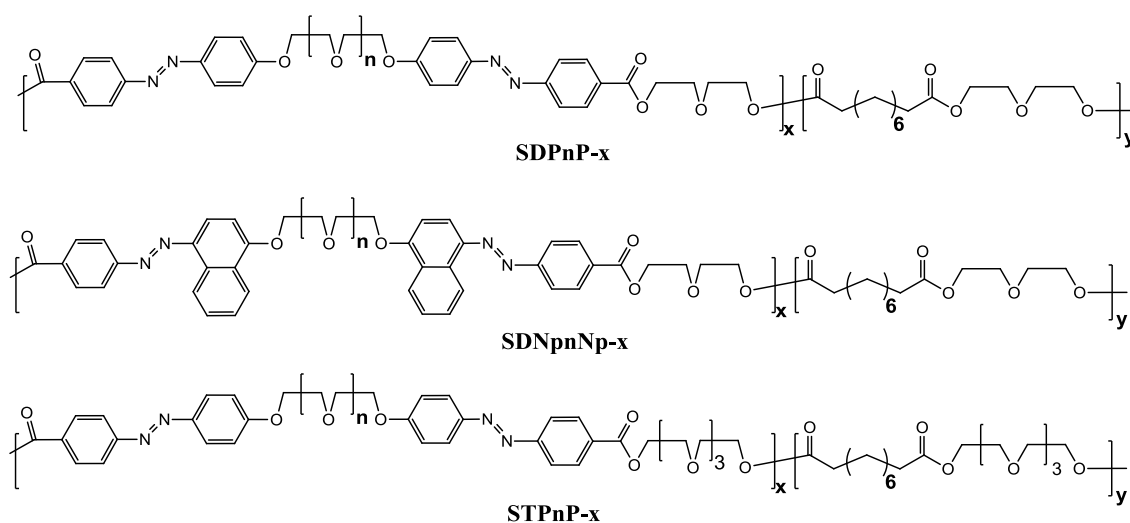
The SEC analysis showed single peak for all molecules confirming their purity. In the HRMS or MALDI-TOF analysis, molecular ion m , or $m+1$ radicals were obtained. Scheme 2.2 shows the incorporation of the twin azobenzenes into a main chain

polyester backbone by melt polycondensation. The most widely used reactions for the preparation of polyesters are direct esterification of diacid/diacid chloride with diol or transesterification of diester with diol which are usually performed at high temperature in the melt. Generally the degradation temperature of the azobenzene chromophore is lower than the melting temperature; thereby making it impossible to carry out melt polycondensation. On the other hand, solution polymerization generally result in very low molecular weight oligomers, as the poor solubility leads to its precipitation from the polymerization medium before build-up of high molecular weight occurs.^{7a,c,d}

Synthesis of AzoCopolymer series



Scheme 2.2 Synthesis of random azo copolymers from Phenyl and Naphthyl twin azobenzenes.



Scheme 2.3 Structure of random azo copolymers.

These difficulties were overcome in the polymerization reported here by designing the azobenzene dimethyl ester as a twin molecule with oligooxyethylene units which not only lowered the melting temperatures but also improved the solubility and the miscibility in the molten reaction medium. Dimethyl sebacate (DMS) and di/tetra ethylene glycol were used as the AA and BB monomers respectively into which varying amounts of the different azo twin dimethyl esters were introduced as the A'A' monomer. Two homopolyesters of dimethyl sebacate with diethylene glycol (DEG) named as (**SD-homo**) and with tetraethylene glycol (TEG) named as (**ST-homo**) were synthesized. For the copolymers the total mole equivalents of AA (dimethyl sebacate) and A'A' (dimethylester of azotwin) were kept equal to that of the BB (diol), i.e. sum of AA and A'A': BB = 1:1. Scheme 3 shows the general structure of the random azo copolymers. The incorporation of the azo molecule into the aliphatic polyester backbone was determined from the proton NMR spectra. Table 2.1 gives the list of different copolymer compositions that were made with the actual incorporation of the azo content determined from ^1H NMR analysis given in brackets. The polymers based on sebacate/DEG were named as **SDPnP-x%** and **SDNpNp-x%** respectively, where the **n** represented the number of central ethylene glycol units in the azo twin segment and **x** represented the mole % incorporated. Similarly, the polymers based on sebacate/TEG were named as **STPnP-x%**. Two sets of twin molecules were chosen to be incorporated into polyester; **P2P** (the smallest spacer twin which was not liquid

crystalline) and **P6P** (the largest spacer twin which was liquid crystalline). For the copolymers the highest azo solid content that could be taken in the feed was ~ 30 mole % for the higher spacer twin. For the shorter spacer twins, the poor solubility/miscibility of the azo molecule in the other molten components limited the feed to ~15 mole %. Thus in the **P2P** polymer series, 5 and 15 mol % incorporation of **P2P** could be achieved with both DEG and TEG.

Table 2.1 Polymer designation, molecular weight, polydispersity index, viscosity data (η_{inh}), and LC nature of polymers.

Twin	Polymer (% Azo incorporation from ¹H NMR)	Mn^a	Mw^a	PDI	LC
DEG series					
P2P	SDP2P-5 (4.5)	8300	13000	1.57	√
	SDP2P-15 (14)	14400	26200	1.80	√
P6P	SDP6P-5 (5.4)	13800	19000	1.37	X
	SDP6P-30 (25)	4000	5030	1.24	√
Np2Np	SDNp2Np-5 (5)	46800	67800	1.44	X
Np6Np	SDNp6Np-5 (5)	16300	25900	1.59	X
	SDNp6Np-30 (30)	7400	13800	1.86	X
TEG series					
P2P	STP2P-5 (5)	25300	38000	1.50	X
	STP2P-15 (17)	12700	22720	1.78	√
P6P	STP6P-5 (6)	13660	19540	1.43	X
	STP6P-30 (31)	18900	32900	1.73	X
Homopolymers					
	DMS/DEG	8700	12400	1.42	X
	DMS/TEG	18000	28400	1.57	X

a. Molecular weights as determined by gel permeation chromatography in THF at 30 °C using polystyrene standards for calibration.

b. Inherent viscosity measured in chloroform solvent (0.5 dL/g) at 30 °C ± 0.1 °C.

Although a 30 mole % **P2P** in the feed was attempted, the polymerization could not be practically carried out due to the large solid content of **P2P** which was immiscible in the other two components, namely 100 mol % DEG/TEG and 70 mol % dimethyl sebacate. In the **P6P** polymer series 5 and 30 mol % incorporated polymers were synthesized using both DEG and TEG. The proton NMR signals of the copolymers were identified by comparison of the NMR spectra of the corresponding twin molecule with the homopolymer. The formation of the polymer was confirmed by the appearance of the new peak at 4.5 ppm (indicated by circle in Figure 2.5) corresponding to the new aromatic ester linkage. The integrated area of the aromatic protons of azobenzene was compared with the $-(O-C(O)-CH_2)-$ protons of the sebacate to determine the mol incorporation of the azobenzene into the polymer backbone.

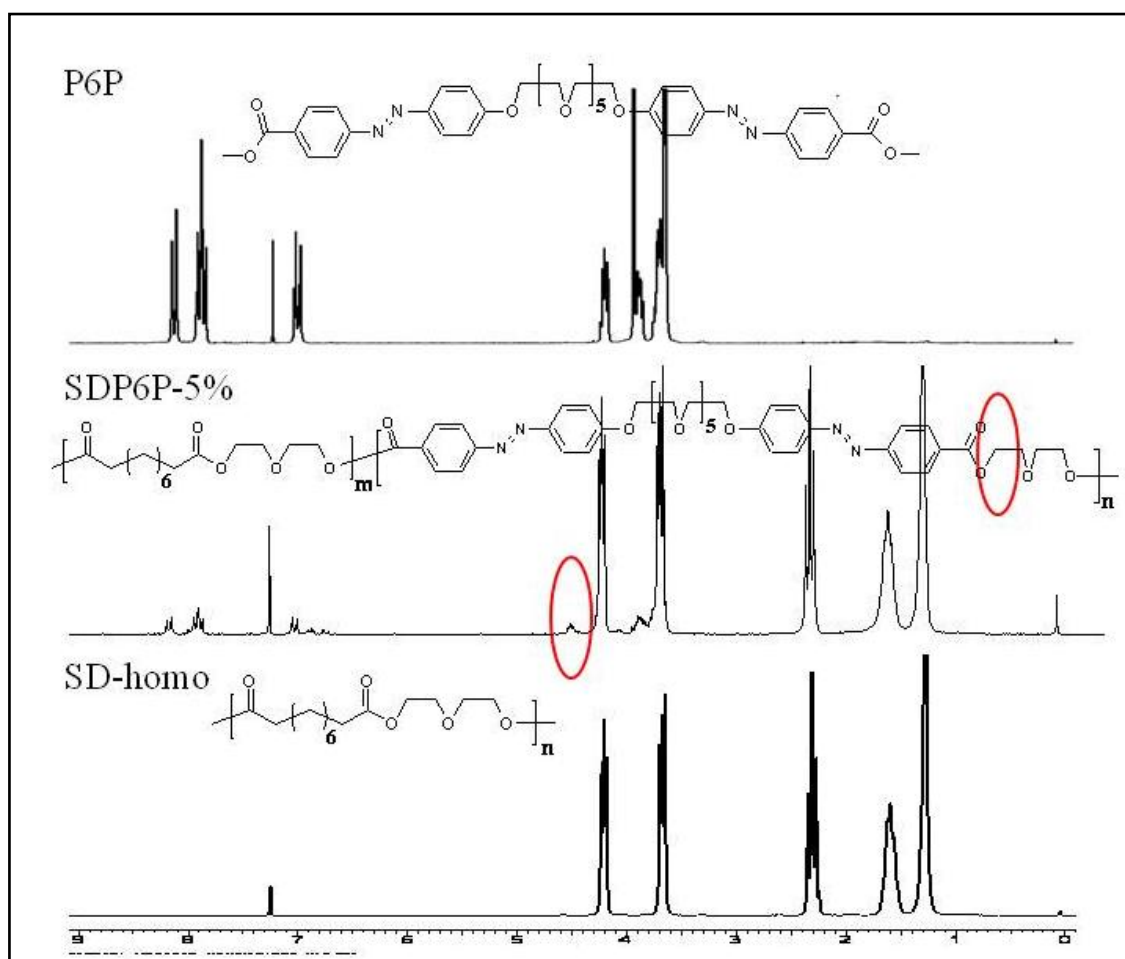


Figure 2.5 $^1\text{H-NMR}$ of phenyl twin azobenzene **P6P**, homopolymer **SD-homo** and random azo co-polymer **SDP6P5**.

Figure 2.5 shows the representative proton NMR spectra of the twin molecule **P6P** and its copolymer with sebacate and diethylene glycol – **SDP6P-5%**. Similarly, Figure 2.6 shows $^1\text{H-NMR}$ spectra for the Naphthyl azo copolymers – **SDNp2Np-5%**, **SDNp6Np-5%** and **SDNp6Np-30%**.

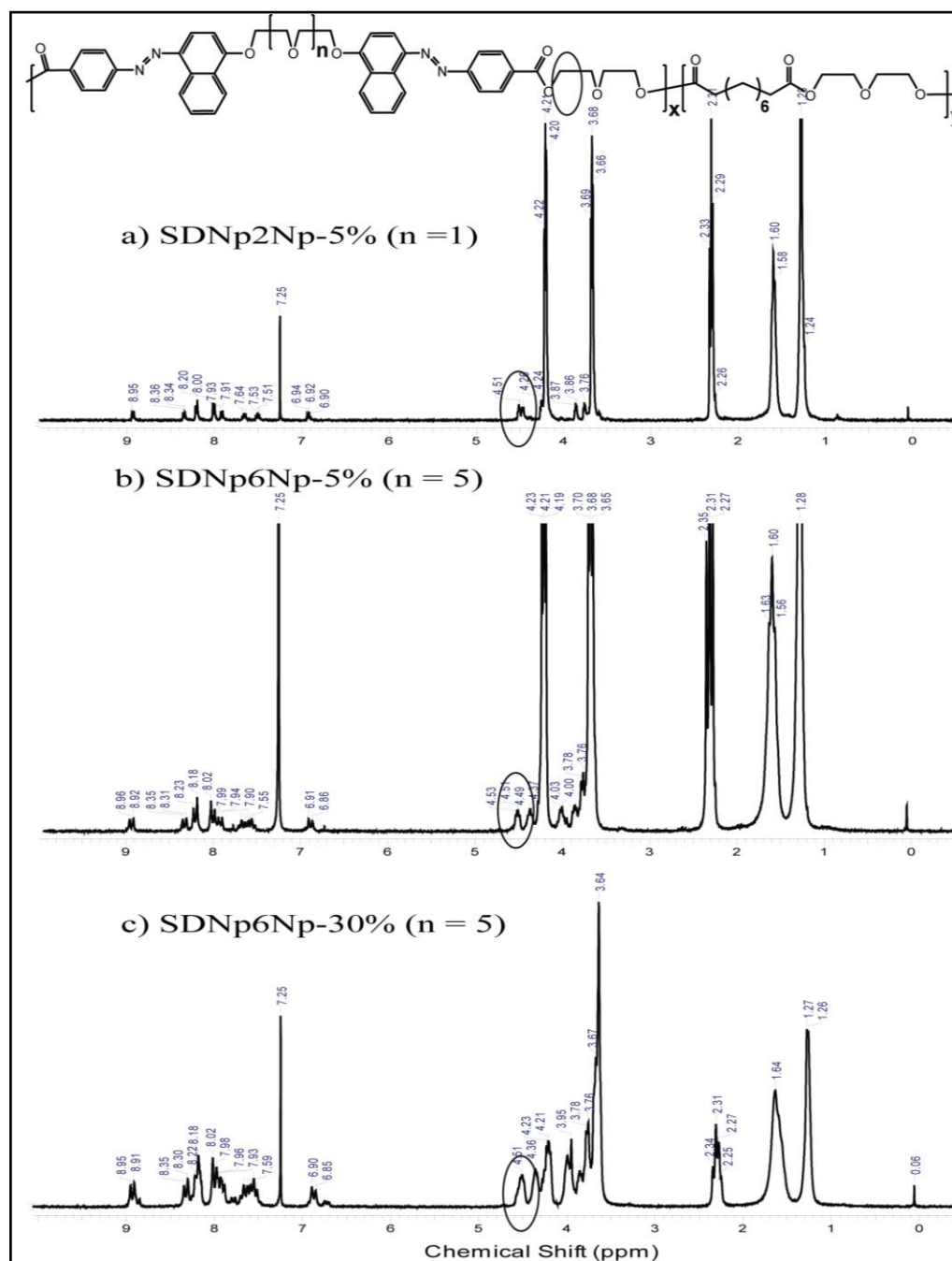


Figure 2.6 $^1\text{H-NMR}$ spectra of Naphthyl azo co-polymers **SDNp2Np-5%**, **SDNp6Np-5%** and **SDNp6Np-30%**.

The new peak corresponding to new aromatic ester linkage with naphthyl core appeared at 4.5 ppm is indicated by circle in Figure 2.6, confirming the covalent incorporation of naphthylazo twin into the polymer backbone. All the random copolymers thus developed had good solubility in common organic solvents such as CHCl_3 , DCM, THF, DMF, DMSO etc. The molecular weight and polydispersity of the polymers were determined by GPC (Figure 2.7) and the values are given in Table 2.1. In general, it was observed that the molecular weight of the DEG based copolymers were lower compared to that of the TEG copolymers. In the DEG copolymer series, higher (30 mole %) incorporation of azo dye resulted in a drastic reduction of the molecular weight.

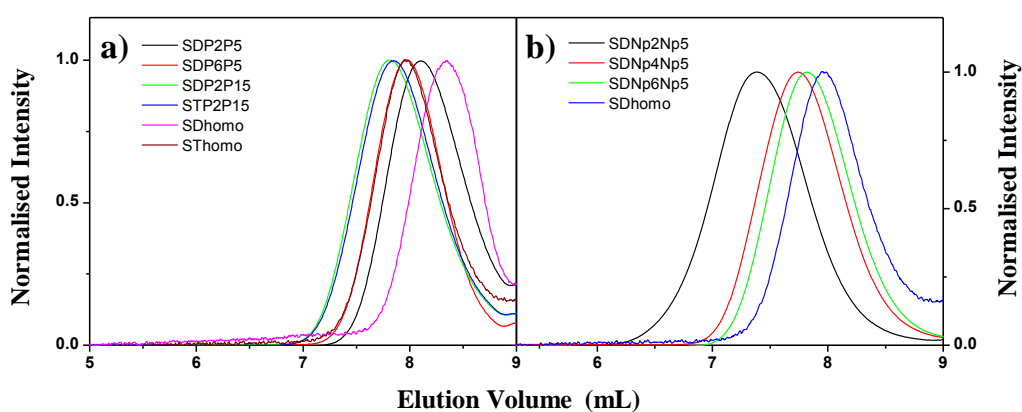


Figure 2.7 GPC Chromatogram of homo polymer *SDhomo*, *SThomo*, and random azo copolymers in THF solvent: a) *SDPnP* b) *SDNpnNp*.

2.3.1 Photophysical Properties

The absorption spectra of the twin molecules and polymers were recorded in THF and the peak absorption values are given in Table 2.2. The absorption spectra of typical azobenzene consist of three major bands. The lowest energy transition occurs at approximately 430-440 nm and is assigned to the $n-\pi^*$ transition. The second transition occurs in the UV region around 320 nm and is assigned to the $\pi-\pi^*$ transition for trans azobenzene (for cis azobenzene the $\pi-\pi^*$ band occurs around 280 nm).¹³ The peak maximum of this band is sensitive to the polarity and also to the presence of substituents. The third energy transition around 230-240 nm is considered to arise from the $\pi-\pi^*$ transition in the phenyl rings.

Table 2.2 Absorption and photoisomerization data of the Phenyl and Naphthyl based twin azobenzene series in THF solvent.

Compound	λ_{\max} Abs ($\epsilon, \text{M}^{-1}, \text{cm}^{-1}$)	Photoisomerization (%)
P0	253, 355, 445	92
P2P	253, 355, 447	80
P3P	253, 355, 447	91
P4P	253, 355, 447	90
P6P	253, 356, 447	90
Np0	280, 415	42
Np2Np	280, 415	42
Np4Np	280, 415	47
Np6Np	280, 415	52

In push-pull substituted aromatic azobenzene systems there is an overall red shift of the π - π^* transitions. Thus the simple phenol based azobenzene molecules, for example **P0** with the ester group at one end and methoxy group at the other end had the n - π^* transition at ~ 445 nm, the π - π^* transition at 355 nm and the aromatic phenyl π - π^* transition at ~ 253 nm. On the other hand in the more conjugated naphthol based azobenzene series the n - π^* band was almost wholly overlain by the bathochromically shifted π - π^* band which appeared at 411 nm. The aromatic phenyl π - π^* transition was observed at ~ 279 nm. Figure 2.8 compares the absorption spectra of **P0** and **Np0** in THF. The twin molecules as well as copolymers had the absorption spectra similar to that of the respective model compounds. The twin azobenzenes were irradiated with a 75 watt short arc mercury vapor lamp with an output wavelength in the range 280-450 nm in combination with either a 360 nm (for Phenylazo series) or a 450 nm (for the naphthylazo series) Oriel bandpass filter. The samples in THF (1×10^{-6} M) were kept in the dark overnight followed by irradiation and the absorption was recorded at every 5-10 seconds interval to trace the trans to cis photoisomerization. The change in absorption spectra of **P0** and **Np0** as representative samples of the **PnP** and **NpNp**

series upon UV irradiation is shown in Figure 2.9 and the inset in the figure shows the % conversion as a function of photoirradiation time.

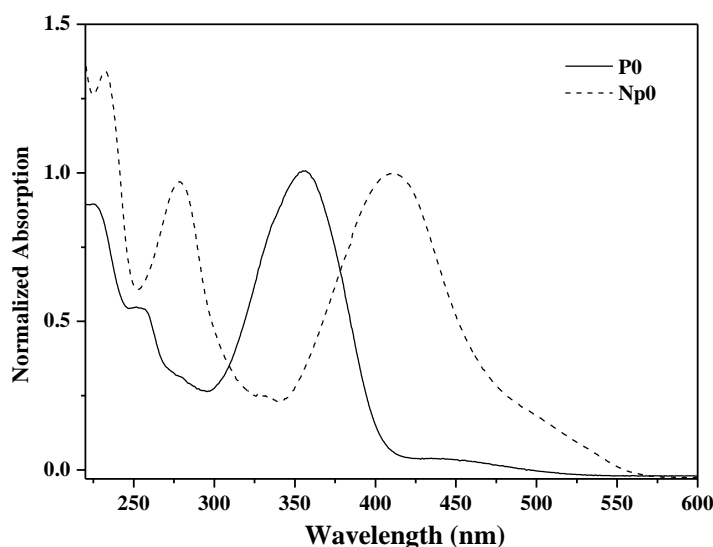


Figure 2.8 Normalized UV absorption spectrum of **P0** and **Np0** in THF.

The % trans to cis conversion upon UV irradiation is estimated using equation (1).¹⁴

$$Y = \frac{1 - A/A_{\text{dark}}}{1 - \epsilon_{\text{cis}}/\epsilon_{\text{trans}}} \dots\dots\dots 1$$

Where, A_{dark} = peak initial absorbance with only trans isomer in dark, A = absorbance at wavelength λ after UV irradiation, ϵ_{cis} , ϵ_{trans} = molar absorption coefficient of trans and cis isomers, respectively at wavelength λ ($\epsilon_{\text{cis}}/\epsilon_{\text{trans}} = 0.050$).¹⁴

Table 2.2 shows the % trans to cis conversion at the photostationary state for both series. The phenylazo series reached the photostationary state with more than 80 % conversion within 15 seconds of irradiation. The phenylazo twin series exhibited increasing extent of trans to cis photoisomerization with increase in the central oligooxyethylene spacer length. The longer members like the **P4P** and **P6P** had the highest extents of isomerization of 90 %, similar to the isolated chromophore **P0** (92 %). The reversibility of the photoisomerization was confirmed by following the back conversion to the trans state upon keeping in the dark overnight. Molecules of both series attained the original trans absorption spectra fully upon keeping in the dark.

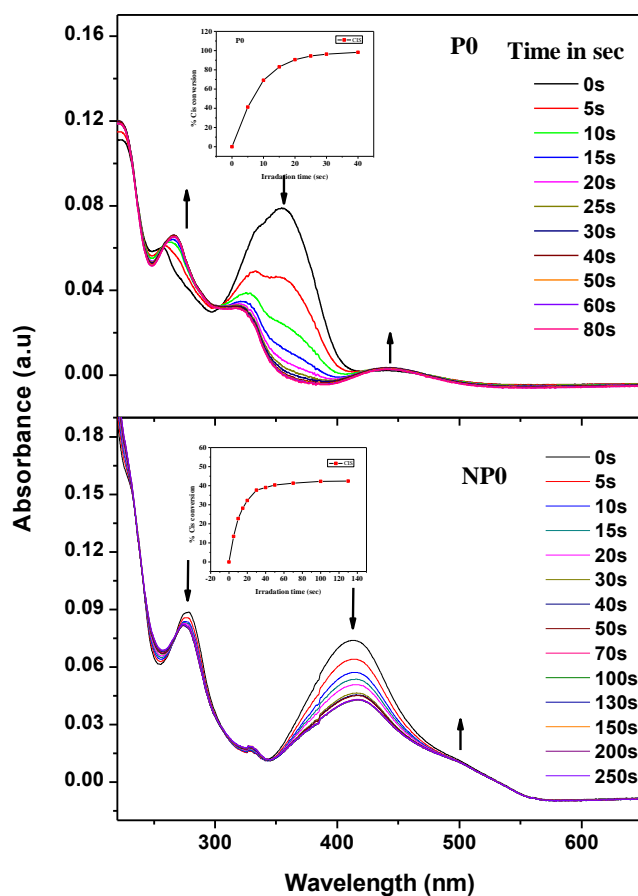


Figure 2.9 Photoisomerization studies of model compounds (a) *P0* and (b) *Np0* in *THF*.

The reduced isomerization efficiency of the naphthyl azo twins in comparison with the phenyl azo series is due to its bulky nature which hindered the motion. The photoisomerization in the copolyesters were similar to those observed for the corresponding twin molecules. One would have expected the covalent linkage of azobenzene group to the polymer main chain backbone to result in fewer degrees of freedom and hence to a lower extent of photoisomerization compared to the twin molecule. But no such difference in extent of photoisomerization was observed indicating that the polymer backbone provided enough flexibility for the alignment of azo groups in the main chain.¹⁵

2.3.2 Thermal Mesophase Characteristics of Twin Molecules

The thermal stability of the azotwins was determined by TGA under nitrogen atmosphere and is shown in Figure 2.10. No weight loss was observed until they were

heated up to 200 °C. Table 2.3 compares the 10 wt % decomposition temperature of the single azochromophore (**P0** and **Np0**) with that of the respective azotwin series. The twin molecules had much higher decomposition temperatures compared to the single chromophore. The connection of two mesogens to form a dimeric or twin structure is known to afford better thermal as well as mesogenic stability compared to the single molecule. The thermotropic liquid crystalline tendency of the azo twin series were studied using differential scanning calorimetry (DSC) analysis coupled with polarized light microscopy (PLM) and temperature dependent wide angle X ray diffraction (WXR) studies.

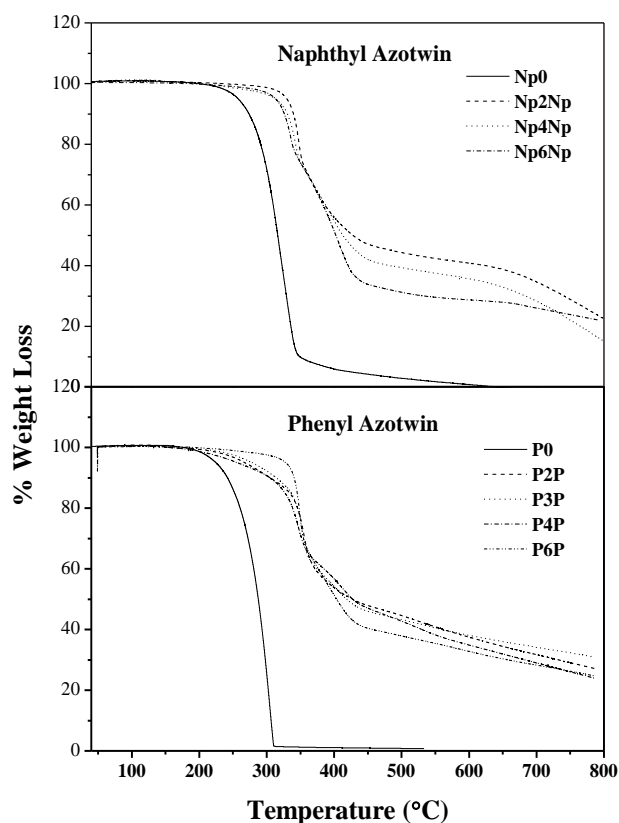


Figure 2.10 Thermal analysis of model compound (**P0** and **Np0**), naphthyl and phenyl twin azobenzenes.

In the phenylazo twin series monotropic mesophases were exhibited by members having spacer length greater than 2. Thus, **P3P**, **P4P** and **P6P** exhibited smectic A (S_A) phases upon cooling, with **P3P** additionally exhibiting nematic phase also. Figure 2.11-a shows the second heating and cooling scans in the DSC thermogram of

the phenyl twin azochromophores **P3P**, **P4P**, **P6P**. The enthalpy values and phase transition temperature are given in Table 2.3. The melting (heating cycle) and isotropic to LC transition (cooling cycle) decreased with increase in spacer length. The model compound **P0** was not liquid crystalline and exhibited a sharp melting at 168 °C in the heating cycle. In the cooling cycle two transitions were observed at 163 °C and 149 °C which corresponded to the isotropic to crystal and crystal to crystal transitions, which were confirmed by the PLM.

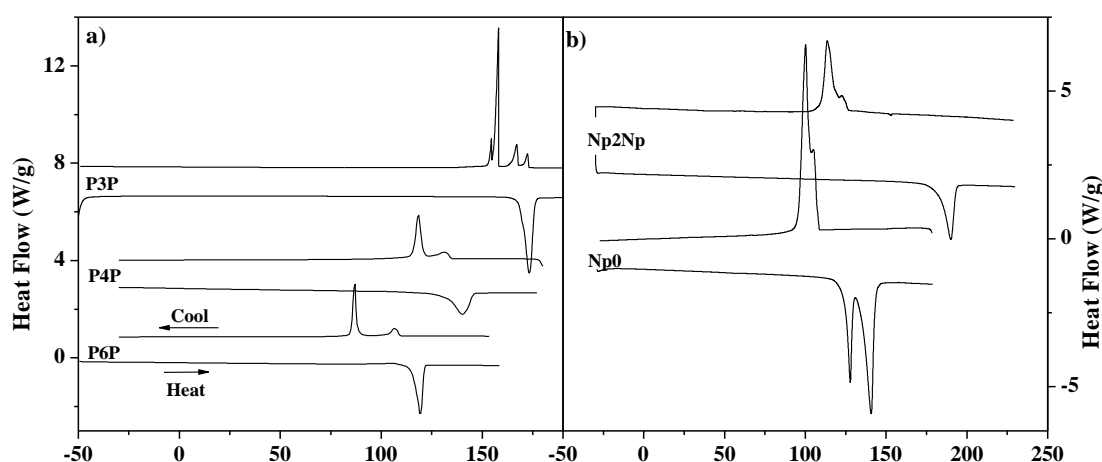


Figure 2.11 DSC thermograms of a) Phenyl twin azobenzenes **P3P**, **P4P** and **P6P** b) Naphthyl twin azobenzenes **Np0** and **Np2Np**.

The twin molecule **P2P** also did not exhibit a mesophase during the heating or cooling cycle and had a melting transition at 215 °C. On the other hand **P3P** was monotropic and exhibited multiple transitions in the cooling cycle which were confirmed to be liquid crystalline phases based on observation under the PLM. There was only one melting transition in the second heating cycle at 173 °C with an enthalpy of 84 J/g. While cooling, sharp transitions were observed at 172 °C, 166 °C, 158 °C and at 155 °C. Although DSC did not show any transition above 172 °C (while cooling), typical nematic textures were observed at 178 °C in the PLM as shown in Figure 2.12-a upon cooling from the isotropic melt. This nematic threads remained only for 2-3 °C, which was too weak to be detected by DSC and then batonnets started appearing at 173 °C which coalesced into the typical focal conic textures of smectic A (S_A) (Figure 2.12 b-c). The focal conic textures remained until 169 °C, then suddenly the texture changed

into multi-colored grainy features which corresponded to the second transition observed in DSC with peak maxima at 166 °C.

Table 2.3 Thermal data of twin azobenzenes (*PnP*, *NpnNp*), and random azo copolymers (*SDPnP-x%*, *STPnP-x%*).

Sample	T _m ^a (C- LC) (°C)	ΔH _m ^a (C- LC) (J/g)	T _{cl} ^a (C/LC -I) (°C)	ΔH _{cl} ^a (C/LC- I) (J/g)	T _c ^b (I/Lc- LC/C) (°C)	ΔH _c ^b (I/LC- LC/C) (J/g)	T _c ^b (LC/ C-C) (°C)	ΔH _c ^b (LC/ C-C) (J/g)	T _D ^e (°C)
P0	-	-	169	129.2	163	- 114.8	149	- 6.49	241
P2P	-	-	215	114.5	205	- 115.9			304
P3P	-	-	173	84.1	*178 172 169.5	-4.8 -10.8	158.1 3	-54.9	315
P4P	-	-	140	47.2	132	- 6.9	118	- 32.9	304
P6P	-	-	119	95.4	106	- 14.4	87	- 55	339
Np0	128	25.4	141	54.3	106	-	101	- 93.7	267
Np2Np	-	-	190	78.0	123	-	113	- 63.0	331
Np4Np	19 ^c	-	139 ^d	87.34	-	-	-	-	325
Np6Np	-6 ^c	-	34	6.97			-	-	331
SDP2P5	34	44.6	66.5	3.9	*25	-	-5.2	46.6	385
SDP2P15	24	14.5	90	8.4	75 47	-9.3	-13.6	-13.3	360
SDP6P30	45 64 79.5	0.5 1.7 7.8	117	0.48	90	-	64	-13.5	335
STP2P15	8	0.7	99	8.7	*80	-	25	-11	364

^a During second heating cycle with 10 °C/min. ^b During second cooling cycle with 10 °C/min. ^cGlass Transition (T_g) during second heating cycle. ^d During first heating cycle. ^eT_D- 10 % weight loss under N₂ atmosphere in TGA. T_m- melting temperature. T_{cl}- Clearing temperature. T_c- cooling cycle. Note- ‘*’ transitions observed in PLM.

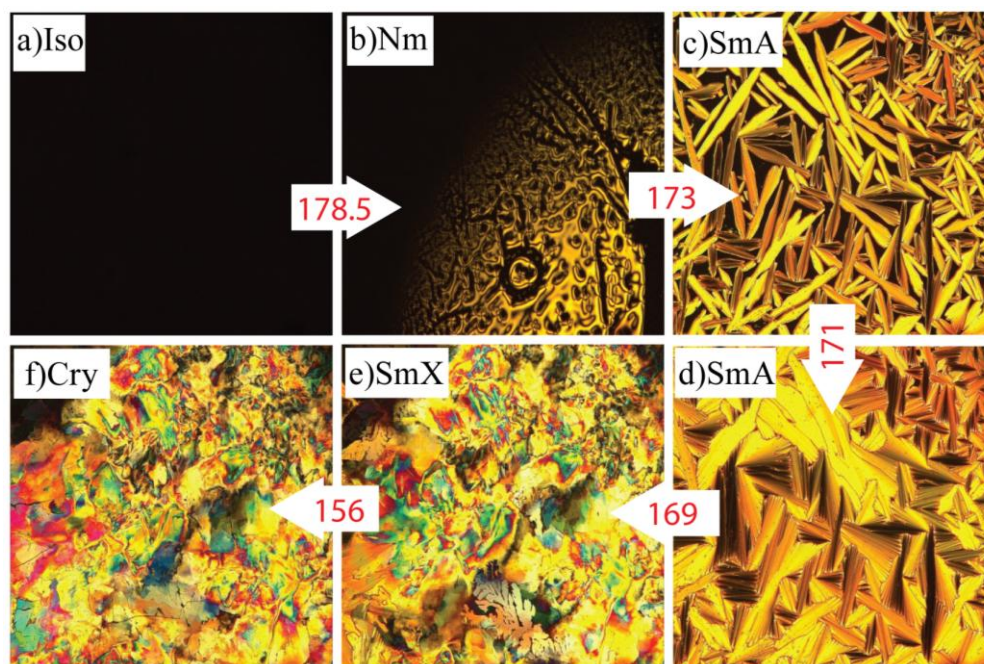


Figure 2.12 Polarized Light microscope images of phenyl twin azobenzene **P3P** (b) at 178 °C (Schlieren texture) (c) at 172 °C (Batonnets) (d) at 170 °C (focal conic texture - S_A) (e) at 166 °C (unidentified S_X phase) and (f) at 155 °C (Crystalline phase).

Beyond this temperature DSC showed transitions at 158 °C and 155 °C associated with huge enthalpy change of 54.9 J/g (compared to the smaller values of 10.8 J/g and 4.8 J/g of the LC transitions); but under the PLM, sharp changes were not discernible. This transition at 158 °C was confirmed to be crystallization based on the large enthalpy change as well as from the variable temperature WXRd measurements which showed the appearance of multiple sharp peaks corresponding to crystallization around this temperature (Figure 2.13, plot f). The overall LC window exhibited by P3P was thus ~ 20 °C (from 178 to 158 °C). Figure 2.13 shows the VT-WXRd data as a plot of intensity vs. 2θ recorded from $2\theta = 3-35^\circ$ at various temperature intervals while cooling from the isotropic phase. The plot “a” at 185 °C corresponded to the isotropic phase, plot “b” at 178 °C in Figure 2.13 showed a broad peak around $2\theta = 20^\circ$ which could be assigned to the lateral distance between mesogens of about 4 Å, characteristic of the nematic phase. Plot ‘c’ at 172 °C corresponded to the S_A phase and plot ‘d’ corresponded to the colored grainy LC phase as observed under the PLM. Although WXRd did not show any characteristic features of smectic phase until 164

°C, room temperature WXRd recorded for the low angle region of $2\theta = 0.5$ to 10° (Figure 2.14) clearly showed the existence of a peak at low angle corresponding to molecular length of 33.5 \AA around $2\theta = 2.8^\circ$.

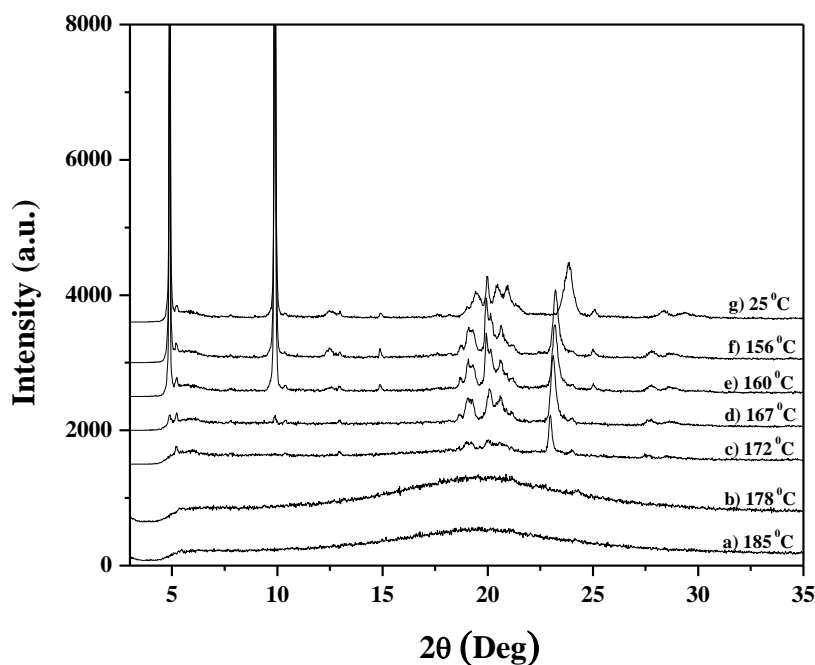


Figure 2.13 Variable temperature wide angle X-ray diffraction of phenyl twin azobenzene *P3P*.

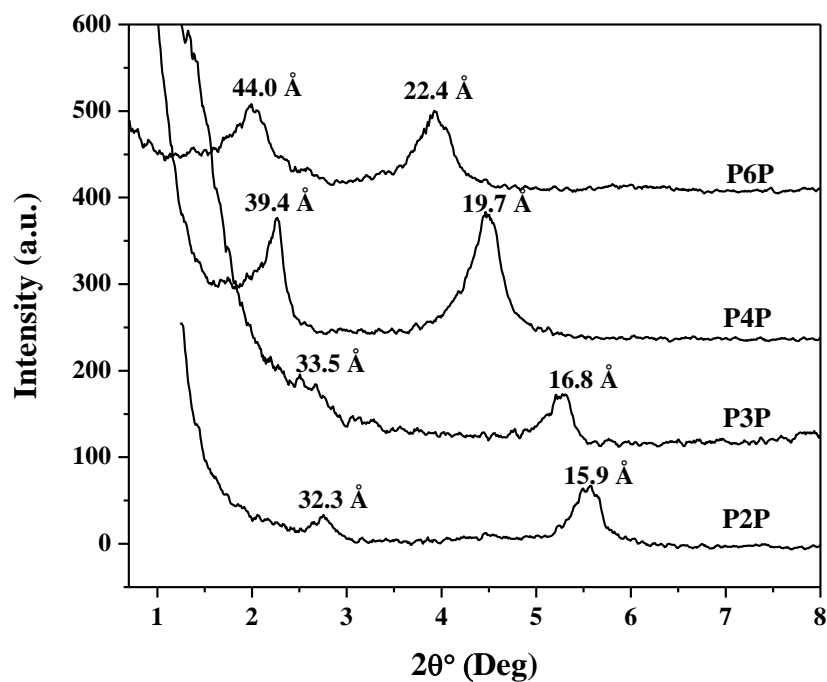


Figure 2.14 Low angle X-ray diffraction patterns of phenyl twin azobenzenes.

P4P exhibited monotropic behavior with two transitions observed only during the cooling cycle. Figure 2.15 a-b shows the focal conic fan-shaped textures typical of smectic A phases observed at 125 °C upon cooling from the isotropic melt.

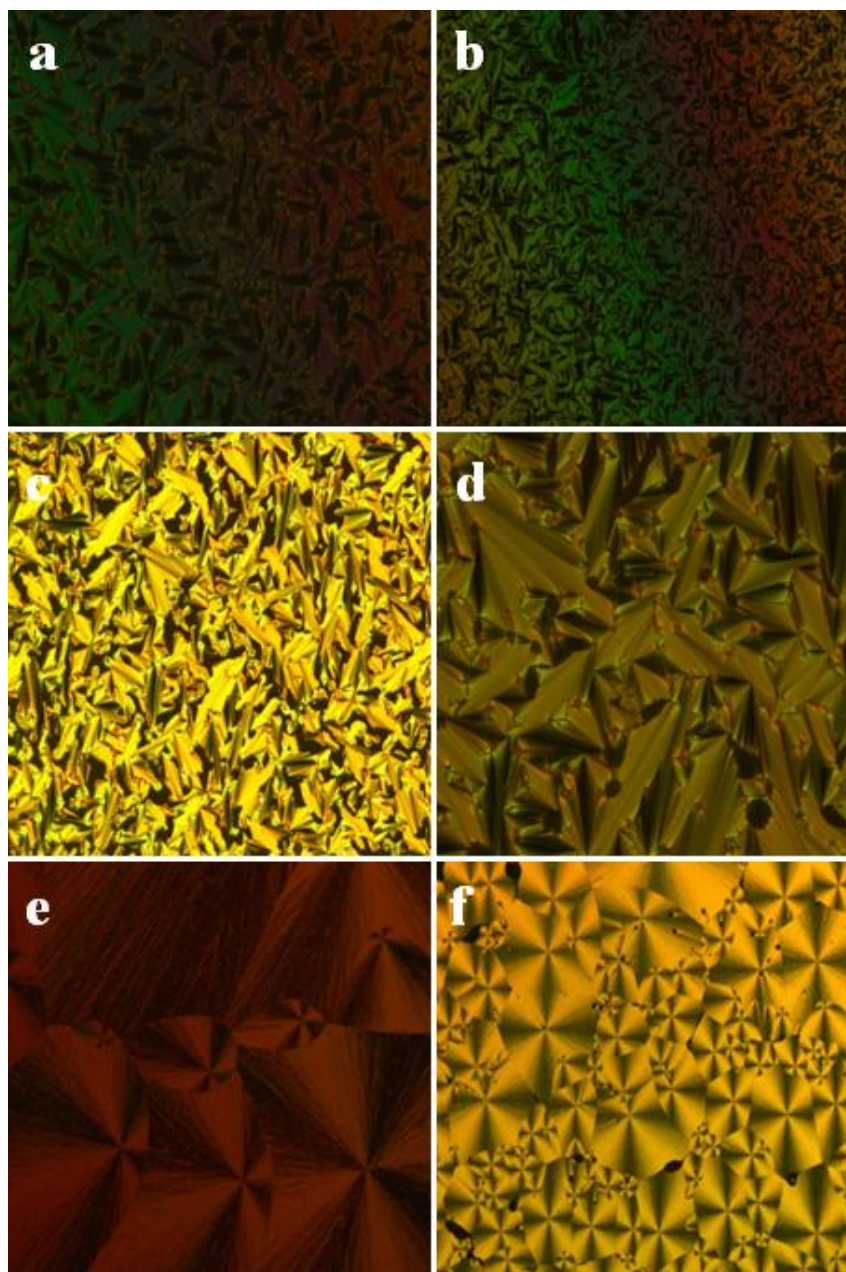


Figure 2.15 Polarized Light microscope images of Phenyl and Naphthyl twin azobenzenes (a) **P4P**-136 °C (focal conic texture- S_A , 40X magnification) (b) **P4P**-128 °C (focal conic texture- S_A) (c) **P6P**-109.7 °C (fan like texture- S_A) (d) **P6P**-104.8 °C (focal conic texture- S_A , 40X magnification) (e) **Np0**- 30 °C (Spherulitic texture) (f) **Np2Np**- 30 °C (Spherulitic texture).

The LC window was around 14 °C. **P6P** also exhibited similar behavior as **P4P** with a monotropic transition corresponding to broken fan-like smectic texture and an LC window of 20 °C. The variable temperature WXRd plot of **P4P** and **P6P** are given in the Figure 2.16. A surprising feature observed in the variable temperature WXRd plot of the three molecules **P3P**, **P4P** and **P6P** were the appearance of sharp crystalline like d spacings during the mesophase in the 2θ region from 20 to 25° which corresponded to the packing of oligooxyethylene units. Similar observation has been reported for azoxy based liquid crystalline polyesters where this has been attributed to

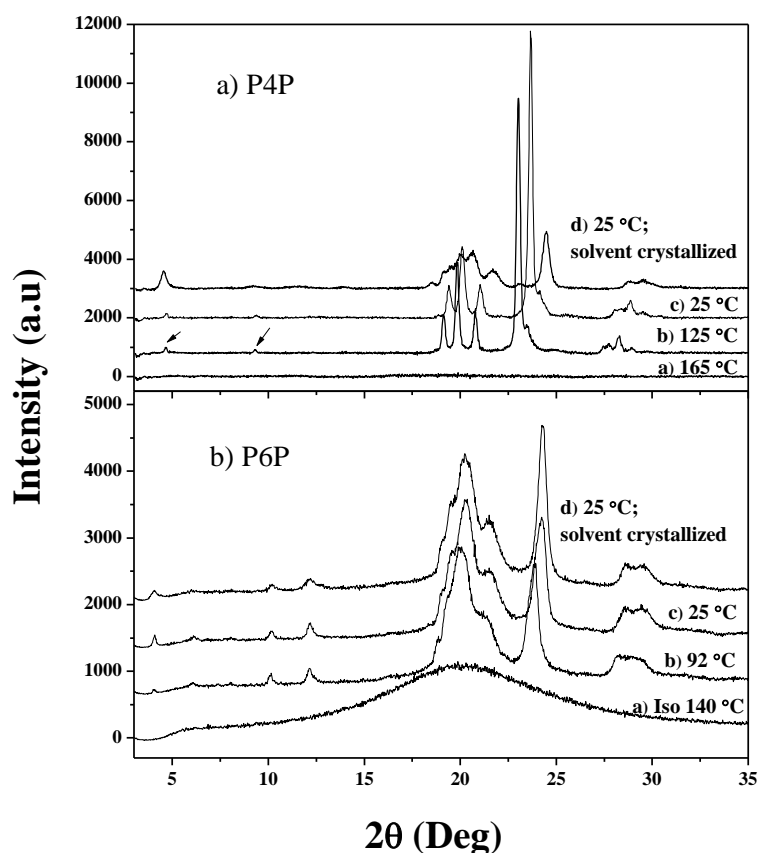


Figure 2.16 Variable temperature wide angle X-ray diffraction of phenyl twin azobenzene **P4P** and **P6P**.

the retention of order of the solid in the mesophase also.¹⁶ In a highly ordered smectic mesophase, the layered order of the solid state would be maintained. **P4P** and **P6P** also exhibited peaks at multiple intervals indicating layered structure in the LC phase. For instance in the LC phase at 125 °C, **P4P** showed two reflections at $2\theta = 4.53^\circ$ and 9.31° which corresponded to the d-spacing values of 19.74 and 9.50 Å respectively

(Figure 2.16a). Similarly, **P6P** also showed peaks at $2\theta = 6.02^\circ$ and 12.05° which corresponded to d-spacing values of 14.80 and 7.36 Å respectively (Figure 2.16b). In all these molecules, existence of the low angle peak corresponding to molecular length gave support for the smectic LC Phase (Figure 2.14).¹⁷ The Figure 2.14 compares the low angle X-ray measurements for the **PnP** series at room temperature which clearly indicated a shift in the peak position to lower angle with an increase in the oligooxyethylene segment indicating longer periodicity for the higher spacer members. Also noteworthy was the observation of the sharp peak around $2\theta \sim 25^\circ$ corresponding to a d spacing of ~ 3.5 Å in these **PnP** twin molecules which in aromatic molecules is usually attributed to the π stacking interaction. This feature was a clearly distinguishing one while comparing the packing in the **NpnNp** twin series (described below).

Compared with the phenylazo twin series, the naphthylazo twin series had lower clearing temperatures. This was expected since a lateral substitution on the core is known to cause reduction in clearing temperature. In the naphthylazo twin series, multiple transitions were observed in the DSC thermogram of **Np0** and **Np2Np**. Figure 2.11b shows the second heating and cooling scans in the DSC thermogram of **Np0** and **Np2Np** of the naphthyl series and their enthalpy values and phase transitions are given in Table 2.3. Model compound **Np0** exhibited two transitions both in the heating (126°C and 141°C) and cooling cycle (106°C ; 101°C) and observation under the PLM indicated spherulitic textures as shown in Figure 2.15e. The spherulitic phase remained frozen until room temperature and the texture was stable even after a month. The twin molecule **Np2Np** also exhibited spherulitic texture at 123°C upon cooling, (Figure 2.15f), which remained stable until room temperature. This was supported by the variable temperature WXR data of **Np0** and **Np2Np** taken at various intervals during cooling from the isotropic melt. Compared to the **PnP** series, **Np0** and **Np2Np** were crystalline and had several sharp reflections both in the low angle and wide angle region. But the oligooxyethylene segment packing that was observed in **PnP** series $\sim 2\theta = 20\text{-}25^\circ$ as well as the π stacking interaction observed $\sim 2\theta = 25^\circ$ were not observable in **Np2Np**. **Np4Np** and **Np6Np**, on the other hand, exhibited glass transition T_g during heating and cooling as shown in Figure 2.17. **Np4Np** also exhibited a melting transition at 139°C during the first heating cycle.

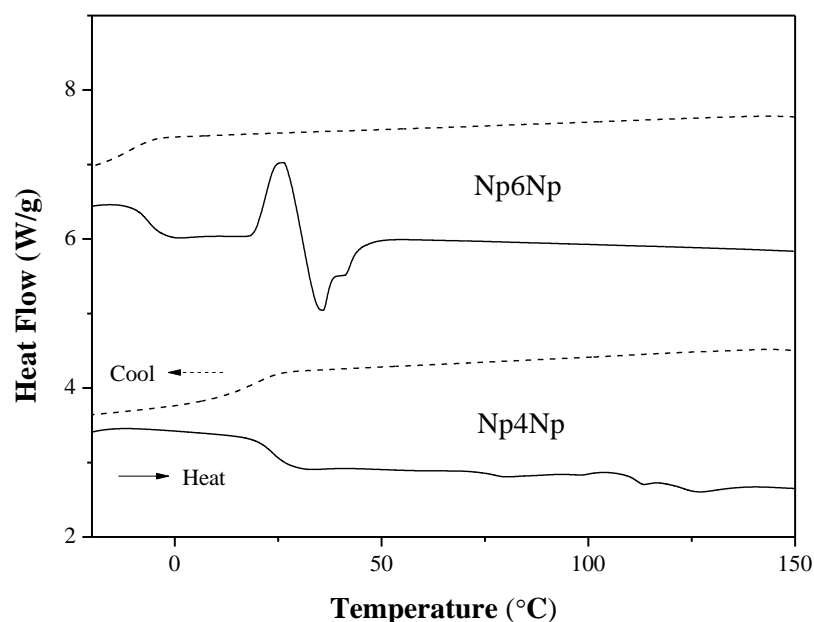


Figure 2.17 DSC thermograms of naphthyl twins *Np4Np* and *Np6Np*.

Subsequent cooling and heating cycles showed only a $T_g \sim 19^\circ\text{C}$. In the case of **Np6Np**, a melting transition was observed in the first heating cycle following which it showed a $T_g \sim -6^\circ\text{C}$ in the cooling cycle. In the second heating cycle, in addition to T_g a large cold crystallization exotherm and a sharp small endotherm were observed at 26°C and 36°C respectively, which could be attributed to the crystallization of the oligooxyethylene component. The lower glass transition temperature for **Np6Np** implied increased plasticization due to increased flexibility of the hexaethylene glycol spacer compared to tetraethylene glycol. From the above observation it was clearly evident that in **Np4Np** and **Np6Np** the thermal properties were determined mostly by the spacer than by the aromatic units.

2.3.3 Thermal Mesophase Characteristics of Azobenzene Copolymers

Linear aliphatic polyesters are generally crystalline and have low melting points (less than 100°C) with the melting points increasing with the number of methylene groups between the ester groups. When the diols are polyethylene glycols, the melting transition as well as the percentage crystallinity of the polymer decreases and for higher glycols, the polymers become amorphous. When aromatic units in the form of aromatic dicarboxylic acids are introduced into the polyester backbone, they not only

increased the melting transition but also induce thermotropic liquid crystallinity to the polymer. Additionally, π bond stabilization in the form of azo linkages have been shown to contribute to the rigidity of the ring, which also stabilizes the mesophase formation.¹⁸ For instance, the literature reports the mesophase characteristics of a series of low molecular weight polyesters formed by 4,4'-azodibenzoyl chloride with di, tri and tetra ethylene glycol.^{8c,19} The DEG based azo copolymers exhibited mesophase whereas the tri and tetra ethylene glycol based azo copolymers were not liquid crystalline.

The homopolymers of dimethyl sebacate with diethylene glycol and tetraethylene glycol – SD-homo and ST-homo were characterized for their thermal stability and crystallinity using TGA and DSC measurements. The homo as well as copolyesters were thermally stable till 300 °C (Figure 2.18). SD-homo was semicrystalline and exhibited cold crystallization and double melting peaks while heating, whereas sharp crystallization was observed at 8 °C while cooling.

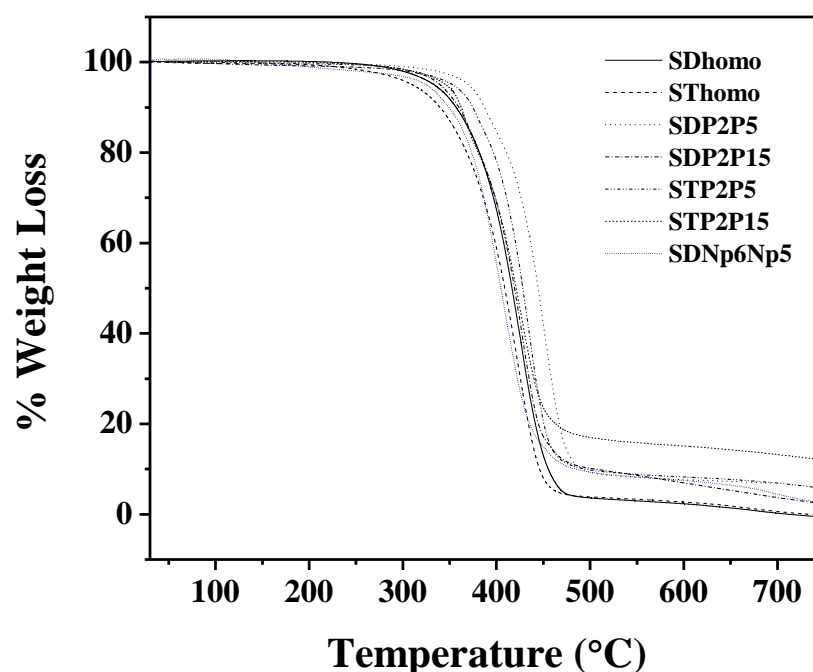


Figure 2.18 Thermal analysis of SD-homo, ST-homo, SDP2P15, STP2P15 and SDNp6Np5.

Such double melting transitions have been observed for the crystallization of other polymers also where it has been shown that it is an after effect of annealing during the DSC scan which results in crystallites with different degrees of perfection.²⁰ The

lower endotherm transition (at 34 °C) is due to the melting of initial crystallites produced during the crystallization process, while the higher temperature endotherm (47 °C) corresponds to crystal reorganization during melting (melting of more perfect crystals). Figure 8a shows the spherulitic crystals of SD-Homo observed under PLM after annealing the sample at 25 °C for one hour. On the other hand, increasing the chain length from di to tetra ethylene glycol resulted in a completely amorphous homopolymer – ST-homo. The DEG based copolymers incorporating varying mol % of the twin molecules **P2P** (short non-LC twin) and **P6P** (long LC twin) were analyzed for their thermal characteristics. Figure 2.19 compares the second heating and cooling cycles of twin molecule **P2P** and homopolymer SD-homo along with the respective copolymers **SDP2P-5** and **SDP2P-15**. **P2P** was not liquid crystalline and had a melting transition at 215 °C, which crystallized at 205 °C in the cooling cycle. The 5 mol % incorporation of **P2P** (**SDP2P-5**) exhibited a sharp melting transition at 34 °C (enthalpy of 44.6 J/g) with another broad weak transition around 65 °C (3.9 J/g). While cooling, a broad exotherm was observed (30 to -13 °C) with a sharp peak centered at -5 °C. Annealing the sample at 25 °C and observation under PLM showed the typical thread like pattern of the nematic phase as shown in Figure 2.20. An isothermal crystallization experiment was carried out by annealing the sample at 25 °C for 30 minutes, followed by rapid cooling to -5 °C. The sample was then heated at a rate of 10 °C/min which is also plotted (in red) along with the second heating cycle in Figure 2.19. It showed two endothermic transitions at 33 and 45 °C respectively similar to that of the SD-Homo. The isothermal annealing in the nematic phase followed by rapid cooling allowed for the reorganization of the crystals which was observed as the double melting in the following heating cycle.²⁰ Upon increasing the incorporation of **P2P** from 5 to 15 mole %, biphasic nature was evident in the DSC transitions with coexistence of two distinct phases. The first one corresponded to the crystalline regions of the sebacate and DEG polymer and the second corresponded to the liquid crystalline phase of the aromatic unit. In the first heating cycle, transition corresponding to the melting of the reorganized crystallites at 45 °C was visible along with two more transitions at lower temperatures 22 and 7 °C; and a higher one corresponding to the nematic to isotropic transition of the aromatic units at 92 °C.

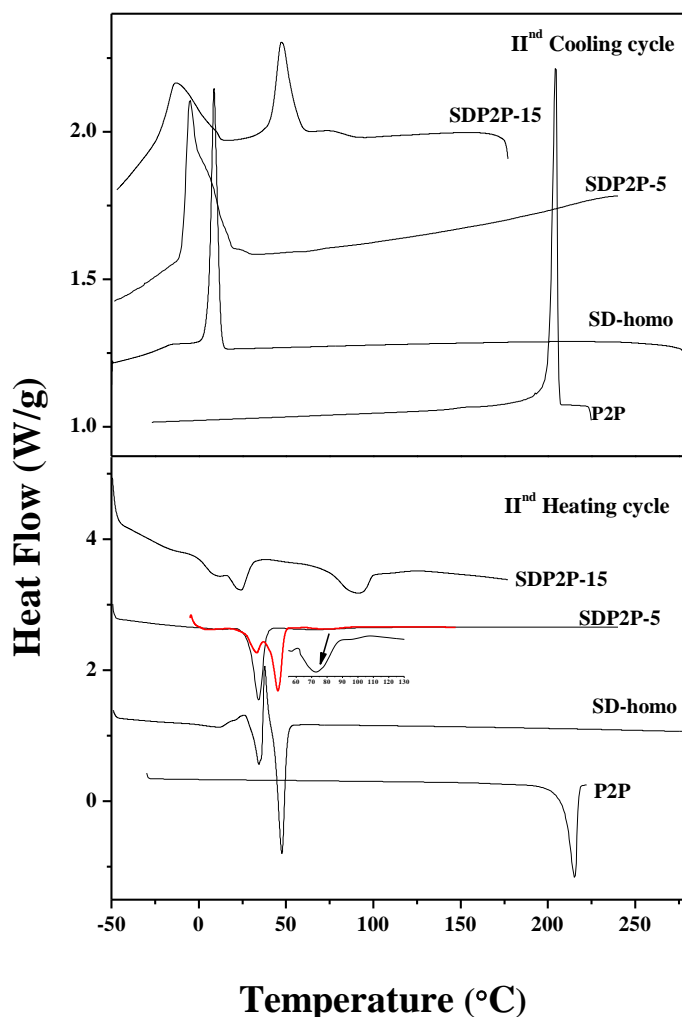


Figure 2.19 DSC thermograms of P2P, SD-homo, SDP2P-5 and SDP2P-15.

In the second heating cycle three endothermic transitions were observed at 10 °C, 24 °C (enthalpy 14.5 J/g) and 90 °C (enthalpy 8.4 J/g). Upon cooling, a grainy texture (figure 2.20c) was observed under PLM around 100 °C which produced typical nematic threads upon further cooling. Correspondingly, in DSC a weak transition (enthalpy 0.44 J/g) was observed around 92 °C. Variable temperature WXR D of **SDP2P-15** is given in Figure 2.21. The XRD pattern of the polymer was broad and had lesser number of peaks compared to that of the twin molecule indicating the lower crystallinity. Plots 'a' and 'b' at 140 and 100 °C respectively corresponded to isotropic phase, whereas plots 'c' and 'd' recorded at 88 and 85 °C respectively corresponded to the nematic phase. DSC showed a broad transition having a large

enthalpy of 9.3 J/g with a peak centered at 47 °C. Observation under PLM showed a change in texture around this temperature indicating formation of a more ordered smectic phase (Figure 2.20-d).²¹

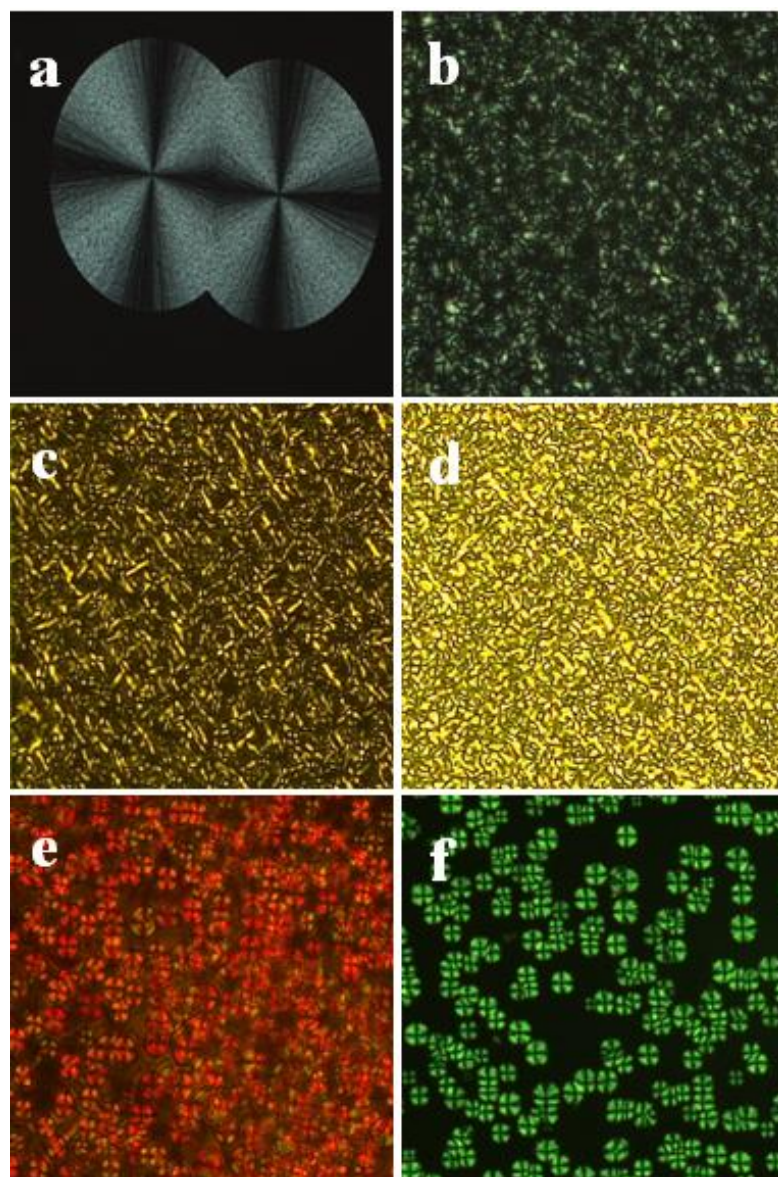


Figure 2.20 Polarized light microscope images of homopolymer and random azo copolymer a) *SD-homo*- 30 °C (Spherulitic crystalline phase) b) *SDP2P5*-30 °C (Nematic texture) c) *SDP2P15*- 77 °C (Nematic texture) d) *SDP2P15*- 45 °C (Smectic phase) e) *SDP6P30*- 91 °C (Nematic droplets) f) *STP2P15*- 30 °C (Nematic droplets). This was further confirmed by the appearance of more reflections in the wide angle region of the variable temperature WXRd recorded at this temperature (plot ‘e’).

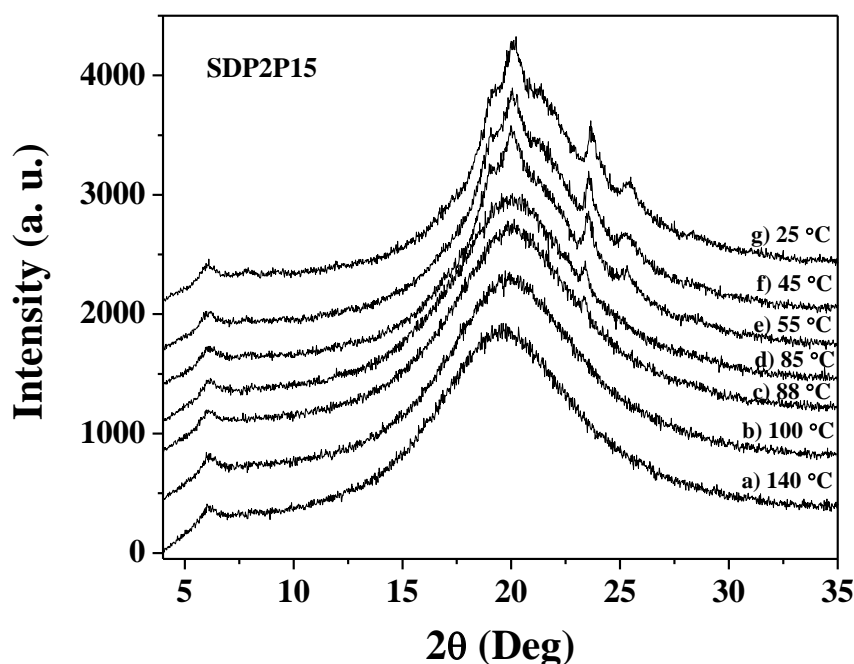


Figure 2.21 Variable temperature wide angle X-ray diffraction of random azo copolymer *SDP2P15*.

This ordered phase was retained until room temperature of 25 °C as observed under PLM as well as WXR. Higher incorporation of **P2P** in the DEG copolymer series was not possible due to practical reasons; however, the longer spacer twin molecule **P6P** could be incorporated up to 30 mole %. **SDP6P-5** did not exhibit a LC phase but only a melting and crystallization in the heating and cooling cycles respectively. Figure 2.22 compares the second heating and cooling cycles of **P6P**, **SD-Homo** along with that of **SDP6P-5** and **SDP6P-30** copolymers. Here also, at higher incorporation biphasic regions were distinguishable in the DSC thermogram, corresponding to the crystalline sebacate/DEG domains and liquid crystalline azoaromatic domains. Thus, multiple transitions were observed in the heating cycle of **SDP6P-30** and while cooling, nematic droplets were observed at around 90 °C under the PLM (Figure 2.20-e).

Three copolymers of the naphthylazo twin series were synthesized – **SDNp2Np-5**, **SDNp6Np-5** and **SDNp6Np-30** and were analyzed for their thermal characteristics. They did not exhibit any thermotropic liquid crystalline behavior. Compared to the phenylazo twin series, only the lowest member of the naphthylazo

twin molecule - **Np2Np** exhibited LC behavior; with the higher members already having lost the flexible/rigid balance required for mesophase formation.

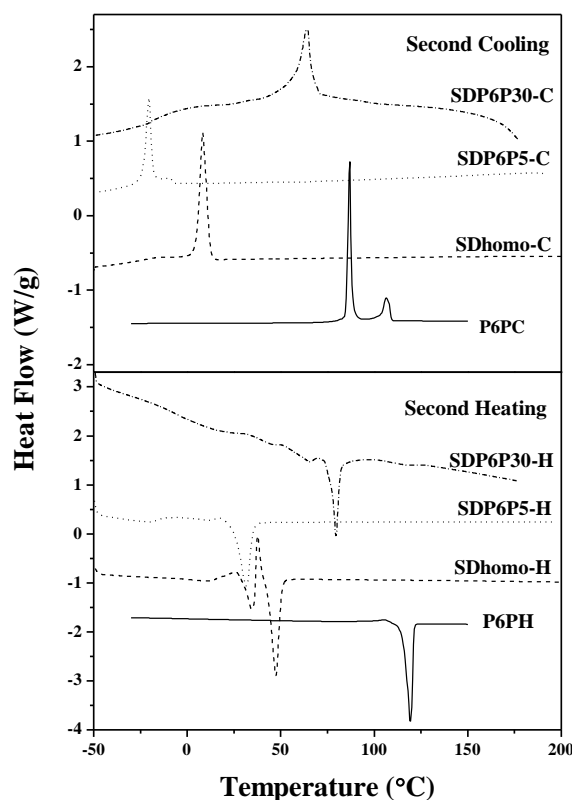


Figure 2.22 DSC thermograms of phenyl twin azobenzene **P6P**, homo polymer **SD-homo**, random azo-copolymers **SDP6P5** and **SDP6P30**.

The introduction of more flexible segments via copolymerization would be counter intuitive in inducing mesophase abilities in the **NpnNp** copolymer series.

A series of copolymers were developed using tetraethylene glycol (TEG) as the BB monomer instead of diethylene glycol. Since the naphthylazo copolymers did not exhibit any LC tendencies with DEG, the probability of mesophase formation with a more flexible TEG could be ruled out. Therefore only **P2P** and **P6P** were incorporated into copolyesters with dimethyl sebacate and TEG. 5 and 15 mole % incorporated **P2P**, viz., **STP2P-5** and **STP2P-15** were analyzed for their thermal properties. The DEG based copolymers were all obtained as solid powders whereas **STP2P-5** was a viscous liquid. The DSC thermogram of the ST-homo with that of its 5 and 15 mol% azo copolymers **STP2P-5** and **STP2P-15** shown in Figure 2.23. The ST homopolymer did not show any transition in the heating or cooling cycles.

STP2P-5 exhibited a cold crystallization followed by melting at 6 °C in the first heating cycle but in the subsequent cycles no transitions were observed.

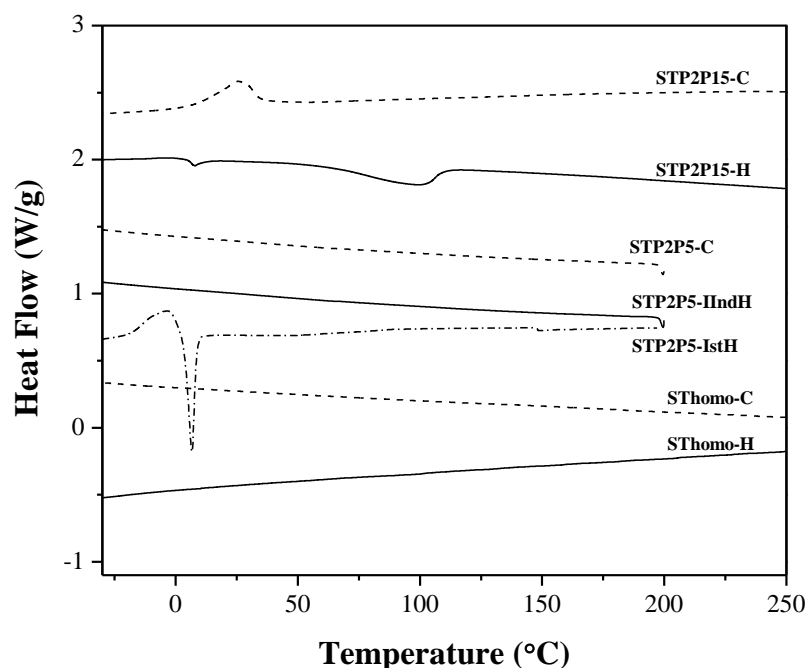


Figure 2.23 DSC thermograms of homopolymer *ST-homo*, random azo copolymers *STP2P5* and *STP2P15*.

After 15 mole % incorporation of **P2P**, new transitions were observed in the DSC thermogram of **STP2P-15**. Two transitions were observed at 8 and 99 °C while heating but only one transition was observed at around 25 °C while cooling. Annealing the sample at 80 °C resulted in the formation of nematic droplets (Figure 2.20-f) under the PLM. The copolymers **STP6P-5** and **STP6P-30** did not exhibit any mesophases when observed under PLM and their DSC also was devoid of any transitions.

2.4 Summary

Two new homologous azotwin series were synthesized and studied for the effect of varying central spacer length on liquid crystalline characteristics. These twin moieties were used as AA type monomers for the synthesis of segmented main chain azo copolyesters composed of sebacate and di or tetraethylene glycol. The short ($n = 2$) and long ($n = 6$) spacer twins in both **PnP** and **NpnNp** series were incorporated in varying mole ratios into main chain aliphatic copolyesters. At higher incorporation of the **PnP** twins, biphasic regions were observed in the DSC thermograms of both DEG and TEG copolymers and they exhibited liquid crystalline phases. On the other hand, **NpnNp** twins were unsuccessful in inducing mesogenicity even upon 30 mole % incorporation in DEG copolymers.

The liquid crystalline phase analysis of the two series of twin monomers and their main chain copolyesters thus showed that they were dependant on the length of oligooxyethylene spacer as well as the nature of azo chromophore (phenylazo vs. naphthylazo). Incorporation of “rigid azoaromatic twin” units into a non-mesogenic polymer helped to induce mesogenicity in the copolymer. Although the twin molecules exhibited smectic LC phases, their incorporation in the copolymer in low mole ratios resulted mostly in nematic LC phase. The randomness of the sequence along the copolymer chain would impose restrictions upon the translational mobility of the monomeric units of the polymer, thereby making it unfavorable for the formation of the layered smectic phases. The study presented here clearly showed that polymers incorporating the same mesogen (DEG and TEG copolymers) can behave differently depending on the nature of the flexible co monomer. The observation of mesogenicity is a complex phenomenon, especially in a random copolymer and both the “rigid” and the “flexible” spacer would be expected to have almost equal contribution in deciding the final outcome.

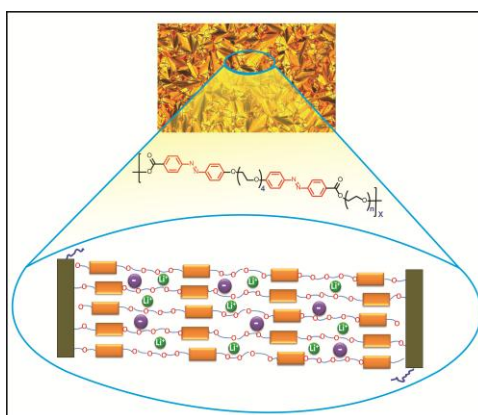
2.5 References

- (1) Hafiz, H. R.; Nakanishi, F. *Nanotechnology* **2003**, *14*, 649.
- (2) Ikeda, T.; Tsutsumi, O. *Science* **1995**, *268*, 1873-1875.
- (3) Kurihara, S.; Masumoto, K.; Nonaka, T. *App. Phys. Lett.* **1998**, *73*, 160-162.
- (4) Mativetsky, J. M.; Pace, G.; Elbing, M.; Rampi, M. A.; Mayor, M.; Samorì, P. *J. Am. Chem. Soc.* **2008**, *130*, 9192-9193.
- (5) Abrakhi, S.; Peralta, S.; Fichet, O.; Teyssié, D.; Cantin, S. *Langmuir* **2013**, *29*, 9499-9509.
- (6) Bai, S.; Zhao, Y. *Macromolecules* **2002**, *35*, 9657-9664.
- (7) (a) Smitha, P.; Asha, S. K.; Pillai, C. K. S. *J. Polym. Sci., Part A: Polym. Chem.* **2005**, *43*, 4455-4468 (b) Howe, L. A.; Jaycox, G. D. *J. Polym. Sci., Part A: Polym. Chem.* **1998**, *36*, 2827-2837 (c) Heldmann, C.; Schulze, M.; Wegner, G. *Macromolecules* **1996**, *29*, 4686-4696 (d) Xu, C.; Wu, B.; Becker, M. W.; Dalton, L. R.; Ranon, P. M.; Shi, Y.; Steier, W. H. *Chem. Mater.* **1993**, *5*, 1439-1444.
- (8) (a) Griffin, A. C.; Britt, T. R. *J. Am. Chem. Soc.* **1981**, *103*, 4957-4959 (b) Nieri, P.; Ramireddy, C.; Wu, C. N.; Munk, P.; Lenz, R. W. *Macromolecules* **1992**, *25*, 1796-1800 (c) Volksen, W.; Yoon, D. Y.; Cotts, P. M. *Macromolecules* **1989**, *22*, 3846-3850.
- (9) Imrie, C. T.; Henderson, P. A. *Chem. Soc. Rev.* **2007**, *36*, 2096-2124.
- (10) (a) Mingos, D. M. P.; Imrie, C. In *Liquid Crystals II*; Springer Berlin Heidelberg, 1999; Vol. 95 (b) Emsley, J. W.; Luckhurst, G. R.; Shilstone, G. N.; Sage, I. *Mol. Cryst. Liq. Cryst.* **1984**, *102*, 223-233.
- (11) (a) Kitazawa, S.; Kimura, K.; Shono, T. *Bull. Chem. Soc. Jpn.* **1983**, *56*, 3253-3257 (b) Judeinstein, P.; Roussel, F. *Adv. Mater.* **2005**, *17*, 723-727 (c) Djurado, D.; Delabouglise, D.; Caix-Cecillon, C.; Cecchetto, L.; Decker, I.; Petit, J. P. *Solid State Ionics* **2002**, *154-155*, 29-35.

- (12) Perrin D. D.; Armarego W. L. F.; Perrin D. R. *Purification of Laboratory Chemicals*; Pergamon Press, 1966.
- (13) Zollinger, H. *Azo and Diazo Chemistry, Aliphatic and Aromatic Compounds*; Interscience Publishers: New York, 1961.
- (14) Victor, J. G.; Torkelson, J. M. *Macromolecules* **1987**, *20*, 2241-2250.
- (15) Chen, D. T.-L.; Morawetz, H. *Macromolecules* **1976**, *9*, 463-468.
- (16) Iimura, K.; Koide, N.; Ohta, R.; Takeda, M. *Makromol. Chem.* **1981**, *182*, 2563-2568.
- (17) Although low angle peak from $2\theta = 0.5$ to 10° was recorded only at room temperature (25 °C), its existence could be expected in the smectic LC phase temperature also.
- (18) Braun, D.; Cherdron, H.; Rehahn, M.; Ritter, H.; Voit, B. *Polymer Synthesis: Theory and Practice : Fundamentals, Methods, Experiments*; Springer-Verlag Berlin Heidelberg, 2005.
- (19) Xu, Z.-S.; Drnoyan, V.; Natansohn, A.; Rochon, P. *J. Polym. Sci., Part A: Polym. Chem.* **2000**, *38*, 2245-2253.
- (20) Carpaneto, L.; Marsano, E.; Valenti, B.; Zanardi, G. *Polymer* **1992**, *33*, 3865-3872.
- (21) (a) Sepelj, M.; Lesac, A.; Baumeister, U.; Diele, S.; Nguyen, H. L.; Bruce, D. W. *J. Mater. Chem.* **2007**, *17*, 1154-1165 (b) Han, D.; Tong, X.; Zhao, Y.; Galstian, T.; Zhao, Y. *Macromolecules* **2010**, *43*, 3664-3671.

Chapter 3

Thermo and Photoresponsive Ionic Conductivity probed in Main Chain Liquid Crystalline Azobenzene Polyesters



Three series of main chain thermotropic liquid crystalline azobenzene polymers were synthesized using azobenzene twin molecules as the AA monomer and oligoxyethylene diols as the BB comonomer. The twin azobenzene moieties were terminally functionalized with $-C(O)OMe$ units to facilitate transesterification with diols to form polyesters. The combination of polar oligoxyethylene unit with non-polar rigid aromatic azo chromophore produced stable smectic mesophases in all the polymers and most of the polymers showed higher ordered smectic mesophase transition. One of the polymers - **Poly(P4PTEG)** was chosen to prepare composite polymer electrolytes with $LiCF_3SO_3$ and ionic conductivity was measured by a.c impedance spectroscopy. The polymer/0.3 Li salt complex exhibited a maximum ionic conductivity in the range of $10^{-5} S cm^{-1}$ at room temperature ($25\text{ }^\circ C$), which increased to $10^{-4} S cm^{-1}$ above $65\text{ }^\circ C$. Reversible ionic conductivity switching was observed upon irradiation of the polymer/0.3 Li salt complex with alternate UV and visible irradiation.

3.1 Introduction

Liquid crystalline azobenzene polymers have generated a lot of interest due to their potential application in a variety of areas like optical data storage, molecular switches, display devices, photomechanical systems, etc.¹ Main chain azobenzene polymers that have a large liquid crystalline window in the processable temperature range $< 200\text{ }^{\circ}\text{C}$ are very interesting. Liquid crystalline polymers, oligomers and low molecular weight compounds based on poly(ethylene oxide) (PEO) have shown promise as solid electrolytes.² The oligoethylene oxide segment can bind to alkali metals through ion-dipole interactions which can stabilize as well as induce various self organized liquid crystalline phases.^{2a,3} For instance, a rod coil polymer containing PEO upon complexation with LiCF_3SO_3 exhibited phase transitions from the highly ordered smectic phase followed by cubic and finally cylindrical micellar mesophase upon increasing Li ion salt concentration.⁴ Recently Kato *et al.* showed anisotropic ion conduction in free standing film of a side chain LC polymer containing oligoethylene oxide unit (Figure 3.1).

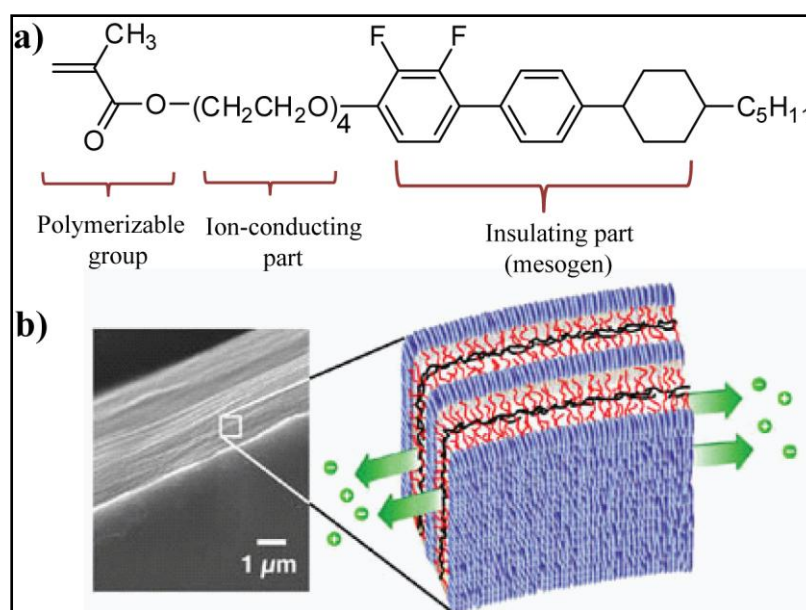


Figure 3.1-a) Chemical structure of ion conductive LC monomer and b) macroscopically oriented self standing film FE-SEM image, carton depicts 2D ion conduction in LC aligned film. (Adapted from *J. Am. Chem. Soc.* **2003**, 125, 3196-3197).

The LC aligned monomer was photopolymerized to get layered nanostructure at room temperature.^{2a} However, the PEO-salt complexes have an inherent tendency for crystallization which retards effective ion transport through polymer matrix. The incorporation of PEO into various polymer architectures like copolymers, block copolymers, comb shaped polymers, hyperbranched polymers etc. have been attempted to circumvent the problem of crystallization by forming amorphous polymers (Figure 3.2).⁵

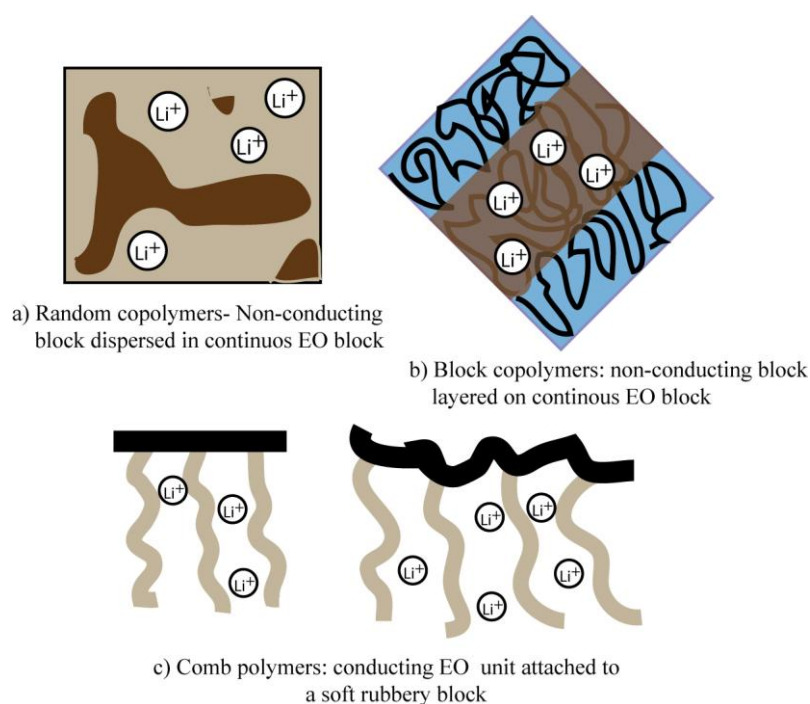


Figure 3.2 Common copolymer templates for the synthesis of solid polymer electrolytes (SPEs).

The structural design consisting of a rigid mesogen and flexible oxyethylene units is expected to lead to ion conductive liquid crystalline materials. The LC materials have simultaneous fluidity as well as ordering, which can help fast transport of ions. Due to their ordered fluidic characteristic, LCs could be ideal candidate for solvent free electrolytes. The segmental mobility on the molecular scale affords faster ion transport and the ordered structures on the nanometer scale impart mechanical strength. The utilization of the photoresponsive azobenzene as the rigid mesogen has the added advantage of providing a photoinduced ion-conductive switching.⁶

Extensive research in the early 1990's by the group of Kimura *et al.* addressed the effectiveness of a combination of materials like suitable polymer matrix for processability, liquid crystalline molecule for thermal stimuli, azobenzene units for photostimuli, crown ether derivatives as ion conducting carriers and lithium salt for ionic conductivity for developing higher-performing ionically conducting composite films.^{6a} They also prepared vinyl polymers having varying mole ratios of crowned azobenzene and mesogenic biphenyl moieties in the side chain as single polymeric photoresponsive ion conducting materials (Figure 3.3).^{6d} The reversible photoisomerization of the azobenzene in the side chain perturbed the liquid crystalline organization, which in turn, disrupted the ionic conductivity through the ion-hopping crown ether sites resulting in reversible photoswitching.

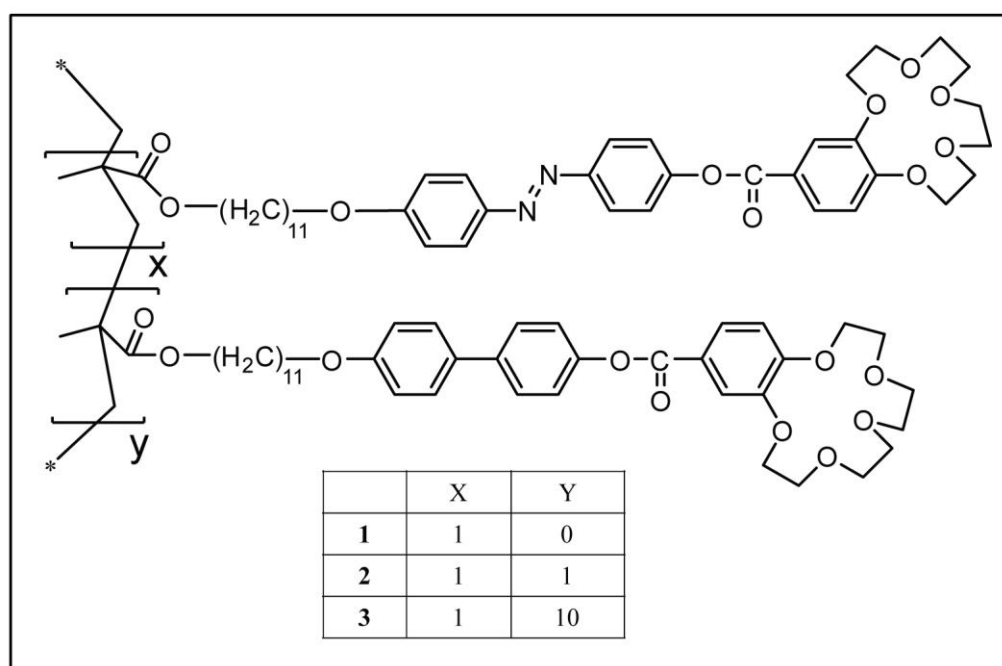


Figure 3.3 Photoresponsive ion-conducting vinyl copolymers carrying crowned azobenzene and biphenyl moieties in the side chain.^{6d}

In the previous chapter we presented a twin molecular design having the structure azobenzene-oligooxy ethylene-azobenzene as a versatile AA-type monomer for melt polycondensation polymerization.⁷ The twin monomer design successfully addressed two issues, firstly it lowered the melting temperature of the molecule as

well as improved its solubility thereby enabling the melt condensation at lower temperatures which would have otherwise degraded the azo monomer and secondly the balance of rigid and flexible units resulted in stable mesophases due to the mutual non solubility. The previous chapter described incorporation of two types of azotwin molecules - a phenyl azotwin and a naphthyl azotwin (A-A type monomer) into a main chain copolyester backbone in various ratios along with dimethyl sebacate (A'-A' type monomer) where di or tetra ethylene glycol (DEG/TEG) was used as the B-B type monomer. In the present chapter, we have explored main chain polyesters of the phenylazo twin molecule with various diols (BB monomer) like diethylene glycol (DEG), tetraethylene glycol (TEG) and hexaethylene glycol (HEG) to form three homologous series of polyesters. The polymers were structurally characterized and their mesophase characteristics were determined using differential scanning calorimetry (DSC), polarizing light microscope (PLM) and variable temperature wide angle X-ray diffraction (VT-WXRD) studies. One of the polymers – **Poly(P4PTEG)** – was further complexed with LiCF_3SO_3 salt and its ionic conductivity was measured at room temperature as well as in the liquid crystalline (LC) and isotropic phases. The photo response of ionic conductivity was studied at room temperature by alternate UV and visible light irradiation on films formed by the polymer/Li salt complex.

3.2 Experimental section

3.2.1 Materials

Di, tetra and hexa ethylene glycol, p-amino benzoic acid, phenol, titanium tetrabutoxide ($\text{Ti}(\text{OBu})_4$), p-toulene sulphonyl chloride and lithium triflate (LiCF_3SO_3) were purchased from Aldrich Company Ltd and were used as such. Sodium nitrite, potassium carbonate and potassium iodide were purchased from Merck Chemicals Ltd. Dimethyl formamide (DMF), tetrahydrofuran (THF), acetone and methanol were purchased Merck Chemicals Ltd. and purified using standard procedures.

3.2.2 Instrumentation

^1H -NMR and ^{13}C -NMR spectra of polymers were recorded on a Bruker-AVANCE 200 MHz spectrometer using CDCl_3 or CDCl_3/TFA as solvent. The molecular weight

of the polymers was determined using a Polymer Laboratories PL-GPC-220 Gel Permeation Chromatography (GPC) with CHCl_3 as eluent. The inherent viscosity (η_{inh}) of the polymers was measured for 0.5 g/dL concentration solutions in chloroform as solvent. Infrared spectra were recorded using Bruker FT-IR (ATR mode) spectrophotometer in the range of 4000-600 cm^{-1} . The thermal characterization of the polymers were carried out using a PerkinElmer STA-6000 thermogravimetric analyser (TGA) under nitrogen atmosphere from 40-800 °C at 10 °C /min as well as a TA Q10 model Differential Scanning Calorimeter (DSC). The DSC instrument was calibrated with indium standards and scanned at 10 °C/min under nitrogen atmosphere. The phase behaviour of the polymers were analyzed using LIECA DM2500P polarized optical microscope equipped with Linkam TMS 94 heating and cooling stage connected to a Linkam TMS 600 temperature programmer. Wide Angle X-ray Diffractograms (WXR) was performed using a Rigaku, MicroMax-007HF with high intensity Microfocus rotating anode X-ray generator. All the samples were recorded in the (2θ) range of 2–50 degrees and data was collected with the help of Control Win software. The radiation used was $\text{CuK}\alpha$ (1.54 Å) with a Ni filter, and the data collection was carried out using an Aluminium holder. Variable temperature in situ X-ray diffraction of samples was carried out in a PANalytical X'pert Pro dual goniometer diffractometer. An X'celerator solid-state detector was employed in wide-angle experiments. The radiation used was $\text{Cu K}\alpha$ (1.54 Å) with a Ni filter and the data collection carried out in an Anton-Paar XRK900 reactor. Ionic conductivity of the polymer complexes was measured using a Bio-Logic instrument with Potentio electrochemical impedance spectroscopy (PEIS) technique. The response of the material was recorded in the form of Nyquist plot in the frequency range of 1 MHz to 100 mHz with an amplitude of 10 mV. The photoisomerization was performed as described previously using a DYMAX Blue Wave 75 watt short arc mercury vapor lamp as light source with an output wavelength in the range 280-450 nm using a 360 nm bandpass filter for UV irradiation and 450 nm bandpass filter for visible light irradiation.⁸

3.2.3 Synthesis and Characterization

Synthesis of twinazobenzene monomers

The synthesis and detailed structural characterization of phenyl azo twin monomers was already given in previous chapter.

Synthesis of main chain azo polymers:

Poly(P2PDEG): The polymerization was carried out in a homemade test tube shaped polymerization apparatus by taking monomers α, ω -bis(4-diethyleneoxyphenyl-4'-azophenyl)methylbenzoate (P2P) (0.500 g, 0.858 mmol) and diethylene glycol (DEG) (0.091 g, 0.858 mmol). The contents were melted in an oil bath at 160 °C with constant stirring and a small amount (0.5 mL) of DMAc solvent was added. After homogenous melt formation, the reaction mixture was cooled to room temperature (25 °C) and 1 mol % of titaniumtetrabutoxide (Ti(OBu)₄) catalyst was added. Continuous nitrogen purge was provided to make the polycondensation apparatus oxygen and moisture free. The reaction mixture was further heated to 160 °C with slow nitrogen purge for 4 h. The resultant precondensate was further subjected to high vacuum (0.01 mm of Hg) at 170 °C for 2 h. The formed polymer was dispersed in methanol and filtered to get the main chain azo polyester. The polymer was further purified by soxhlet extraction in acetone and hexane, dried in vacuum oven at 45 °C for 24 h. Yield = 0.55 g (89 %). ¹H NMR (200 MHz CDCl₃+TFA): δ (ppm): 8.12 (4H, d, Ar), 7.92 (8H, m, Ar), 7.04 (4H, d, Ar), 4.60 (4H, t, Ar-C(O)-OCH₂-CH₂O), 4.33 (4H, t, Ar-OCH₂-CH₂O), 4.15-3.99 (8H, m, oligoethyleneoxy region), 3.76-3.62 (16H, m, oligoethyleneoxy region). FTIR (ATR) (cm⁻¹): 2921, 2871, 1709, 1589, 1493, 1445, 1403, 1239, 1133, 1092, 921, 832, 766, 722, 686.

Poly(P2PTEG): A similar procedure to that of **Poly(P2PDEG)** was adopted using α, ω -bis(4-diethyleneoxyphenyl-4'-azophenyl)methylbenzoate (P2P) (0.500 g, 0.858 mmol) and tetraethylene glycol (TEG) (0.167 g, 0.858 mmol). The polymer was purified by soxhlet extraction in acetone and hexane, dried in vacuum oven at 45 °C for 24 h.

Yield = 0.57 g (90 %). ¹H NMR (200 MHz CDCl₃): δ (ppm): 8.16 (4H, d, Ar), 7.89 (8H, m, Ar), 7.02 (4H, d, Ar), 4.48 (4H, t, Ar-C(O)-OCH₂-CH₂O), 4.24 (4H, t, Ar-

OCH₂-CH₂O), 3.97 (Ar-C(O)-OCH₂-CH₂O), 3.83 (4H, t, Ar-OCH₂-CH₂O), 3.69-3.66 (8H, m, oligoethyleneoxy region). ¹³C NMR (CDCl₃) δ ppm: 166.01, 161.74, 155.32, 147.11, 131.17, 130.66, 130.55, 125.15, 122.33, 114.91, 77.32, 76.69, 70.71, 70.69, 69.85, 69.19, 67.78, 64.28. FTIR (ATR) (cm⁻¹): 2916, 2872, 1711, 1593, 1495, 1451, 1404, 1241, 1092, 923, 831, 766, 722, 686.

Poly(P2PHEG): A similar procedure to that of **Poly(P2PDEG)** was adopted using α,ω -bis(4-diethyleneoxyphenyl-4'-azophenyl)methylbenzoate (P2P) (0.800 g, 1.373 mmol) and hexaethylene glycol (HEG) (0.387 g, 1.373 mmol). The polymer was purified by soxhlet extraction in acetone and hexane, dried in vacuum oven at 45 °C for 24 h.

Yield = 0.80 g (73 %). ¹H NMR (200 MHz CDCl₃): δ (ppm): 8.16 (4H, d, Ar), 7.90 (8H, m, Ar), 7.02 (4H, d, Ar), 4.48 (4H, t, Ar-C(O)-OCH₂-CH₂O), 4.24 (4H, t, Ar-OCH₂-CH₂O), 3.97 (Ar-C(O)-OCH₂-CH₂O), 3.83 (4H, t, Ar-OCH₂-CH₂O), 3.69-3.66 (12H, m, oligoethyleneoxy region). ¹³C NMR (CDCl₃) δ ppm: 166.01, 161.74, 155.32, 147.11, 131.17, 130.66, 130.55, 125.14, 122.32, 114.91, 70.67, 70.59, 70.55, 69.85, 69.16, 67.78, 64.29. FTIR (ATR) (cm⁻¹): 2912, 2875, 1713, 1595, 1497, 1453, 1408, 1245, 1098, 928, 853, 771, 690.

Poly(P4PDEG): The polymerization was carried out in a homemade test tube shaped polymerization apparatus by taking monomers α,ω -bis(4-tetraethyleneoxyphenyl-4'-azophenyl)methylbenzoate (P4P) (0.500 g, 0.745 mmol) and diethylene glycol (DEG) (0.079 g, 0.745 mmol). The contents were melted in an oil bath at 170 °C with constant stirring. After homogenous melt formation, the reaction mixture was cooled to room temperature (25 °C) and 1 mol % of titaniumtetrabutoxide (Ti(OBu)₄) catalyst was added. Continuous nitrogen purge was provided to make the polycondensation apparatus oxygen and moisture free. The reaction mixture was further heated to 170 °C with slow nitrogen purge for 4 h. The resultant precondensate was further subjected to high vacuum (0.01 mm of Hg) at 170 °C for 2 h. The formed polymer was dissolved in chloroform, filtered to remove the catalyst and precipitated twice in cold methanol to get the main chain azo polyester.

Yield = 0.41 g (77 %). ^1H NMR (200 MHz CDCl_3): δ (ppm): 8.13 (4H, d, Ar), 7.85 (8H, m, Ar), 6.97 (4H, d, Ar), 4.53 (4H, t, Ar-C(O)-OCH₂-CH₂O), 4.19 (4H, t, Ar-OCH₂-CH₂O), 3.93 (3H, s Ar-C(O)-CH₃ from end group), 3.90-3.87 (8H, m, oligooxyethylene region), 3.76-3.62 (4H, m, oligooxyethylene region). ^{13}C NMR (CDCl_3) δ ppm: 166.58, 161.84, 155.28, 147.04, 131.16, 130.62, 130.54, 125.12, 122.34, 114.88, 70.87, 70.69, 69.57, 67.76, 64.09, 52.23. FTIR (ATR) (cm^{-1}): 2948, 2866, 1714, 1594, 1496, 1437, 1276, 1247, 1135, 1100, 1056, 944, 835, 770, 724, 689.

Poly(P4PTEG): A similar procedure as that reported for **Poly(P4PDEG)** was adopted using α,ω -bis(4-tetraethyleneoxyphenyl-4'-azophenyl) methylbenzoate (P4P) (0.500 gm, 0.746 mmol) and tetraethylene glycol (TEG) (0.145 gm, 0.746 mmol). The methanol precipitated polymer was further purified by soxhlet extraction in acetone and hexane, dried in vacuum oven at 45 °C for 24 h.

Yield = 0.48 g (80 %). ^1H NMR (200 MHz CDCl_3): δ (ppm): 8.15 (4H, d, Ar), 7.88 (8H, m, Ar), 7.01 (4H, d, Ar), 4.48 (4H, t, Ar-C(O)-OCH₂-CH₂O), 4.19 (4H, t, Ar-OCH₂-CH₂O), 3.93 (s Ar-C(O)-CH₃ from end group), 3.92-3.77 (8H, m, oligooxyethylene region), 3.74-3.66 (12H, m, oligooxyethylene region). ^{13}C NMR (CDCl_3) δ ppm: 166.00, 161.82, 155.28, 146.99, 130.64, 130.53, 125.11, 122.31, 114.86, 70.86, 69.55, 67.72, 64.26, 52.25. FTIR (ATR) (cm^{-1}): 2901, 2868, 1713, 1596, 1497, 1453, 1406, 1248, 1129, 1100, 928, 841, 772, 689.

Poly(P4PHEG): A similar procedure as that reported for **Poly(P4PDEG)** was adopted using α,ω -bis(4-tetraethyleneoxyphenyl-4'-azophenyl) methylbenzoate (P4P) (0.400 g, 0.596 mmol) and hexaethylene glycol (HEG) (0.168 g, 0.596 mmol). The methanol precipitated polymer was further purified by soxhlet extraction in acetone and hexane, dried in vacuum oven at 45 °C for 24 h.

Yield = 0.44 g (82 %). ^1H NMR (200 MHz CDCl_3): δ (ppm): 8.15 (4H, d, Ar), 7.89 (8H, m, Ar), 7.01 (4H, d, Ar), 4.48 (4H, t, Ar-C(O)-OCH₂-CH₂O), 4.20 (4H, t, Ar-OCH₂-CH₂O), 3.93 (1H, s Ar-C(O)-CH₃ from end group), 3.92-3.77 (8H, m, oligooxyethylene region), 3.78-3.55 (24H, m, oligooxyethylene region). ^{13}C NMR

(CDCl₃) δ ppm: 165.99, 161.85, 155.27, 146.98, 131.10, 130.64, 125.12, 122.29, 114.87, 70.83, 70.58, 70.52, 69.52, 67.73, 64.27, 52.25. FTIR (ATR) (cm⁻¹): 2901, 2867, 1711, 1596, 1498, 1453, 1407, 1363, 1247, 1096, 928, 838, 771, 690.

Poly(P6PDEG): A similar procedure to that of **Poly(P4PDEG)** was adopted using α,ω -bis(4-hexaethyleneoxyphenyl-4'-azophenyl)methylbenzoate (P6P) (0.400 g, 0.527 mmol) and diethylene glycol (DEG) (0.059 g, 0.527 mmol). The polymer was dissolved in CHCl₃, filtered to remove catalyst and precipitated in cold methanol twice to obtain the azo main chain polyester.

Yield = 0.55 g (79 %). ¹H NMR (200 MHz CDCl₃): δ (ppm): 8.12 (4H, d, Ar), 7.92 (8H, m, Ar), 7.04 (4H, d, Ar), 4.60 (4H, t, Ar-C(O)-OCH₂-CH₂O), 4.33 (4H, t, Ar-OCH₂-CH₂O), 4.15-3.99 (8H, m, oligoethyleneoxy region), 3.76-3.62 (16H, m, oligoethyleneoxy region). ¹³C NMR (CDCl₃) δ ppm: 166.56, 161.82, 155.26, 146.99, 131.12, 130.52, 125.09, 122.31, 114.86, 70.83, 70.56, 69.51, 67.71, 52.22. FTIR (ATR) (cm⁻¹): 2921, 2871, 1709, 1589, 1493, 1445, 1403, 1239, 1133, 1092, 921, 832, 766, 722, 686.

Poly(P6PTEG): A similar procedure to that of **Poly(P4PDEG)** was adopted using α,ω -bis(4-hexaethyleneoxyphenyl-4'-azophenyl)methylbenzoate (P6P) (0.450 g, 0.593 mmol) and tetraethylene glycol (TEG) (0.115 g, 0.593 mmol). The polymer was dissolved in CHCl₃, filtered to remove catalyst and precipitated in cold methanol twice to obtain the azo main chain polyester.

Yield = 0.57 g (91 %). ¹H NMR (200 MHz CDCl₃): δ (ppm): 8.16 (4H, d, Ar), 7.89 (8H, m, Ar), 7.02 (4H, d, Ar), 4.48 (4H, t, Ar-C(O)-OCH₂-CH₂O), 4.24 (4H, t, Ar-OCH₂-CH₂O), 3.97 (Ar-C(O)-OCH₂-CH₂O), 3.83 (4H, t, Ar-OCH₂-CH₂O), 3.69-3.66 (8H, m, oligoethyleneoxy region). ¹³C NMR (CDCl₃) δ ppm: 166.00, 161.83, 155.30, 146.99, 131.09, 130.64, 130.53, 125.11, 122.30, 114.87, 70.84, 70.66, 70.58, 69.52, 69.16, 67.72, 64.25, 63.45, 62.83, 52.23. FTIR (ATR) (cm⁻¹): 2916, 2872, 1711, 1593, 1495, 1451, 1404, 1241, 1092, 923, 831, 766, 722, 686.

Poly(P6PHEG): A similar procedure to that of **Poly(P4PDEG)** was adopted using α,ω -bis(4-hexaethylenoxyphenyl-4'-azophenyl)methylbenzoate (P6P) (0.500 g, 0.659 mmol) and hexaethylene glycol (HEG) (0.186 g, 0.659 mmol). The polymer was dissolved in CHCl_3 , filtered to remove catalyst and precipitated in cold methanol twice to obtain the azo main chain polyester.

Yield = 0.52 gm (80 %). ^1H NMR (200 MHz CDCl_3): δ (ppm): 8.16 (4H, d, Ar), 7.90 (8H, m, Ar), 7.01 (4H, d, Ar), 4.48 (4H, t, Ar-C(O)-OCH₂-CH₂O), 4.20 (4H, t, Ar-OCH₂-CH₂O), 3.93 (1H, s Ar-C(O)-CH₃ from end group), 3.92-3.77 (8H, m, oligoethyleneoxy region), 3.78-3.55 (32H, m, oligoethyleneoxy region). ^{13}C NMR (CDCl_3) δ ppm: 166.55, 165.99, 161.85, 155.27, 146.98, 131.10, 130.64, 130.52, 125.12, 122.29, 114.87, 70.83, 70.63, 70.58, 70.52, 69.52, 69.13, 67.73, 64.27, 52.22. FTIR (ATR) (cm^{-1}): 2916, 2870, 1711, 1597, 1498, 1454, 1407, 1353, 1248, 1092, 943, 835, 771, 723, 690.

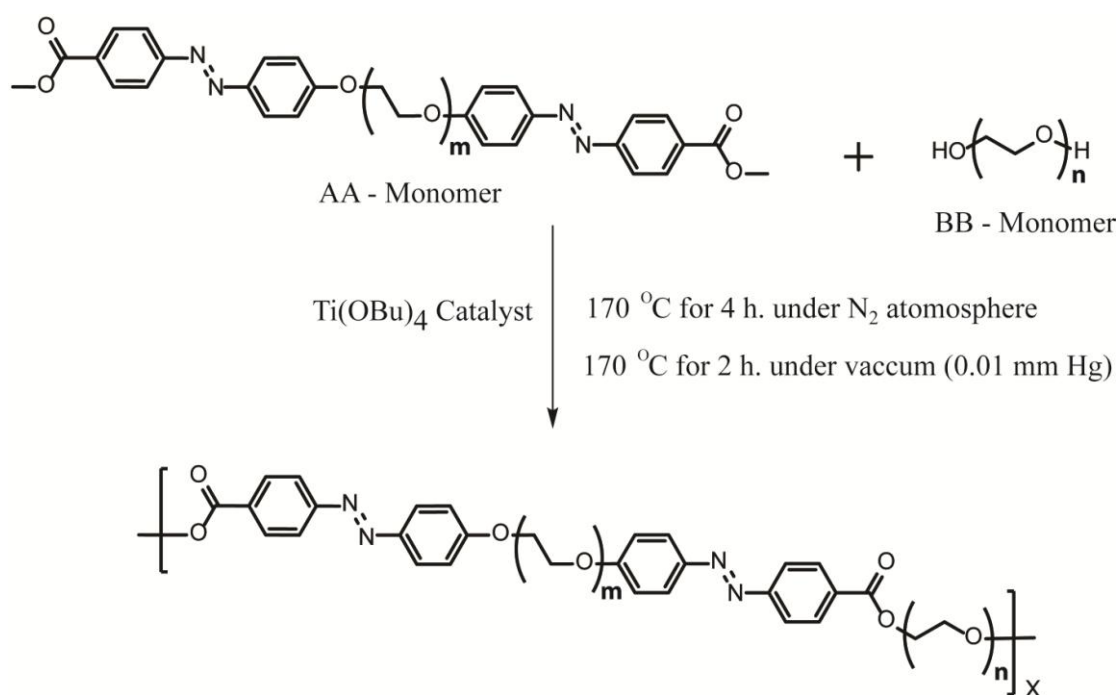
Preparation of Complexes:

Complexes of **Poly(P4PTEG)** with lithium triflate were prepared by mixing solutions of **Poly(P4PTEG)** (10 mg/mL) in dry THF solvent with an appropriate amount of lithium triflate salt. The solution was stirred for 24 h under N_2 atmosphere followed by slow evaporation of the solvent at room temperature and subsequent drying in vacuum oven at 50 °C. The polymer to lithium triflate salt ratio was varied from 0.01, 0.03, 0.05, 0.1, 0.2 to 0.3 moles per ethyleneoxy unit (total ethyleneoxy unit in the repeating unit).

3.3 Results and Discussion

The detailed procedure for synthesis and thermal characterization of twin azo monomers has been already discussed in previous chapter. The synthesis of azo main chain polyesters are shown in Scheme 3.1. The main chain polyesters were synthesized by polycondensation reaction of azo twin dimethyl esters (**P2P**, **P4P** and **P6P**; AA type monomer) with oligoethoxy ethylene (BB type monomer) namely DEG, TEG and HEG. All polymers except the **P2P** series were synthesized using melt polycondensation route; a small amount of dimethyl acetamide (DMAc) as a solvent

had to be added during first step of polymerization for the short spacer **P2P** based polymers due to the rather high melting point of **P2P** (< 200 C azobenzene



	P2P Series (m=2)	P4P Series (m=4)	P6P Series (m=6)
n=2	Poly(P2PDEG)	Poly(P4PDEG)	Poly(P6PDEG)
n=4	Poly(P2PTEG)	Poly(P4PTEG)	Poly(P6PTEG)
n=6	Poly(P2PHEG)	Poly(P4PHEG)	Poly(P6PHEG)

Scheme 3.1 Synthesis of main chain azo copolyesters.

decomposition). A step wise temperature protocol was followed during the polymerization, details of which are given in the synthesis part. The incorporation of azobenzene in the main chain polyester backbone was confirmed by $^1\text{H-NMR}$ spectroscopy. The $^1\text{H-NMR}$ spectra of P2P series of azo polymers e.g. **Poly(P2PDEG)**, **Poly(P2PTEG)** and **Poly(P2PHEG)** are shown in Figure 3.4. The new peak at ~ 4.5 ppm (highlighted by arrow) corresponding to the new aromatic ester linkage between twin azo and diol monomer confirmed covalent incorporation of azo dye in the polymer backbone. Similar observation was observed in the case of **P4P** and **P6P** series of polymers, which are shown in Figure 3.5 and 3.6 respectively. The molecular weight and molecular weight distribution of polymers was determined

by gel permeation chromatography (GPC) in chloroform as solvent and the values are given in Table 3.1. The GPC plot is given in Figure 3.7. The **Poly(P2PDEG)** was not soluble enough to record the GPC.

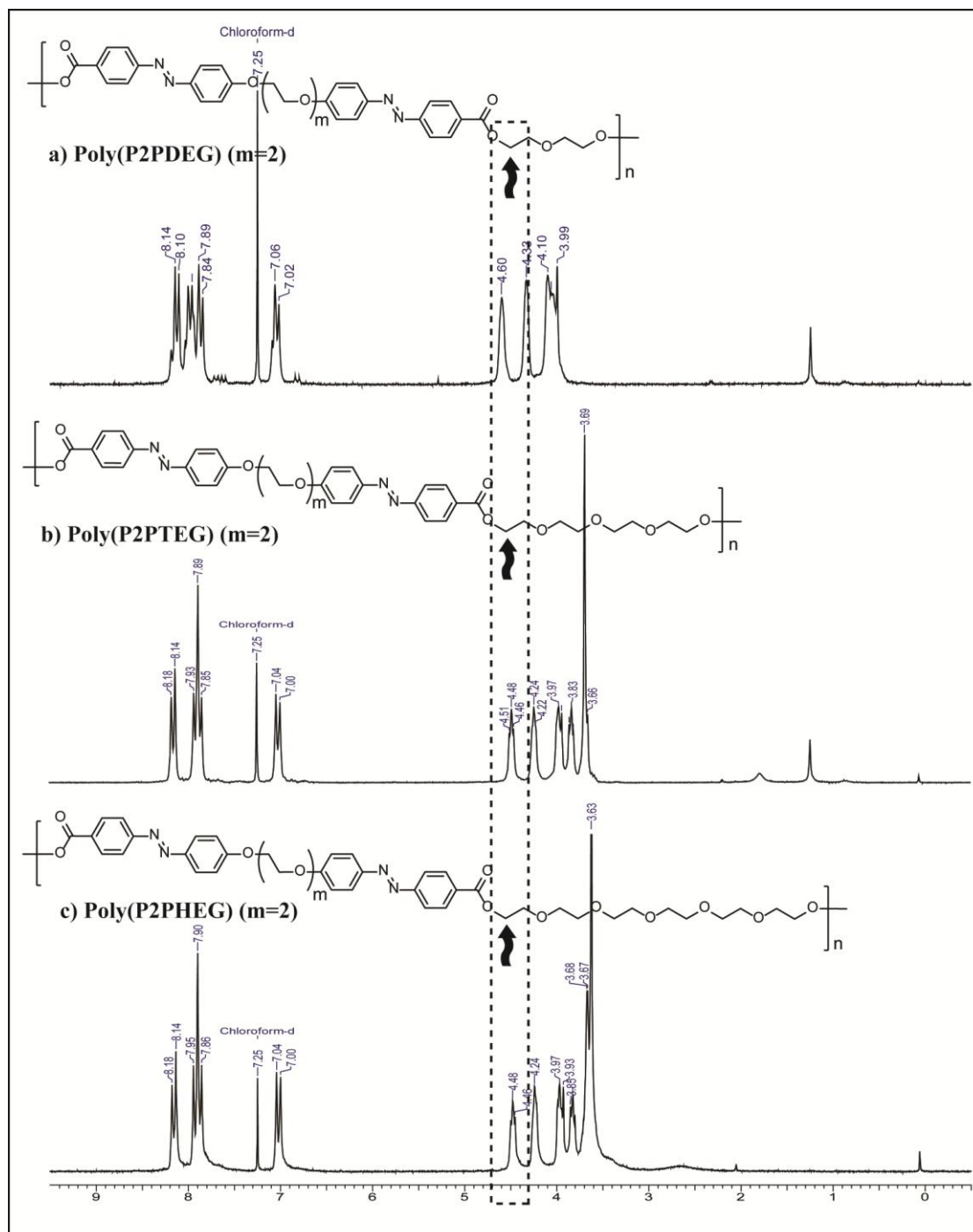


Figure 3.4 $^1\text{H-NMR}$ spectra of main chain azo polymers **Poly(P2PDEG)**, **Poly(P2PTEG)** and **Poly(P2PHEG)** recorded in CDCl_3 .

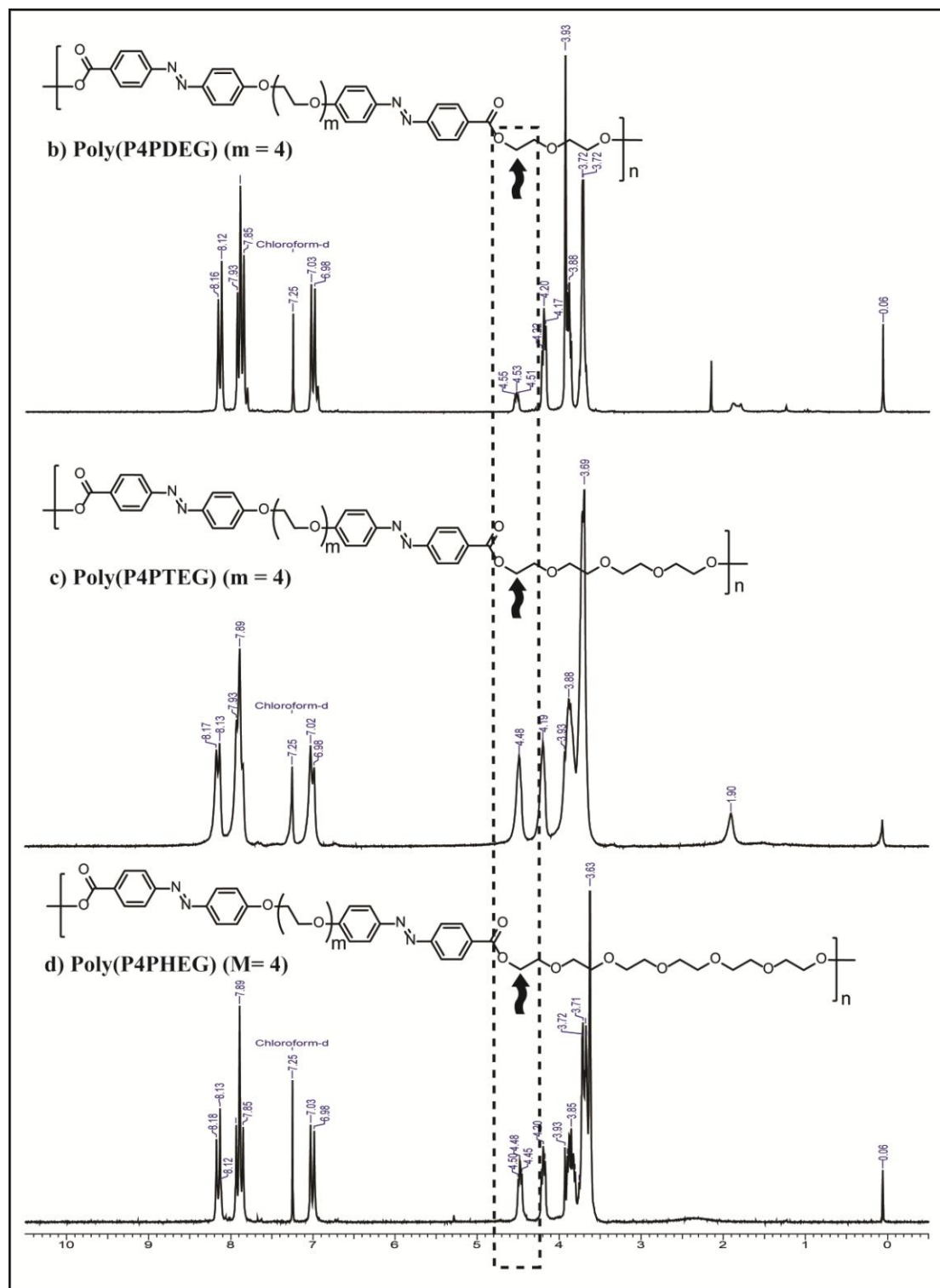


Figure 3.5 $^1\text{H-NMR}$ spectra of main chain azo polymers **Poly(P4PDEG)**, **Poly(P4PTEG)** and **Poly(P4PHEG)** recorded in CDCl_3 .

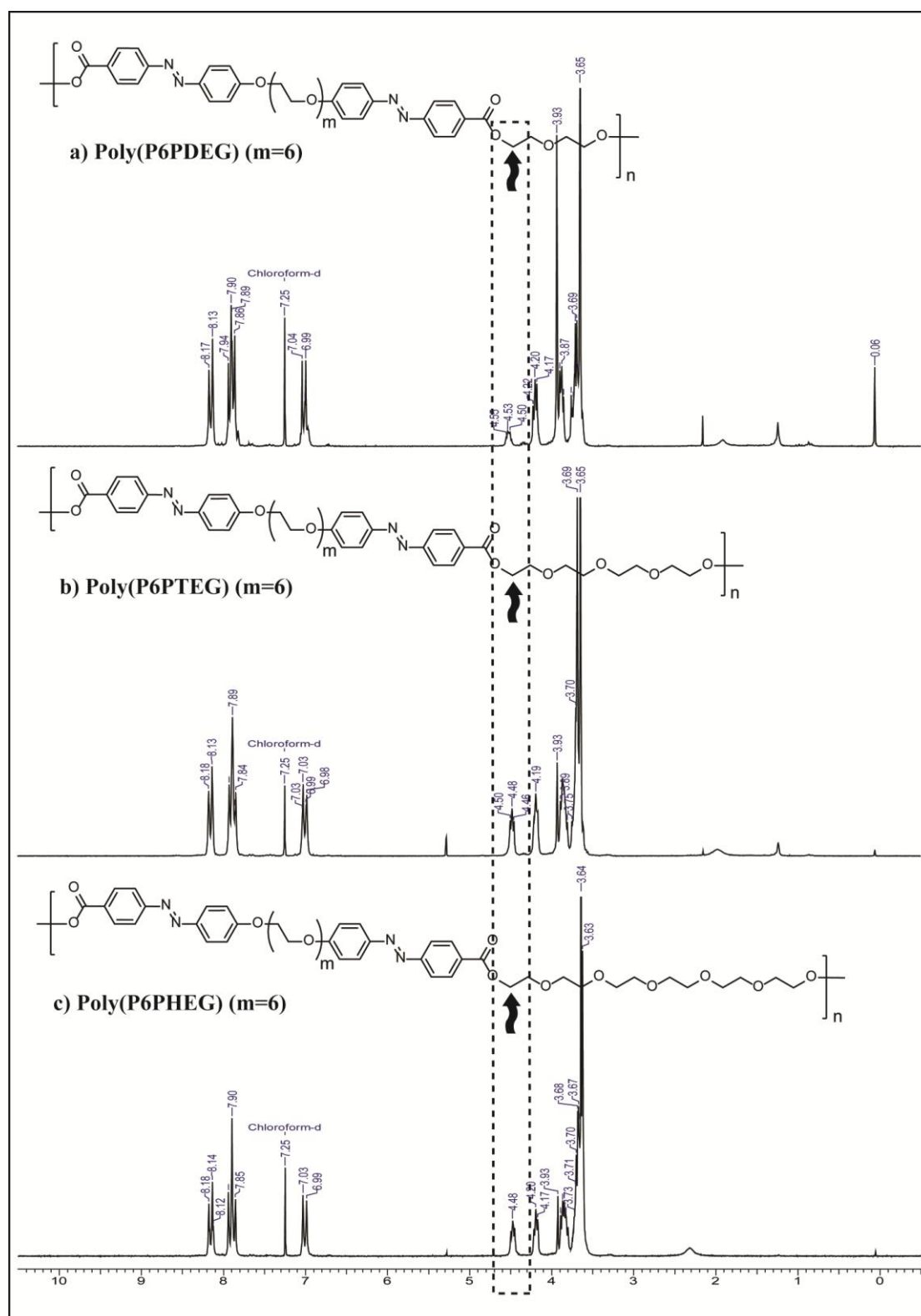


Figure 3.6 $^1\text{H-NMR}$ spectra of main chain azo polymers *Poly(P6PDEG)*, *Poly(P6PTEG)* and *Poly(P6PHEG)* recorded in CDCl_3 .

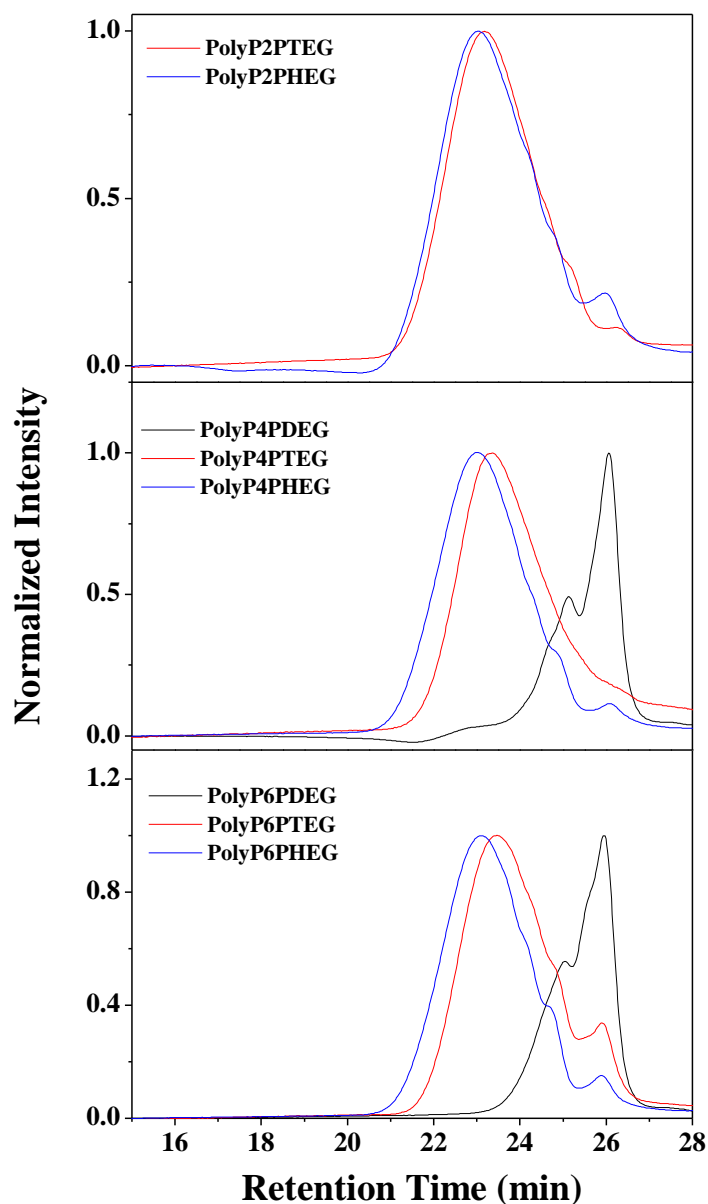


Figure 3.7 Gel permeation chromatograms (GPC) of main chain azo polyester in $CHCl_3$.

In general, it was observed that when the azo twin was polymerized with short spacer diol monomer (DEG) a lower degree of polymerization was observed (2 or 3). The GPC chromatogram of the DEG based polymers **Poly(P4PDEG)** and **Poly(P6PDEG)** showed a huge peak around 26 minutes corresponding to the elution of unreacted starting azobenzene twin monomer. From the GPC data, it was obvious that only dimeric or oligomeric species was formed when DEG was used as the diol monomer for polymerization. A small shoulder corresponding to the respective twin ester

monomer was present in the other polymers also. The P2P series of polymers **Poly(P2PTEG)** and **Poly(P2PHEG)** as well as the P4P series polymers **Poly(P4PTEG)** and **Poly(P4PHEG)** could be purified and the unreacted P2P or P4P twin could be removed to a large extent by soxhlet extraction using acetone and hexane solvent. This purification strategy could not be adopted for the P6P series due to similar solubilities of the polymer and twin molecule. The molecular weight reported in literature for main chain azo polymers generally indicates incorporation of ~6-8 repeating units.⁹ In the polymers reported here, the extent of formation of new ester linkage could be estimated based on the integration of the new ester peak at 4.48 ppm (methylene ester) from the corresponding ¹H-NMR spectra.

Table 3.1 Polymer designation, molecular weight, polydispersity index, viscosity data (η_{inh}), and yield of polymers.

Polymer	Mn ^a	Mw ^a (g mol ⁻¹)	PDI ^a	Viscosity η_{inh} (dL/g) ^b	Yield (%)
Poly(P2PDEG)*	-	-	-	-	89
Poly(P2PTEG)	7460	11200	1.5	0.25	90
Poly(P2PHEG)	8500	13700	1.6	0.27	73
Poly(P4PDEG)	1200	1500	1.3	0.12	77
Poly(P4PTEG)	5100	9000	1.8	0.20	80
Poly(P4PHEG)	8600	14000	1.6	0.27	82
Poly(P6PDEG)	1400	1900	1.3	0.07	79
Poly(P6PTEG)	4000	8100	2.0	0.16	91
Poly(P6PHEG)	7400	11800	1.5	0.20	80

a. Molecular weights as determined by gel permeation chromatography in CHCl₃ at 30 °C using polystyrene standards for calibration.

b. Inherent viscosity measured in chloroform solvent (0.5 dL/g) at 30 °C ± 0.1 °C.

* CHCl₃ insoluble polymer.

The actual peak integration value and the percentage of new ester linkage are given in the Table 3.2 **Poly(P2PDEG)** could be fully dissolved in CDCl_3 after the addition of a few drops of trifluoroacetic acid (TFA). The fully matching integration for new ester link formation suggested high molecular weight for **Poly(P2PDEG)** (Figure 3.4). **Poly(P4PDEG)** and **Poly(P6PDEG)** showed very low percentage formation of new ester linkage (21 and 29 %, respectively) and this was in confirmation with their low molecular weights determined from GPC. The other polymers which showed moderate molecular weight based on GPC data also showed percentage formation of new ester linkage in the range of 85-95 %.

Table 3.2 Percentage formation of new ester linkage from ^1H NMR spectra of main chain polymers.

Polymer	New ester linkage (integration value)	% New ester linkage
Poly-P2PDEG	4.00	100**
Poly-P2PTEG	3.82	95.5
Poly-P2PHEG	3.69	92.3
Poly-P4PDEG	0.84	21
Poly-P4PTEG	4.00	100
Poly-P4PHEG	3.81	95.2
Poly-P6PDEG	1.18	29.5
Poly-P6PTEG	3.18	79.5
Poly-P6PHEG	3.44	86

** determined from proton NMR spectra after the addition of few drops of trifluoroacetic acid (TFA) to CDCl_3 .

Inherent viscosities were also measured for all polymers except **Poly(P2PDEG)** using an ubbelodhe viscometer at $30\text{ }^\circ\text{C} \pm 0.1\text{ }^\circ\text{C}$ in chloroform at a concentration of 0.5 g/dL and the values are given in Table 3.1. The viscosity values observed were in the

range of 0.16 - 0.27 dL/g for most of polymers. The two polymers with low molecular weights namely **Poly(P4PDEG)** and **Poly(P6PDEG)** showed low viscosity values of 0.12 and 0.07 dL/g, respectively in accordance with GPC and proton NMR studies.

3.3.1 Thermal Mesophase Characteristics

The thermal stability of the azo polymers was determined by thermogravimetric analysis (TGA) under nitrogen atmosphere. Figure 3.8 shows the TGA curves of the polymers recorded at a heating rate of 10 °C /min from 40 - 800 °C. All polymers were thermally stable up to 300 °C and exhibited one single major degradation step around 350 °C with a total remaining residue of 30-40 %. Table 3.3 compares the 10 % weight loss of azo polymers which was in the range of 360 - 380 °C.

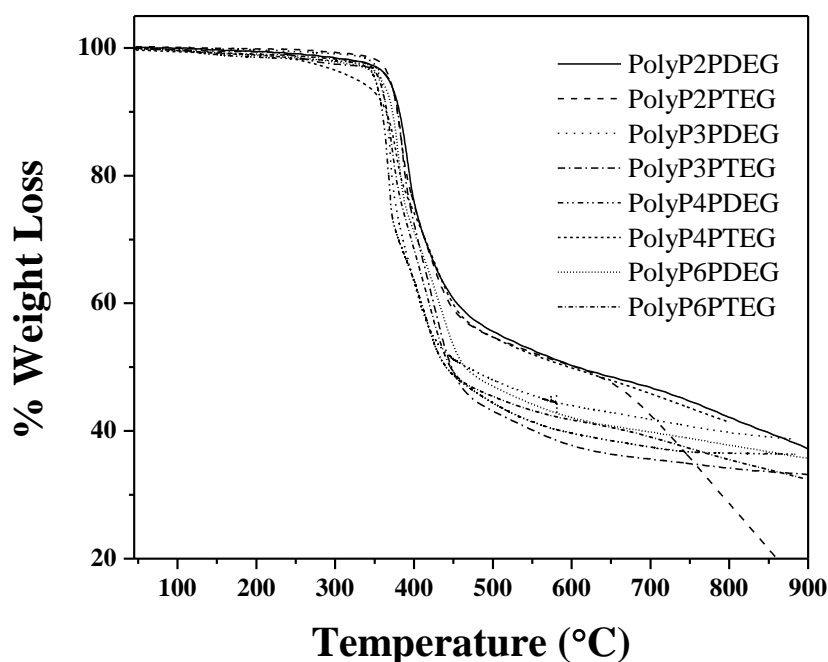


Figure 3.8 Thermogravimetric analysis (TGA) of main chain azo polyester.

The thermotropic liquid crystalline behavior of azo polymers were studied using differential scanning calorimetry (DSC), polarized light microscope (PLM) and variable temperature wide angle X-ray diffraction (VTXRD) studies. Figure 3.9 compares the cooling DSC thermograms of the three **Poly(PnP)** based polymers. The DSC thermogram of the corresponding twin molecule PnP is also given for the sake of comparison. Table 3.3 gives the phase transition temperature as well as the

corresponding enthalpies of all the polymers. Plot a in Figure 3.9 compares the **Poly(P2P)** polymer series. The P2P twin molecule was not liquid crystalline and exhibited a single melting and crystallization (215 °C and 205 °C) upon heating and cooling, respectively.

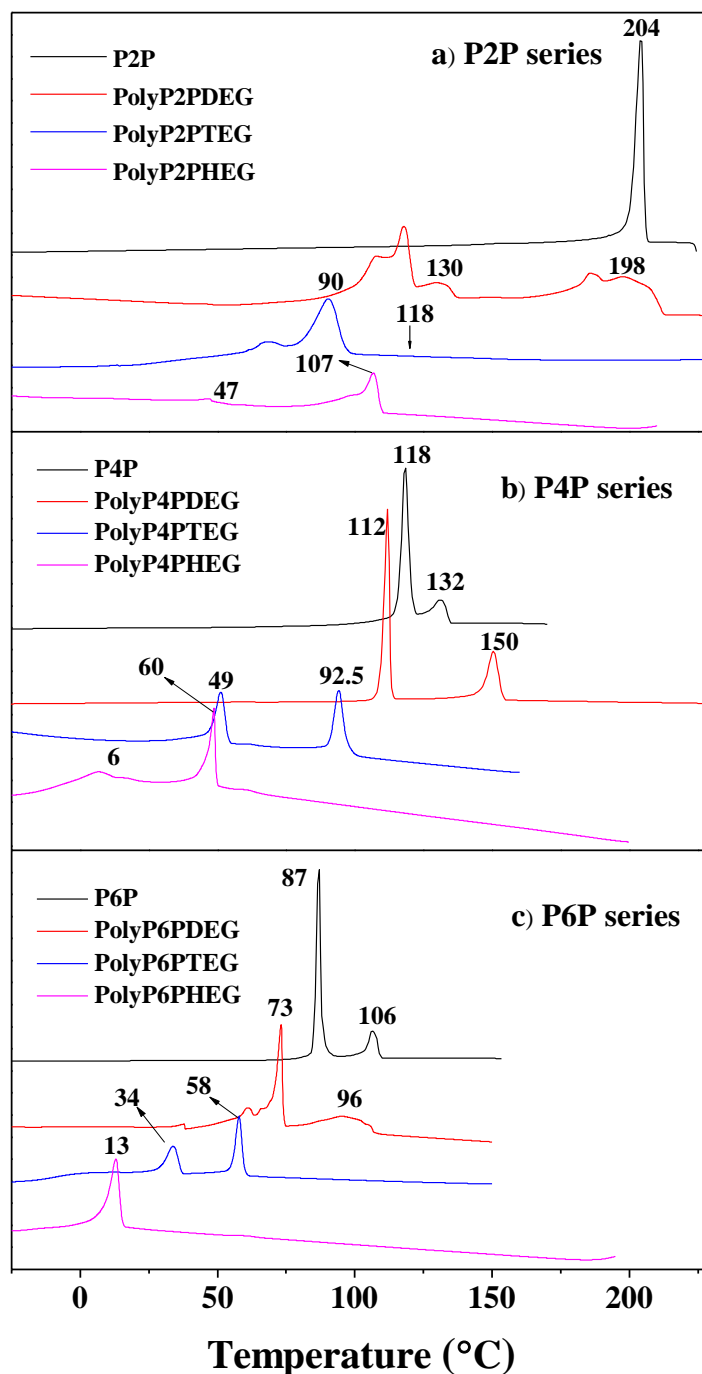


Figure 3.9 DSC thermograms in the cooling cycle of the Poly(*PnP*) azo polymers along with the respective twin azo twin monomers (*PnP*).

Table 3.3 Thermal characteristics of main chain azo polyesters.

Sample	T_{cl}^a (°C) (Lc/C-I)	ΔH_{cl}^a (KJ/ mol)	T_c^b (°C) I-Lc	ΔH_c^b (KJ/ mol)	T_c^b (°C) (Lc-C) / (Lc-Lc)	ΔH_c^b (KJ/ mol)	T_D^c (°C)
Poly(P2PDEG)	212.6	4.0	198.6 S_A	9.3	130 Cr	12.4	380
Poly(P2PTEG)	131	23.7	118 S_A	-	90 S_E	21.0	381
Poly(P2PHEG)	128	25.4	106.8 S_A	18.4	47 S_E	2	360
Poly(P4PDEG)	157	11.1	150.4 S_A	12.1	112 Cr	22.8	360
Poly(P4PTEG)	103	11.9	92.5 S_A	7.5	48.9 S_E	7.1	366
Poly(P4PHEG)	80	0.10	60.8 S_A	0.13	5.7 S_E	5.0	365
Poly(P6PDEG)	116.5	2.2	96.7 S_A	6.3	73 S_E	14.7	372
Poly(P6PTEG)	78.4	4.5	57.9 S_A	5.3	33.7 S_E	4.6	366
Poly(P6PHEG)	80	0.2	60.6 S_A	0.24	13	12.6	362

a. Transitions in DSC during heating cycle, b. Transitions in DSC during cooling cycle, c. 10 % weight loss in TGA under N_2 atmosphere.

Upon polymerization with diols like DEG, TEG and HEG all three polymers exhibited thermotropic liquid crystalline characteristics. **Poly(P2PDEG)** exhibited multiple transitions with the LC phase appearing at 198 °C (9.3 KJ/mol) upon cooling from the isotropic state, which further transformed in to crystalline phase around 138 °C with an enthalpy of (12.4 KJ/mol). **Poly(P2PTEG)** showed two prominent exothermic peaks at 90 °C (11.8 KJ/mol) which transformed in to another phase at 68 °C, which remained stable up to room temperature in the cooling cycle. However, as will be described later on under the section on PLM studies, LC textures were visible under the microscope at 118 °C, which could not be traced in the DSC thermogram. **Poly(P2PHEG)** showed monotropic LC behavior - only a clearing transition was observed during heating cycle (Figure 3.10); while cooling the LC phase transition

was observed at 107 °C (18.4 KJ/mol) which transformed in to crystalline phase at 47 °C (2 KJ/mol). Thus, a clear reduction in the LC transition temperature was observed in going from the small molecule to the HEG based polymer.

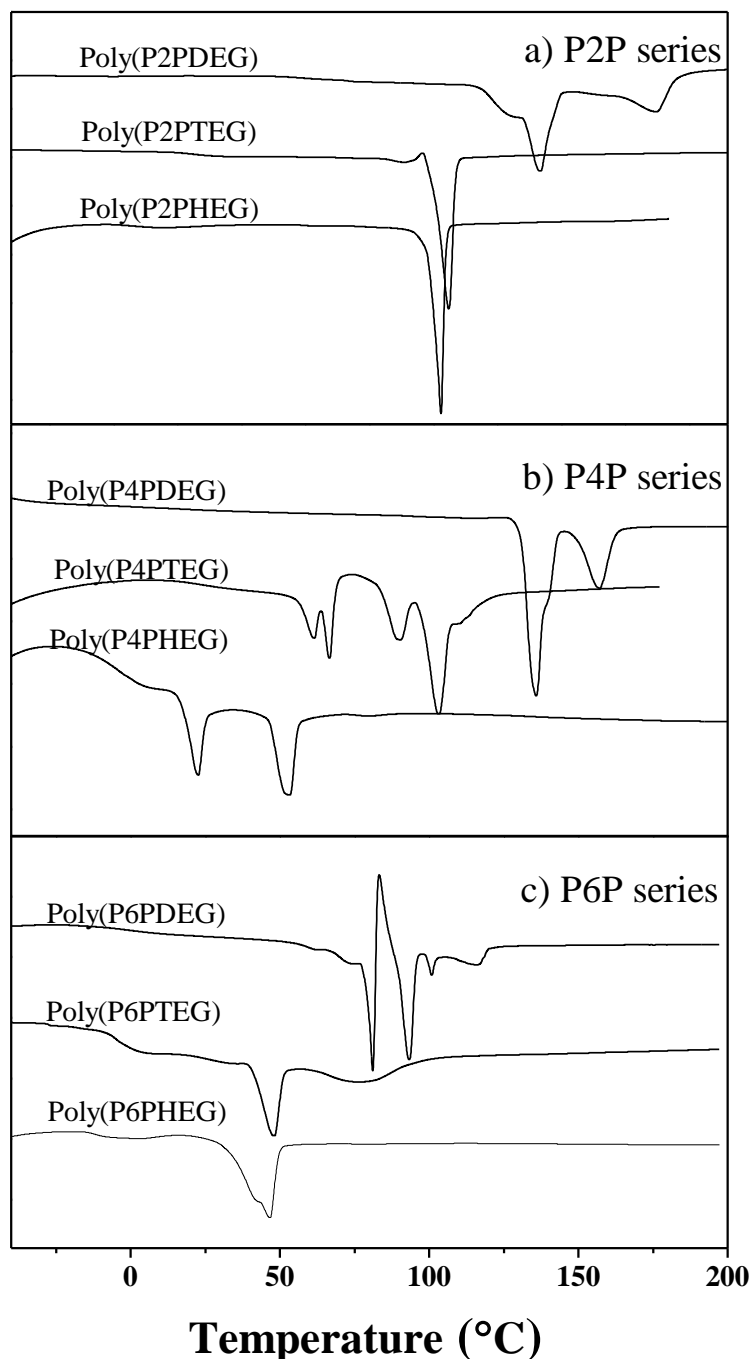


Figure 3.10 DSC thermograms in the heating cycle of the Poly(PnP) azo polymers along with the respective twin azo twin monomers (PnP).

In the P4P series (plot b, Figure 3.9), the twin P4P was liquid crystalline with a clear LC and crystalline transition at 132 °C and 118 °C respectively upon cooling. The DEG, TEG and HEG based polymers of P4P also exhibited thermotropic liquid crystalline behavior. **Poly(P4PDEG)** exhibited isotropic to LC phase transitions at 150.4 °C (12.1 KJ/mol), followed by transformation to crystalline phase at 112 °C (22.8 KJ/mol). The probable reason for unexpected higher transition temperatures for this polymer in comparison with the P4P twin molecule could be its low molecular weight. The dimeric or low oligomeric species would tilt the balance in favor of higher rigidity in contrast to flexibility. **Poly(P4PTEG)** showed two exothermic transitions corresponding to isotropic to LC phase at 92.5 °C (7.9 KJ/mol) and LC to LC phase transition (confirmed later on based on PLM and VT-WXRD studies) at 48.9 °C (8.2 KJ/mol). **Poly(P4PHEG)** exhibited two exothermic transitions corresponding to isotropic to LC around 48 °C (3.82 KJ/mol) and another at 7 °C (4 KJ/mol).

The P6P series is given in plot c, Figure 3.9; the twin P6P was liquid crystalline with a clear LC and crystalline transition at 106 and 87 °C respectively upon cooling. **Poly(P6PDEG)**, **Poly(P6PTEG)** and **Poly(P6PHEG)** also showed thermotropic liquid crystalline behavior. The low molecular weight polymer **Poly(P6PDEG)** showed isotropic to LC transition at 96 °C (6.3 KJ/mol) which transformed in to another LC phase at 73 °C (14.7 KJ/mol). The LC phase remained stable up to room temperature. Upon cooling, **Poly(P6PTEG)** showed an isotropic to LC transition at 58 °C (5.3 KJ/mol) which subsequently transformed in to another LC phase at 33.7 °C. For **Poly(P6PHEG)**, the LC phase appeared at 13 °C in the cooling cycle, which was the lowest isotropic to LC transition temperature recorded among the entire series. Overall, in each **Poly(PnP)** polymer series the HEG based polymers exhibited the lowest transition temperatures. When, the polymers were organized as DEG, TEG and HEG series, where the trend within the twin members could be easily visualized. For instance, among the twin molecules, P6P contributed to the lowest transition temperatures within each polymer series.

3.3.2 Polarized Light Microscopy (PLM)

The LC phase textures were visualized using polarized light microscopy studies. Figure 3.11 shows selected LC images of some of the main chain azobenzene polymers. Figure 3.11-a shows the typical broken fan-like structures of smectic

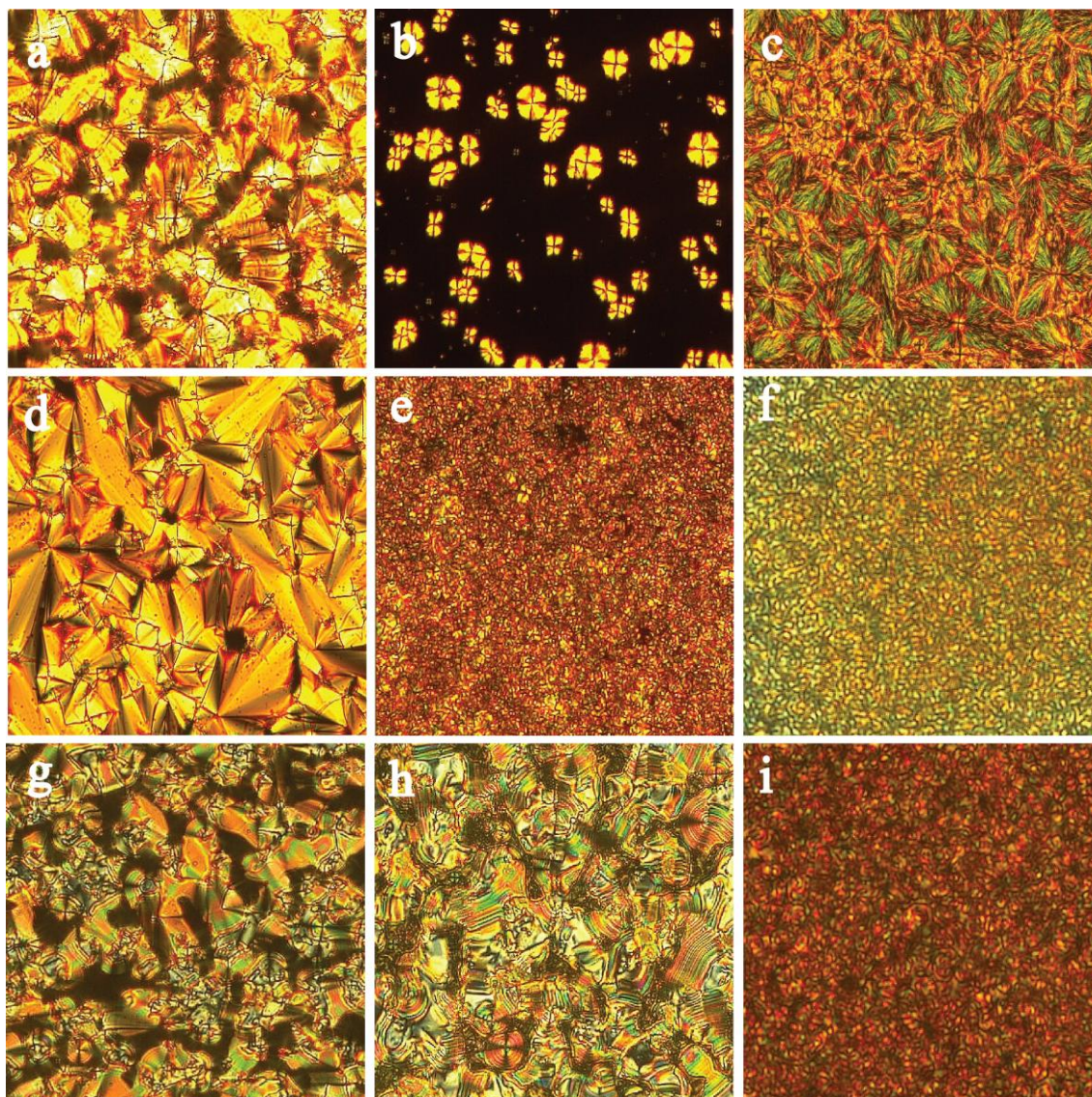


Figure 3.11 PLM images of main chain azo polymers - a) broken fan like structure (S_A) of **Poly(P2PDEG)** at 184 °C (20X), - b) focal conic structure (S_A) of **Poly(P2PTEG)** at 118 °C (20X) c) S_E phase of **Poly(P2PTEG)** at 80 °C (40X), d) Focal conic growth of S_A phase of **Poly(P4PDEG)** at 155 °C (20X), e) S_A phase of **Poly(P4PTEG)** at 93.5 °C (20X), f) S_A phase of **Poly(P4PHEG)** at 25 °C (20X), g)

Focal conic growth of S_A phase of Poly(P6PDEG) at 86.5 °C (40X), h) S_E phase of Poly(P6PDEG) at 69 °C (40X) and i) S_A phase of Poly(P6PTEG) at 52 °C (20X).

mesophase (S_A) exhibited by **Poly(P2PDEG)** at 184 °C upon cooling from the isotropic phase. The crystalline phase observed beyond 138 °C during cooling cycle. Figure 3.11-b shows the growth of focal conic smectic mesophase at 118 °C shown by **Poly(P2PTEG)** which was not observed in the DSC thermogram. The Figure 3.11-c shows the higher ordered LC phase formed beyond 80 °C by the same polymer, which remained stable until room temperature. Figure 3.11-d in the middle row shows the typical broken fan-like texture of smectic phase (S_A) exhibited by **Poly(P4PDEG)** at 155 °C while cooling. This smectic phase transformed into a crystal phase beyond 112 °C. Figure 3.11-e and 3.11-f shows the grainy birefringence texture exhibited by **Poly(P4PTEG)** and **Poly(P4PHEG)** at 93.5 °C and at 25 °C respectively in the cooling cycle. The bottom row images Figure 3.11-g and 3.11-h corresponds to the typical broken focal conic texture of the smectic (S_A) phase exhibited by **Poly(P6PDEG)** at 86.5 °C followed by its transformation to the higher ordered ring banded focal conic structure at 69 °C respectively in the cooling cycle. The ring banded texture remained stable until room temperature. The bottom row Figure 3.11-i shows grainy texture of the smectic phase (S_A) for **Poly-P4PTEG** during cooling cycle.

3.3.3 Wide angle X-ray diffraction (WXR)

Further characterization of the phase characteristics of the polymers were done using wide angle X-ray diffraction studies. Figure 3.12a-c compares the normalized room temperature WXR pattern of the **Poly(P2P)** polymer series both in the as-solvent precipitated powder form as well as after heating to isotropic state followed by cooling to room temperature. The ‘as-solvent precipitated’ powder and ‘as cooled from isotropic’ powder of **Poly(P2PDEG)** exhibited several sharp reflections in the low as well as wide angle region confirming the crystalline nature. Figure 3.13-i shows the WXR data collected at various temperatures during heating and cooling for the same polymer sample. The data was collected in a horizontal sample placement mode using a Bruker D8 Advance diffractometer. The peaks were not very sharp – especially in the $2\theta < 15^\circ$ range, compared to the room temperature data

collected in vertical sample placement mode collected with a Rigaku instrument having high intensity Microfocus rotating anode X-ray source (Figure 3.12). The data collected in the LC phase at 175 °C while cooling (Plot-d in supporting figure S10A) showed two diffraction peaks in the low angle range at $2\theta = 5.35^\circ$ ($d = 16.44 \text{ \AA}$) and $2\theta = 10.7^\circ$ ($d = 8.26 \text{ \AA}$) along with a broad hallow peak at $2\theta = 19.5^\circ$ ($d = 4.54 \text{ \AA}$) due to the diffuse packing of oligoethylene chains. This confirmed the smectic S_A nature of the mesophase.¹⁰

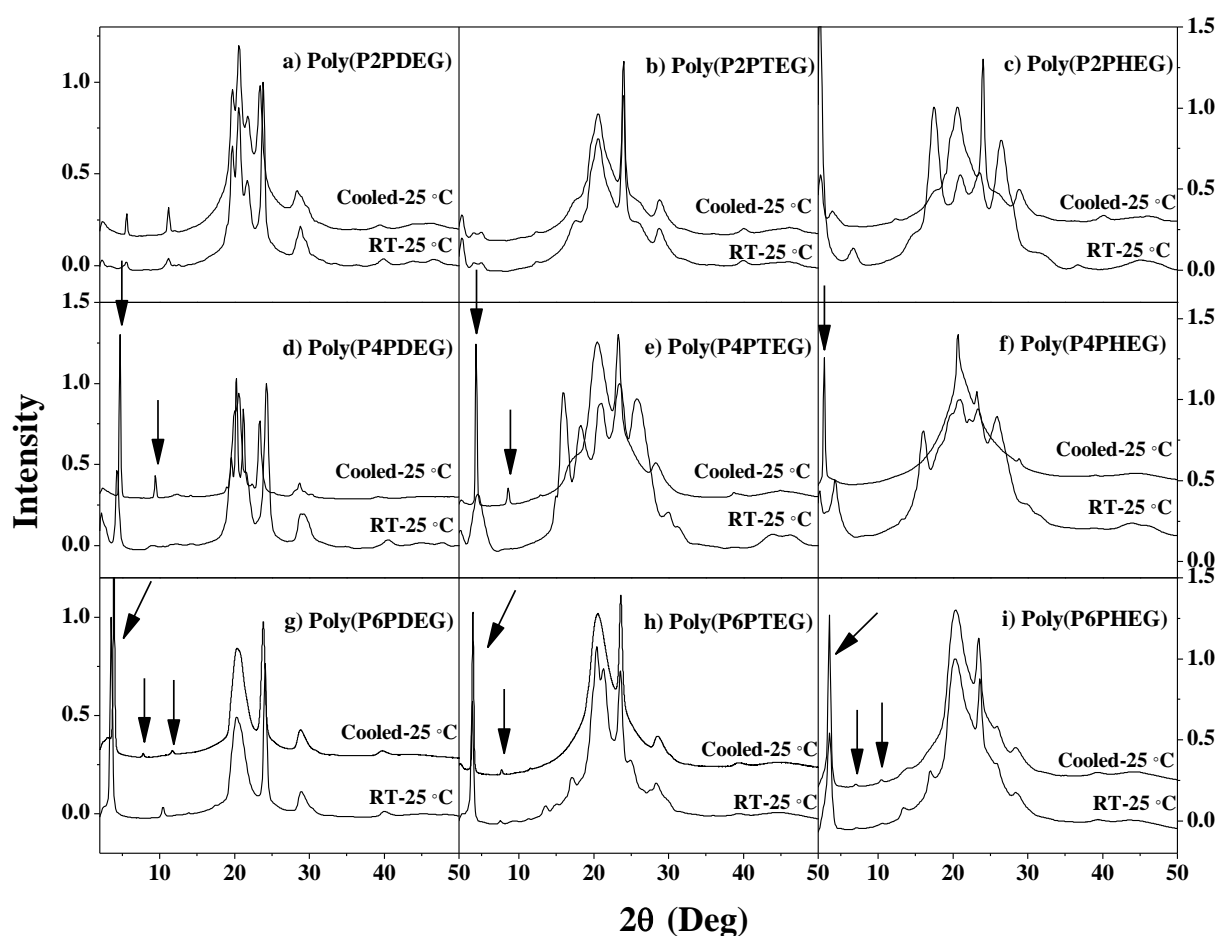


Figure 3.12 X-ray diffraction of main chain azo polymers (*RT-25* represent diffraction pattern for 'as solvent precipitated' powder sample recorded at 25 °C and *Cooled-25* represent diffraction pattern at 25 °C for the cooled sample from the isotropic phase).

Figure 3.13-ii compares the variable temperature WXR D data for **Poly(P2PTEG)**. The WXR D pattern of **Poly(P2PTEG)** at 86 °C in the cooling cycle was characterized by a reflection in low angle at $2\theta = 5.41^\circ$ (16.32 Å) and in the wide angle region a broad diffraction centered around $2\theta = 20.6^\circ$ (4.3 Å) due to diffuse packing of oligoethylene chain with characteristic sharp reflections at 24° (3.7 Å), 28.7° (3.1 Å) and 32° (2.8 Å) indicative of higher ordered LC phases was observed.¹¹ In Figure 3.12-b it was observed that the ‘cooled from isotropic’ sample retained the diffraction pattern in the LC phase which was in agreement with the observation from the PLM also. Such sharp wide angle diffraction patterns are very closely associated with smectic E mesophase where the mesogen is packed in orthorhombic pattern within the smectic layers.¹⁰⁻¹¹

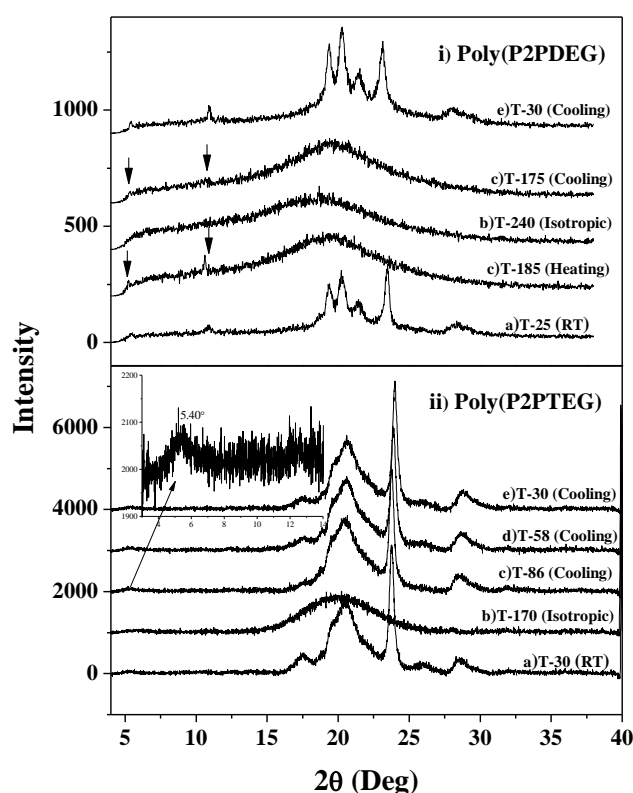


Figure 3.13 Variable temperature X-ray diffraction (VTXRD) of polymers A) **Poly(P2PDEG)** and B) **Poly(P2PTEG)**.

Poly(P2PHEG) (Figure 3.12-c) showed multiple sharp reflections in the wide angle region for “as solvent precipitated sample indicative of crystalline nature. Upon

heating to isotropic followed by cooling, two low angle diffractions along with broad peak in the wide angle region with new sharp diffractions at $2\theta = 24^\circ$, 28.8° and 40.2° associated with higher order mesophase like smectic E phase was observed.

Figure 3.12-d to 3.12-f shows the WXR D pattern for the P4P polymer series collected at room temperature in the ‘as-solvent’ precipitated form and ‘cooled from isotropic melt’ form. Similar to the observation in the case of the **Poly(P2PDEG)** polymer, **Poly(P4PDEG)** also underwent LC to crystalline transition at room temperature retaining a lamellar crystalline phase. The variable temperature WXR D pattern recorded for **Poly(P4PDEG)** (Figure 3.14-i) at 148°C in the LC phase confirmed the S_A mesophase with two reflections in the low angle region at $2\theta = 4.75^\circ$ (18.4 \AA) and $2\theta = 9.23^\circ$ (9.5 \AA) in addition to the broad halo peak centered at $2\theta = 20^\circ$ (4.3 \AA) corresponding to diffuse alkyl chain packing of the oligoethyleneoxy units.

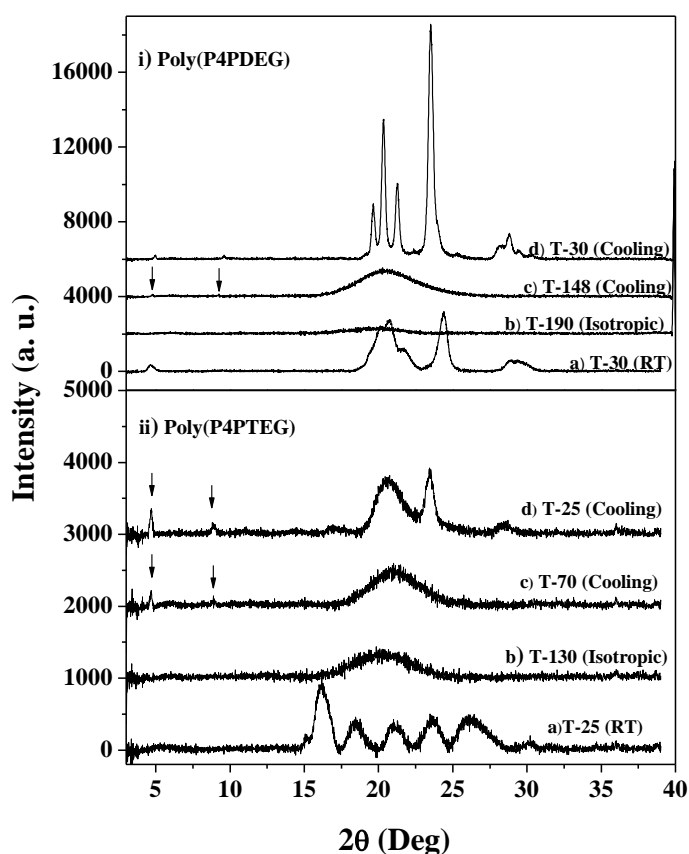


Figure 3.14 Variable temperature X-ray diffraction (VTXRD) of polymers A) **Poly(P4PDEG)** and B) **Poly(P4PTEG)**.

Although **Poly(P4PTEG)** showed several sharp peaks indicating crystalline nature for the ‘as-solvent’ precipitated powder, the ‘cooled from isotropic melt’ sample showed three reflections in the low angle region at $2\theta = 4.30^\circ$ (20.5 \AA), $2\theta = 8.56^\circ$ (10.3 \AA) and $2\theta = 12.9^\circ$ (6.85 \AA) with multiplicity of 1: 1/2 : 1/3 and in the wide angle region a broad peak (20.5 \AA) with three new characteristic reflections were observed at $2\theta = 23.3^\circ$, 28.3° and 38.7° which were indicative of higher ordered smectic mesophase like smectic E phase. Assuming the two wide angle reflections at 20.5 \AA and 23.3 \AA to be the d_{110} and d_{200} of an orthorhombic mode of packing within smectic layers, the lattice parameters were estimated as $a = 0.764$ and $b = 0.524$.^{10,11b} In a similar way the reflections were indexed for **Poly(P4PHEG)** and are given in Table 3.4.

Figure 3.12 g-i shows the WXR D pattern for the P6P polymer series collected at room temperature in the ‘as-solvent’ precipitated form and ‘cooled from isotropic melt’ form. In confirmation with the transformation to higher ordered ring-banded

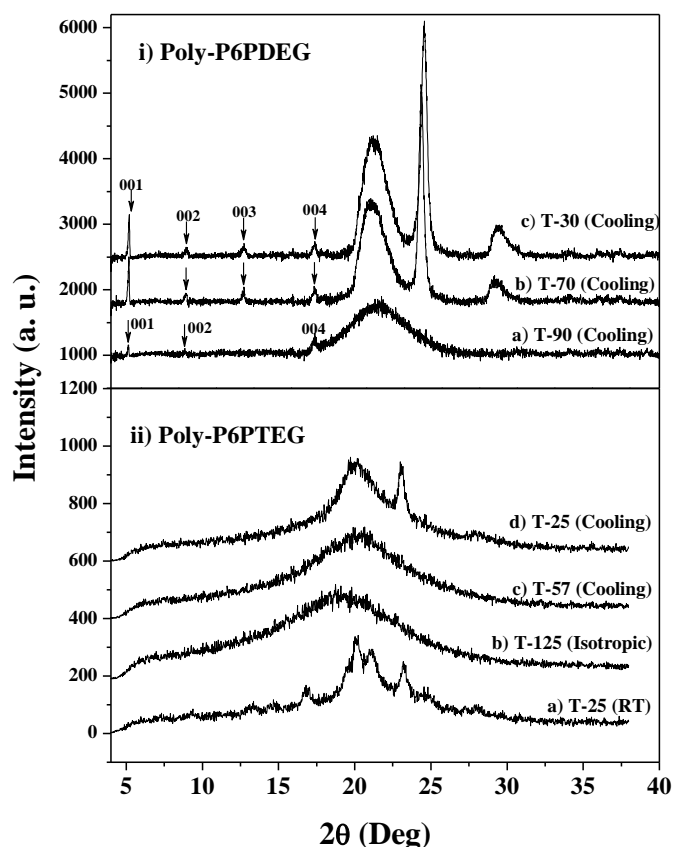


Figure 3.15 Variable temperature wide angle X-ray diffraction (VTXRD) of polymers A) Poly(P6PDEG) and B) Poly(P6PTEG).

structure which was retained till room temperature (observation from PLM), the WXR pattern (Figure 3.12 g) of the ‘cooled from isotropic melt’ sample of **Poly(P6PDEG)** was different from its pattern collected in the ‘as-solvent’ precipitated form.

Table 3.4 *d*-spacing of polymers *Poly(P2PTEG)*, *Poly(P2PHEG)*, *Poly(P4PTEG)*, *Poly(P4PHEG)*, *Poly(P6PDEG)*, *Poly(P6PTEG)* and *Poly(P6PHEG)* collected after cooling the samples from isotropic melt. The values in brackets indicate the orthorhombic lattice parameters.

Poly(P2PTEG) (a= 0.742 nm, b= 0.527 nm)			Poly(P2PHEG) (a= 0.739 nm, b= 0.526 nm)		
d_{hkl}	d_{calcd}/nm	d_{obsd}/nm	d_{hkl}	d_{calcd}/nm	d_{obsd}/nm
110	0.431	0.431	110	0.430	0.430
200	0.371	0.371	200	0.370	0.370
210	0.302	0.309	210	0.302	0.309
220	0.214	0.224	020	0.262	0.278
			220	0.214	0.224
Poly(P4PTEG) (a= 0.764 nm, b= 0.524 nm)			Poly(P4PHEG) (a= 0.768 nm, b= 0.518 nm)		
d_{hkl}	d_{calcd}/nm	d_{obsd}/nm	d_{hkl}	d_{calcd}/nm	d_{obsd}/nm
110	0.429	0.429	110	0.430	0.430
200	0.379	0.379	200	0.384	0.384
210	0.308	0.315	210	0.308	0.309
120	0.247	0.232			
Poly(P6PDEG) (a= 0.743 nm, b= 0.531 nm)			Poly(P6PTEG) (a= 0.750 nm, b= 0.524 nm)		
d_{hkl}	d_{calcd}/nm	d_{obsd}/nm	d_{hkl}	d_{calcd}/nm	d_{obsd}/nm
110	0.433	0.433	110	0.431	0.431
200	0.372	0.372	200	0.376	0.376
210	0.304	0.309	210	0.304	0.313
220	0.215	0.226	220	0.214	0.228
Poly(P6PHEG) (a= 0.757 nm, b= 0.532 nm)					
d_{hkl}	d_{calcd}/nm	d_{obsd}/nm			
110	0.436	0.436			
200	0.379	0.379			
-	-	0.344			
210	0.308	0.314			
220	0.217	0.230			

The WXRD data collected in the first LC transition around 90 °C (Figure 3.15-i) corresponded to the typical smectic S_A mesophase with two sharp reflections in the low angle region at $2\theta = 4.15^\circ$ (21.2 Å) and $2\theta = 7.95^\circ$ (11 Å) along with broad reflection in the wide angle centered around $2\theta = 20.8^\circ$ (4.3 Å). The supporting figure shows that at 70 °C, this WXRD peak pattern altered with four new reflections appearing in the low angle region at $2\theta = 4.16^\circ$ (20.9 Å), $2\theta = 8.03^\circ$ (11 Å), $2\theta = 11.85^\circ$ (7.4 Å) and $2\theta = 16.5^\circ$ (5.3 Å). In the wide angle region also, new reflections appeared at $2\theta = 23.6^\circ$ (3.73 Å) and $2\theta = 28.6^\circ$ (3.1 Å) indicative of higher ordered mesophase. The nature of the higher ordered mesophase could be tentatively attributed to a S_B or S_E phase based on the observation that the fundamental reflection in the low angle at 90 °C and 70 °C did not show any shift in 2θ position indicating absence of tilt within smectic layer organization. Besides this fact, a multiplicity could be attributed to the peaks in the low angle region with that observed for the sharp peaks in the wide angle region. The S_B phase is associated with the hexatic packing mode of mesogen within the smectic layer. However, the d-spacing (d_{hkl}) diffraction pattern observed in the wide angle did not exhibit the relationship of hexagonal packing mode; which is $d_{100}:d_{110}:d_{210}:1:1/\sqrt{3}:1/\sqrt{7}$ thereby ruling out the possibility of a S_B mesophase.⁴⁰ On the other hand, the S_E phase is associated with orthorhombic mode of packing within smectic layer. If the two wide angle reflections at 20.4° and 23.8° were assumed as the (110) and (200) diffraction respectively of an orthorhombic mode of packing, the lattice parameters a and b could be calculated as; $a = 0.743$ nm and $b = 0.530$ nm. On the basis of this, the other reflections could be indexed as shown in Table 3.4 The calculated d-spacing closely matched with the observed d-spacing, indicating a probable orthorhombic mode of packing of mesogen within smectic layer (S_E phase). Figure 12-h and 12-i corresponds to the ‘as-solvent’ precipitated form and ‘cooled from isotropic melt’ form of **Poly(P6PTEG)** and **Poly(P6PHEG)** respectively. The ‘cooled from isotropic melt’ powder of **Poly(P6PTEG)** indicated a higher ordered mesophase that was retained at room temperature. Table 3.4 shows the d-spacing calculated for the polymer **Poly(P6PTEG)** and **Poly(P6PHEG)** assuming the sharp reflection in the wide angle

around $2\theta = 23^\circ$ and $2\theta = 28^\circ$ as the (110) and (200) diffraction respectively of the orthorhombic packing.

3.3.4 Ionic Conductivity and Phase Transitions

One of the polymers – **Poly(P4PTEG)** was chosen for ionic conductivity studies in combination with varying amounts of lithium salt (LiCF_3SO_3) using complex impedance spectroscopy. The complex was prepared by mixing the polymer with varying amounts of LiCF_3SO_3 salt dissolved in tetrahydrofuran (THF) solvent, followed by removal of the solvent and drying the polymer/Li salt complex. The amount of lithium added was varied in equivalents of oxyethylene ($\text{CH}_2\text{CH}_2\text{O}$) units per repeat unit of the polymer.^{2b,3b} For instance compositions corresponding to 0.01, 0.03, 0.05, 0.1, 0.2 and 0.3 equivalents of lithium per $-\text{CH}_2\text{CH}_2\text{O}-$ repeat unit were prepared. DSC thermograms were recorded for all the polymer complexes. Figure 3.16 shows the second cooling (a) and heating (b) scans in the DSC thermograms of the complexes along with that of the uncomplexed **Poly(P4PTEG)**. Except for the complex corresponding to highest lithium content - 0.3 moles Li, all complexes retained the LC nature. In the case of the poly/Li 0.3 complex, phase transitions were observed in the first heating cycle; however in the first cooling scan as well as the subsequent heating cycles only a glass transition was observed at around 69°C , indicating the amorphous nature of the polymer complex with high lithium salt content. Poly/Li 0.2 complex exhibited an isotropic to LC transition upon cooling; however unlike the other polymer/lithium complexes with lower lithium content, the second higher order LC transition (around 50°C) was not observed. The LC phase was frozen into a glass around 37°C as shown in the DSC thermogram in Figure 3.16a. The LC nature of the complexes was further confirmed using polarized light microscope. The LC texture of three representative compositions namely poly/Li 0.01, 0.05 and 0.2 after cooling from isotropic melt is shown in Figure 3.17b-d. For comparison, the smectic LC texture of the neat polymer is also shown in Figure 3.17a. Additional conformation regarding the layered nature of the LC phase of the polymer/lithium complexes was obtained from the WXR D data. Figure 3.18 compares the WXR D pattern of the complexes in the ‘as solvent’ precipitated form and ‘cooled from isotropic melt’ form. The polymer/lithium salt complexes with low lithium

content like the poly/Li 0.01, poly/0.03 (Figure 3.18-a, b) were almost identical to the neat polymer in their WXR D pattern (see Figure 3.12e for data of neat polymer).

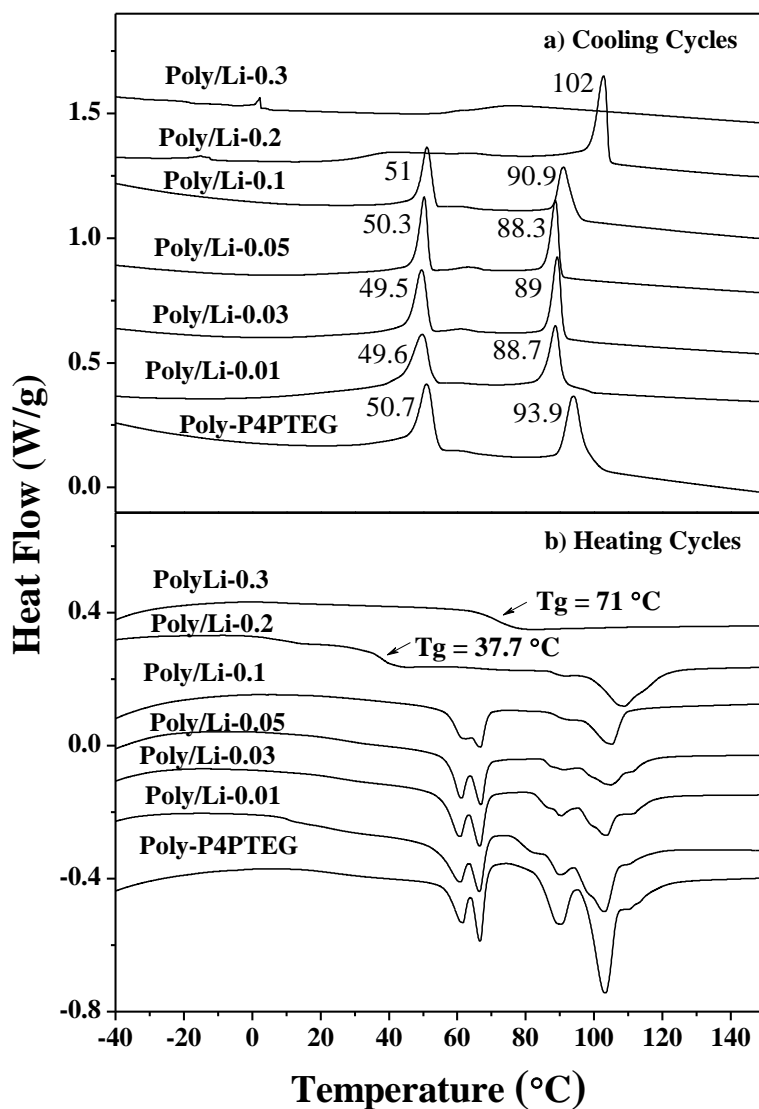


Figure 3.16 DSC thermogram (IInd cooling and heating cycles) of polymer complexes of *Poly(P4PTEG)* with LiCF_3SO_3 salt by varying the mole ratio of Li with respect to ethyleneoxy unit (Transition temperature labeled in °C).

However, with higher lithium content - poly/Li 0.05, poly/0.1 complexes exhibited new peaks at $2\theta = 2.79^\circ$ and 5.67° corresponding to d spacing 31.68 \AA and 15.57 \AA respectively (highlighted by arrow in Figure 3.18- c and d) in addition to those of the neat polymer.

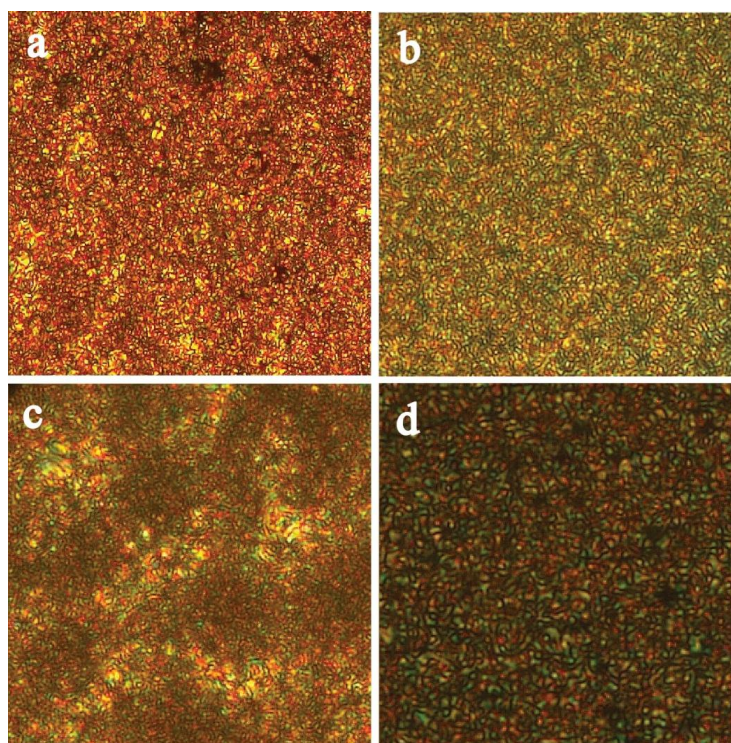


Figure 3.17 PLM images of Poly-Li complexes with neat polymer **Poly(P4PTEG)** also included for comparison. a) S_A phase of **Poly(P4PTEG)** at 93.5 °C, (b) **Poly(P4PTEG)/Li-0.01** at 25 °C, (c) **Poly(P4PTEG)/Li-0.05** at 25 °C and (d) **Poly(P4PTEG)/Li-0.2** at 58.5 °C.

The multiplicity in the peak pattern in these new peaks indicated new layered organization in presence of lithium. As the lithium content increased the new layering became more intense at the cost of the existing layered structure. For instance, in poly/0.2 the peak pattern of the neat polymer disappeared totally and only peaks corresponding to the new layered structure, namely those at $2\theta = 3.27^\circ$, 6.5° and 9.87° corresponding to d spacing 27 Å, 13.56 Å and 8.95 Å were observed. The inset in Figure 18-e shows the expanded region in the 2θ range 2-15° of the WXRd plot highlighting the new layered peak pattern. The absence of the reflections in the wide angle region of $2\theta = 28.3^\circ$ (3.8 Å) and 38.7° (3.1 Å) was in confirmation with the observation from DSC which also indicated absence of higher ordered smectic mesophase in the polymer complexes with lithium content > 0.1 . The polymer complex with the highest lithium content - poly/0.3 complex (Figure 18-f) also was characterized by broad diffuse diffraction pattern centered at $2\theta = 20.4^\circ$ (4.4 Å) as a

result of the interchain packing in oligooxyethylene region, confirming the amorphous nature of the complex at room temperature.

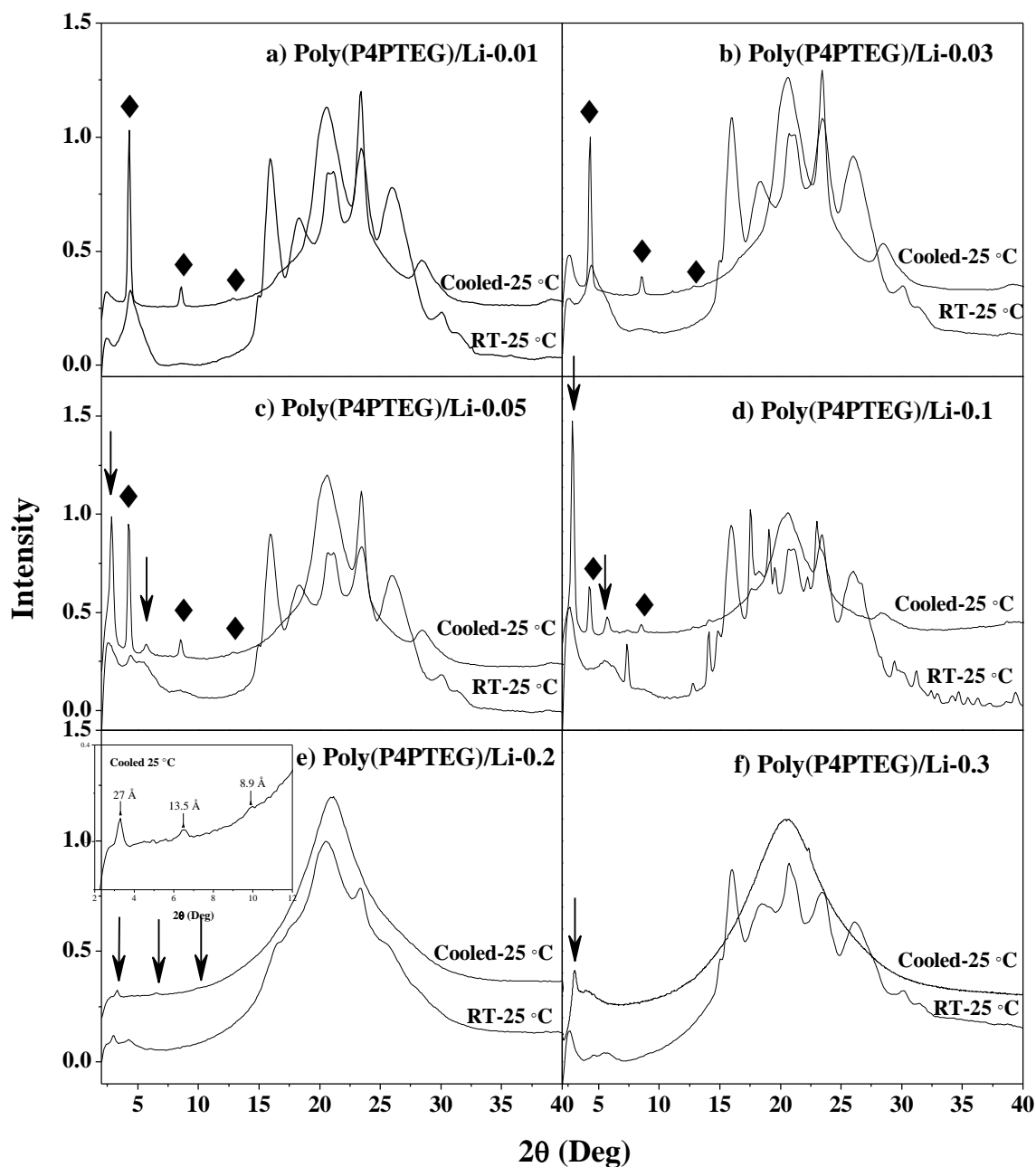


Figure 3.18 X-ray diffraction patterns of main chain azo polymer-Li salt complexes (Black line diffraction pattern for ‘as solvent precipitated’ powder sample recorded at 25 °C and red line diffraction pattern at 25 °C for the cooled sample from the isotropic phase).

The schematic representation of the cell used for the conductivity measurement of LC polydomain sample is shown in Figure 3.19. The cell consisted of a pair of indium tin oxide (ITO) electrodes separated by 80 μm Teflon spacer.

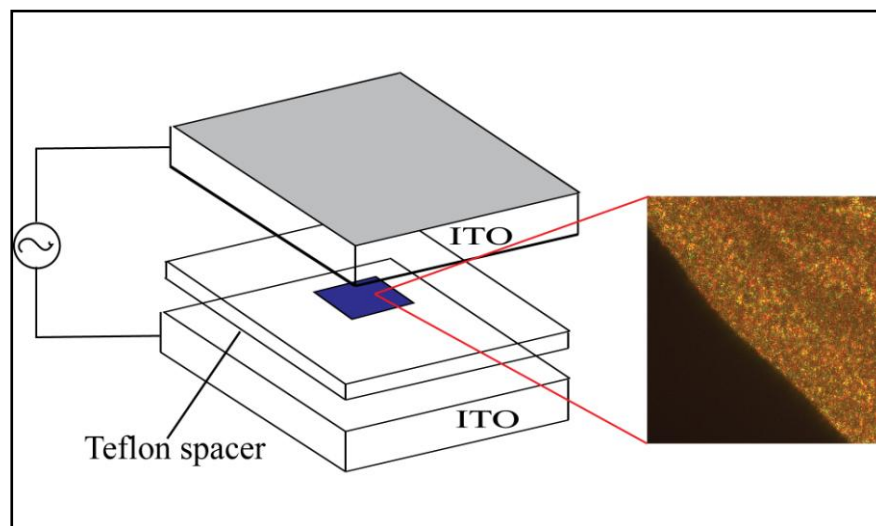


Figure 3.19 Schematic view of the cell used for ionic conductivity measurement with ITO electrode.

The samples were sandwiched between two electrodes and heated to 70 $^{\circ}\text{C}$ followed by slow cooling to room temperature for better surface contact. During the measurements, the sample was gradually heated to various temperature intervals for ionic conductivity measurement. The variation in the ionic conductivity as a function of Li content and temperature (25 $^{\circ}\text{C}$ to 150 $^{\circ}\text{C}$) was studied. The data presented as a Cole-Cole plot presented classical semicircle shape from which the intercept with the real impedance (Z') axis at the low frequency was used to extract the bulk resistance.¹² The ionic conductivity (σ) of poly/Li complexes was calculated according to equation -1.¹³

$$\sigma = d/(R \times S) \dots \dots (1)$$

where 'd' is the thickness of the solid polymer electrolyte layer, 'S' is the area and 'R' is the bulk resistance extracted from Nyquist plot of impedance spectroscopy.

The typical semicircle shaped Nyquist plots of the imaginary component of the impedance (Z'') versus the real component (Z') for the polymer complexes was

observed. Figure 3.20A shows the Nyquist plots of the imaginary component of the impedance (Z'') versus the real component (Z') for the **Poly/Li-0.3** complex at various temperature intervals. Figure 3.20B compares the temperature dependence of ionic conductivity for all the four polymer complexes and the values are given in Table 3.5. For the polymer complexes with the lithium ratio less than 0.2, the ionic conductivity was too low to measure at room temperature, whereas for **Poly/Li-0.2** and **Poly/Li-0.3** complexes, conductivity in the order of $10^{-7} \text{ S cm}^{-1}$ and $10^{-5} \text{ S cm}^{-1}$ respectively was obtained at 30 °C itself. The temperature dependence of ionic conductivity was compared with the phase transitions occurring in the sample by plotting the ionic conductivity ($\log \sigma$) along with the second heating scan in the DSC thermogram as a function of temperature as shown in Figure 3.20C (i to iv). It could be observed that the conductivity increased with the temperature for all complexes. The highest ionic conductivity was observed for the polymer complex with highest lithium salt content (**Poly/Li-0.3**), which reached a value of $\sim 7 \times 10^{-4} \text{ S cm}^{-1}$ at around 130 °C. A sharp change in the slope was observed in the ionic conductivity for **Poly/Li-0.3** between the temperature range 50 - 70°C, which coincided with the start of the broad glass transition temperature (T_g) observed in the DSC thermogram between 50 - 90°C (Figure 20C-i). Polymer segmental mobility that is initiated at the glass transition temperature facilitates movement of the ions, which is immediately reflected as a jump in the ionic conductivity values. In the case of **Poly/Li-0.2** complex, T_g was observed at much lower temperature of ~ 35 °C (Figure 3.20C-ii). A similar sharp change in the slope of ionic conductivity could be observed around 35 – 40 °C. The increase in ionic conductivity with temperature beyond ~ 60 °C, when the sample was in the liquid crystalline phase was slower. For the complexes **Poly/Li-0.1** and **Poly/Li-0.05**, reasonable ionic conductivity could be extracted only beyond 60 °C and 80 °C respectively when the sample was already in the liquid crystalline phase. The ionic conductivity leveled off beyond the clearing transition when the sample transformed to the isotropic phase.

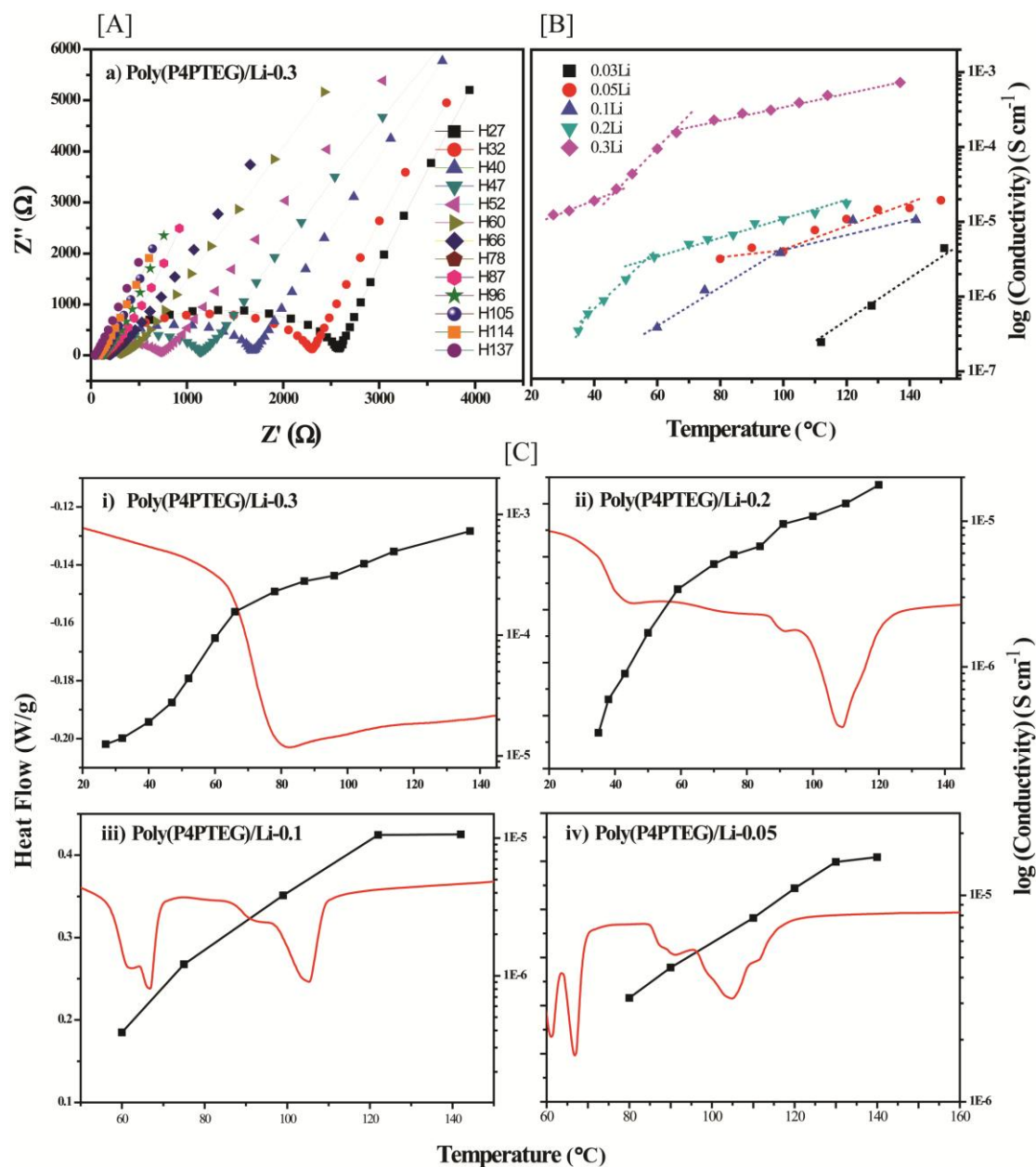


Figure 3.20 [A] Nyquist plots of the imaginary component of the impedance (Z'') versus the real component (Z') at various temperature interval for the **Poly/Li-0.3** complex, [B] Variation of the ionic conductivity (σ) with temperature for complexes **Poly-Li 0.01, Poly-Li 0.03, Poly-Li 0.05, Poly-Li 0.1, Poly-Li 0.2 and Poly-Li 0.3** [C] Variation of the ionic conductivity ($\log \sigma$) with temperature (black line spectra) and corresponding second heating DSC thermogram (red line spectra) for (i) **Poly/Li-0.3**, ii) **Poly/Li-0.2**, iii) **Poly/Li-0.1** and iv) **Poly/Li-0.05** complexes.

Table 3.5 Ionic conductivity of Poly-Li complexes at various temperatures during heating cycle.

Poly(P4PTEG)/Li-0.03		Poly(P4PTEG)/Li-0.05	
Temperature	Ionic Conductivity	Temperature	Ionic Conductivity
112 °C	2.45E-7	80 °C	3.18E-6
128 °C	7.57E-7	100 °C	4.00E-5
151 °C	4.44E-6	110 °C	7.75E-5
Poly(P4PTEG)/Li-0.1		120 °C	1.08E-5
60 °C	3.89E-7	130 °C	1.45E-5
75 °C	1.21E-6	140 °C	1.53E-5
99 °C	3.83E-6	150 °C	1.93E-5
122 °C	1.05E-5	Poly(P4PTEG)/Li-0.3	
142 °C	1.06E-5	27 °C	1.25E-5
Poly(P4PTEG)/Li-0.2		32 °C	1.40E-5
35 °C	3.52E-7	40 °C	1.91E-5
38 °C	5.96E-7	47 °C	2.76E-5
43 °C	8.97E-7	52 °C	4.38E-5
50 °C	1.71E-6	60 °C	9.46E-5
59 °C	3.40E-6	66 °C	1.56E-4
70 °C	5.06E-6	78 °C	2.30E-4
76 °C	5.89E-6	87 °C	2.80E-4
84 °C	6.72E-6	96 °C	3.10E-4
91 °C	9.56E-6	105 °C	3.90E-4
100 °C	1.08E-5	114 °C	4.92E-4
110 °C	1.32E-5	137 °C	7.27E-4
120 °C	1.77E-5		

Overall, it could be seen that the glass transition had a higher influence on the ionic conductivity compared to the ordered liquid crystalline phase. This is reasonable also since the movements of ions are more closely related to the segmental mobility of the ethylene glycol chains in the polymer. The liquid crystalline order associated with

the rigid azo units in these poly domain samples could be expected to have only an indirect influence on the ions that are complexed to the ethylene glycol units along the polymer chains.

3.3.5 Photoresponsive Ionic Conductivity

The azobenzene moiety is well studied for the trans-cis isomerization. Thin film (dropcast from THF) as well as THF solutions of **Poly(P4PTEG)** was irradiated with a DYMAX Blue Wave 75 light source with an output wavelength in the range 280-450 nm in combination with a 360 nm Oriel bandpass filter for UV and 450 nm for the visible source. The actual photograph of set up is shown in Figure 3.21.

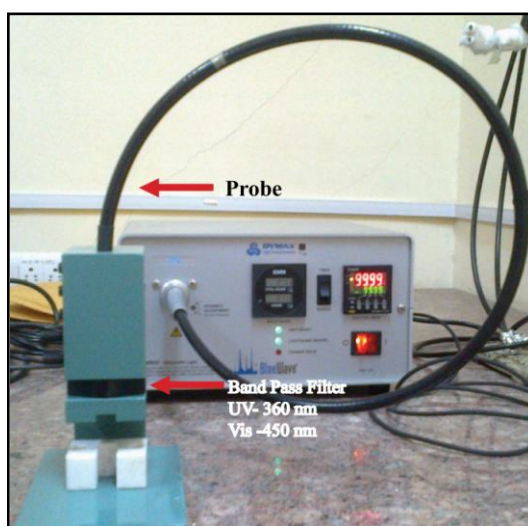


Figure 3.21 Photograph of photoisomerization set-up (for UV irradiation 360 nm and visible light 450 nm band pass filter was used).

The typical absorption spectra for the azobenzene in solution state consists of three characteristic absorption peaks: a low energy transition around 430-450 nm assigned for the $n-\pi^*$ transition, a second transition around 350-360 nm assigned for $\pi-\pi^*$ transition of trans azobenzene (for the cis azobenzene $\pi-\pi^*$ transition occurs around 280 nm) and a third high energy transition around 230-240 nm assigned for the $\pi-\pi^*$ transition of phenyl ring.¹⁴ Figure 3.22a shows the changes in absorption spectra upon UV irradiation in THF solution. Upon photoisomerization, the intensity of $\pi-\pi^*$ transition at 360 nm decreased with simultaneous increase of the $n-\pi^*$ band at 440 nm.¹⁵

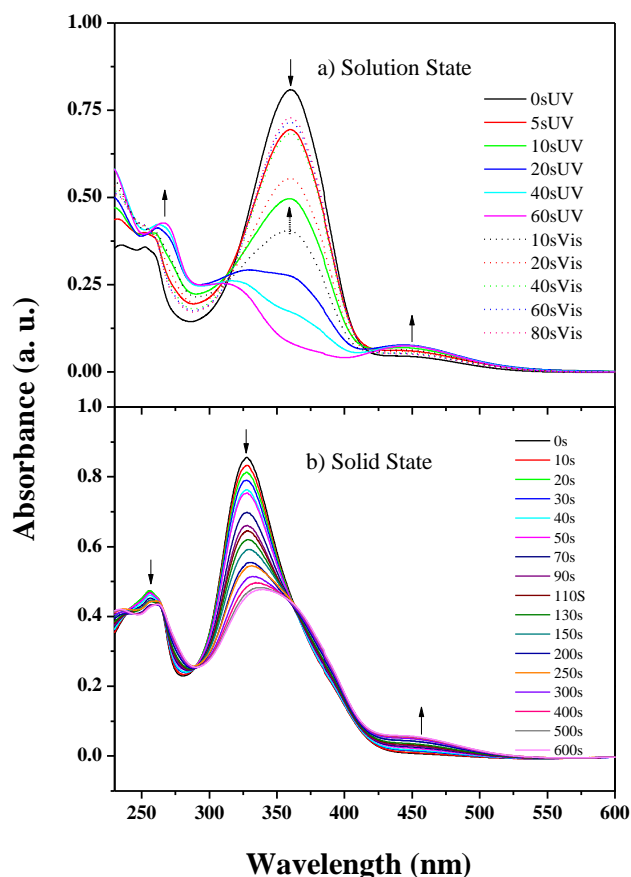


Figure 3.22 Photoisomerization of polymer *Poly(P4PTEG)* a) Solution state in THF solvent and b) Spin coated thin film from THF solvent. (Dotted line spectrum indicates back recovery of trans form upon visible light irradiation (450 nm)).

The extent of cis isomer fraction formed upon UV irradiation was calculated using equation (1) and results were summarized in Table 3.6.¹⁶

$$Y = \frac{1 - A/A_{\text{dark}}}{1 - \epsilon_{\text{cis}}/\epsilon_{\text{trans}}} \dots\dots\dots (1)$$

Where, A_{dark} = Absorption in dark at λ , for only trans isomer, A = absorption after UV irradiation at λ and ϵ_{cis} , ϵ_{trans} = molar absorption coefficient for cis and trans isomer, respectively at λ .

Table 3.6 Extent of photoisomerization (fraction of cis and trans isomers) of Poly(P4PTEG) polymer in solution and thin film.

Poly(P4PTEG) (Solution State)		Poly(P4PTEG) (Solid State)	
Time (s)	Trans: Cis	Time (s)	Trans: Cis
0	100:0	0	100:0
5	85:15	10	97:3
10	60:40	20	95:5
20	30:70	50	88:12
40	21:79	100	80:20
60	6:94	200	63:37
		400	54:46
		600	51:49

An almost 90 % conversion of trans to cis isomer occurred within 60 s of UV irradiation, while an 80 % recovery from cis to trans isomer occurred upon irradiation with 450 nm light in about 80 s. Figure 3.22b follows the corresponding changes in thin spin coated films (from THF) of the polymer. The film thickness was maintained to obtain an optical density < 1.0. Compared to the solution spectra the absorption in thin film was blue shifted by 33 nm indicating aggregation due to excitonic interaction of aromatic chromophore forming H-aggregates.¹⁷ Upon UV irradiation, decrease in intensity of the aggregated peak with a shift in peak maxima towards non-aggregated peak position along with slight increase of the $n-\pi^*$ band was observed. Even after irradiation for 600 s only 49 % conversion of the trans to cis isomer was observed.

The effect of photochemical switching on the ionic conductivity was studied for the Poly(P4PTEG)/Li-0.3 complex, which had exhibited room temperature ionic conductivity in the range of 10^{-5} S cm⁻¹. The experiment was carried out with alternate irradiation of UV and visible light (at intervals of 10 minutes each) on thin polymer electrolyte film (80 μ m). Figure 3.23 compares the absorption spectra of the

polymer/Li complex after each irradiation. The thin film absorption spectra of the polymer/Li complex was more blue shifted than the thin film of the neat polymer sample indicating higher levels of aggregation. Upon 10 minutes irradiation with UV light a dramatic increase in the absorption intensity with pronounced red shift of the peak maxima was observed.

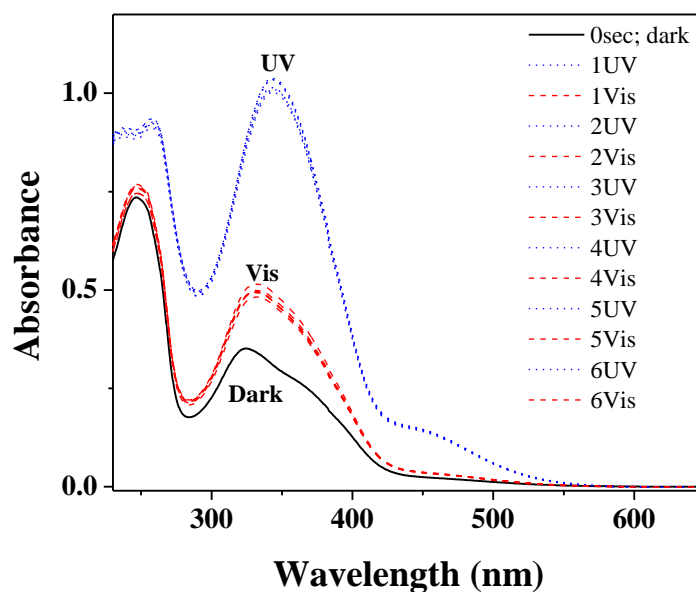


Figure 3.23 Photoisomerization of spin coated thin film (from THF solvent) of polymer *Poly(P4PTEG)/Li0.3* complex. Solid line spectra indicates for as spin coated film (from dark), dotted line indicates spectra after 10 min UV light irradiation using Band Pass Filter of 360 nm and dashed line indicates spectra after 10 min of visible light irradiation using Band Pass Filter of 450 nm.

The extent of trans to cis isomerization could not be calculated due to the overall increase in intensity of the peak maxima. The red shifted (wrt spectra before irradiation) peak maxima indicated less aggregation compared to the initial state; however compared to the un aggregated neat polymer in solution, the spectra was still blue shifted. Consequent irradiation with visible radiation for 10 minutes resulted in reduction in peak intensity and blue shift of peak maxima, but it did not return to the initial aggregated level. The UV and visible irradiation was repeated for 4 or 5 cycles to establish the reversible switching between less aggregated cis isomer to more aggregated trans isomer. The complex impedance spectra were measured for fresh

samples of the **Poly(P4PTEG)/Li-0.3** under similar photoirradiation conditions and data collected after each irradiation step. Figure 3.24-a shows the complex impedance spectra of **Poly(P4PTEG)/Li-0.3** after alternate UV/Vis light irradiation.

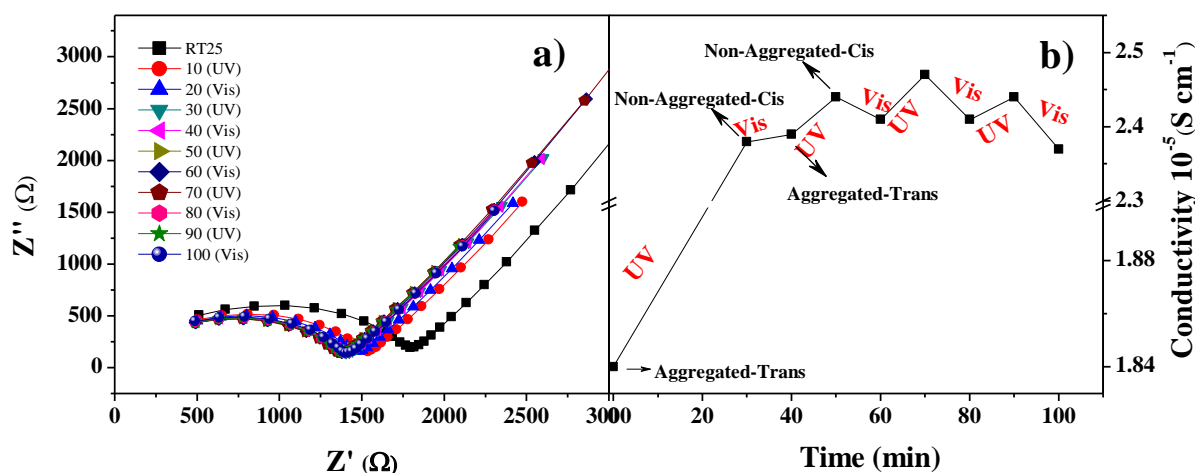


Figure 3.24 (a) Complex impedance spectra of **Poly(P4PTEG)/Li-0.3** complex after alternate UV (360 nm) and Visible irradiation (450 nm) (b) Corresponding change in ionic conductivity upon UV (360 nm) and Visible irradiation (450 nm).

The black line-square impedance spectrum was the initial room temperature measurement, which showed the typical semicircle behaviour in charge transfer region having conductivity in the range of $1.8 \times 10^{-5} \text{ S cm}^{-1}$. An initial increase in ionic conductivity to an overall value of $2.4 \times 10^{-5} \text{ S cm}^{-1}$ was observed for both UV as well as visible light irradiation. A similar observation was reported in literature also.¹⁸ From Figure 3.24b it can be seen that photoswitching behavior was observed in the ionic conductivity value beyond 40 minutes of irradiation. UV light irradiation resulted in an increase in the conductivity whereas visible light irradiation resulted in reduction in ionic conductivity.^{6c} The range of switching observed for ionic conductivity values upon irradiation was similar to those reported in literature.^{6a,b,d} The photoconductivity behavior of **Poly(P4PTEG)/Li-0.3** was in accordance with the observation from the absorption spectra recorded as a function of UV and visible irradiation steps which indicated reduction in aggregation. The absorption spectra gave information regarding the state of aggregation of the azo segment brought about by the complexation of lithium ions to the connecting oligoethylene oxy segments.

The cis isomer which was formed by UV irradiation is unfavorable for chromophore aggregation due to its bent structure, but indirectly favored improved mobility due to reduced aggregation.

3.4 Summary

Twin azobenzene is a versatile design for the synthesis of segmented azobenzene oligo(ethylene oxide) polyesters. This chapter demonstrated the fine tuning of mesophase and transition temperature using twin azobenzene diesters which were designed as AA type monomer and polymerized with diols such as DEG, TEG and HEG in a melt polycondensation polymerization to obtain main chain liquid crystalline polyesters. These main chain liquid crystalline polymers containing photoresponsive azobenzene as well as the oligo(ethylene oxide) segments facilitated ionic conduction and served as good thermo as well as photoresponsive ion conducting materials upon complexation with Li-salt. Ionic conductivity in the range of 10^{-5} S/cm⁻¹ could be obtained at room temperature (25 °C) in case of polymer/0.3 Li complex, which could be further increased up to 10^{-4} S/cm⁻¹ at 65 °C. The temperature dependant ionic conductivity was compared with phase transitions occurring in the sample and it was observed that the glass transition (T_g) had more influence on ionic conductivity of these polymers compared to the ordered liquid crystalline phase transition. The improved segmental motion of oligo(ethylene oxide) segments during glass transition facilitated faster transport of ions compared to liquid crystalline phase transition in these polydomain samples. With the help of azobenzene unit as photoresponsive handle, reversible ionic conductivity switching was observed upon irradiation of the polymer/0.3Li salt complex with alternate UV and visible irradiation. An increase in ionic conductivity upon UV light irradiation followed by reduction in ionic conductivity upon visible light irradiation was observed.

3.4 References

- (1) (a) Hafiz, H. R.; Nakanishi, F. *Nanotechnology* **2003**, *14*, 649 (b) Barrett, C. J.; Mamiya, J.-i.; Yager, K. G.; Ikeda, T. *Soft Matter* **2007**, *3*, 1249-1261 (c) Mativetsky, J. M.; Pace, G.; Elbing, M.; Rampi, M. A.; Mayor, M.; Samorì, P. *J. Am. Chem. Soc.* **2008**, *130*, 9192-9193 (d) Ikeda, T.; Tsutsumi, O. *Science* **1995**, *268*, 1873-1875.
- (2) (a) Kishimoto, K.; Yoshio, M.; Mukai, T.; Yoshizawa, M.; Ohno, H.; Kato, T. *J. Am. Chem. Soc.* **2003**, *125*, 3196-3197 (b) Imrie, C. T.; Ingram, M. D.; McHattie, G. S. *J. Phys. Chem. B* **1999**, *103*, 4132-4138 (c) Kang, Y.; Kim, H. J.; Kim, E.; Oh, B.; Cho, J. H. *J. Power Sources* **2001**, *92*, 255-259 (d) Ohtake, T.; Ogasawara, M.; Ito-Akita, K.; Nishina, N.; Ujiie, S.; Ohno, H.; Kato, T. *Chem. Mater.* **2000**, *12*, 782-789 (e) Cho, B.-K. *RSC Adv.* **2014**, *4*, 395-405.
- (3) (a) Kato, T. *Science* **2002**, *295*, 2414-2418 (b) Kimura, M.; Moriyama, M.; Kishimoto, K.; Yoshio, M.; Kato, T. *Liq. Cryst.* **2007**, *34*, 107-112 (c) Song, J.; Cho, B.-K. *Chem. Commun.* **2012**, *48*, 6821-6823 (d) Kishimoto, K.; Suzawa, T.; Yokota, T.; Mukai, T.; Ohno, H.; Kato, T. *J. Am. Chem. Soc.* **2005**, *127*, 15618-15623.
- (4) Lee, M.; Oh, N.-K.; Lee, H.-K.; Zin, W.-C. *Macromolecules* **1996**, *29*, 5567-5573.
- (5) (a) Percec, V.; Tomazos, D. *J. Mater. Chem.* **1993**, *3*, 643-650 (b) Fish, D.; Khan, I. M.; Smid, J. *Makromol. Chem., Rapid Commun.* **1986**, *7*, 115-120 (c) Bouchet, R.; Maria, S.; Meziane, R.; Aboulaich, A.; Lienafa, L.; Bonnet, J.-P.; Phan, T. N. T.; Bertin, D.; Gigmès, D.; Devaux, D.; Denoyel, R.; Armand, M. *Nature Mater.* **2013**, *12*, 452-457 (d) Okamoto, Y.; Yeh, T. F.; Lee, H. S.; Skotheim, T. A. *J. Polym. Sci., Part A: Polym. Chem.* **1993**, *31*, 2573-2581 (e) Panday, A.; Mullin, S.; Gomez, E. D.; Wanakule, N.; Chen, V. L.; Hexemer, A.; Pople, J.; Balsara, N. P. *Macromolecules* **2009**, *42*, 4632-4637 (f) Trapa, P. E.; Acar, M. H.; Sadoway, D. R.; Mayes, A. M. *J. Electrochem. Soc.* **2005**, *152*, A2281-A2284 (g) Ruzette, A.-V. G.; Soo, P. P.; Sadoway, D. R.; Mayes, A. M. *J. Electrochem. Soc.* **2001**, *148*, A537-A543 (h) Zuo, X.; Liu, X.-M.; Cai, F.; Yang, H.; Shen, X.-D.; Liu, G. *J. Mater. Chem.* **2012**, *22*, 22265-22271 (i) Hawker, C. J.; Chu, F.; Pomery, P. J.; Hill, D. J. T. *Macromolecules* **1996**, *29*, 3831-3838.

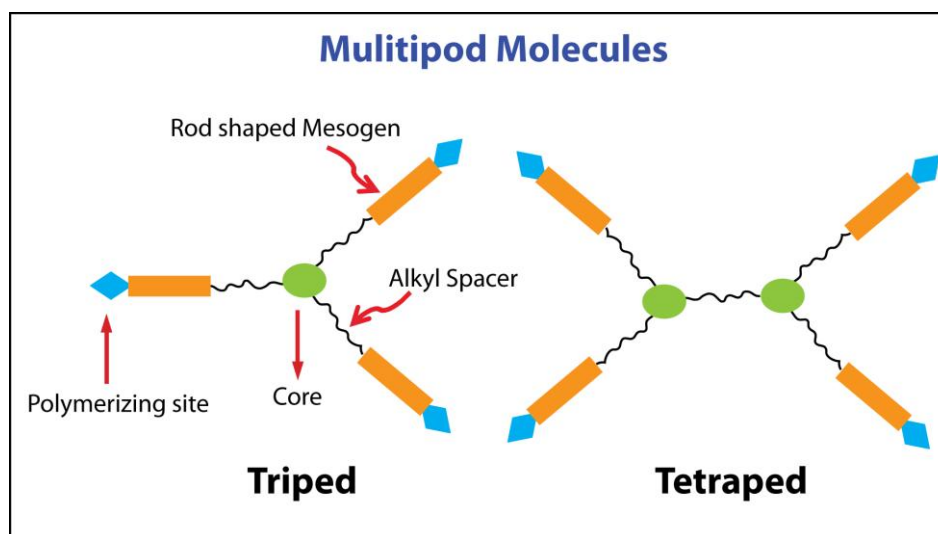
- (6) (a) Kimura, K.; Morooka, H.; Yokoyama, M. *J. App. Poly. Sci.* **1991**, *43*, 1233-1239 (b) Tokuhisa, H.; Yokoyama, M.; Kimura, K. *Chem. Mater.* **1993**, *5*, 989-993 (c) Tokuhisa, H.; Yokoyama, M.; Kimura, K. *Macromolecules* **1994**, *27*, 1842-1846 (d) Tokuhisa, H.; Yokoyama, M.; Kimura, K. *J. Mater. Chem.* **1998**, *8*, 889-891.
- (7) Nardele, C. G.; Asha, S. K. *J. Polym. Sci., Part A: Polym. Chem.* **2012**, *50*, 2770-2785.
- (8) Nardele, C. G.; Asha, S. K. *J. Phys. Chem. B* **2014**, *118*, 1670-1684.
- (9) (a) Kumaresan, S.; Kannan, P. *J. Polym. Sci., Part A: Polym. Chem.* **2003**, *41*, 3188-3196 (b) Iimura, K.; Koide, N.; Ohta, R.; Takeda, M. *Makromol. Chem.* **1981**, *182*, 2563-2568 (c) Izumi, A.; Teraguchi, M.; Nomura, R.; Masuda, T. *Macromolecules* **2000**, *33*, 5347-5352.
- (10) Sato, M.; Mizoi, M.; Uemoto, Y. *Macromol. Chem. Phys.* **2001**, *202*, 3634-3641.
- (11) (a) Wutz, C.; Stribeck, N.; Gieseler, D. *Colloid Polym. Sci.* **2000**, *278*, 1061-1069 (b) Yonetake, K.; Soga, J.; Masuko, T. *Polym. J.* **1997**, *29*, 500-507 (c) Xie, H.-L.; Jie, C.-K.; Yu, Z.-Q.; Liu, X.-B.; Zhang, H.-L.; Shen, Z.; Chen, E.-Q.; Zhou, Q.-F. *J. Am. Chem. Soc.* **2010**, *132*, 8071-8080.
- (12) (a) Takeoka, S.; Ohno, H.; Tsuchida, E. *Polym. Adv. Technol.* **1993**, *4*, 53-73 (b) Qian, X.; Gu, N.; Cheng, Z.; Yang, X.; Wang, E.; Dong, S. *J. Solid State Electrochem.* **2001**, *6*, 8-15.
- (13) Simone, P. M.; Lodge, T. P. *ACS Appl. Mater. Interfaces* **2009**, *1*, 2812-2820.
- (14) Zollinger, H. *Azo and Diazo Chemistry, Aliphatic and Aromatic Compounds*; Interscience Publishers, New York, 1961.
- (15) Moniruzzaman, M.; Talbot, J. D. R.; Sabey, C. J.; Fernando, G. F. *J. App. Poly. Sci.* **2006**, *100*, 1103-1112.
- (16) Victor, J. G.; Torkelson, J. M. *Macromolecules* **1987**, *20*, 2241-2250.

(17) (a) Kuiper, J. M.; Engberts, J. B. F. N. *Langmuir* **2004**, *20*, 1152-1160 (b) M. Kasha; H. R. Rawls; El-Bayoumi, M. A. *Pure Appl. Chem.* **1965**, *11*, 371-392.

(18) Djurado, D.; Delabouglise, D.; Caix-Cecillon, C.; Cecchetto, L.; Decker, I.; Petit, J. P. *Solid State Ionics* **2002**, *154–155*, 29-35.

Chapter 4

Liquid Crystalline Triped and Tetraped Azobenzene Molecules



Triped and tetraped liquid crystalline molecules incorporating the azobenzene moiety was designed using a phloroglucinol core connected to three or four azobenzene moieties via a pentyl or decyl alkyl spacer segment. The mesophase properties and phase behavior were investigated using various instrumentation techniques like differential scanning calorimetry (DSC), polarized light microscopy (PLM) and variable temperature XRD (VTXRD). The triped and tetraped molecules exhibited liquid crystalline (LC) behavior. Reversible isothermal Smectic-Isotropic phase transition photoswitching was achieved with UV irradiation in <1 sec in the azo multipod molecules. These triped and tetraped molecules were suitably substituted with terminal methyl carboxylic ester groups, which could be used as the B_3 and B_4 type of monomers for the synthesis of hyperbranched polymers with suitable A_2 comonomer.

4.1 Introduction

Multipodes have a structural architecture in which mesogenic or premesogenic arms are connected to a central core. If the mesogens are bound end-on or side-on via flexible spacer- (typically long aliphatic chain or oligo ethylene chain) to form flexible mesogenic oligomers, they are called polypedes or polypedals.¹ Among the various versatile designs for multipode (multiarm) mesogens, especially those with a symmetric triped geometry consisting of a central core attached to three mesogenic arms through flexible spacers depicted in Figure 4.1 are very interesting.² The driving force for the self assembly of these molecules in liquid crystalline (LC) phases is based on the nanosegregation of chemically and physically different building blocks and the tendency to efficiently fill the space in the condensed matter.³ The large void space and the flexible nature of the spacer allows for various modes of packing resulting in the observation of various phases like the nematic, columnar and lamellar mesophases in these systems.^{2a,4}

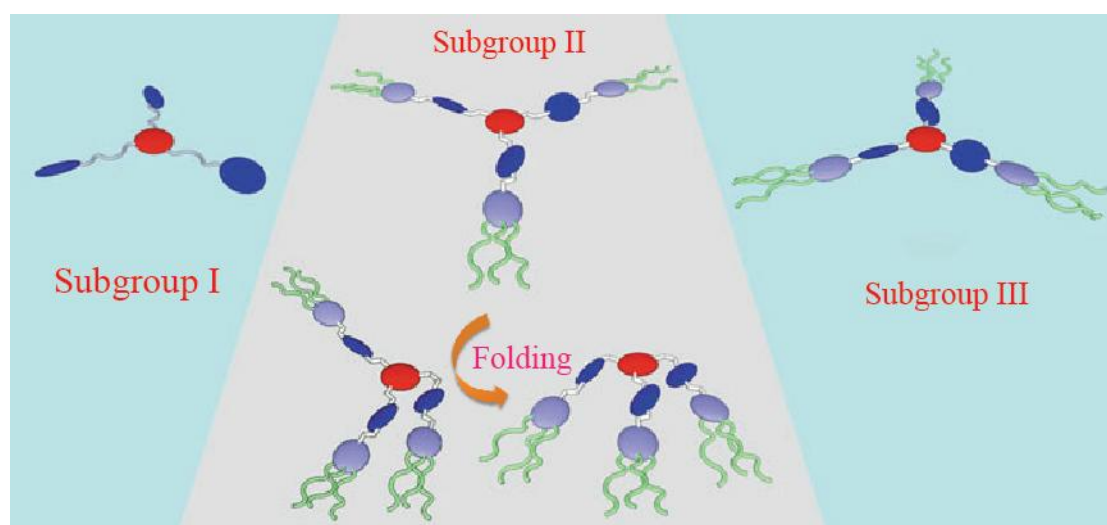


Figure 4.1 Classification of three arm (tripod) mesogens. Flexible (Subgroup I), semi-flexible (Subgroup II) and shape-persistent (Subgroup III). Folding tripod semi-flexible to λ - and E shaped mesogens (Adapted from Lehmann, M. *Chem. Eur. J.* **2009**, *15*, 3638-3651).

The choice of mesogenic arm substitution on central core plays a vital role in deciding the final LC outcome and its function. The multipodes have various

advantages as compared to the linear monomer and oligomers: (i) Structural diversity due to different arms and library of accessible cores (ii) their often high glass transitions and therefore stable glassy LC phases and (iii) their good solubility.

Zhang *et al.* demonstrated a triped design having symmetric mesogenic arms, which exhibited a broad liquid crystalline window that was retained in a glassy liquid crystalline phase at room temperature. (Figure 4.2-a).^{2e}

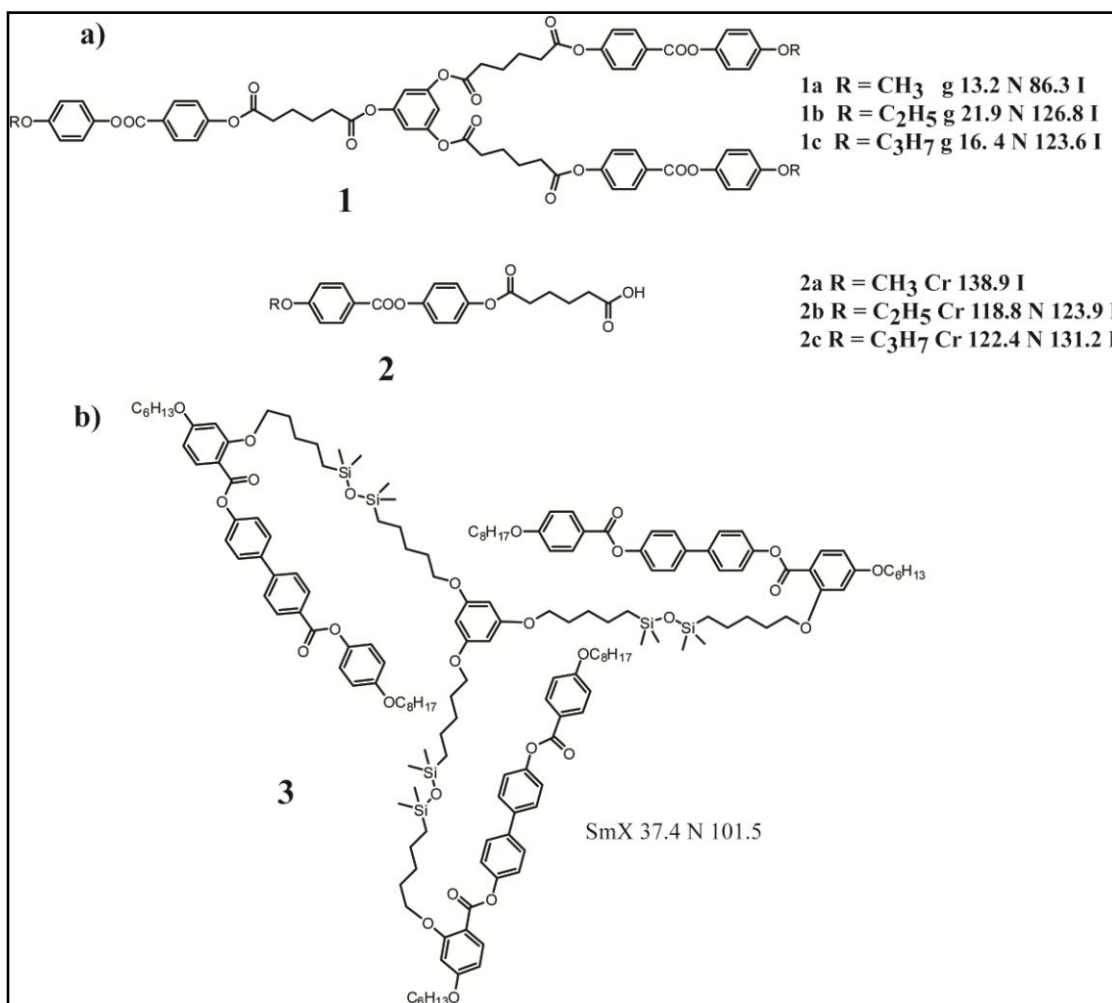


Figure 4.2 a) LC properties with fixed spacer length and peripheral chains. compound (2,3)^{2e} b) Triped LC design with laterally situated nematogen showing biaxial nematic mesophase.^{2d}

Gallardo and co-workers were successful in obtaining liquid crystalline (LC) luminescent materials by symmetric substitution of oxadiazole moiety in the triped structure.^{4b} Lehmann *et al.* reported a star shaped oligobenzoates that were equipped

with naphthalene chromophores, which helped to promote fast charge carrier mobility.⁵ Recently, Kocot *et al.* observed thermotropic biaxial nematic phase traced by polarized IR studies in tripod LC design having laterally attached nematogens (Figure 4.2-b).^{2d} The lateral attachment of the mesogens restricted the rotation about the molecules long axis and therefore favoured a biaxial ordering. All the above discussed examples were limited to small molecules or oligomers because of the lack of suitable functionality on them for further polymerization. Multipodes having terminally installed polymerizable functionality an interesting monomer design for the preparation of functional dendritic architecture. There are reports in literature where in situ polymerization were attempted in the ordered and fluid columnar LC media formed by the tripod monomers functionalized with olefinic or acetylenic bonds by UV irradiation and thermal annealing.⁶ However, the above design had very limited scope because of extremely specific structural requisite and polymerization condition which limited its application and further exploitation.

The Azobenzene is a well-known mesogen as well as photoresponsive chromophore which has found wide application in optical storage, optical displays, molecular switches, photomechanical systems, photo-switchable coatings etc.⁷ Branched LC molecules incorporating azobenzene units are promising structures for the preparation of LC materials with lower viscosity due to their fast switching response in device.⁸ A detailed structure-property relationship analyzing the effect of branching on the mesogenic characteristics by the systematic variation of branching to three-armed stars (tripod) to four-armed stars (tetrapod) is very relevant to material science in order to fine tune properties to generate suitable materials for various applications.⁹ The properties like photoswitching response in going from a simple tripod structure to more branched tetrapod is expected to be different.

This chapter describes the design and synthesis of tripod and tetrapod architectures incorporated with photoresponsive azobenzene moiety. In the design, azobenzene unit served the role of mesogen as well as photoswitching handle for modulating LC properties. The tripod design consisted of three azobenzene mesogens connected to a phloroglucinol core through a poly methylene spacer (5 or 10 alkyl units). The tetrapod design consisted of dimeric structure in which two phloroglucinol core was separated by poly methylene spacer and each phloroglucinol core was

connected to two azobenzene arms via variable alkyl spacer (5 or 10 alkyl units). The terminal unit of the triped and tetraped molecules was suitably functionalized with methyl carboxyl ester groups which could be further polymerized with appropriate A₂ comonomer using transesterification methodology. A comparative study of the LC phases of the triped and tetraped molecules as to the effect of variation of spacer length in each of these classes of materials as well as effect of branching on the LC characteristics of triped vs tetraped molecules was undertaken. A detailed study of the characterization of the LC phases using various instrumentation techniques like differential scanning calorimetry (DSC), polarized light microscopy (PLM) coupled with variable temperature X-ray diffraction is presented. Photoswitching behavior in the LC state as well as in spin coated thin films using an UV irradiation source was also undertaken.

4.2 Experimental section

4.2.1 Materials

Phloroglucinol, 1, 5-dibromopentane, 1, 10-dibromodecane, p-amino benzoic acid, phenol and 18-crown-6 were purchased from Aldrich Company Ltd. and were used as such. Sodium nitrite and potassium carbonate, were purchased from Merck Chemicals Ltd and were used as such. Thionyl chloride, dimethyl formamide (DMF), acetonitrile (CH₃CN), tetrahydrofuran (THF), chloroform (CHCl₃), acetone and methanol were purchased from Merck Chemicals Ltd. and were purified using standard procedures.

4.2.2 Instrumentation

¹H-NMR and ¹³C-NMR spectra of all molecules were recorded on a Bruker-AVANCE 400 MHz spectrometer. Chemical shifts are reported in ppm at 25 °C using CDCl₃ as solvent containing small amount of tetramethylsilane (TMS) as internal standard. The purity of the compounds was determined by elemental analysis as well MALDI-TOF in combination with size exclusion chromatography (SEC). Elemental analysis was done by Thermofinnigan flash EA 1112 series CHNS analyzer. Infrared spectra were recorded using Bruker FT-IR (ATR mode) spectrophotometer in the range of 4000-600 cm⁻¹. UV-Vis spectra were recorded using a Perkin Elmer Lambda-35 UV-Vis spectrometer. The thermal stability of all the model compounds and

multipod molecules were analyzed using Perkin Elmer: STA 6000 thermogravimetric analyzer (TGA) under nitrogen atmosphere from 40-800 °C at 10 °C/min. Differential Scanning Calorimetry (DSC) was performed using a TA Q10 model. About 2–3 mg of the sample was taken in aluminium pan, sealed and scanned at 10 °C/min under nitrogen atmosphere. The instrument was calibrated with indium standards before measurements. The phase behavior of the molecules was analyzed using LIECA DM2500P polarized optical microscope equipped with Linkam TMS 94 heating and cooling stage connected to a Linkam TMS 600 temperature programmer. The various phase transitions was monitored during heating and cooling cycles. Powder X-ray diffraction of all the samples were recorded by a DY 1042-Empyrean XRD with Programmable Divergence Slit(PDS) and PIXcel 3D detector using Cu K α (1.54 Å) emission. The spectra were recorded in the range of (2θ) 3–50° and analyzed using X'pert software. Variable temperature in situ XRD experiments were carried out in an Anton-Paar XRK900 reactor. Single crystal X-ray diffraction data was collected on a Super Nova Dual source X-ray Diffractometer system (Agilent Technologies) equipped with a CCD area detector and operated at 250 W (50 kV, 0.8 mA) to generate Mo K α radiation ($\lambda = 0.71073$ Å). The crystal reported in this paper was mounted on Nylon CryoLoops (Hampton Research) with Paraton-N (Hampton Research).

4.2.3 Synthesis of triped and tetraped bromo intermediates

1,3,5-tris(5-bromopentyloxy)benzene and 1,5-bis(3,5-bis(5-bromopentyloxy)phenoxy)pentane:

To a stirred solution of 1, 5-dibromobutane (8.20 g, 35.67 mmol) and K₂CO₃ (6.56 g, 47.57 mmol) in DMF 20 mL was added phloroglucinol (1 g, 7.92 mmol) in 6 mL DMF over a period of 30 min. The reaction mixture was stirred for 48 h at room temperature and reaction mixture was filtered. The filtrate was poured in 400 mL water and stirred well; the resultant solution was extracted with dichloromethane. The combined organic layer was washed with brine, dried over sodium sulphate and evaporated under reduced pressure to afford the crude oily product. Further separation of two products was carried out by silica column chromatography, pet ether/EtOAc. The 1,3,5-tris(5-bromopentyloxy)benzene afforded oily liquids in pet ether/EtOAc

(95:5 v/v) whereas 1,5-bis(3,5-bis(5-bromopentyloxy)phenoxy)pentane eluted in pet ether/ Ethyl acetate (95:6 v/v) as oily liquid.

1,3,5-tris(5-bromopentyloxy)benzene (T3Br5Phg): Yield (2.3 g, 51 %), ^1H NMR (400 MHz CDCl_3): δ (ppm): 6.04 (3H, s, Ar-phg), 3.91 (6H, t, Arphg- $\text{OCH}_2\text{-CH}_2\text{-}$), 3.43 (6H, t, Br- $\text{CH}_2\text{-CH}_2\text{-}$) 1.99-1.51 (18H, m, $\text{-CH}_2\text{-CH}_2\text{-}$), ^{13}C NMR (CDCl_3) δ ppm: 160.75, 93.79, 67.53, 33.59, 32.42, 28.33, 24.80 FTIR (KBr) (cm^{-1}): 2937, 2867, 1593, 1459, 1386, 1252, 1150, 1059, 816, 736, 681, 642. MALDI-TOF (m) 570.87, (m+Na) 592.84, (m+k) 608.87.

1,5-bis(3,5-bis(5-bromopentyloxy)phenoxy)pentane (T4Br5bisPhg): Yield (1.23 gm, 17%), ^1H NMR (400 MHz CDCl_3): δ (ppm): 6.04 (6H, s, Ar-phg), 3.91 (12H, t, Arphg- $\text{OCH}_2\text{-CH}_2\text{-}$), 3.43 (8H, t, Br- $\text{CH}_2\text{-CH}_2\text{-}$) 2.04-1.51 (30H, m, $\text{-CH}_2\text{-CH}_2\text{-CH}_2\text{-CH}_2\text{-}$), ^{13}C NMR (CDCl_3) δ ppm: 160.78, 93.85, 67.56, 33.58, 32.45, 28.96 28.37, 24.83, 22.73 FTIR (KBr) (cm^{-1}): 2924, 2854, 1595, 1460, 1384, 1252, 1153, 1059, 817, 724, 681, 643. MALDI-TOF (m) 916.92, (m+Na) 938.88, (m+k) 954.83.

1,3,5-tris(10-bromodecyloxy) benzene and 1,10-bis(3,5-bis(10-bromodecyloxy) phenoxy) decane:

A similar procedure as above was adopted using 1, 10-dibromodecane (10.70 g, 35.67 mmol) and phloroglucinol (1 g, 7.92 mmol). The crude product was purified by silica column chromatography using hexane-ethyl acetate solvent mixture. 1,3,5-tris(10-bromodecyloxy) benzene was eluted in pet ether/EtOAc (98:2 v/v) mixture as oily liquid whereas 1,10-bis(3,5-bis(10-bromodecyloxy)phenoxy)decane was eluted in pet ether/ EtOAc (97:3 v/v) solvent as oily liquid.

1,3,5-tris(10-bromodecyloxy) benzene (T3Br10Phg): Yield (1.5 g, 25 %), ^1H NMR (400 MHz CDCl_3): δ (ppm): 6.04 (3H, s, Ar-phg), 3.88 (6H, t, Arphg- $\text{OCH}_2\text{-CH}_2\text{-}$), 3.40 (6H, t, Br- $\text{CH}_2\text{-CH}_2\text{-}$) 1.91-1.67(12H, m, $\text{-CH}_2\text{-CH}_2\text{-}$), 1.46-1.24 (36H, m, $\text{-CH}_2\text{-CH}_2\text{-}$). ^{13}C NMR (CDCl_3) δ ppm: 160.89, 93.78, 67.98, 34.05, 32.79, 29.41, 29.33, 29.29, 29.19, 28.71, 28.13, 25.99 FTIR (KBr) (cm^{-1}): 2922, 2852, 1596, 1461, 1385, 1260, 1158, 1060, 804, 722, 681, 644. MALDI-TOF (m) 780.32, (m+Na) 803.28.

1,10-bis(3,5-bis(10-bromodecyloxy)phenoxy)decane (T4Br10bisPhg): Yield (0.6 g, 10 %), ^1H NMR (400 MHz CDCl_3): δ (ppm): 6.04 (6H, s, Ar-phg), 3.88 (12H, t, Arphg- $\text{OCH}_2\text{-CH}_2\text{-}$), 3.39 (8H, t, Br- $\text{CH}_2\text{-CH}_2\text{-}$), 1.91-1.67 51 (20H, m, $\text{-CH}_2\text{-CH}_2\text{-}$), 1.50-1.24 (60H, m, $\text{CH}_2\text{-CH}_2\text{-CH}_2\text{-CH}_2\text{-}$), ^{13}C NMR (CDCl_3) δ ppm: 160.89, 93.68,

67.90, 34.00, 32.77, 29.27 29.91, 28.69, 28.11, 25.98 FTIR (KBr) (cm^{-1}): 2924, 2854, 1595, 1460, 1384, 1252, 1153, 1059, 817, 724, 681, 643. MALDI-TOF (m) 1262.47, (m+Na) 1290.60, (m+k) 1306.

4.2.4 Synthesis of triped and tetraped molecules

T3star5: A mixture of 1,3,5-tris(5-bromopentyloxy)benzene (0.94 g, 1.64 mmol), 4-(4'-hydroxy phenyl azo)-benzoic acid methyl ester (1.68 g, 6.55 mmol), K_2CO_3 (1.13 g, 8.18 mmol) and 18 crown 6 (catalyst) in CH_3CN (60 mL) solvent was refluxed for 20 h. For workup, the reaction mixture was cooled to room temperature and the solvent was removed under reduced pressure. The resultant crude product was dissolved in water, filtered and dried in vacuum oven for overnight. The product was purified by flash column chromatography (SiO_2 , PhMe/EtOAc 95:5 v/v) resulting in an orange solid. Yield (1.24 g, 69 %), mp = 185 °C.

$^1\text{H-NMR}$ (400 MHz CDCl_3): δ (ppm): 8.15 (6H, d, ArAzo), 7.91 (12H, m, ArAzo), 6.99 (6H, d, ArAzo), 6.07 (3H, s, Ar-phg), 4.06 (6H, t, Azo- $\text{OCH}_2\text{-CH}_2\text{-}$), 3.94 (15H, m, Phg- $\text{OCH}_2\text{-CH}_2\text{-}$, Azo- COOCH_3), 1.98-1.57 (18H, m, $\text{CH}_2\text{-CH}_2\text{-CH}_2\text{-CH}_2$) ^{13}C NMR (CDCl_3) δ ppm: 166.64, 162.17, 160.85, 155.33, 146.85, 131.10, 130.57, 125.19, 122.33, 114.75, 93.82, 68.13, 67.68, 52.29, 28.89, 22.71 FTIR (ATR) (cm^{-1}): 2944, 2870, 1714, 1595, 1498, 1463, 1438, 1395, 1277, 1247, 1162, 1140, 1104, 1060, 1013, 977, 861, 829, 771, 728, 688, 634. MALDI-TOF (m+1) 1100.84, (m+Na) 1122.27, (m+K) 1138.9 Elemental analysis calculated for $\text{C}_{63}\text{H}_{66}\text{N}_6\text{O}_{12}$: C, 68.84; H, 6.05; N, 7.65. Found: C, 68.56; H, 6.15; N, 7.62.

T3star10: A similar procedure as that reported for **T3star5** was adopted using 0.25 g (0.32 mmol) of 1,3,5-tris(10-bromodecyloxy) benzene. The final product after column purification (SiO_2 , PhMe/EtOAc 97:3 v/v) was obtained as an orange solid. Yield (0.22 g, 53 %), mp = 167 °C.

$^1\text{H-NMR}$ (400 MHz CDCl_3): δ (ppm): 8.15 (6H, d, ArAzo), 7.91 (12H, m, ArAzo), 6.99 (6H, d, ArAzo), 6.05 (3H, s, Ar-phg), 4.03 (6H, t, Azo- $\text{OCH}_2\text{-CH}_2\text{-}$), 3.94 (9H, m, Azo- COOCH_3), 3.89 (6H, t, phg- $\text{OCH}_2\text{-CH}_2\text{-}$), 1.88-1.70 (12H, m, $\text{CH}_2\text{-CH}_2\text{-CH}_2\text{-CH}_2$), 1.50-1.22 (36H, m, $\text{CH}_2\text{-CH}_2\text{-CH}_2\text{-CH}_2$) ^{13}C NMR (CDCl_3) δ ppm: 166.62, 162.35, 160.98, 155.41, 146.88, 131.13, 130.56, 125.19, 122.32, 114.80, 93.86, 68.43, 68.00, 52.22, 29.45, 29.15, 26.03. FTIR (KBr) (cm^{-1}): 2920, 2852, 1724,

1592, 1497, 1470, 1436, 1393, 1280, 1251, 1179, 1146, 1104, 1018, 863, 804, 691. MALDI-TOF (m + isotopic) 1315.64, (m+Na) 1331.61. Elemental analysis calculated for $C_{78}H_{96}N_6O_{12}$: C, 71.53; H, 7.39; N, 6.42 Found: C, 71.10; H, 7.23; N, 6.62.

T4star5: A mixture of 1,5-bis(3,5-bis(5-bromopentyloxy)phenoxy)pentane (0.40 g, 0.44 mmol), 4-(4'-hydroxy phenyl azo)-benzoic acid methyl ester (0.67 g, 2.61 mmol), K_2CO_3 (0.36 g, 2.62 mmol) and 18 crown 6 (cat) in CH_3CN (30 mL) solvent was refluxed for 20 hrs. For workup, the reaction mixture was cooled to room temperature and the solvent was removed under reduced pressure. The resultant crude product was dissolved in water, filtered and dried in vacuum oven for overnight. The product was purified by flash column chromatography (SiO_2 , PhMe/EtOAc 94:6 v/v) resulting in an orange solid. Yield (0.350 g, 50 %), mp = 160 °C.

1H -NMR (400 MHz $CDCl_3$): δ (ppm): 8.15 (2H, d, ArAzo), 7.91 (4H, m, ArAzo), 6.99 (2H, d, ArAzo), 6.07 (6H, s, Ar-phg), 4.06 (8H, t, Azo- OCH_2-CH_2-), 3.94 (24H, m, Phg- OCH_2-CH_2- , Azo- $COOCH_3$), 2.04-1.50 (30H, m, $CH_2-CH_2-CH_2-CH_2$). ^{13}C NMR ($CDCl_3$) δ ppm: 166.58, 162.17, 160.82, 155.27, 146.81, 130.53, 125.18, 122.30, 114.73, 93.81, 68.10, 67.65, 52.22, 28.91, 28.85, 22.67. FTIR (KBr) (cm^{-1}): 2921, 2852, 1717, 1593, 1500, 1461, 1390, 1253, 1139, 1098, 1055, 1015, 862, 804, 723, 686. MALDI-TOF (m+Na) 1640.45 Elemental analysis calculated for $C_{93}H_{100}N_8O_{18}$: C, 69.04; H, 6.23; N, 6.93. Found: C, 68.79; H, 6.39; N, 6.72.

T4star10: A similar procedure as that reported for **T4star5** was adopted using 0.29 g (0.23 mmol) of 1,10-bis(3,5-bis(10-bromodecyloxy)phenoxy)decane. The final product after column purification (SiO_2 , PhMe/EtOAc 96:4 v/v) was obtained as an orange solid. Yield (0.210 g, 47 %), mp = 132 °C.

1H -NMR (400 MHz $CDCl_3$): δ (ppm): 8.15 (2H, d, ArAzo), 7.91 (4H, m, ArAzo), 6.99 (2H, d, ArAzo), 6.05 (6H, s, Ar-phg), 4.03 (8H, t, Azo- OCH_2-CH_2-), 3.94 (12H, s, Azo- $COOCH_3$), 3.89 (12H, m, Phg- OCH_2-CH_2-), 1.90-1.60 (20H, m, $CH_2-CH_2-CH_2-CH_2$), 1.57-1.22 (60H, m, $CH_2-CH_2-CH_2-CH_2$). ^{13}C NMR ($CDCl_3$) δ ppm: 166.60, 162.37, 160.91, 155.26, 146.75, 131.08, 130.55, 125.25, 122.30, 114.77, 93.71, 68.38, 67.93, 52.24, 29.31, 26.02, 26.03. FTIR (KBr) (cm^{-1}): 2921, 2852, 1717, 1593, 1461, 1251, 1138, 1100, 1055, 1014, 808, 774, 685. MALDI-TOF (m+Na)

1991.0. Elemental analysis calculated for $C_{118}H_{150}N_8O_{18}$: C, 72.00; H, 7.68; N, 5.69. Found: C, 71.97; H, 7.78; N, 5.42.

4.2.5 Synthesis of Model Compound

P5Br: 4-(4'-hydroxy phenyl azo)-benzoic acid methyl ester (1 g, 3.89 mmol) with 1, 5-dibromopentane (2.68 g, 11.65 mmol) was taken in two neck 100 mL round bottom flask in 45 mL of dry acetone in the presence of excess of anhydrous K_2CO_3 (1.07 g, 7.78 mmol) and catalytic amount of potassium iodide (KI). The reaction mixture was stirred at 65 °C for 15 h. After cooling the reaction mixture to room temperature, excess of solvent was removed under reduced pressure. The resultant crude product was poured in to 300 mL of water and extracted with dichloromethane. The combined organic layer was washed with water, brine, dried over sodium sulphate and evaporated under reduced pressure to afford a crude orange solid. The column purification (SiO_2 , pet ether/EtOAc 90:10) afforded orange solid. Yield (1.20 g, 76 %), mp = 118 °C.

1H NMR (400 MHz $CDCl_3$): δ (ppm): 8.16 (2H, d, Ar), 7.91 (4H, m, Ar), 7.00 (2H, d, Ar), 4.05 (3H, t, -ArO- CH_2 - CH_2 -), 3.94 (3H, s, -C(O)O CH_3), 3.40 (2H, t, - CH_2 - CH_2 Br), 1.99-1.75 (4H, m, - CH_2 - CH_2 - CH_2 -), 1.50-1.69 (2H, m, - CH_2 - CH_2 - CH_2 -). ^{13}C NMR ($CDCl_3$) δ ppm: 166.28, 161.74, 154.99, 146.56, 130.79, 130.23, 124.85, 121.99, 114.41, 67.62, 51.93, 33.18, 32.07, 31.50, 27.98, 26.43, 24.43 FTIR (KBr) (cm^{-1}): 2934, 2857, 1713, 1585, 1490, 1460, 1429, 1393, 1236, 1096, 999, 841, 811, 764, 723 687. MALDI-TOF (m) 405.08 Elemental analysis calculated for $C_{15}H_{14}N_2O_3$: C, 56.31; H, 5.22; N, 6.91. Found: C, 55.97; H, 4.90; N, 6.79.

P10Br: 4-(4'-hydroxy phenyl azo)-benzoic acid methyl ester (1 g, 3.89 mmol) with 1, 10-dibromodecane (3.50 g, 11.68 mmol) taken in two neck 100 mL round bottom flask in 45 mL of dry acetone in the presence of excess of anhydrous K_2CO_3 (1.07 g, 7.78 mmol) and catalytic amount of potassium iodide (KI). The reaction mixture was stirred at 65 °C for 15 h. After cooling the reaction mixture to room temperature excess of solvent was removed under reduced pressure. The resultant crude product was poured in to 300 mL of water and extracted with dichloromethane. The combined organic layer was washed with water, brine, dried over sodium sulphate and evaporated under reduced pressure to afford crude orange solid. The column

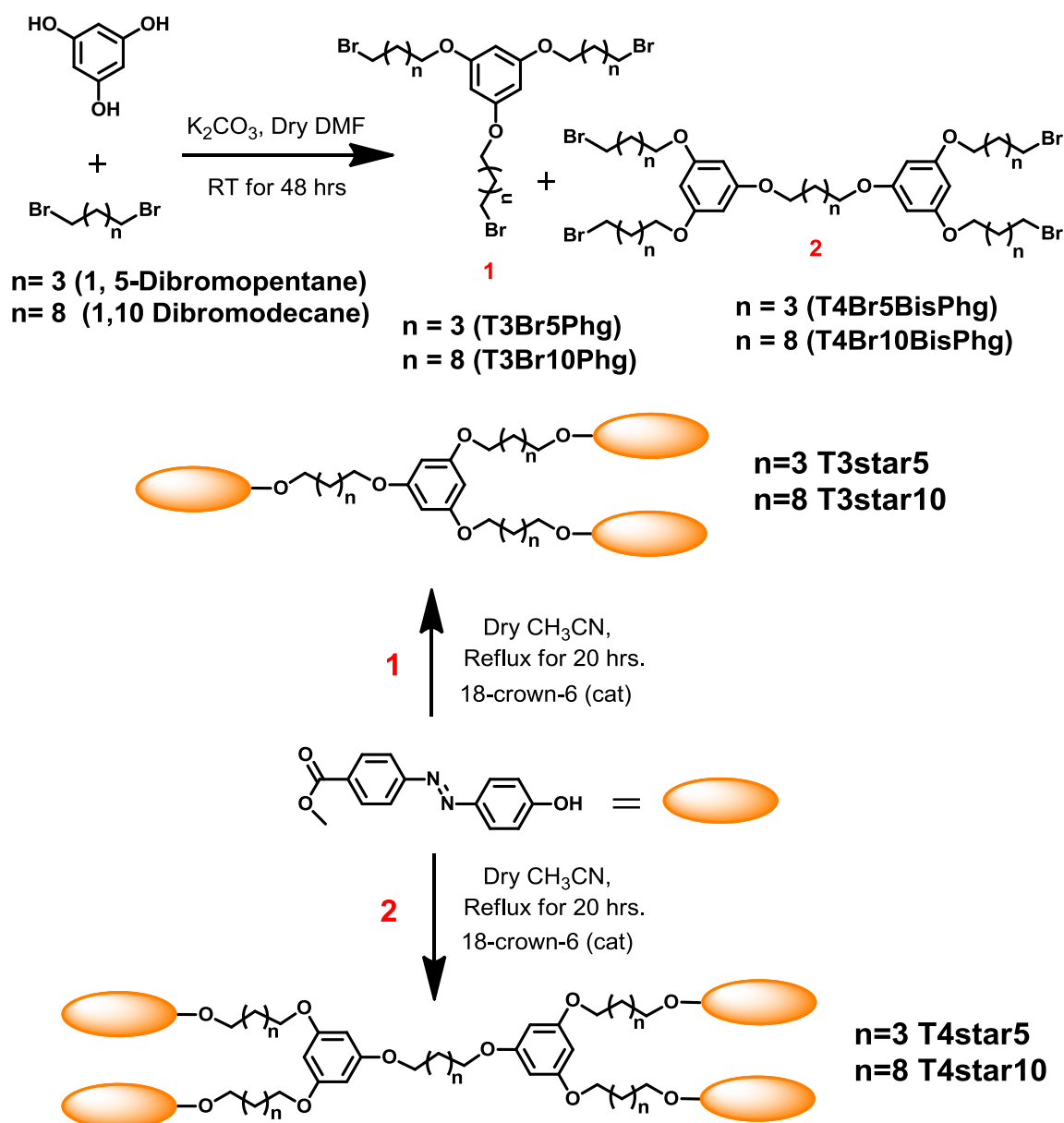
purification (SiO₂, pet ether/EtOAc 95:5) afforded orange solid. Yield (0.90 g, 48 %), mp = 116 °C.

¹H NMR (400 MHz CDCl₃): δ (ppm): 8.16 (2H, d, Ar), 7.92 (4H, m, Ar), 7.00 (2H, d, Ar), 4.04 (3H, t, -ArO-CH₂-CH₂-), 3.94 (3H, s, -C(O)OCH₃), 3.40 (2H, t, -CH₂-CH₂Br), 1.99-1.75 (4H, m, -CH₂-CH₂-CH₂-), 1.54-1.22 (12H, m, -CH₂-CH₂-CH₂-). ¹³C NMR (CDCl₃) δ ppm: 166.62, 162.32, 155.38, 146.84, 130.56, 125.18, 122.32, 114.78, 68.38, 52.23, 39.97, 32.79, 29.39, 28.71, 28.13, 25.95. FTIR (KBr) (cm⁻¹): 2920, 2851, 1718, 1577, 1494, 1464, 1428, 1389, 1273, 1101, 1009, 946, 864, 778, 732, 694. MALDI-TOF (m) 475.11, (m+k) 513.09 Elemental analysis calculated for C₂₄H₃₁BrN₂O₃: C, 60.63; H, 6.57; N, 5.89. Found: C, 60.42; H, 6.67; N, 5.70.

4.3 Results and Discussion

4.3.1 Synthesis and characterization

Phloroglucinol is a readily available commercial tri functional core which has been used to develop an array of C₃-symmetric compounds.^{5,10} A triped monomer core was designed by coupling phloroglucinol with 1, 5-dibromopentane or 1, 10-dibromodecane as shown in Scheme 4.1. An excess (4.5 equivalents) of the α,ω-dibromoalkane was used in the coupling to drive the reaction to completion. However, along with the desired tri bromo alkoxy benzene derivative (1), the dimeric structure (2) as shown in Scheme 4.1 was also obtained after column purification in reasonably good yields. Thus, a 50 % yield of the pentyloxy substituted triped and 17 % yield of the pentyloxy substituted tetraped was obtained; whereas the yields were 50 % for the decyloxy substituted triped and 10 % for the decyloxy substituted tetraped derivative, respectively. These bromo tri and tetraped intermediates were characterized with ¹H-NMR spectroscopy and also confirmed by mass analysis using MALDI-TOF. The ¹H-NMR spectra for the bromo triped (**T3Br5Phg**) and tetraped (**T4Br5Phg**) were shown in Figure 4.3. The azobenzene coupled tri and tetraped derivatives of the 5 and 10 alkyl spacers were further synthesized from compounds (1) and (2) by reaction with the azo dye in dry acetonitrile in presence of 18-crown-6 as catalyst (detailed synthesis of the starting azo dye is given in chapter 2).¹¹



Scheme 4.1 Synthesis of azo triped (B_3 type) and tetraped (B_4 type) molecules.

For instance, the triped **T3star5** azobenzene monomer was synthesized by etherification reaction of 1,3,5-tris(5-bromopentyloxy)benzene with 4-(4'-hydroxy-phenylazo)-benzoic acid methyl ester. The tetraped (dimeric structure) **T4star5** monomer was synthesized by etherification of 1,5-bis(3,5-bis(5-bromopentyloxy)phenoxy)pentane with 4-(4'-hydroxy-phenylazo)-benzoic acid methyl ester. Two model compounds bearing the azobenzene moiety and terminated

by either bromo pentyl (**P5Br**) or bromo decyl (**P10Br**) spacer units were also synthesized as shown in Scheme 4.2.

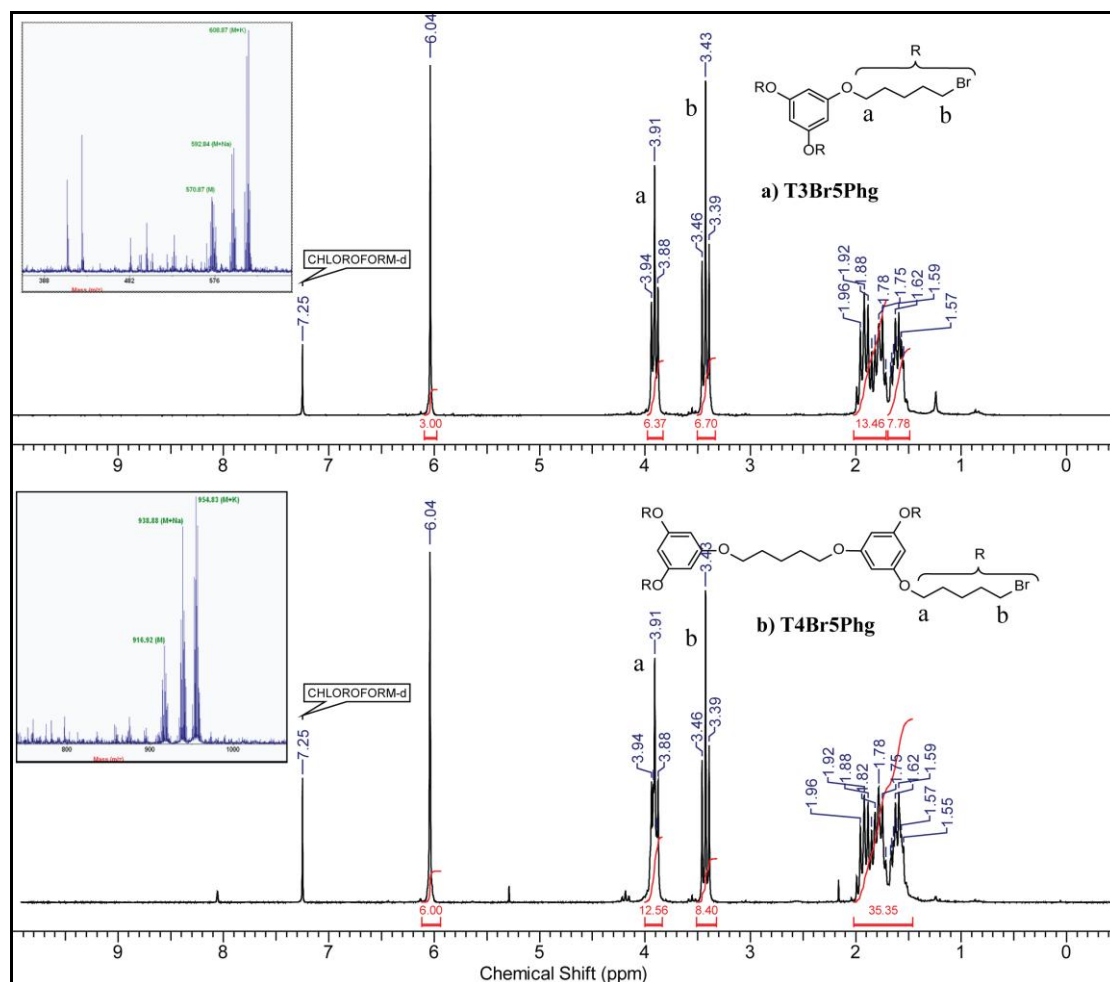
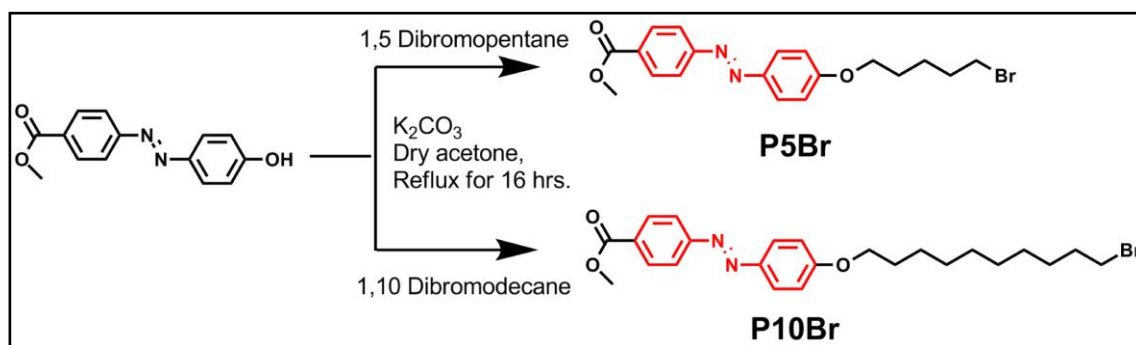


Figure 4.3 $^1\text{H-NMR}$ spectra of bromo intermediate and a) triped - **T3Br5Phg** and b) tetraped - **T4Br5Phg** in CDCl_3 solvent. Inset shows MALDI-TOF spectra of corresponding molecules.



Scheme 4.2 Synthesis of model compounds **P5Br** and **P10Br**.

They were synthesized by refluxing 4-(4'-hydroxy-phenylazo)-benzoic acid methyl ester (azo dye) in presence of 1, 5-dibromopentane and 1, 10-dibromodecane respectively in acetone. The triped and tetrapod molecules and the model compounds were structurally well characterized using $^1\text{H-NMR}$ and $^{13}\text{C-NMR}$ spectroscopy. The $^1\text{H-NMR}$ spectra of tri and tetrapod molecules having spacer length five are shown in Figure 4.4 and spacer length ten were shown in Figure 4.5. The signal corresponding to phloroglucinol aromatic core proton appeared at 6.07 ppm and the azobenzene core proton showed three sets of protons in the range of 6.97-8.18 ppm. Comparing the integration values of phloroglucinol core proton to that of the azobenzene aromatic protons, confirmed the symmetric placement of the azobenzene chromophore on phloroglucinol core.

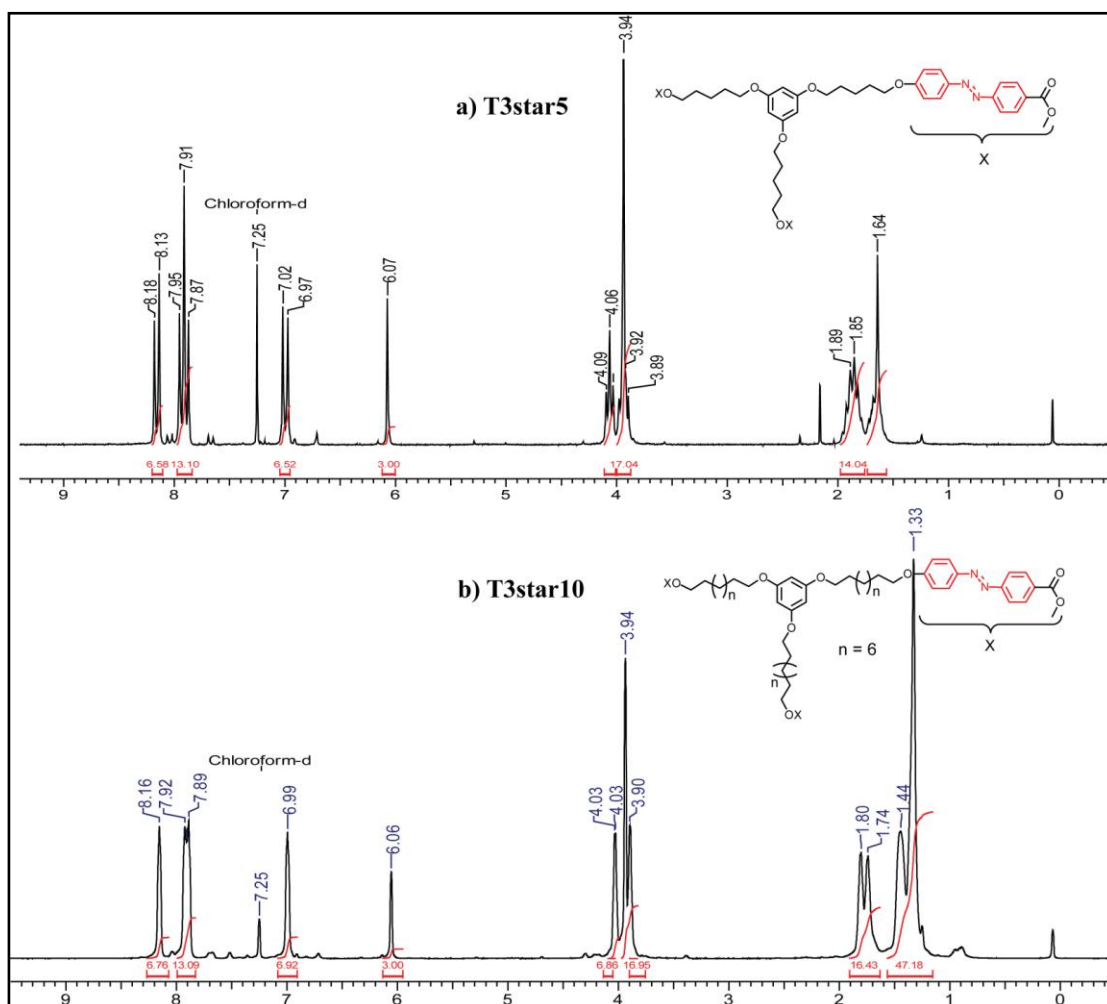


Figure 4.4 $^1\text{H-NMR}$ of triped azobenzene molecules a) *T3star5* and b) *T3star10* in CDCl_3 as solvent.

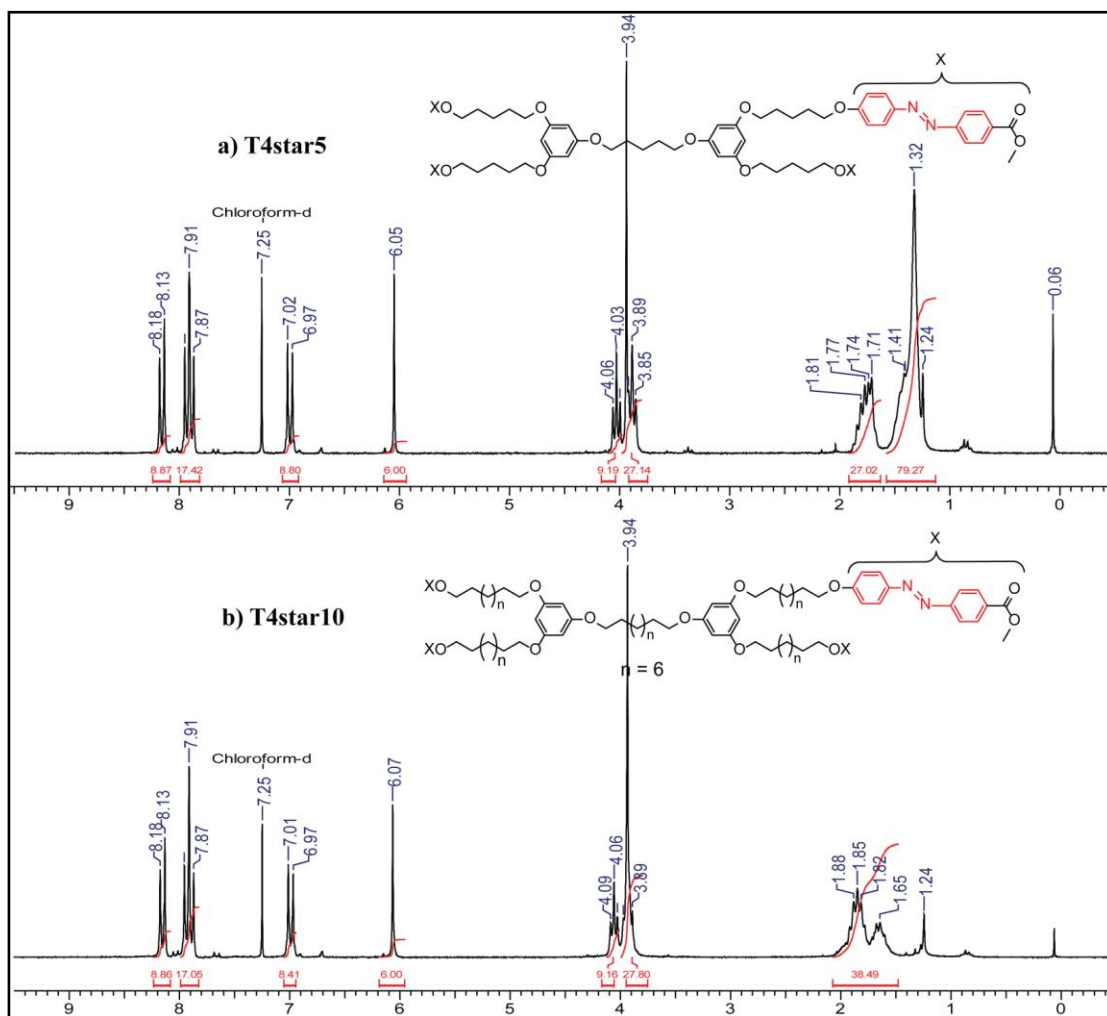


Figure 4.5 $^1\text{H-NMR}$ of tripod azobenzene molecules a) **T4star5** and b) **T4star10** in CDCl_3 as solvent.

The $^1\text{H-NMR}$ spectra for the two model compounds **P5Br** and **P10Br** are shown in Figure 4.6. The purity of molecules and model compounds were confirmed by mass analysis using MALDI-TOF and by single peak in gel permeation chromatography (GPC) as well as elemental analysis. The gel permeation chromatogram of all molecules and model compounds are shown in Figure 4.7. The single peak in size exclusion chromatography, confirms purity of the molecules.

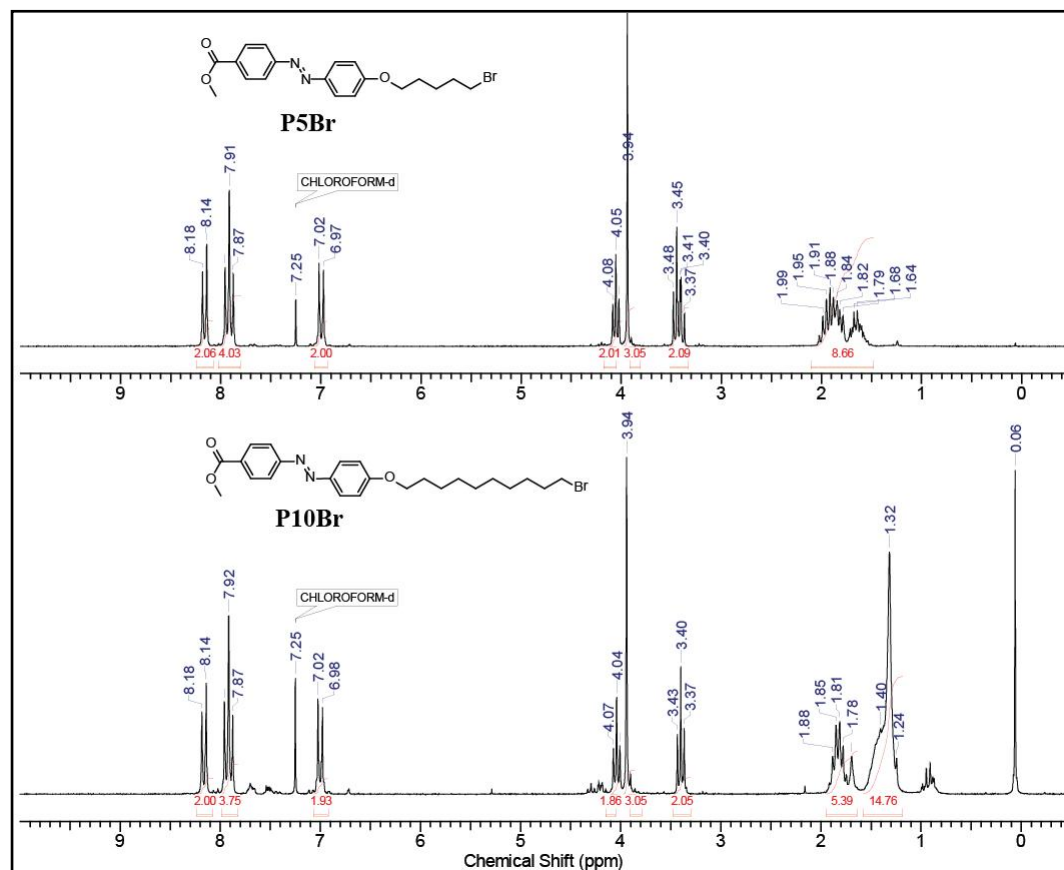


Figure 4.6 $^1\text{H-NMR}$ spectra of model compounds a) **P5Br** and b) **P10Br**.

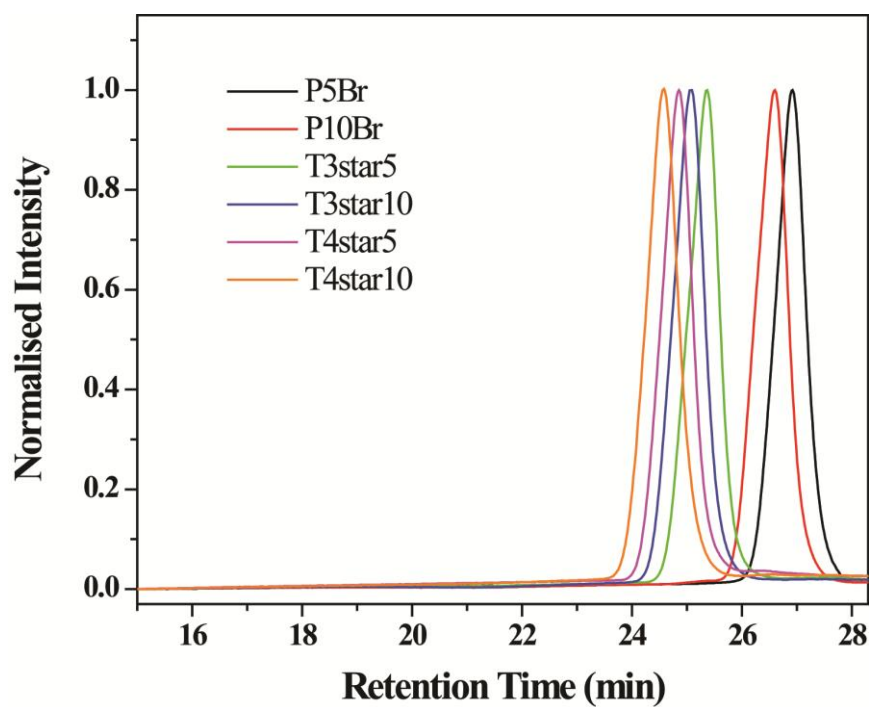


Figure 4.7 Gel permeation chromatogram (GPC) of molecules in CHCl_3 solvent.

4.3.2 Mesophase Characteristics of Triped and Tetraped Molecules

The thermal stability of the model compounds, triped and tetraped molecules were determined by TGA under N₂ atmosphere (Figure 4.8). All molecules were observed to be thermally stable up to 300 °C except for the **T3star10**, which exhibited lower thermal stability (10 % weight loss ~ 220 °C). Table 4.1 compares the 10 wt % decomposition temperature of the model compounds (**P5Br** and **P10Br**) with that of the respective triped and tetraped azo molecules. The triped and tetraped molecules showed enhanced thermal stability compared to the respective rod-type model compounds. The thermotropic liquid crystalline behavior of tri and tetraped molecules and model compounds were studied using differential scanning calorimetry (DSC) analysis coupled with polarized light microscope (PLM) as well as temperature dependant X-ray diffraction (VTXRD). The model compounds **P5Br** and **P10Br** were conventional calamitic type molecules and showed monotropic behaviour in DSC thermogram as shown in Figure 4.9. **P5Br** exhibited only a clearing transition at 118 °C (29.7 kJ/mol) during the heating cycle; while cooling it showed isotropic to LC transition at 109.5 °C (2 kJ/mol), which was further transformed in to crystalline phase at 92.4 °C (24.8 kJ/mol).

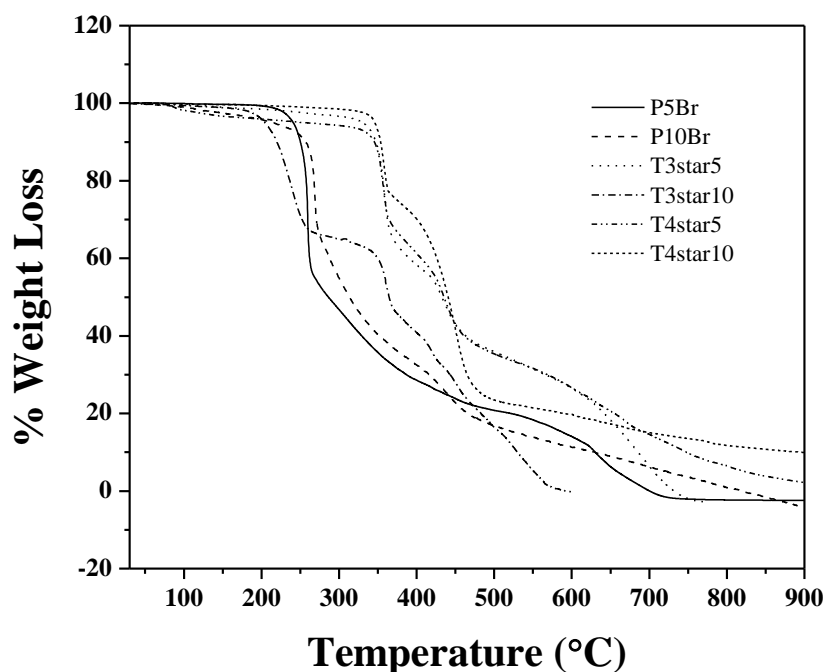


Figure 4.8 Thermogravimetric analysis (TGA) of model compounds and molecules.

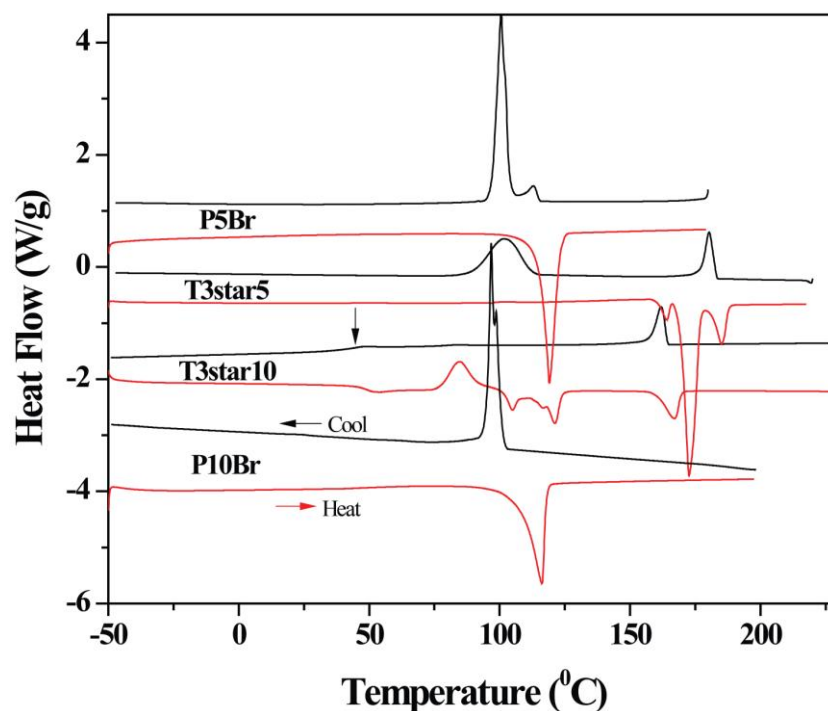


Figure 4.9 DSC thermograms of triped molecules (*T3star5* and *T3star10*) with model compound of *P5Br* and *P10Br*.

The LC texture confirmed by PLM (Figure 4.10) showed characteristic smectic phase (SmA) at 118 °C and its crystalline phase transformation was clearly observable around 116 °C. The VT XR D data showed sharp diffraction at $2\theta = 4.66^\circ$ ($d = 18.53 \text{ \AA}$) with broad peak around $2\theta = 20^\circ$ ($d = 4.30 \text{ \AA}$) confirming the LC nature (Figure 4.11).

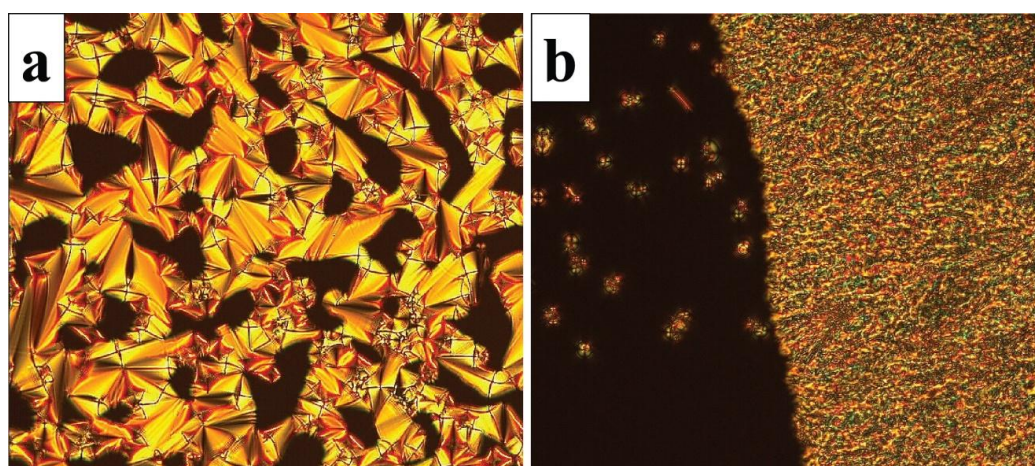


Figure 4.10 PLM images of model compound *P5Br* - a) 106.5 °C (SmA) and b) *P10Br* -99 °C (SmA).

The fundamental peak ($d = 18.53 \text{ \AA}$) corresponded to the (001) plane based on indexing from single crystal X-ray diffraction data (Figure 4.11).¹²

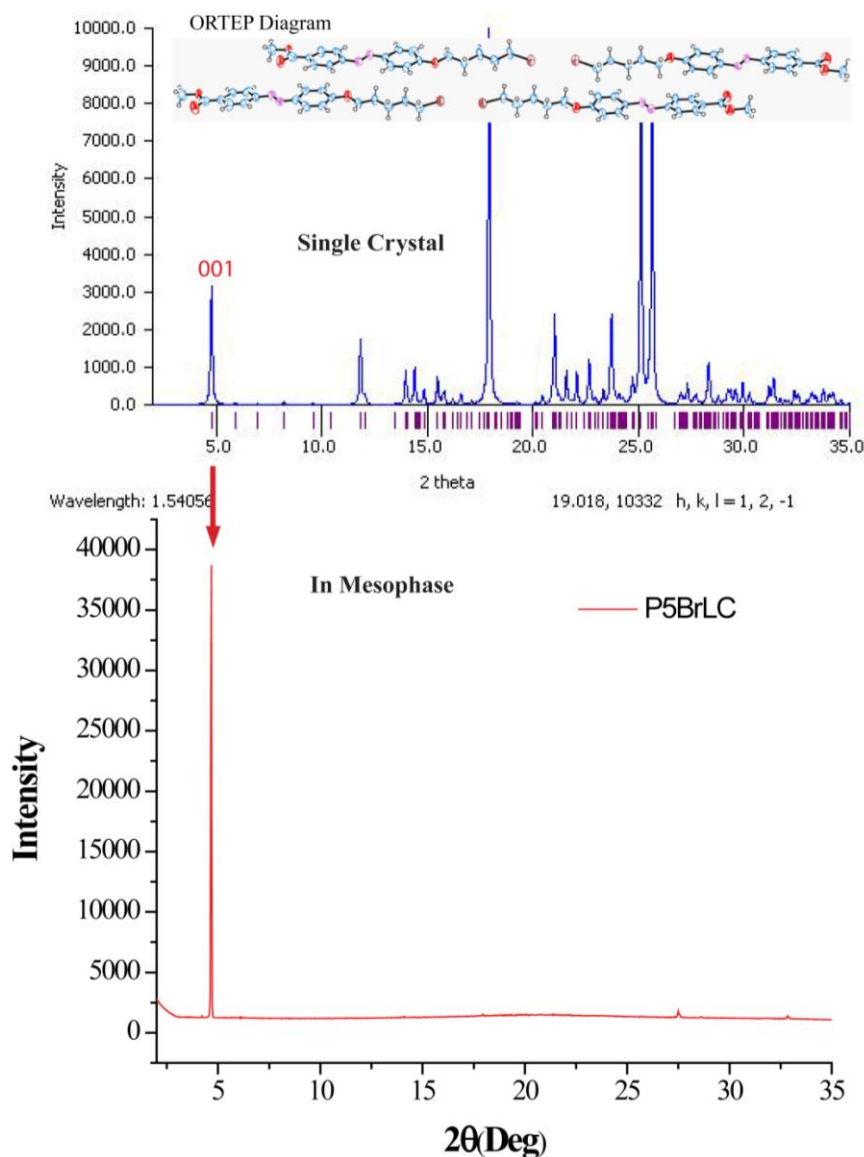


Figure 4.11 Single crystal ORTEP diagram of **P5Br** and its comparison of simulated X-ray diffraction with X-ray diffraction in mesophase (*Sm*).

The model compound **P10Br** also exhibited monotropic LC behavior in the DSC thermogram with a very small LC window observed in the cooling cycle. The isotropic to LC transition was observed at $98 \text{ }^\circ\text{C}$, immediately followed by crystallization at $96 \text{ }^\circ\text{C}$. This was also confirmed by the PLM images taken during the LC transition which indicated characteristic smectic phases (Figure 4.10). Figure 4.9

also compares the second heating and cooling cycles of the triped azo molecules **T3star5** and **T3star10**. Multiple transitions were observed in the second heating cycles of both the triped molecules. However, only two transitions were observed in the cooling cycle of **T3star5** with the isotropic to LC transition at 180 °C (21.5 kJ/mol) and the LC to crystallization around 101 °C with enthalpy 60.7 kJ/mol. In the case of **T3Star10**, the first heating cycle corresponding to the as-solvent-crystallized sample was rather simple with only two transitions (Figure 4.12), one at 135 °C (110.2 kJ/mol) and the clearing transition at 167 °C (22.8 kJ/mol). In the cooling cycle, the isotropic to LC transition was observed at 161 °C (24.5 kJ/mol) followed by LC to LC transitions at 82.3 °C and 46 °C, with the LC texture remaining stable up to room temperature.

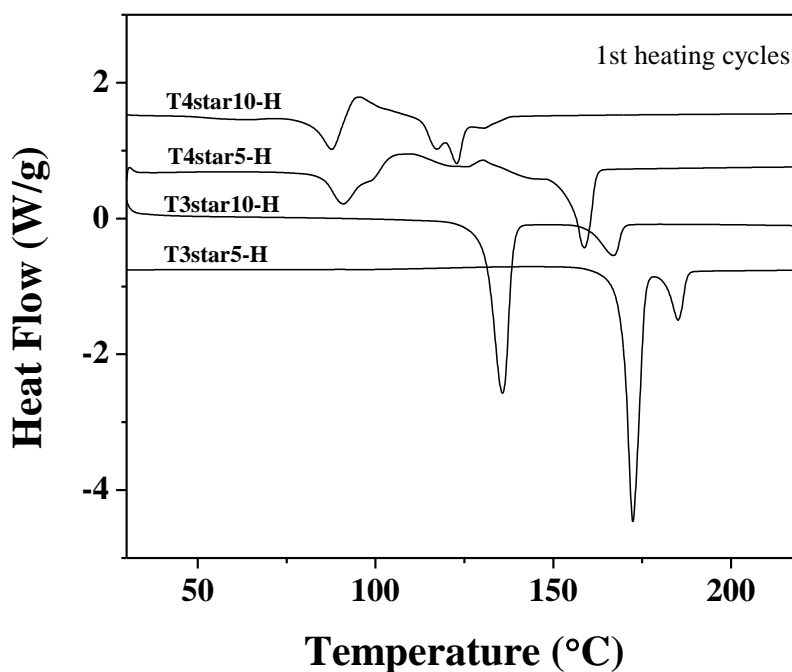


Figure 4.12 DSC thermograms during first heating cycle of tri and tetraped molecules.

The total enthalpy during the cooling cycle did not match with that of the first heating cycle. However, during the second heating cycle, a cold crystallisation was observed for **T3star10** with an enthalpy of (36.7 kJ/mol) followed by several smaller endothermic transitions. The melting to isotropic phase was identical for both the first and second heating cycles – at 167 °C. Compared to the LC window of a few degrees for the model compounds, **P5Br** and **P10Br**, the LC window during the cooling cycle

increased to more than 80 °C in the two triped molecules. Incorporation of the alkoxy azobenzene moiety into a triped architecture as in **T3star5** and **T3star10** stabilized the mesophase. Among the triped molecules, the LC phase remained stable until room temperature for the one with longer alkyl spacer – the **T3star10**. The PLM images of both the triped samples exhibited characteristic focal conic features of SmA phase as shown in Figure 4.13.

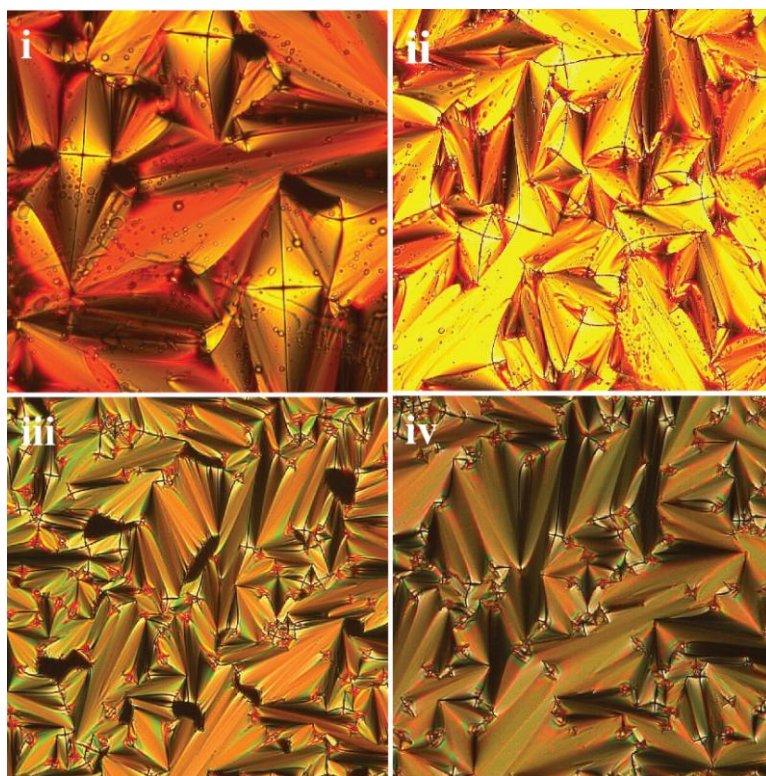


Figure 4.13 Crossed polarized optical micrographs of **T3star5** i) 185 °C (SmA), ii) 155 °C (SmA) and **T3star10** iii) 164 °C (SmA) iv) 40 °C (SmA).

The variable temperature X-ray diffraction recorded at various intervals of temperature during the cooling cycle of **T3star5** is shown in Figure 4.14. Plot-b recorded during the LC phase at 150 °C showed a sharp diffraction in the small angle region at $2\theta = 3.80^\circ$ ($d = 23.23 \text{ \AA}$) along with a broad diffraction at $2\theta = 20.17^\circ$ ($d = 4.39 \text{ \AA}$) attributed to the diffused alkyl chain packing in the mesophase. The PLM images along with the WXR D reflections confirmed the LC phase to be SmA. The length of one arm of the molecule from the end of the azobenzene unit to the phloroglucinol core was obtained as 24.5 \AA based on energy minimized structures

calculated using Density Functional Theory (DFT). The fundamental reflection ($d = 23.23 \text{ \AA}$) observed in the small angle region of the WXR D data was in close agreement with this length calculated from DFT.

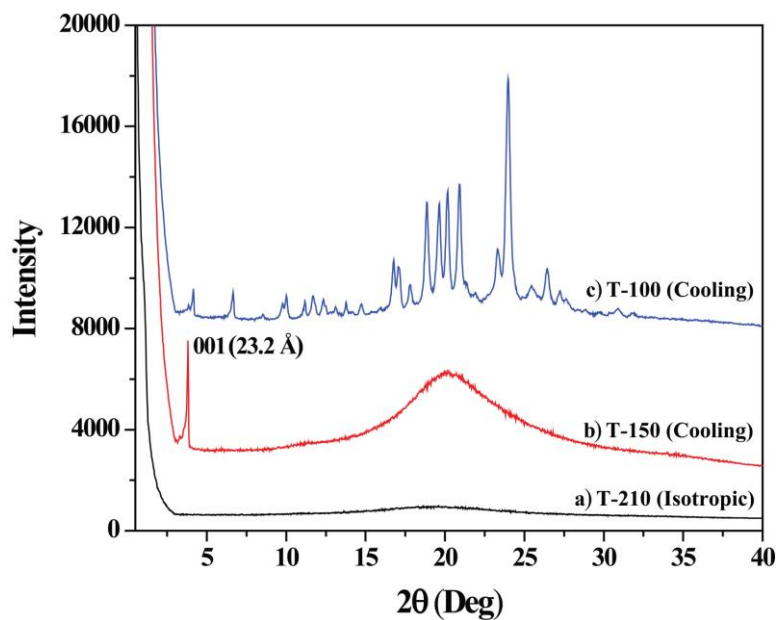


Figure 4.14 Variable temperature X-ray diffraction of triped *T3star5*.

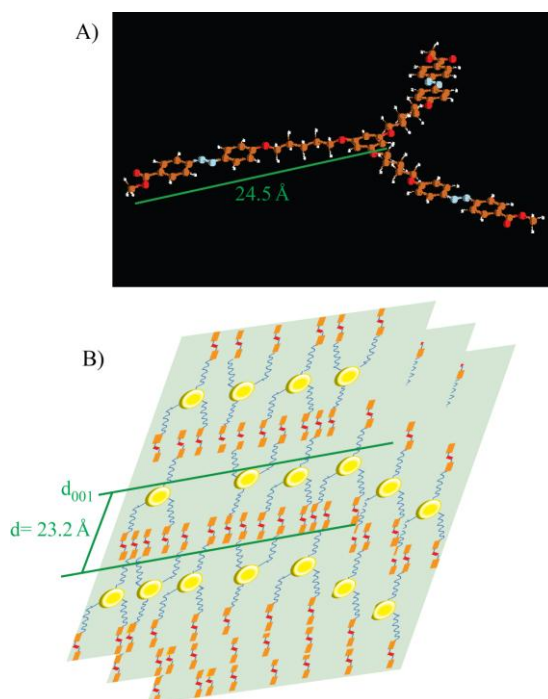


Figure 4.15 A) DFT energy minimized structure of *T3star5*. B) Schematic diagram of the plausible layered packing (SmA phase) of *T3star5*.

Figure 4.15-A shows the energy minimized structure obtained from DFT along with a schematic representation (Figure 4.15-B) of the layered packing in the smectic phase (SmA) of **T3star5**. Figure 4.16 compares the DSC thermograms of the tetraped series of molecules; the **P5Br** and **P10Br** are also given for comparison. Multiple transitions were observed both in the first as well as second heating cycles of the tetraped molecules. During the cooling cycle, isotropic to LC transition was observed at 141 °C (20.5 kJ/mol) for **T4star5** whereas it was observed at 127 °C (28 kJ/mol) for **T4star10**. Another broad transition with a shoulder was observed around 50 °C for both the samples.

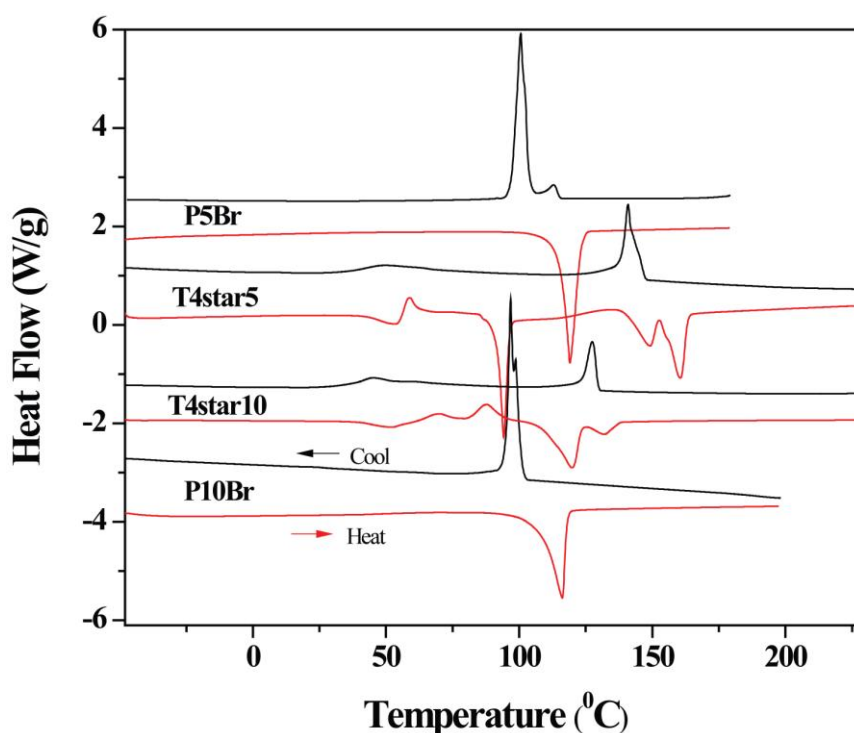


Figure 4.16 DSC thermograms of tetraped molecules (**T4star5** and **T4star10**) with model compound of **P5Br** and **P10Br**.

The nature of the LC phase was further confirmed by PLM. Figure 4.17 shows the LC texture observed for **T4star5** and **T4star10** while cooling from the isotropic melt, which were characteristic of smectic liquid crystalline phases. Further identification of the LC phase was done with VTXRD studies. Plot-a in Figure 4.18 shows the lamellar organization in the LC phase (140 °C) of **T4star5** with reflections corresponding to (d_{001} and d_{002}) in the small angle region at $2\theta = 3.25^\circ$ ($d = 27.12 \text{ \AA}$)

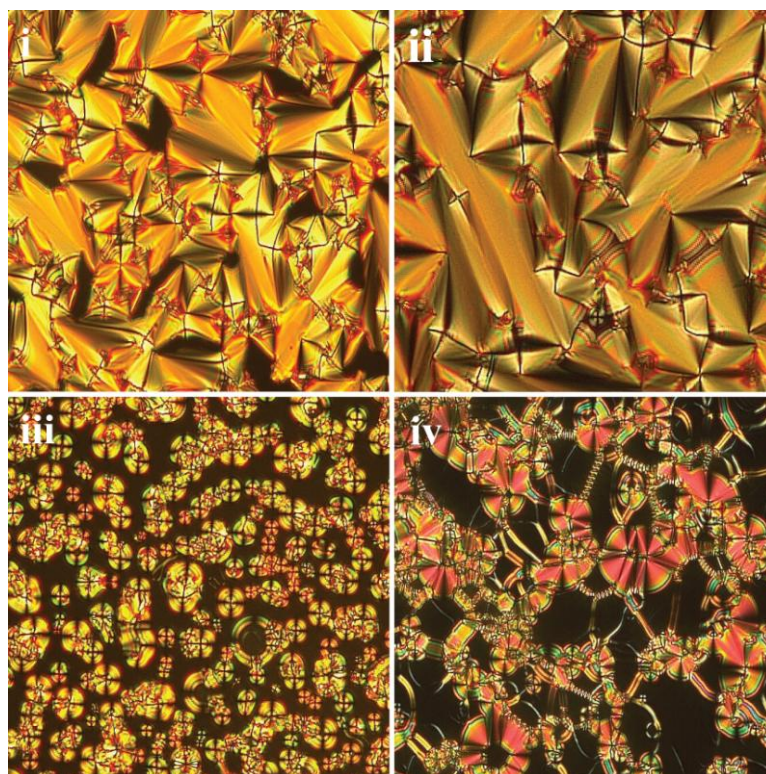


Figure 4.17 Crossed polarized optical micrographs of *T4star5*- i) 140 °C (20X-Sm), ii) RT-25 °C (20X-SmF/H) and *T4star10*- iii) 126 °C (20X-Sm), iv) RT-25 °C (20X-SmF/H).

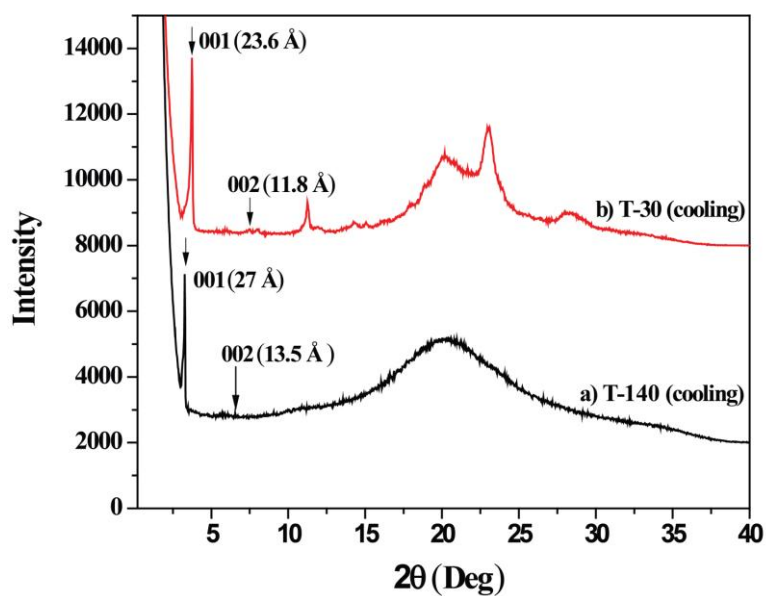


Figure 4.18 Variable temperature X-ray diffraction of tetraped *T4star5*.

and $2\theta = 6.55^\circ$ ($d = 13.5 \text{ \AA}$). Another broad reflection around $2\theta = 20^\circ$ ($d = 4.4 \text{ \AA}$), typical of diffuse alkyl packing in the mesophase was also observed. The DSC thermogram had indicated a transition around 60°C (8.3 kJ/mol) which was supported by small changes observed under the PLM around the same temperature, like appearance of rings at the center of the focal conic points. WXRd recorded at 30°C is shown in plot b of Figure 4.18. Two important features were observable – (1) a shift in the (d_{001} and d_{002}) peaks from $\sim 27 \text{ \AA}$ to 23.6 \AA and 13.5 \AA to 11.8 \AA respectively indicating a tilt and (2) appearance of new reflections in the wide angle region indicative of a higher ordered smectic phase.¹³ Lower ordered smectic phases like SmA and SmC would show only a diffuse halo in the wide angle region, whereas higher ordered soft crystalline phases like SmE, SmG, SmH or hexatic fluidic phases like SmF, and SmI would show more peaks due to more regular packing of mesogens.¹⁴ Among these higher ordered smectic phases, the SmF and SmH phases are known to exhibit tilt of the mesogen based on their orientation with respect to the layer plane. The tilt angle in the higher ordered smectic phase of the **T4star5** was found to be 29° based on the relation $d_{001} = L \cdot \cos\theta$ (where L = half of fully extended molecular length).¹⁵

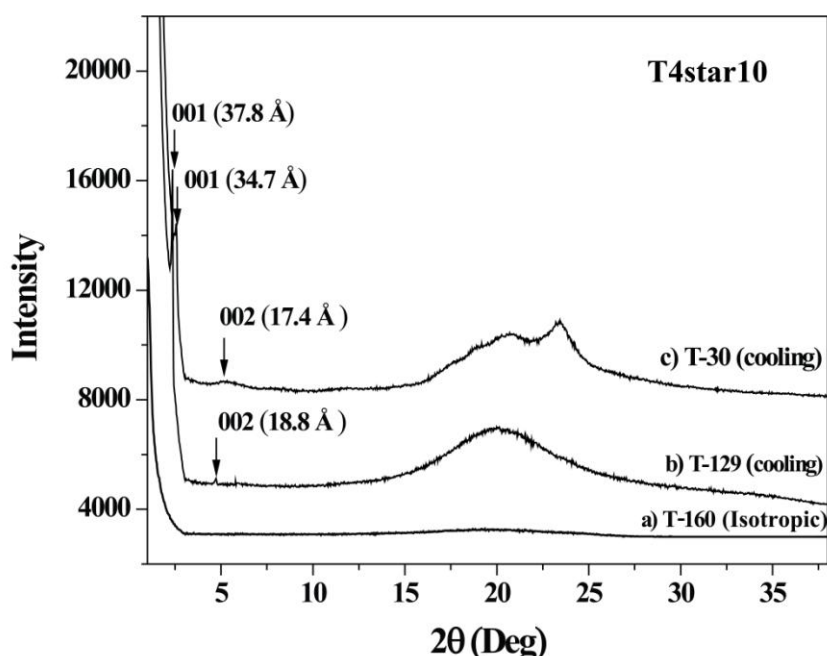


Figure 4.19 Variable temperature X-ray diffraction of tetrapod **T4star10**.

The VTXRD plot of **T4star10** (given in Figure 4.19) also exhibited similar features with a shift in the fundamental diffraction (d_{001}) from 37.7 Å to 34.7 Å on going from 129 °C to 30 °C while cooling, indicating a tilt of 23°. Thus, based on the tilt and peaks in the wide angle region in the XRD as well as the texture from PLM, the higher ordered smectic phases exhibited by **T4star5** and **T4star10** could be SmF or SmH phases. Table 4.1 summarizes the LC transitions and their corresponding enthalpy values (kJ/mol) during the cooling cycle. A clear LC window could be established only for the two model compounds and the **T3star5** because only these three molecules exhibited a clear LC to crystal transition during the cooling cycle. All the other molecules retained the mesophase characteristics until room temperature (25 °C). This ability to freeze-in the liquid crystal ordering below room temperature and form glassy liquid crystals is an important characteristic of the branched molecules which make them useful for various potential applications.¹⁶

Table 4.1. Thermal analysis data of model compound, molecules and hyperbranched polymers

Sample	T_{cl}^a (°C) (Lc/C-I)	ΔH_{cl}^a (KJ/mol)	T_c^b (°C) I-Lc	ΔH_c^b (KJ/mol)	T_c^b (°C) (Lc-C) /(Lc-Lc)	ΔH_c^b (KJ/mol)	LC window ^c (°C)	T_D^d (°C)
P5Br	118	29.7	109.5 (SmA)	2	92.4 (c)	24.8	17	252
P10Br	116.2	37.7	98.7 (SmA)	-	96.8 (c)	37.2	2	258
T3star5	185	16.5	180.3 (SmA)	21.5	101.4 (c)	60.7	79	350
T3star10	167	23.2	161.8 (SmA)	24.5	82.4/46	12.6	-	222
T4star5	160.8	16.5	140.9 (Sm)	20.5	63/50 (SmF/H)	8.3	-	345
T4star10	132.5	14.6	127.5 (Sm)	28	59/45 (SmF/H)	26.2	-	354

^a clearing transitions during heating cycle, ^b phase transitions and corresponding enthalpy values during cooling cycles, ^c LC window during cooling cycle, ^d 10 % weight loss under N₂ atmosphere during TGA.

The influence of branching on the nature of the LC phase observed was very clearly established with both the tetraped molecules exhibiting higher ordered smectic mesophases in contrast to the smectic A phase alone exhibited by the triped molecules. While comparing the effect of five versus ten alkyl spacer length, the longer spacer seemed to favor higher ordered mesophases as indicated by the larger enthalpy values for the isotropic to LC transition. For instance, **T3star10** had an enthalpy of 24.5 kJ/mol whereas **T3star5** had only 21.5 kJ/mol for the isotropic to LC transition. Similarly, **T4star10** showed an enthalpy of 28 kJ/mol, in contrast to only 20.5 kJ/mol for the isotropic to LC transition. Thus, both in terms of architecture as well as spacer length, the **T4star10** had the better structural design to exhibit higher order mesophases. It had the lowest isotropic to LC transition temperature (128 °C) in the whole series and the LC textures also clearly established the higher ordered nature, which was unlike that observed in the others.

4.3.3 Isothermal Photoswitching in the LC state

The cis-trans isomerization of the azobenzene has been used as a photo-switchable trigger to control the molecular order of LC phases; the most widely studied being the photo-induced isothermal nematic to isotropic disordering.^{7d,17} There are very few reports of control of the more ordered smectic LC phases using azobenzenes as the photo trigger.¹⁸ A reversible and controlled isothermal photoswitching from the highly ordered smectic to isotropic phase could be achieved by trans to cis photo isomerization of the triped and tetraped molecules. Thin films of the sample between cover glasses were first heated to the isotropic state and slowly cooled to the LC phase where they were exposed to irradiation from a DYMAX Blue Wave 75 light source (output power: 19 W/cm²) while holding the temperature constant. The irradiation resulted in instantaneous (< 1 sec) disruption of the smectic LC ordering due to the trans to cis molecular rearrangement. Upon removal of the irradiation source, the smectic LC phase reappeared immediately since high temperature favors the thermal cis to trans back isomerization. The samples were exposed to UV irradiation at different temperatures in the LC phase after cooling from the isotropic melt. Figure 4.20 shows the isothermal photoswitching of **T4star10** at 3 different temperatures in the LC phase upon cooling from the isotropic phase around 140 °C.

For instance, figure 4.20-1a shows the formation of the smectic focal conics (magnification 40x) upon cooling from the isotropic melt. Figure 4.20-1b shows the disappearance of birefringence after 1 sec UV irradiation. The second set of images corresponds to the isothermal photoswitching at 136 °C, when more of the smectic focal conics had formed.

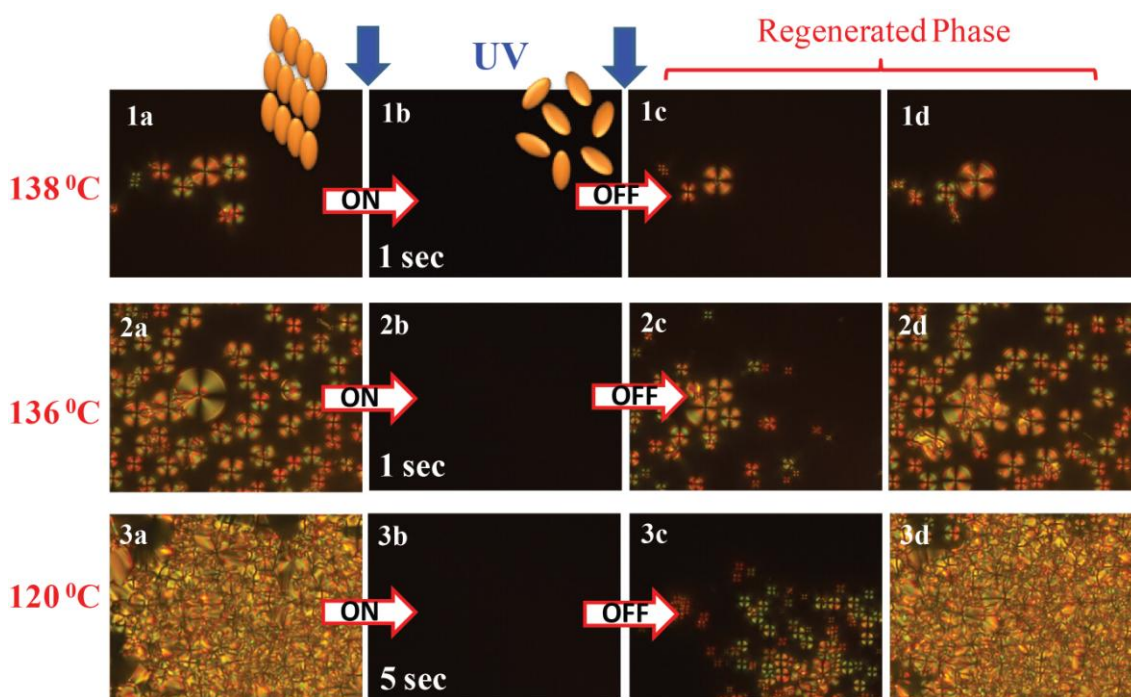


Figure 4.20 Polarized optical microscope images (40 X magnification) depicting the photoinduced isothermal switching behavior of tetrapod **T4star10** at various temperatures upon cooling from isotropic phase at 140 °C. a) LC phase before UV irradiation (b) isotropic state obtained upon UV irradiation (c, d) regeneration of LC ordering upon removal of light source.

Figure 4.20-3a shows the almost complete formation of the smectic phases at 120 °C. 5 seconds of UV exposure was required to bring about total disappearance of birefringence. At all the three temperatures, the full recovery of the smectic LC ordering occurred almost immediately upon removal of the source of irradiation. The Figure 4.21 shows isothermal photoswitching of tripod **T3satr5** at various temperatures in the LC phase upon cooling from isotropic phase around 190 °C.

Similarly, Figure 4.22 shows isothermal photoswitching for the triped **T3star10** at various temperatures during cooling cycle from isotropic phase (171 °C).

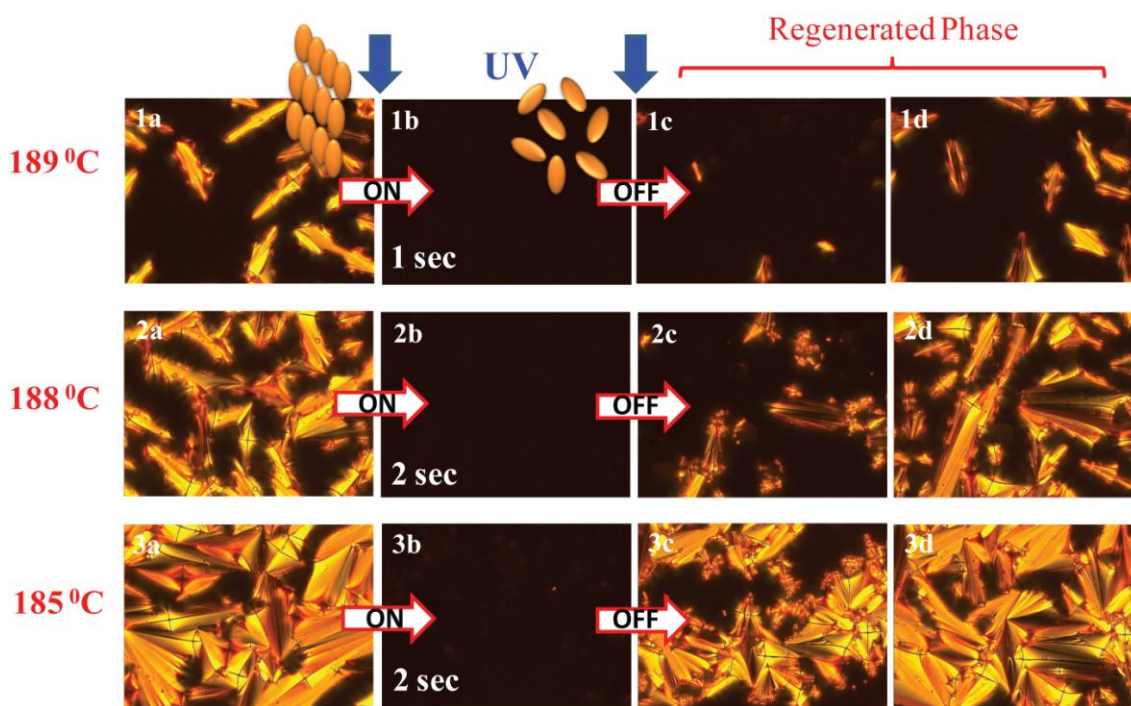


Figure 4.21 Polarized optical microscope images (40 X magnification) depicting the photoinduced isothermal switching behavior of triped **T3star5** at various temperatures upon cooling from isotropic phase at 189.5 °C. a) LC phase before UV irradiation (b) isotropic state obtained upon UV irradiation (c, d) regeneration of LC ordering upon removal of light source.

At temperatures further away from the isotropization, more UV exposure time was required for all samples to show complete disruption of the LC ordering.¹⁸ Compared to doped systems where small amounts of azo chromophores are doped into inert LC matrix to bring about photoswitchability, these multipod molecules where the azo chromophores also acted as the LC mesogens certainly exhibited faster switching response due to the much higher content of the photoactive moiety. In general all multipod molecules showed reversible isothermal photoswitching Smectic-Isotropic phase transition upon UV irradiation in <1 sec exposure time.

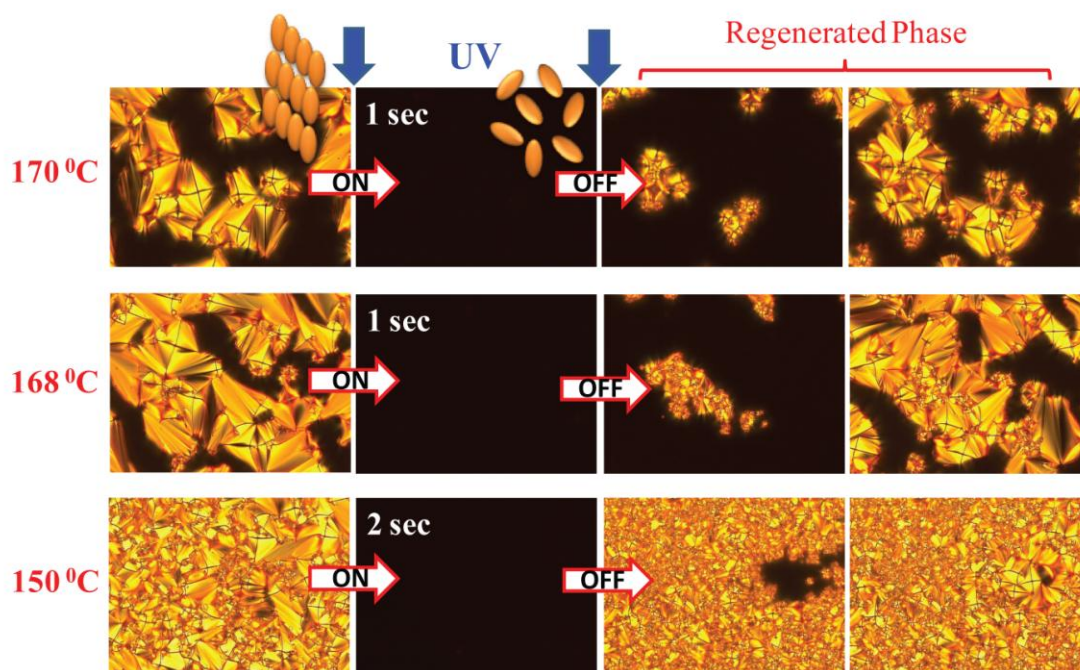


Figure 4.22 Polarized optical microscope images (40 X magnification) depicting the photoinduced isothermal switching behavior of triped **T3star10** at various temperatures upon cooling from isotropic phase at 171 °C a) LC phase before UV irradiation (b) isotropic state obtained upon UV irradiation (c, d) regeneration of LC ordering upon removal of light source.

4.4 Summary

Three and four armed multipod molecules incorporating azobenzene as the rigid mesogen linked to the multicore phloroglucinol via spacers of variable length like pentyl and decyl chains was designed. The triped and tetraped design proved to be interesting building blocks exhibiting smectic liquid crystalline phases. A significant difference was observed in the LC properties of triped compared to tetraped molecules. A tendency towards higher ordered LC phases was observed with increased branching. For instance, the triped with five or ten alkyl spacer showed only SmA phases where as tetraped (dimeric) structures showed higher ordered Smectic phases. All the multipod molecules exhibited fast reversible isothermal photoswitching from Smectic-Isotropic (S-I) phase upon UV irradiation in the LC phase. The melting transitions of these molecules are quite low (< 200 °C) which can therefore be directly used as B₃ (triped) and B₄ (tetraped) type monomers for the synthesis of azo hyperbranched polymers. Overall, the azo containing triped and tetraped multifunctional molecule design described here is a simple and robust one which could also act as versatile monomers for the synthesis of LC hyperbranched polymers thorough melt polycondensation approach.

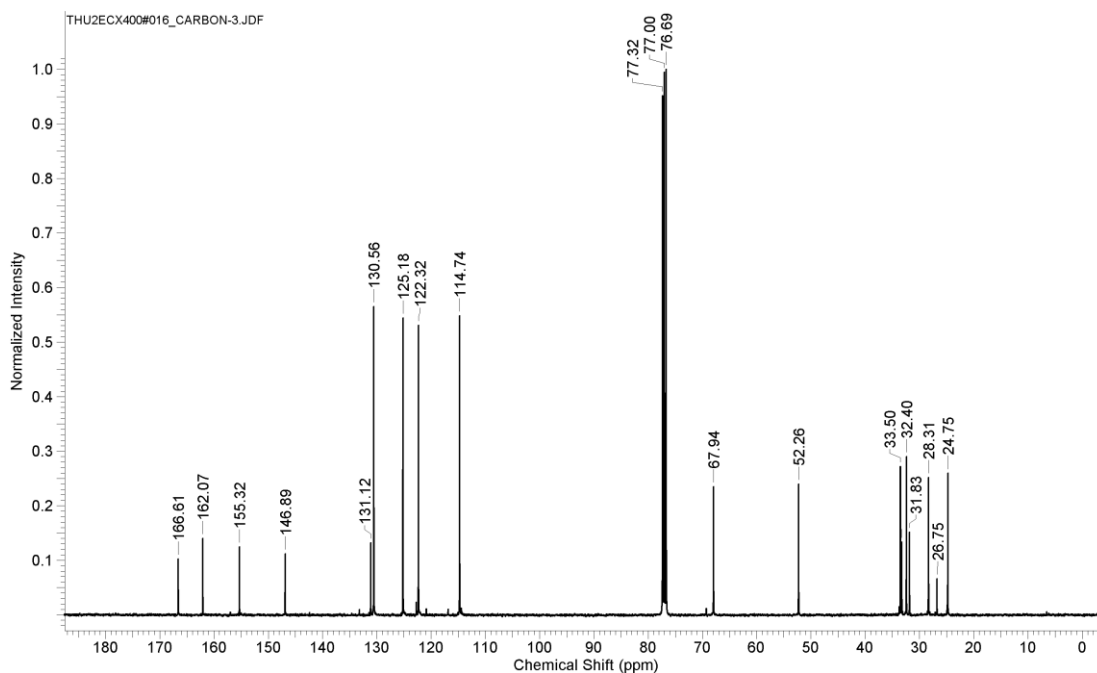
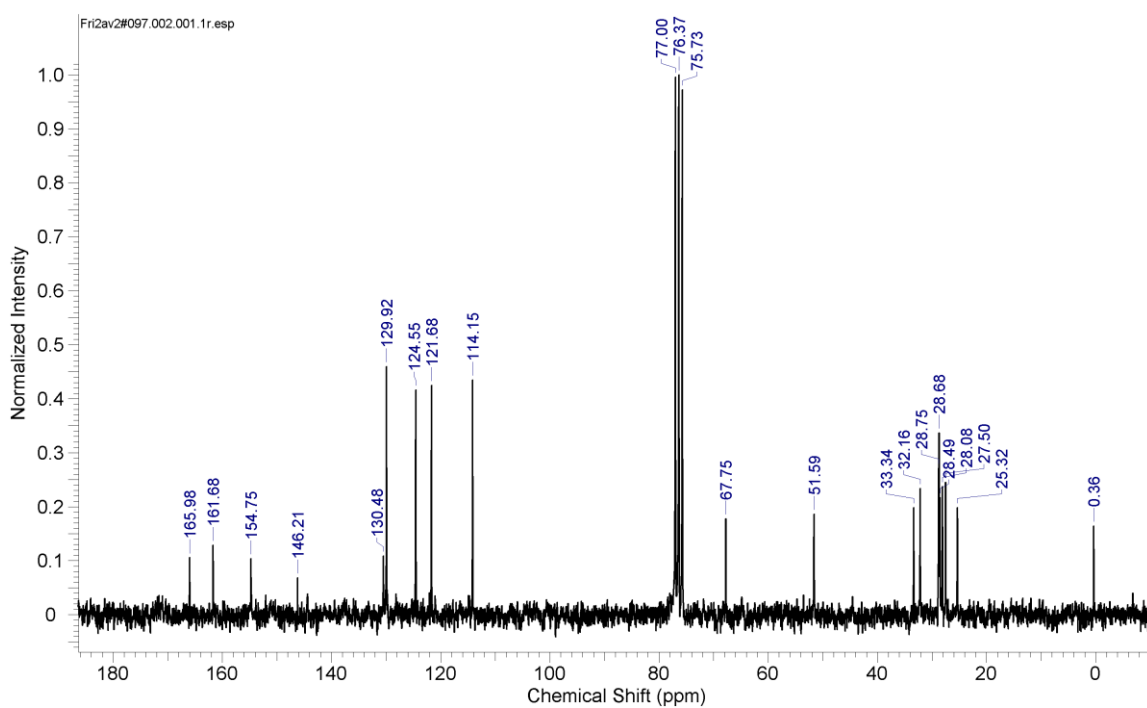
^{13}C -NMR and mass spectral data**Figure** ^{13}C -NMR spectra of model compounds **P5Br** and **P10Br** in CDCl_3 solvent.**P5Br****P10Br**

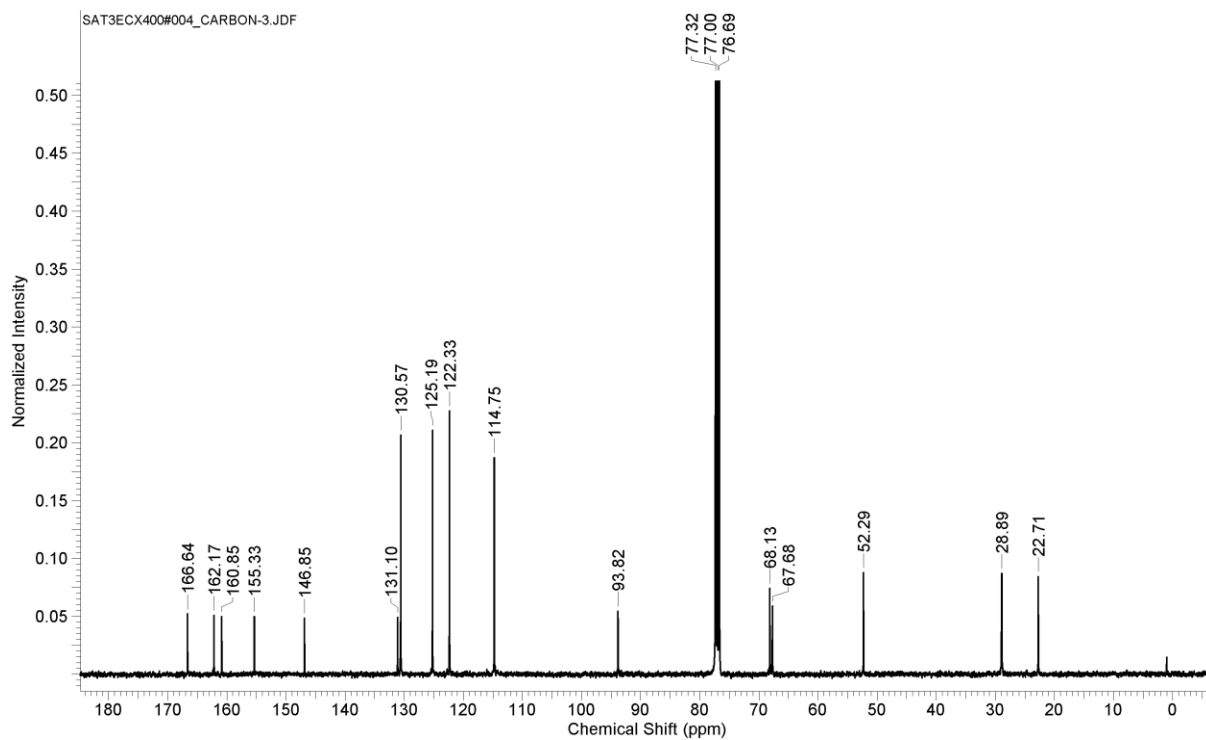
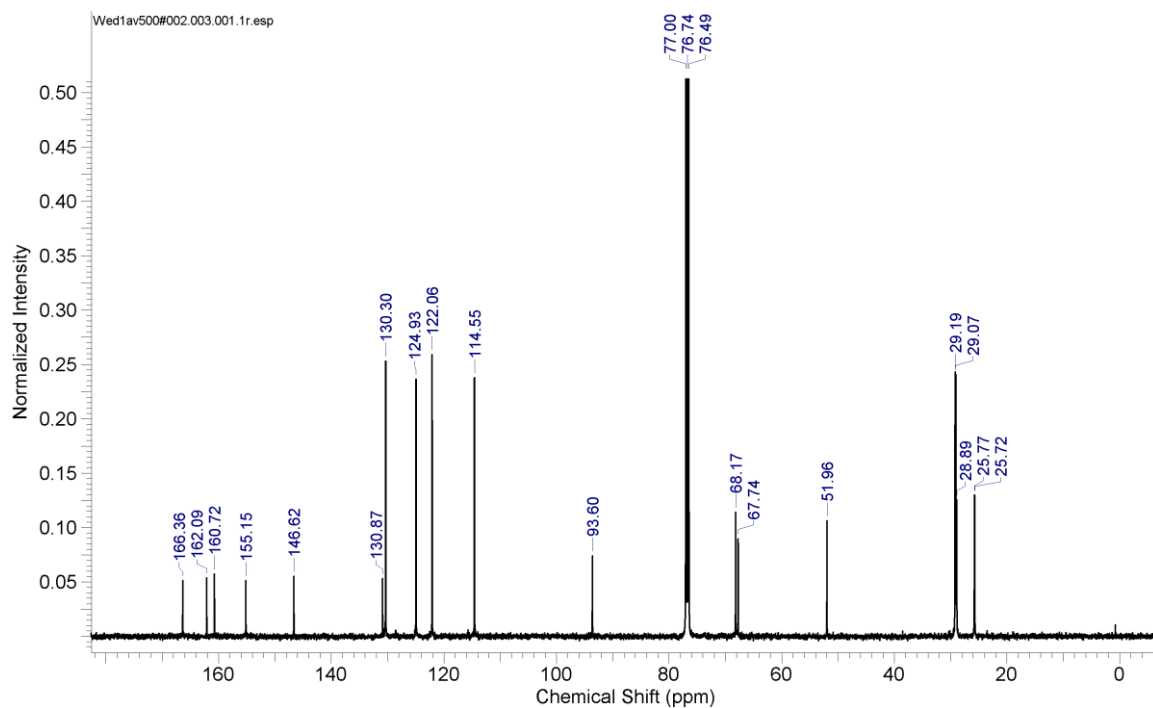
Figure ^{13}C -NMR spectra of triped molecules *T3star5* and *T3star10* in CDCl_3 solvent.**T3star5****T3star10**

Figure ^{13}C -NMR spectra of tetrapod molecules **T4star5** and **T4star10** in CDCl_3 solvent.

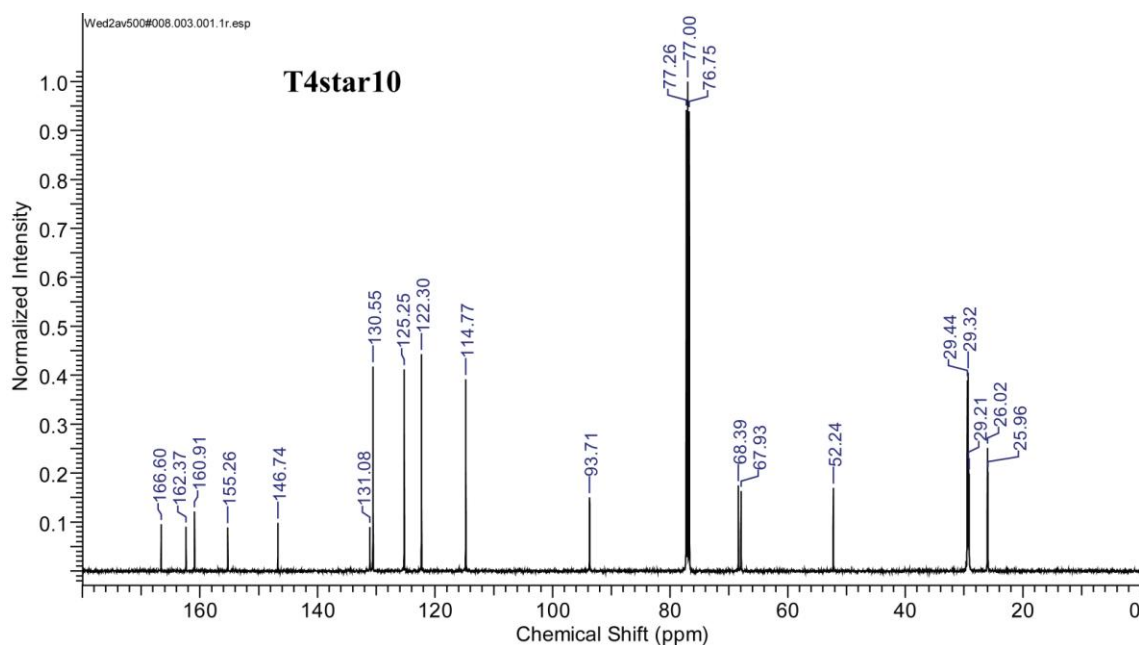
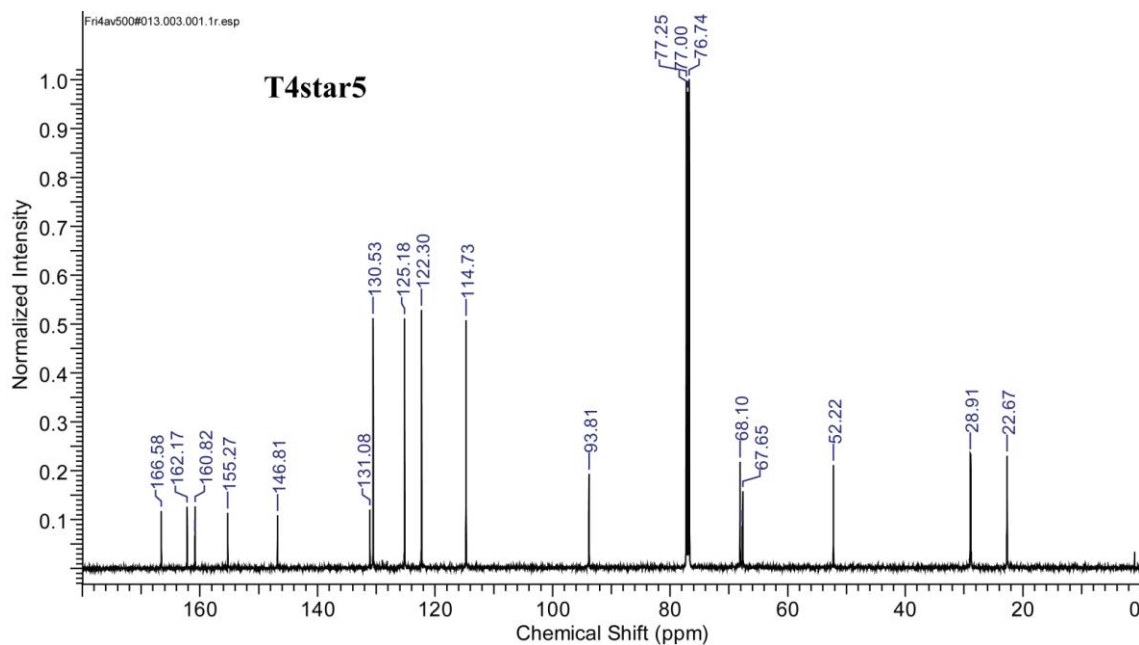


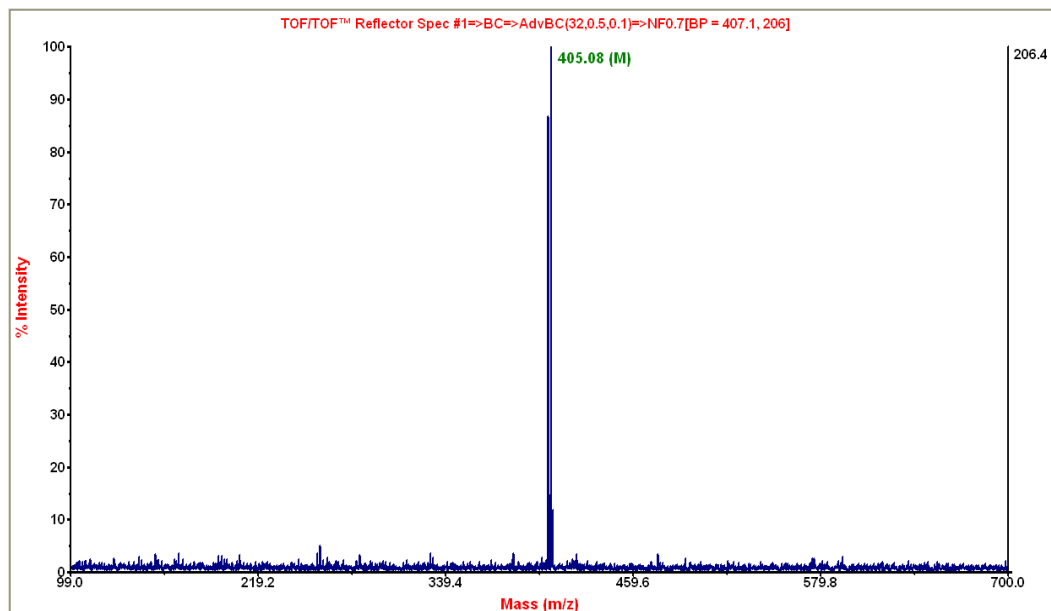
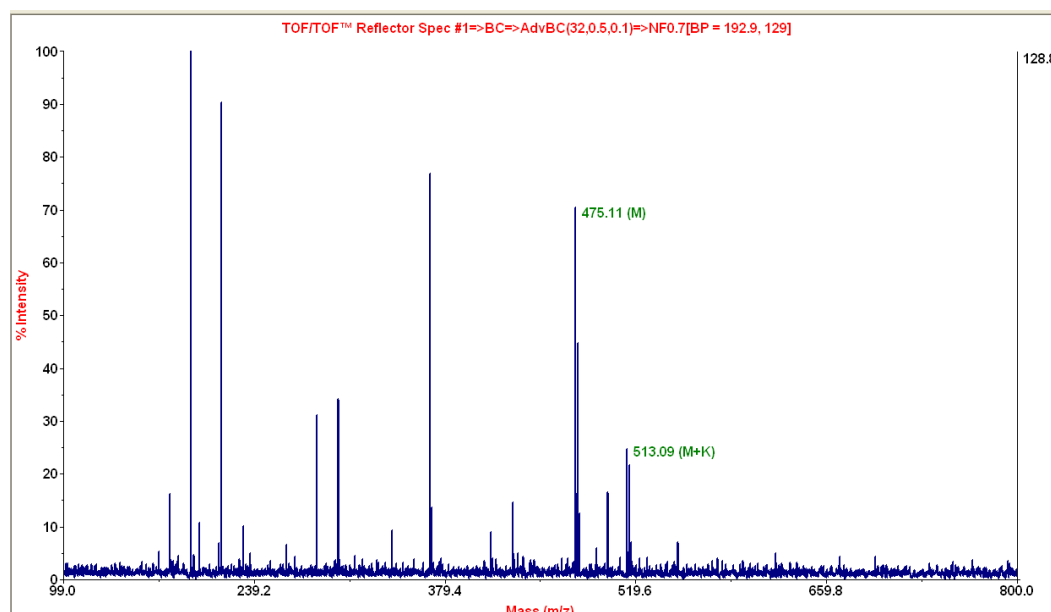
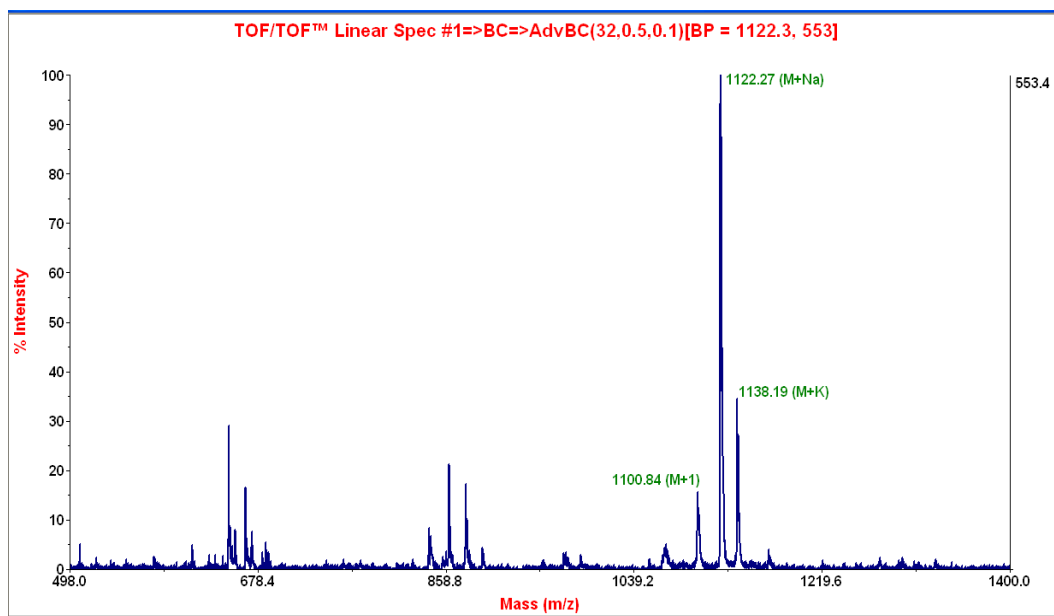
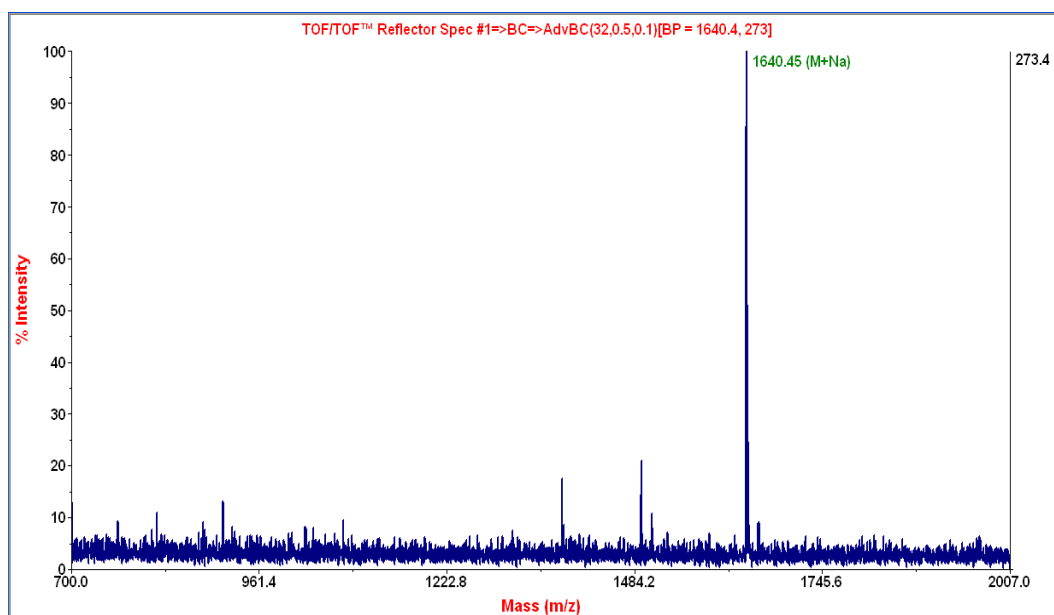
Figure MALDI-TOF spectra of model compounds **P5Br** and **P10Br**.**P5Br****P10Br**

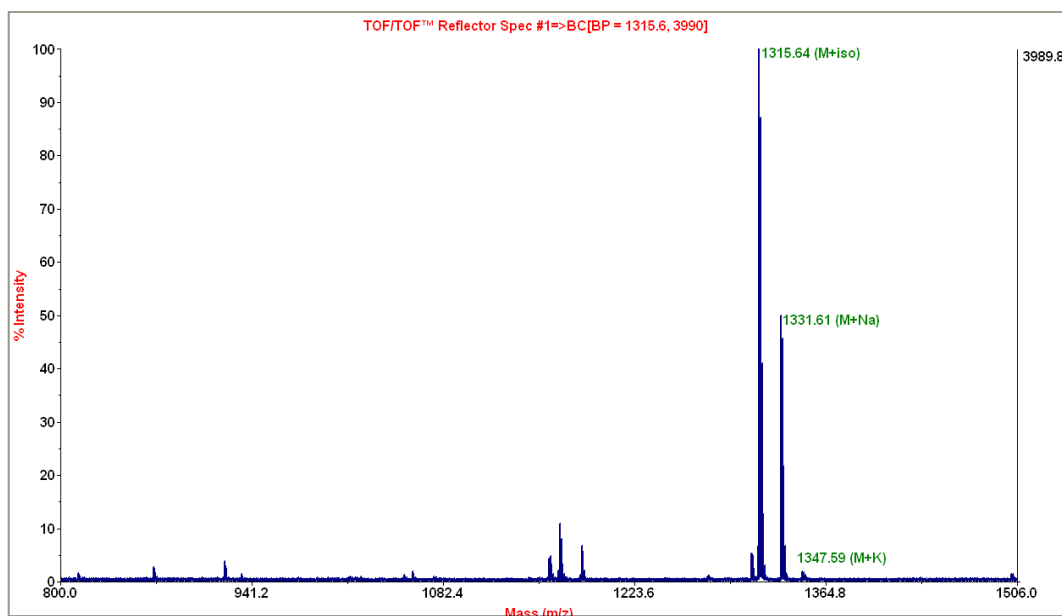
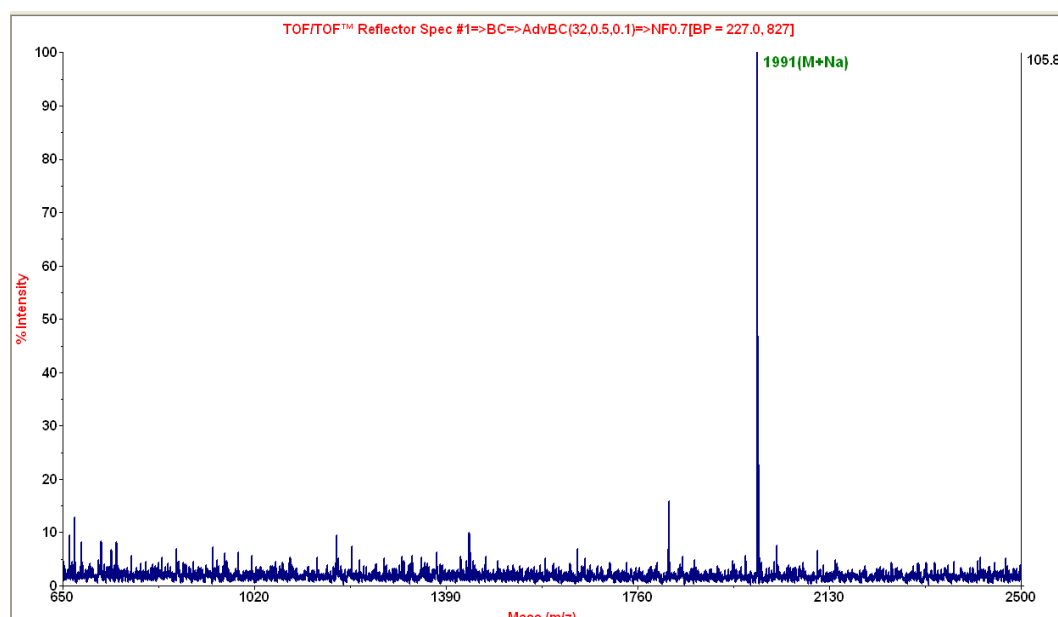
Figure MALDI-TOF spectra of tri and tetraped azo molecules.

T3star5



T4star5



T3star10**T4star10**

4.5 References

- (1) (a) Donnio, B.; Guillon, D. In *Supramolecular Polymers Polymeric Betains Oligomers*; Springer Berlin Heidelberg, 2006; Vol. 201 (b) Goodby, J. W.; Saez, I. M.; Cowling, S. J.; Görtz, V.; Draper, M.; Hall, A. W.; Sia, S.; Cosquer, G.; Lee, S.-E.; Raynes, E. P. *Angew. Chem. Int. Ed.* **2008**, *47*, 2754-2787.
- (2) (a) Kumar, S.; Manickam, M. *Liq. Cryst.* **1999**, *26*, 939-941 (b) Lehmann, M.; Jahr, M.; Donnio, B.; Graf, R.; Gemming, S.; Popov, I. *Chem. Euro. J.* **2008**, *14*, 3562-3576 (c) Yao, D.-S.; Zhang, B.-Y.; Zhang, W.-W.; Tian, M. *J. Mol. Struct.* **2008**, *881*, 83-89 (d) Kocot, A.; Vij, J. K. *Liq. Cryst.* **2010**, *37*, 653-667 (e) Zhang, B.-Y.; Yao, D.-S.; Meng, F.-B.; Li, Y.-H. *J. Mol. Struct.* **2005**, *741*, 135-140.
- (3) (a) Tschierske, C. *J. Mater. Chem.* **2001**, *11*, 2647-2671 (b) Skoulios, A.; Guillon, D. *Mol. Cryst. Liq. Cryst.* **1988**, *165*, 317-332 (c) Tschierske, C. *J. Mater. Chem.* **1998**, *8*, 1485-1508.
- (4) (a) Meier, H.; Lehmann, M.; Holst, H. C.; Schwöppe, D. *Tetrahedron* **2004**, *60*, 6881-6888 (b) Cristiano, R.; Santos, D. M. P. d. O.; Gallardo, H. *Liq. Cryst.* **2005**, *32*, 7-14 (c) Kim, B. G.; Kim, S.; Park, S. Y. *Tetrahedron Lett.* **2001**, *42*, 2697-2699.
- (5) Lehmann, M.; Jahr, M.; Gutmann, J. *J. Mater. Chem.* **2008**, *18*, 2995-3003.
- (6) (a) Chang, J. Y.; Yeon, J. R.; Shin, Y. S.; Han, M. J.; Hong, S.-K. *Chem. Mater.* **2000**, *12*, 1076-1082 (b) Chang, J. Y.; Baik, J. H.; Lee, C. B.; Han, M. J.; Hong, S.-K. *J. Am. Chem. Soc.* **1997**, *119*, 3197-3198.
- (7) (a) Hafiz, H. R.; Nakanishi, F. *Nanotechnology* **2003**, *14*, 649-654
- (b) Mativetsky, J. M.; Pace, G.; Elbing, M.; Rampi, M. A.; Mayor, M.; Samori, P. *J. Am. Chem. Soc.* **2008**, *130*, 9192-9193 (c) Abrakhi, S.; Peralta, S.; Fichet, O.; Teyssié, D.; Cantin, S. *Langmuir* **2013**, *29*, 9499-9509 (d) Ikeda, T.; Tsutsumi, O. *Science* **1995**, *268*, 1873-1875 (e) Liu, D.; Bastiaansen, C. W. M.; den Toonder, J. M. J.; Broer, D. J. *Angew. Chem. Int. Ed.* **2012**, *51*, 892-896 (f) Barrett, C. J.; Mamiya, J.-i.; Yager, K. G.; Ikeda, T. *Soft Matter* **2007**, *3*, 1249-1261.

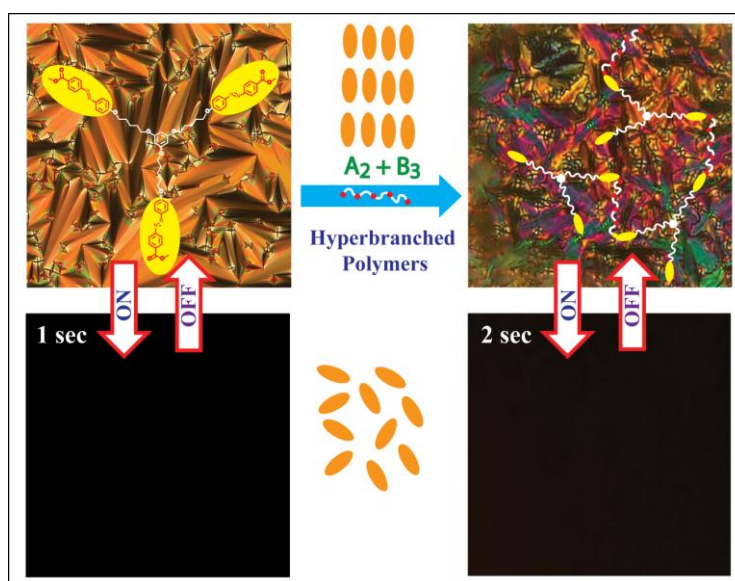
- (8) Marcos, M.; Martin-Rapun, R.; Omenat, A.; Serrano, J. L. *Chem. Soc. Rev.* **2007**, *36*, 1889-1901.
- (9) (a) Lehmann, M. *Chem. Eur. J.* **2009**, *15*, 3638-3651 (b) Lehmann, M. *Top. Curr. Chem.* **2012**, *318*, 193-223 (c) Nagy, Z. T.; Heinrich, B.; Guillon, D.; Tomczyk, J.; Stumpe, J.; Donnio, B. *J. Mater. Chem.* **2012**, *22*, 18614-18622.
- (10) (a) Lehmann, M.; Jahr, M.; Grozema, F. C.; Abellon, R. D.; Siebbeles, L. D. A.; Müller, M. *Adv. Mater.* **2008**, *20*, 4414-4418 (b) Ooi, Y.-H.; Yeap, G.-Y.; Han, C.-C.; Lin, H.-C.; Kubo, K.; Ito, M. M. *Liq. Cryst.*, *40*, 516-527 (c) Lee, S. J.; You, M. K.; Lee, S. W.; Lee, J.; Lee, J. H.; Jho, J. Y. *Liq. Cryst.* **2011**, *38*, 1289-1299.
- (11) Nardele, C. G.; Asha, S. K. *J. Polym. Sci., Part A: Polym. Chem.* **2012**, *50*, 2770-2785.
- (12) The structure of model compound P5Br has been determined by single crystal X-ray diffraction. Crystallographic information: P5Br: C₁₉ H₂₁ Br N₂ O₃, M_r = 405.28, Triclinic, P-1, a = 6.5873(4) Å, b = 15.1475(10) Å, c = 18.7060(6) Å, α = 80.570(4)°, β = 87.305(4)°, γ = 88.026(5)°, V = 1838.57(18) Å³, D_c = 1.464 g cm⁻³, Z = 4, μ = 2.256 mm⁻¹, T = 293 K, CCDC 953910.
- (13) (a) Yonetake, K.; Soga, J.; Masuko, T. *Polym. J.* **1997**, *29*, 500-507 (b) Wutz, C.; Stribeck, N.; Gieseler, D. *Colloid Polym. Sci.* **2000**, *278*, 1061-1069 (c) Xie, H.-L.; Jie, C.-K.; Yu, Z.-Q.; Liu, X.-B.; Zhang, H.-L.; Shen, Z.; Chen, E.-Q.; Zhou, Q.-F. *J. Am. Chem. Soc.* **2010**, *132*, 8071-8080.
- (14) Kapernaum, N.; Knecht, F.; Hartley, C. S.; Roberts, J. C.; Lemieux, R. P.; Giesselmann, F. *Beilstein J. Org. Chem.* **2012**, *8*, 1118-1125.
- (15) Tian, Y.; Watanabe, K.; Kong, X.; Abe, J.; Iyoda, T. *Macromolecules* **2002**, *35*, 3739-3747.
- (16) (a) Chen, H. M. P.; Katsis, D.; Chen, S. H. *Chem. Mater.* **2003**, *15*, 2534-2542 (b) Chen, A. C. A.; Wallace, J. U.; Wei, S. K. H.; Zeng, L.; Chen, S. H.; Blanton, T. N. *Chem. Mater.* **2005**, *18*, 204-213.

(17) Garcia-Amoros, J.; Szymczyk, A.; Velasco, D. *Phys. Chem. Chem. Phys.* **2009**, *11*, 4244-4250.

(18) Zhang, S.; Liu, S.; Zhang, Y.; Deng, Y. *Chem. Asian J.* **2012**, *7*, 2004-2007.

Chapter 5

Photoresponsive Smectic Liquid Crystalline Hyperbranched Azo Polymers



The triped and tetraped molecules with terminal methyl carboxylic ester groups were used as B_3 and B_4 monomers respectively for the synthesis of hyperbranched polymers with tetraethylene glycol as A_2 type co monomer. The polymerization was conducted via melt polycondensation route during which gelation was efficiently suppressed to obtain soluble hyperbranched polyesters with moderate molecular weight and inherent viscosities. The mesophase characteristics of the hyperbranched polymers were analyzed using various instrumentation techniques like differential scanning calorimetry (DSC), polarized light microscopy (PLM) and variable temperature XRD. The all hyperbranched polymers exhibited thermotropic liquid crystalline behavior. Reversible isothermal Smectic-Isotropic phase transition could be achieved by UV irradiation in > 2 sec in the case of the hyperbranched polymers.

5.1 Introduction

Hyperbranched polymers (HBPs) are a class of dendritic polymers having branched tree like structure. The dendritic polymers are widely classified in to two major classes, one is dendrimers having perfectly branched architecture while another class is hyperbranched polymers having random branched architecture. HBPs are usually prepared in a one-pot synthesis, which limits the control on molar mass and branching accuracy and leads to heterogeneous products with a distribution in molar mass and branching. This distinguishes hyperbranched polymers from perfectly branched and monodisperse dendrimers. It is well accounted that a highly branched architecture provides high solubility, lower viscosity and lower crystallinity compared to linear polymeric analogs. In recent years, dendritic polymers, *i.e.* dendrimers as well as hyperbranched polymers have attracted major attention because of their intriguing properties resulting from branched architecture as well as the high number of functional end groups.¹ The tedious multistep synthesis of the dendrimers is a major hurdle for the large scale production which limits its real practical application. However, one pot synthesis of HBPs makes them as an ideal candidate for the variety of application, where a perfect structure is sacrificed for an easy and affordable synthesis.

The Azobenzene is a well recognized mesogen as well as photoresponsive chromophore which has found wide application in optical displays,² optical data storage,³ photocontrollable coatings,⁴ molecular switches,⁵ photomechanical systems etc.⁶ Although there are a few reports on liquid crystalline azobenzene containing hyperbranched polymers, those synthesized via the melt polycondensation route are very few in literature.⁷ For instance, wang *et al.* reported synthesis of hyperbranched polymer containing azobenzene using solvent free ester exchange method with appropriate AB₂ monomer.⁷ One main reason for this is the fact that, as a chromophore azobenzene are prone to degradation prior to its melting transition. Therefore, suitable modification of the azobenzene-bearing monomer has to be made in order to avail the melt transesterification reaction methodology for polymerization.⁷ Hyperbranched LC polymers incorporating azobenzene units are promising structures for the preparation of LC materials having faster switching response due to their lower viscosity in LC

phase.⁸ There is a dearth of promising HB monomer design containing the azobenzene moiety.^{7,9}

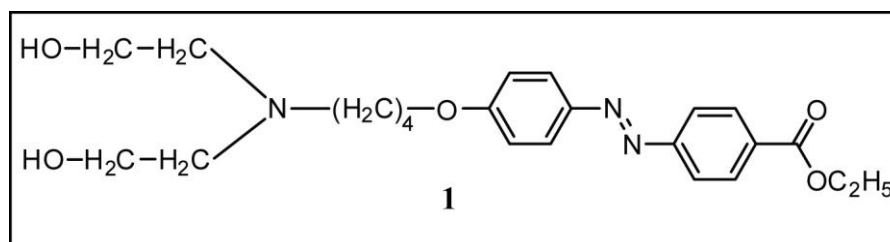


Figure 5.1 Monomer design used for the synthesis of HB polymer through melt ester exchange method.⁷

The azo containing polymerizable trieped (B₃ type) and tetraped (B₄ type) architectures, described in the previous chapter was subjected to melt polycondensation to form liquid crystalline hyperbranched polymers, which is detailed in the present chapter. Unlike the usually reported hyperbranched liquid crystalline polymers (HBLCPs), where the mesogen is either introduced during the polymerization as the branching units,⁹⁻¹⁰ or after the polymerization as terminating group.¹¹ In the present design the mesogenic structure was built-in into the monomer design. The terminal groups of the trieped and tetraped molecules were functionalized with methyl carboxyl ester groups to facilitate polymerization with tetraethylene glycol as the A₂ type comonomer. The rational design of the monomers enabled the adoption of the melt condensation route for polymerization as the melting temperature of the monomers could be brought much further below their decomposition temperature. A thorough study of the LC phases of the HB polymers as to the effect of variation of monomer spacer length in each of these classes of materials as well as effect of branching on the LC characteristics of hyperbranched polymers was undertaken. A detailed study of the characterization of the LC phases using various instrumentation techniques like differential scanning calorimetry (DSC), polarized light microscopy (PLM) and variable temperature XRD is presented. Photoswitching behavior of HBPs in the LC state as well as in spin coated thin films using an UV irradiation source was also undertaken.

5.2 Experimental section

5.2.1 Materials

Tetraethylene glycol (TEG), titanium tetrabutoxide ($\text{Ti}(\text{O}i\text{Bu})_4$) and chloroform-d were purchased from Aldrich Company Ltd. and were used as such. Dimethyl formamide (DMF), acetonitrile (CH_3CN), tetrahydrofuran (THF), acetone, chloroform (CHCl_3) and methanol were purchased from Merck Chemicals Ltd. and purified using standard procedures.

5.2.2 Instrumentation

^1H NMR and ^{13}C spectra of all polymers were recorded on a Bruker-AVANCE 400 MHz spectrometer. Chemical shifts are reported in ppm at 25 °C using CDCl_3 as solvent containing small amount of tetramethylsilane (TMS) as internal standard. The molecular weights with molecular weight distribution of the polymers were determined by using gel permeation chromatography (GPC) polymer lab PL-220 with CHCl_3 used as eluent. The flow rate of CHCl_3 was maintained as 1 $\mu\text{L}/\text{min}$ throughout the experiments and the sample solutions at concentrations 2-3 mg/mL were filtered and injected for recording the chromatograms at 30 °C. The calibration curve was obtained using polystyrene as an internal standard. Infrared spectra were recorded using Bruker FT-IR (ATR mode) spectrophotometer in the range of 4000-600 cm^{-1} . UV-Vis spectra were recorded using a Perkin Elmer Lambda -35 UV-Vis spectrometer. The thermal stability of all azo HB polymers was analyzed using PerkinElmer: STA 6000 thermogravimetric analyser (TGA) under nitrogen atmosphere from 40-800 °C at 10 °C/min. Differential Scanning Calorimetry (DSC) was performed using a TA Q10 model. About 2–3 mg of the sample was taken in aluminium pan, well sealed and scanned at 10 °C/min under nitrogen atmosphere. The instrument was calibrated with indium standards before measurements. The phase behavior of polymers was analyzed using LIECA DM2500P polarized optical microscope equipped with Linkam TMS 94 heating and cooling stage connected to a Linkam TMS 600 temperature programmer. The Transition from isotropic to liquid crystalline phase was monitored by the evolution of characteristic textures. Powder X-ray diffraction of all the samples were recorded by a DY 1042-Empyrean XRD with Programmable Divergence Slit(PDS) and PIXcel 3D detector using $\text{Cu K}\alpha$ (1.54 Å)

emission. The spectra were recorded in the range of (2θ) 3–50° and analyzed using X'pert software. Variable temperature in situ XRD experiments were carried out in an Anton-Paar XRK900 reactor.

Synthesis and detailed structural characterization of multipod monomers used for polymerization were already discussed in previous chapter (Chapter 4).

5.3.3 Synthesis of HB polymers: Melt Polycondensation

HB-T3S5TEG: Tetraethylene glycol (A_2 monomer) (0.066 g, 0.339 mmol) and T3star5 (B_3 monomer) (0.250 g, 0.227 mmol) were taken in a test tube shaped polymerization apparatus and melted by placing in oil bath at 180 °C with constant stirring in order to melt the solid. Once a homogenous mixture was formed, the reaction mixture was cooled to room temperature and 1 mol % of titaniumtetrabutoxide ($Ti(OBu)_4$) was added as a catalyst. The polycondensation apparatus was made oxygen and moisture free by nitrogen purge. The polymerization tube was immersed in the oil bath at 180 °C and the polymerization was carried out with slow nitrogen purge for 4 h. The resultant viscous mass was further condensed by applying high vacuum (0.01 mm of Hg) at 180 °C for 2 h. The polymer was dissolved in $CHCl_3$, filtered to remove catalyst and precipitated in cold methanol twice to obtain the azo HB polyester.

Yield = 0.220 g (61 %). 1H -NMR (400 MHz $CDCl_3$): δ (ppm): 8.16 (6H, d, ArAzo), 7.95-7.80 (12H, m, ArAzo), 6.99 (6H, d, ArAzo), 6.07 (3H, s, Ar-Phg), 4.48 (5H, t, Azo-COOCH₂CH₂O-(expected 12H for 100 % branching), 4.06 (6H, t, Azo-OCH₂-CH₂-), 3.94 (~11H, m, Azo-COOCH₃ from L+T unit, Phg-OCH₂-CH₂-), 3.83 (~ 5H, t, Azo-OCH₂-CH₂-O), 3.75-3.55 (~ 13H, m, Azo-OCH₂-CH₂-O-CH₂), 1.95-1.75 (13H, m, CH₂-CH₂-CH₂-CH₂), 1.72-1.58 (7H, m, CH₂-CH₂-CH₂-CH₂). ^{13}C NMR ($CDCl_3$) δ ppm: 166.83, 166.26, 162.24, 161.11, 155.54, 147.09, 131.32, 130.79, 125.45, 122.56, 115.0, 94.11, 72.70, 70.92, 68.38, 67.93, 64.50, 61.97, 52.48, 29.12, 22.94. FTIR (KBr) (cm^{-1}): 2942, 2870, 1712, 1592, 1498, 1461, 1394, 1246, 1137, 1094, 1013, 862, 829, 770, 724, 686.

HB-T3S10TEG: Tetraethylene glycol (A_2 monomer) (0.077 g, 0.396 mmol) and T3star10 (B_3 monomer) (0.350 g, 0.267 mmol) were used for the polymerization.

Yield = 0.320 g (67 %). $^1\text{H-NMR}$ (400 MHz CDCl_3): δ (ppm): 8.15 (6H, d, ArAzo), 7.91 (12H, m, ArAzo), 6.99 (6H, d, ArAzo), 6.05 (3H, s, Ar-Phg), 4.48 (~ 4H, t (expected 12H), Azo- $\text{COOCH}_2\text{CH}_2\text{O}$ -) 4.03 (6H, t, Azo- $\text{OCH}_2\text{-CH}_2\text{-}$), 3.94 (9H, m, Azo- COOCH_3), 3.89 (6H, t, Phg- $\text{OCH}_2\text{-CH}_2\text{-}$), 3.83 (~ 4H, t, (expected 12H for 100% branching), Azo- $\text{OCH}_2\text{-CH}_2\text{-O}$), 3.69 (~ 8H, t, (expected 24H), Azo- $\text{OCH}_2\text{-CH}_2\text{-O-CH}_2$), 1.88-1.70 (12H, m, $\text{CH}_2\text{-CH}_2\text{-CH}_2\text{-CH}_2$), 1.50-1.22 (36H, m, $\text{CH}_2\text{-CH}_2\text{-CH}_2\text{-CH}_2$) $^{13}\text{C NMR}$ (CDCl_3) δ ppm: 166.61, 166.04, 162.36, 160.97, 155.38, 146.85, 131.14, 130.66, 130.56, 125.21, 122.31, 114.81, 93.85, 70.72, 68.43, 67.99, 64.27, 52.21, 29.44, 29.15, 26.03. FTIR (KBr) (cm^{-1}): 2923, 2851, 1719, 1597, 1501, 1461, 1394, 1258, 1140, 1102, 1057, 1013, 862, 832, 771, 722, 689.

HB-T4S5TEG: Tetraethylene glycol (A_2 monomer) (0.072 g, 0.370 mmol) and T4star5 (B_4 monomer) (0.300 g, 0.185 mmol) were used for the polymerization.

Yield = 0.295 g (71 %). $^1\text{H-NMR}$ (400 MHz CDCl_3): δ (ppm): 8.15 (8H, d, ArAzo), 7.95-7.84 (16H, m, ArAzo), 6.99 (8H, d, ArAzo), 6.07 (6H, s, Ar-Phg), 4.48 (~ 5H, t Azo- $\text{COOCH}_2\text{CH}_2\text{O}$ - expected 16H for 100%) 4.05 (8H, t, Azo- $\text{OCH}_2\text{-CH}_2\text{-}$), 3.93 (18H, m, Azo- COOCH_3 from L+T unit, Phg- $\text{OCH}_2\text{-CH}_2\text{-}$), 3.83 (~ 5H, t, Azo- $\text{OCH}_2\text{-CH}_2\text{-O}$ -), 3.75-3.55 (~ 16H, m, Azo- $\text{OCH}_2\text{-CH}_2\text{-O-CH}_2$), 2.09 (~2H, -OH end group), 1.95-1.75 (20H, m, $\text{CH}_2\text{-CH}_2\text{-CH}_2\text{-CH}_2$), 1.71-1.55 (10H, m, $\text{CH}_2\text{-CH}_2\text{-CH}_2\text{-CH}_2$) $^{13}\text{C NMR}$ (CDCl_3) δ ppm: 166.55, 165.99, 162.16, 160.81, 155.26, 146.80, 131.09, 130.52, 125.18, 122.28, 114.72, 93.81, 72.43, 70.64, 68.10, 67.64, 64.24, 61.70, 52.21, 28.91, 22.67. FTIR (KBr) (cm^{-1}): 2941, 2869, 1714, 1592, 1498, 1460, 1391, 1250, 1138, 1097, 1055, 861, 828, 770, 725, 684.

HB-T4S10TEG:

Tetraethylene glycol (A_2 monomer) (0.059 g, 0.370 mmol) and T4star10 (B_4 monomer) (0.300 g, 0.185 mmol) were used for the polymerization.

Yield = 0.250 g (65 %). $^1\text{H-NMR}$ (400 MHz CDCl_3): δ (ppm): 8.15 (8H, d, ArAzo), 7.91 (16H, m, ArAzo), 6.99 (8H, d, ArAzo), 6.06 (6H, s, Ar-Phg), 4.48 (~ 4H, t (expected 16H for 100% branching, Azo- $\text{COOCH}_2\text{CH}_2\text{O}$ -), 4.03 (8H, t, Azo- $\text{OCH}_2\text{-}$

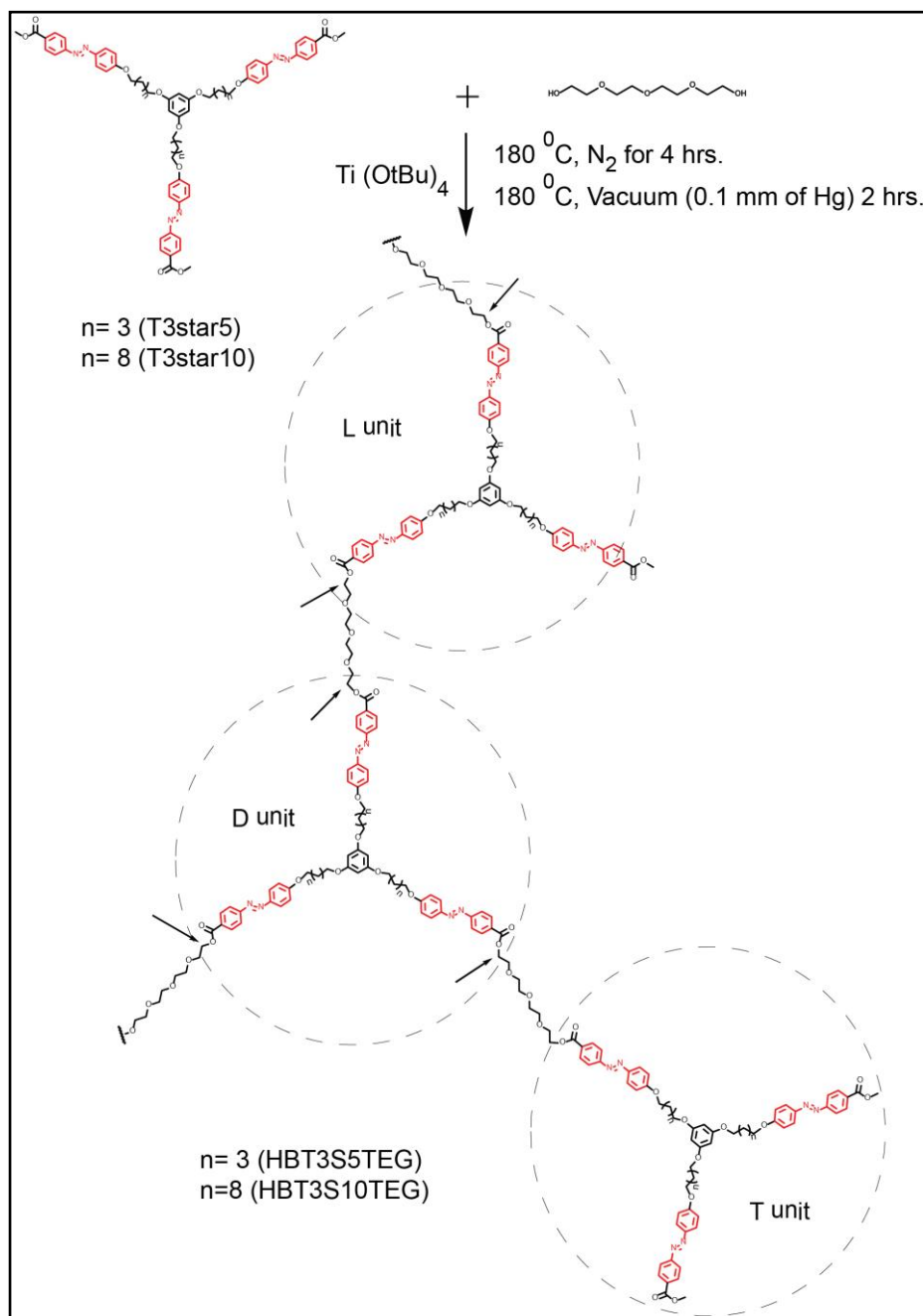
CH₂-), 3.95-3.80 (26H, m, Azo-COOCH₃ from L+T unit, Phg-OCH₂-CH₂, Azo-OCH₂-CH₂-O-), 3.75-3.63 (~ 11 H, m, , Azo-OCH₂-CH₂-O-CH₂), 2.17 (~4H, -OH end group), 1.90-1.60 (24H, m, CH₂-CH₂-CH₂-CH₂), 1.58-1.2 (73H, m, CH₂-CH₂-CH₂-CH₂). ¹³C NMR (CDCl₃) δ ppm: 166.58, 162.38, 160.90, 160.81, 155.22, 146.72, 131.08, 130.52, 130.54, 125.26, 122.29, 114.77, 93.72, 72.47, 70.66, 69.16, 68.39, 67.93, 64.24, 61.70, 52.23, 29.43, 29.30, 29.20, 26.00. FTIR (KBr) (cm⁻¹): 2927, 2866, 1719, 1596, 1498, 1465, 1391, 1255, 1140, 1098, 1057, 863, 825, 770, 727, 683.

5.4 Results and Discussion

5.4.1 Synthesis and characterization of HB-polymers

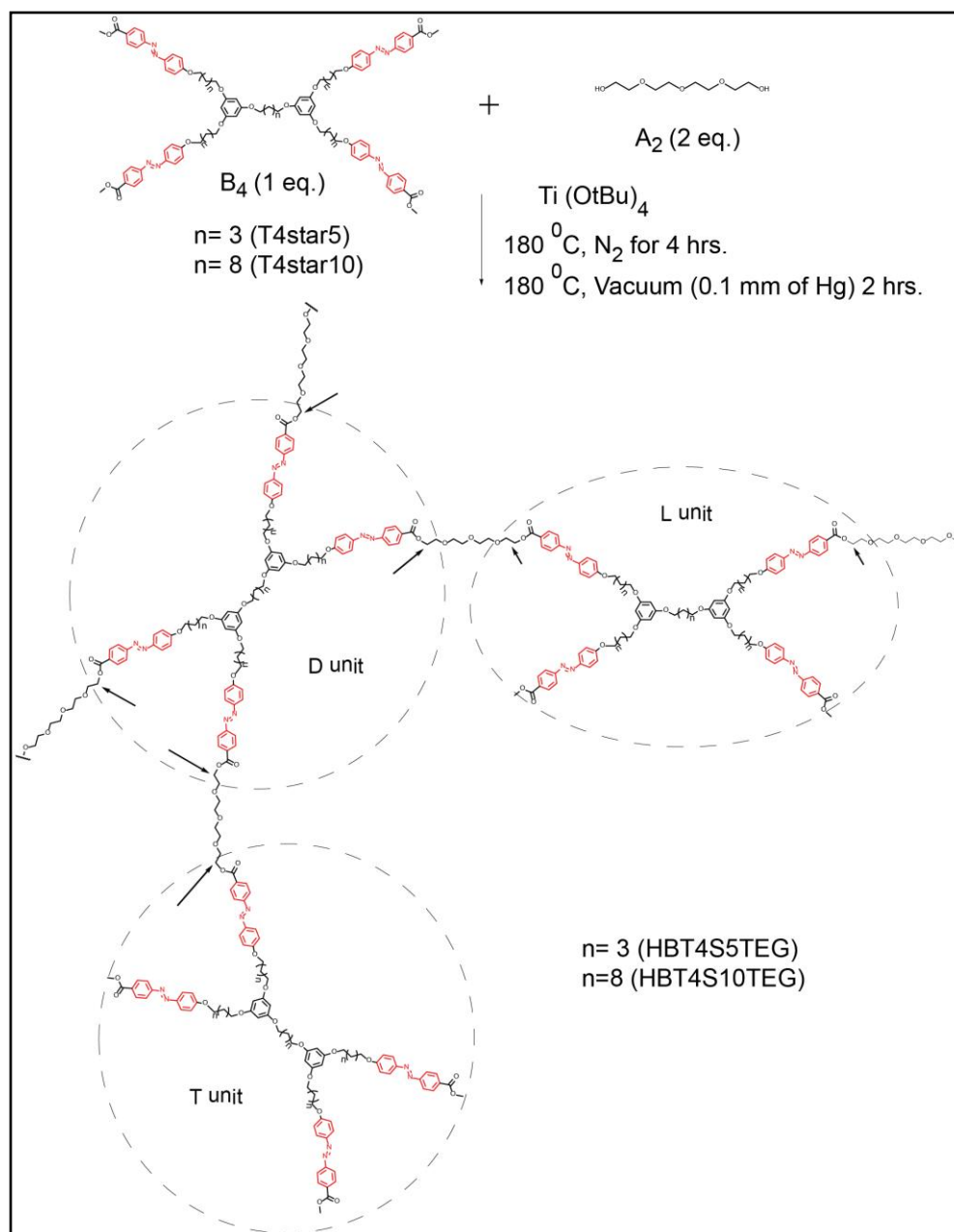
The hyperbranched polymers (HBPs) were synthesized using A₂ and B₃/B₄ monomer approach via melt polycondensation route, where tetraethylene glycol (TEG) was chosen as the A₂ comonomer. The polymerization of A₂ and B₃/B₄ monomers leads not only to branching, but also cross linking.¹² The cross linking can be avoided if the polymerization is kept below the gel point by limiting polymer conversion or by control over stoichiometry of multifunctional monomers.¹²⁻¹³ The critical gelation conversion in the A₂ + B₃ melt polycondensation is (~0.71), whereas it is much lower for the A₂ + B₄ polymerization (~0.58).¹⁴ Although gelation was predicted by Flory at high conversion for these type of branched polymerizations, it has been shown that the high bulk viscosity of the reaction medium has the effect of isolating the growing macromolecules, thereby stopping the polymerization from proceeding to high conversion.¹⁵ The optimal conditions that we adopted to control the polymerization was a reaction temperature of 180 °C, reaction time of six hours with equifunctional groups i.e 3/2 for A₂/B₃ and 2/1 for A₂/B₄. Polymerization was carried out under nitrogen purge for four hours following which vacuum (0.01 mm of Hg) was applied to the viscous mass for two hours. The details of the polymerization procedure are given in the experimental section. The HBPs were named **HB-TmSnTEG**, where m represented the three or four arm and n represented the spacer length of the alkyl chain – 5 or 10. For instance, the HB polymer synthesized from the triped monomer with pentyl spacer was named as **HB-T3S5TEG**. Similarly, the other polymers were named as **HB-T3S10TEG**, **HB-T4S5TEG** and **HB-T4S10TEG**. The synthesis of HB

polymers **HB-T3S5TEG** and **HB-T3S10TEG** using TEG (A_2 monomer) and triped (B_3) monomers in melt condition is shown in Scheme 5.1.



Scheme 5.1 Synthesis of hyperbranched polymer **HB-T3S'*n*'TEG** using tetraethylene glycol (TEG) (A_2) and triped B_3 azobenzene monomers. The arrow indicates the new ester linkages and the circle indicates the dendritic (D), linear (L) and terminal (T) linkages.

The synthesis of polymer **HB-T4S5TEG** and **HB-T4S10TEG** using TEG and tetraped (B_4) monomers in melt condition is shown in Scheme 5.2.



Scheme 5.2 Synthesis of hyperbranched polymer **HB-T4S'n'TEG** using tetraethylene glycol (TEG) (A_2) and tetrapod B_4 azobenzene monomers. The arrow indicates the new ester linkages and the circle indicates the dendritic (D), linear (L) and terminal (T) linkages.

The HBPs were soluble in common organic solvents like dichloromethane, chloroform, tetrahydrofuran etc. which confirmed that the percent conversion of polymer was below their critical gelation point. The structural characterization of the azobenzene HBPs was done using $^1\text{H-NMR}$ and $^{13}\text{C-NMR}$ spectroscopy. Figure 5.2 shows the $^1\text{H-NMR}$ spectra of a) triped monomer **T3star5** (for comparison) along with the corresponding HB polymer b) **HB-T3S5TEG**.

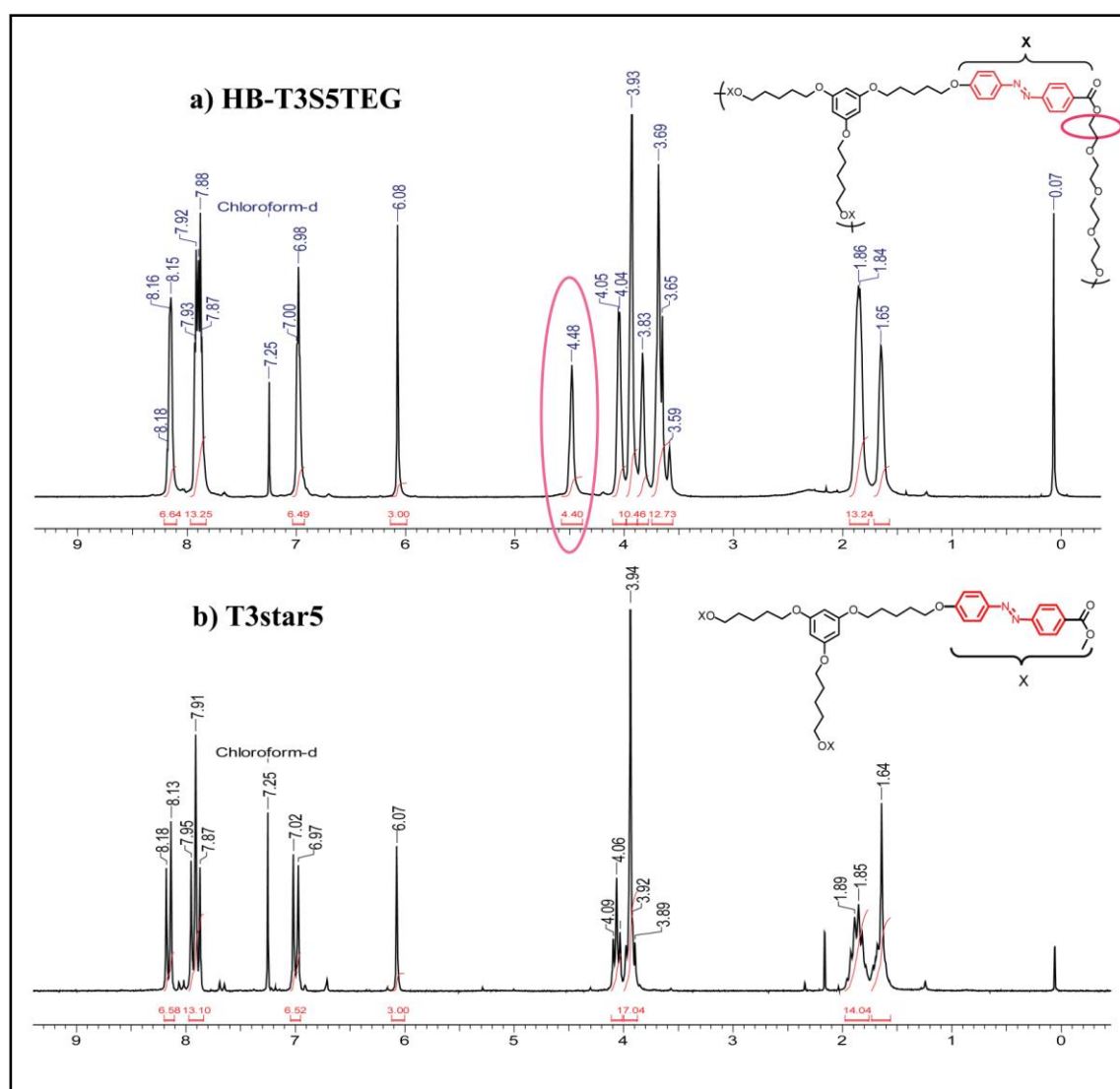


Figure 5.2 $^1\text{H-NMR}$ spectra of a) hyperbranched polymer **HB-T3S5TEG** and b) triped monomer **T3star5** for comparison in CDCl_3 as solvent.

The appearance of a new peak at 4.48 ppm (circled in figure 5.2) in the proton NMR spectra of the hyperbranched polymer corresponding to the new ester linkage (methylene ester) confirmed the covalent incorporation of the triped azo monomer in to the hyperbranched polymer backbone. Similarly, Figure 5.3 shows the ^1H -NMR spectra of a) tetraped monomer **T4star5** (for comparison) **along** with the corresponding HB polymer b) **HB-T4S5TEG**. Here also, the appearance of the new peak at 4.48 ppm confirmed the covalent incorporation of the tetraped monomer into the HB polymer backbone. The new ester linkage is indicated by arrows in Schemes 5.1 and 5.2.

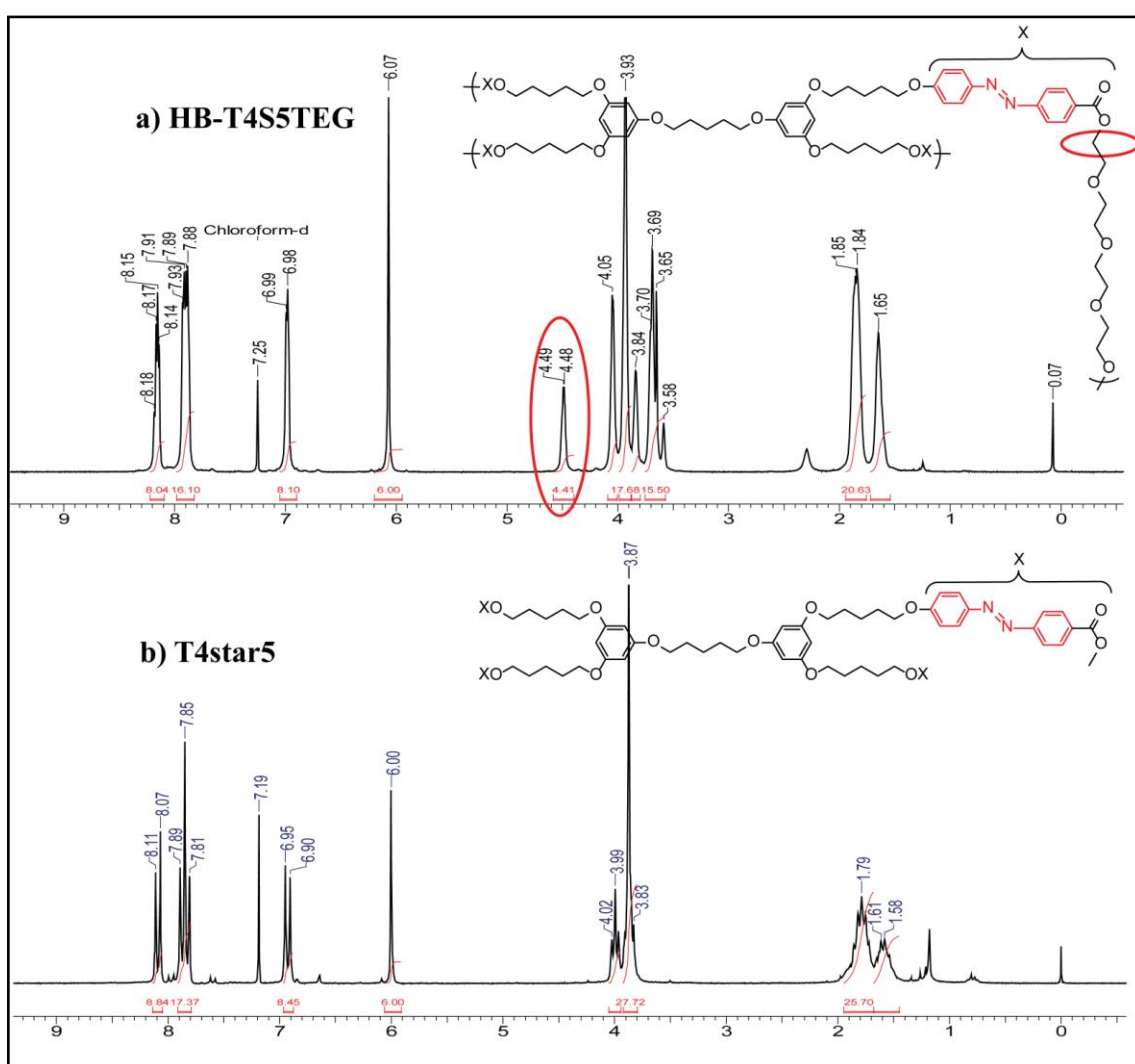


Figure 5.3 ^1H -NMR spectra of a) hyperbranched polymer **HB-T4S5TEG** and b) tetraped monomer **T4star5** for comparison in CDCl_3 as solvent.

As can be seen from the schemes, the point of formation of new ester linkage was far away from the phloroglucinol core to be able to differentiate between dendritic and linear linkages. In fact, no separate peaks corresponding to linear, dendritic and terminal units could be identified from the proton NMR spectra, making it impossible to calculate the degree of branching (DB). However, the extent of formation of the new ester linkage could be estimated based on the integration value of the peaks at 4.48 ppm with that of the aromatic protons. The extent of new ester formation was found to be ~35 % in case of B₃ monomers and ~25 % in case of B₄ monomers. This indicated the lower conversion efficiency of the tetraped monomers compared to the triped ones. Comparing among the short and long spacers also such a tendency was observed shown in Table 5.1. The longer spacer monomers i.e **T3star10** and **T4star10** clearly exhibited lower conversion efficiency compared to their short chain counterparts.

Table 5.1 Percentage of new ester linkage from ¹H NMR spectra of HB polymers.

Polymer	New ester linkage (integration value)	Percentage of new ester linkage (%)
HB-T3S5TEG	4.55	38
HB-T3S10TEG	3.52	30
HB-T4S5TEG	4.60	29
HB-T4S10TEG	3.57	22

The molecular weight and molecular weight distribution (PDI) of HBPs were determined by gel permeation chromatography (GPC). Figure 5.4 shows the GPC chromatograms of the four HB polymers recorded using CHCl₃ as the solvent. The molecular weight and molecular weight distribution (PDI) details of HBPs are given in Table 5.2. The GPC analysis showed multimodal distribution with the PDI values ranging from 2 to 7 which is a typical indication for formation of branched structures.¹⁶ The molecular weight (M_w values) of polymers obtained from the GPC were moderate (data given in Table 5.1). However it should be noted that the GPC

analysis of HB polymers recorded using linear polystyrene as the internal standard for calibration often underestimates the molecular weight of hyperbranched polymers.¹⁷

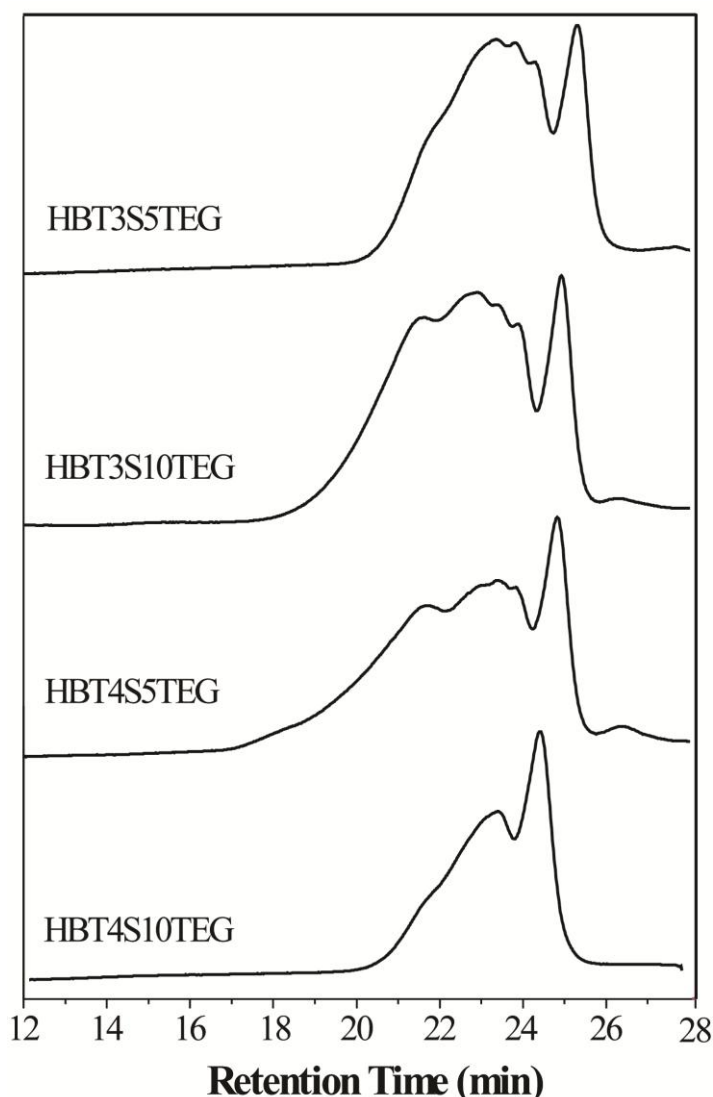


Figure 5.4 GPC chromatograms of Azo HB polymers in $CHCl_3$ solvent.

The inherent viscosity was determined for the two pentyl based hyperbranched polymers **HB-T3S5TEG** and **HB-T4S5TEG** in dimethyl formamide (DMF) to be ~ 0.16 dL/g (the decyl based HB polymers were insoluble in DMF). The GPC data along with the inherent viscosity value confirmed that the molecular weights obtained for these HBPs were in the range of those reported for other HBPs.¹⁸ The sharp peak in the GPC chromatogram corresponded to presence of unreacted triep and tetraep monomers which could not be removed due to the improved solubility of the polymer

upon incorporation of TEG segments. An attempt was made to fractionate one of the polymers, and liquid crystalline characteristics of the different fractions were studied, as will be detailed later on.

Table 5.2 *Molecular weight details of hyperbranched polymers*

Polymer	M_n^a	M_w^a	PDI ^a	Yield (%)
HB-T3S5TEG	4700	13900	2.9	69
HB-T3S10TEG	8400	39700	4.7	66
HB-T4S5TEG	8000	60000	7.4	70
HB-T4S10TEG	6800	13900	2.0	65

^aDetermined by gel permeation chromatography using polystyrene as internal standard in CHCl_3 solvent.

5.4.2 Mesophase Characteristics of Hyperbranched Polymers

The thermal stability of the HB-polymers was determined by TGA under N_2 atmosphere and thermograms are shown in Figure 5.5. All HB-polymers were observed to be thermally stable up to 300 °C and 10 wt % decomposition temperatures were given Table 5.3.

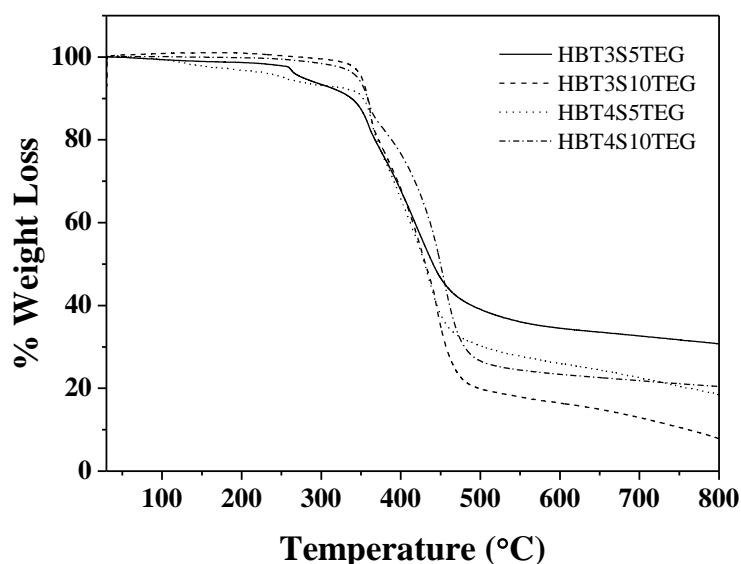


Figure 5.5 *Thermogravimetric analysis (TGA) HB-polymers under N_2 atmosphere.*

The thermotropic liquid crystalline behaviour of hyperbranched polymers were studied using differential scanning calorimetry (DSC) analysis coupled with polarized light microscope (PLM) as well as temperature dependant X-ray diffraction (VTXRD). The second heating and second cooling cycles in the DSC thermogram of the HB polymers is given in Figure 5.6. The transition temperatures and corresponding enthalpy values (J/g) for all polymers are given in Table 5.3. **HB-T3S5TEG** showed two broad transitions both in the heating and cooling cycles. In the heating cycle, the transitions were observed at 76 °C (6 J/g), and at 158 °C (7.4 J/g); while cooling these transitions were observed at 146 °C (8 J/g) and around 54 °C (4.9 J/g).

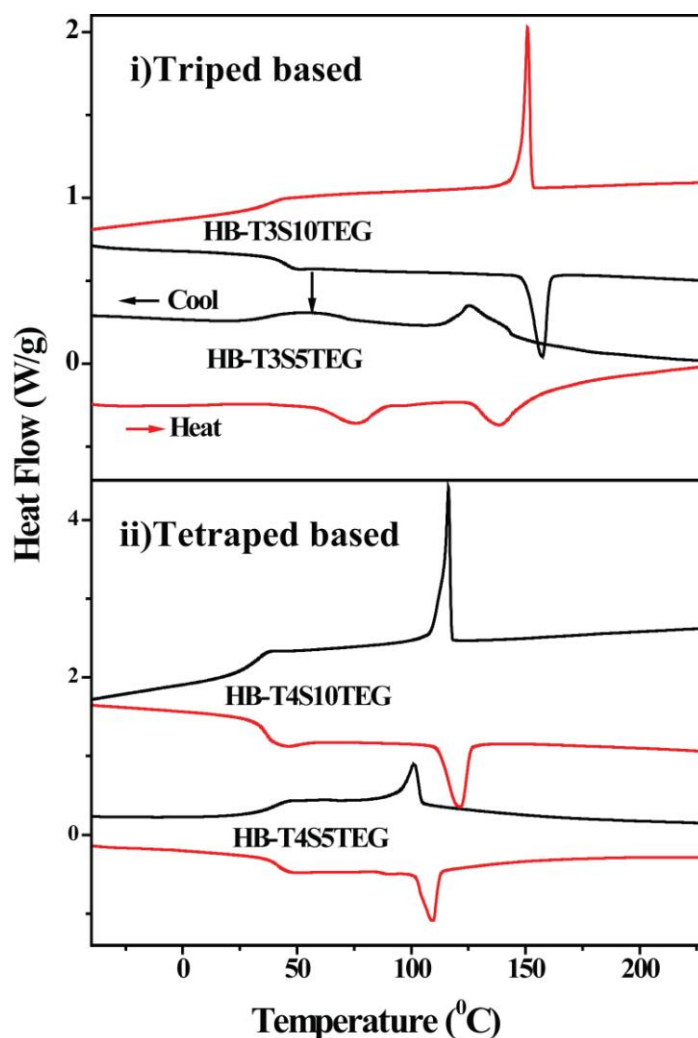


Figure 5.6 DSC thermograms of hyperbranched polymers i) Tripeds based- **HB-T3S5TEG** and **HB-T3S10TEG** ii) Tetrapeds based- **HB-T4S5TEG** and **HB-T4S10TEG**.

Table 5.3 Thermal characteristics of hyperbranched azo polymers.

Sample	T _{cl} ^a (°C) (Lc/C-I)	ΔH _{cl} ^a (J/mol)	T _c ^b (°C) I-Lc	ΔH _c ^b (J/mol)	T _c ^b (°C) (Lc-C) /(Lc-Lc)	ΔH _c ^b (J/mol)	T _D ^c (°C)
HB-T3S5TEG	158	7.7	146 (Sm)	7.9	54 (SmF/H)	4.9	338
HB-T3S10TEG	155	19.6	149 (Sm)	23.2	Glassy	-	360
HB-T4S5TEG	110	6	102 (Sm)	4.8	Glassy	-	356
HB-T4S10TEG	122	12.6	116 (Sm)	12.5	Glassy	-	358

^a clearing transitions during heating cycle, ^b phase transitions and corresponding enthalpy values during cooling cycles, ^c 10 % weight loss under N₂ atmosphere during TGA.

These transitions were confirmed to be that of smectic LC phase based on the textures observed under the PLM as well as the VT XR D pattern. Figure 5.7 shows the characteristic focal conic texture of smectic phase observed while cooling from the isotropic melt. The variable temperature VT XR D plot is also shown in Figure 5.8. The LC phase at 125 °C (plot b in Figure 5.8) upon cooling from the isotropic phase was characterized by a sharp reflection in the low angle region at $2\theta = 3.7^\circ$ ($d = 23.8 \text{ \AA}$) and a broad diffuse reflection in the wide angle region at $2\theta = 20^\circ$ ($d = 4.40 \text{ \AA}$) corresponding to diffuse alkyl chain packing. The second transition around 54 °C, observed in the cooling cycle of the DSC thermogram was confirmed to be a LC to LC transition based on WXR D pattern for the LC frozen sample collected at 25 °C. The DSC thermograms of both the tetraped HB polymers were characterized by a glass transition and clearing transition during heating (Figure 5.6). While cooling, an isotropic to LC transition followed by a glass transition around 50 °C which transformed the LC phase in a glassy state was observed. The transition temperatures and corresponding enthalpy values (J/g) for all polymers are given in Table 5.3. The LC textures obtained for both the tetraped polymers are shown in Figure 5.9.

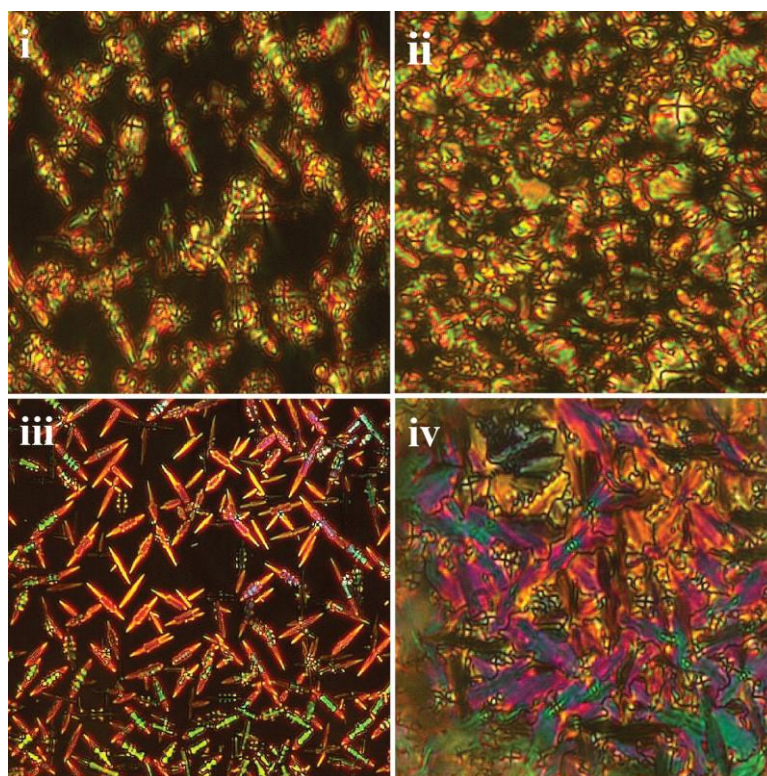


Figure 5.7 Crossed polarized optical micrographs of HB polymers **HBT3S5TEG** i) 96 °C (*Sm*), ii) 30 °C (*SmF/H*), **HBT3S10TEG** iii) 160 °C (*Batonnet-Sm*), iv) 45 °C (*Smectic phase*).

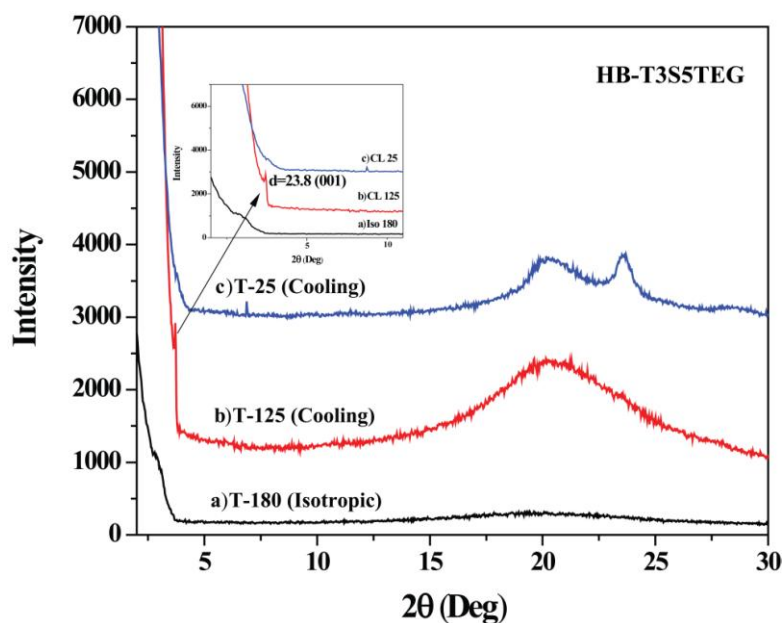


Figure 5.8 Variable temperature X-ray diffraction of HB polymer **HB-T3S5TEG**

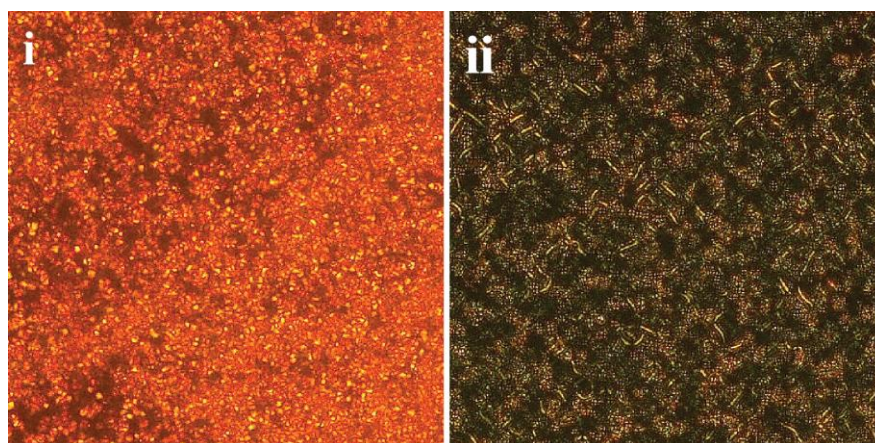


Figure 5.9 Crossed polarized optical micrographs HB-polymers i) **HB-T4S5TEG** 121 °C ii) **HB-T4S10TEG** -120 °C.

One unique feature of the four HB polymers was the fact that the as-solvent precipitated powder sample also exhibited the layered packing observed in the LC phase. Figure 5.10 compares the room temperature (25 °C) powder X-ray diffraction pattern of the four HB polymers.

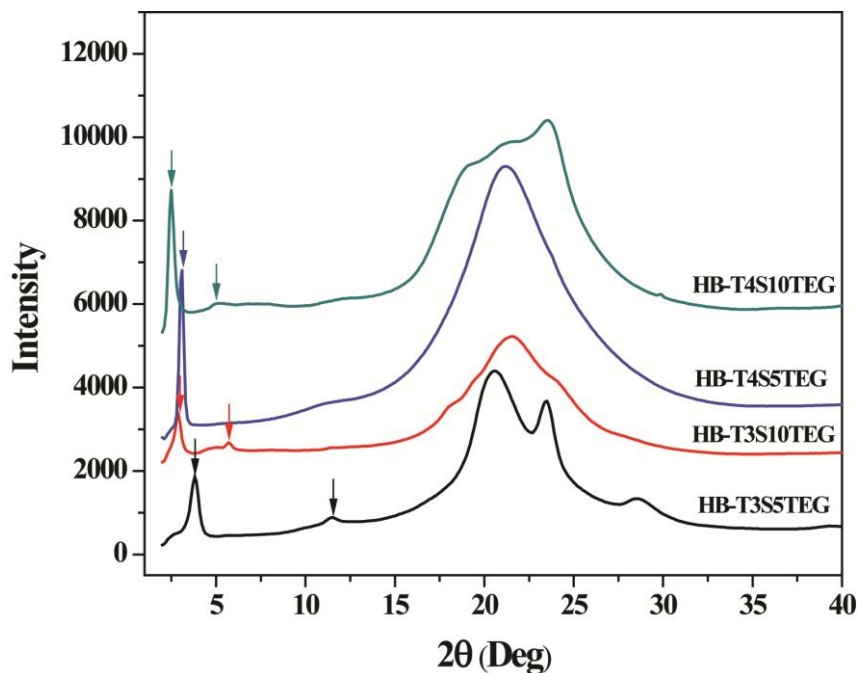


Figure 5.10 Wide angle X-ray diffraction of as-solvent precipitated powder sample of HB-polymers.

Table 5.4 Collected X-ray diffraction data for as-solvent precipitated powder sample of HB polymers.

Polymers	d_{001} Å	d_{002} Å	d_{003} Å	halo (meridian)/Å
HB-T3S5TEG	23.4	-	7.7	4.3
HB-T3S10TEG	31.0	15.7		4.1
HB-T4S5TEG	28.7	-	-	4.2
HB-T4S10TEG	34.4	16.9	-	4.2

The Bragg reflections in 2θ and the corresponding d spacing in Å for all the polymers are given in Table 5.4. From the multiplicity of d_{001} , d_{002} and d_{003} reflections observed in the low angle region for the as-solvent precipitated powder sample, the layered organization prevailing in them was very clear. Another important feature was the observation of the reflection in the wide angle region $\sim 2\theta = 20.17^\circ$ ($d = 4.39$ Å), which was sharp in the case of some HB polymers while it appeared as a shoulder for the other polymers. This reflection in the wide angle region indicated nanosegregation within the lamellar stacks.¹⁹

An attempt was made to fractionate one of the HB polymer – the **HBT3S5TEG** using size exclusion chromatography and to analyze the high molecular weight fractions for their LC characteristics. The GPC plot of the HB polymers given in Figure 5.4 had indicated clearly that the polymers were contaminated by the presence of corresponding unpolymerized tri and tetraped monomers. It was difficult to separate the monomer from the polymer counterpart by conventional solvent precipitation or soxhlet extraction. The analysis of the fractionated polymer sample was undertaken to rule out the possibility that the LC nature observed for the HB polymers was an artifact due to the presence of the contamination by LC monomer. 3.00 mg/mL of the polymer sample dissolved in HPLC grade CHCl_3 was repeatedly injected in the GPC column and three fractions were collected and finally concentrated. The Figure 5.11 shows the GPC plots of the fractionated polymer along with that of the unfractionated sample (dotted line) for comparison.

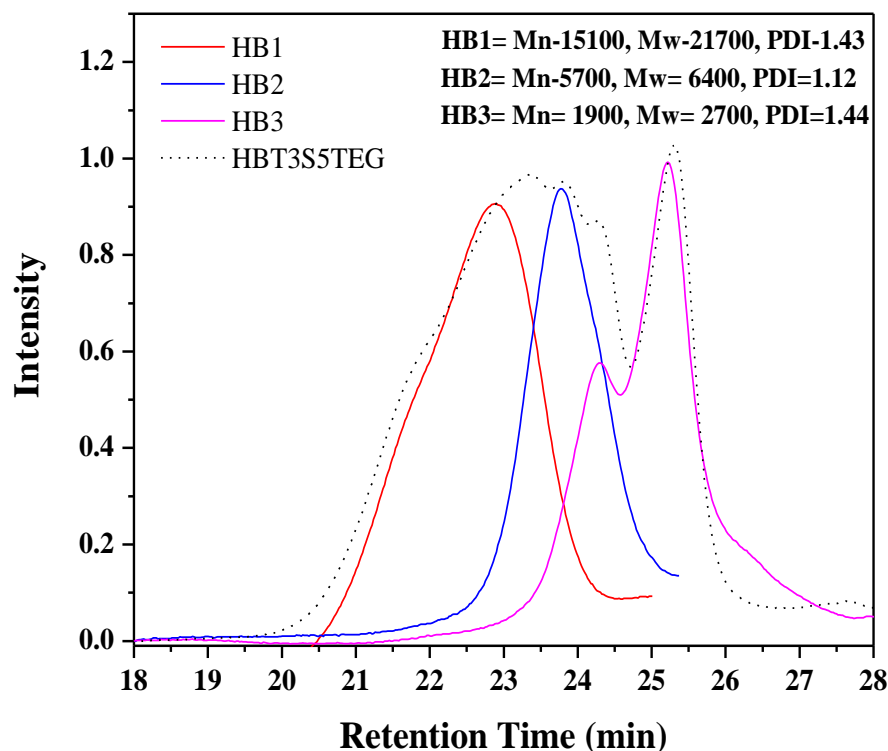


Figure 5.11 Fractionated GPC chromatograms of **HB-T3S5TEG** using chloroform solvent.

The highest molecular weight fraction collected had a M_n of 15,100 and PDI 1.43. The second fraction had a M_n of 5,700 and PDI 1.12. The third fraction was mostly the triped monomer. The fractionated samples collected were just enough to observe their textures under PLM. In Figure 5.12 also shows the textures recorded for the three fractions of **HB-T3S5TEG**. Although the sample thickness was very less, clear focal conic textures could be observed for the second fraction with medium molecular weight. The higher molecular weight fraction also showed smectic mesophase although the formation of larger LC domains was absent. The fractionation experiment thus proved that the LC phase exhibited by the HB polymers was an inherent property of the polymer. Unlike the triped and tetraped molecules a direct analysis of the LC phases of HB polymers based on their architectural or spacer length effect was very difficult considering the fact that the extent of branching as well as molecular weight distribution was different among them.

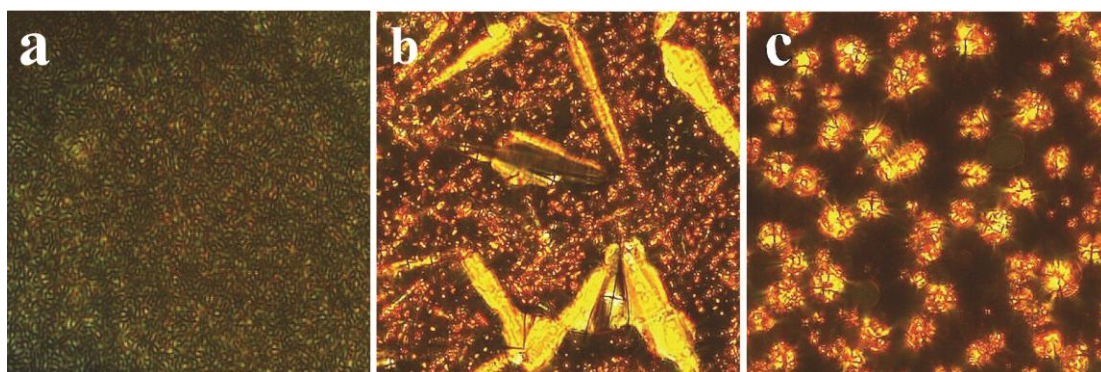


Figure 5.12 Crossed polarized optical micrographs of GPC fractionated polymer **HB-T3S5TEG** a) **HB-1** (33 °C) b) **HB-2** (116 °C) c) **HB-3** (119 °C).

5.4.3 Isothermal Photoswitching in the LC state

Azobenzene chromophore can change its molecular shape that is rod shaped (trans form) to bent shaped (cis form) upon photoirradiation. This property has been used extensively to control the molecular orientation of LC phases by light.²⁰ For instance, the trans form of azobenzene can stabilize LC phase, whereas cis form can destabilize the LC phase because of its bent conformation. Photo-induced isothermal nematic to isotropic disorganization of LC phase structure is well studied in literature.^{3,21} There are very few reports demonstrated the control of the more ordered smectic LC phases using azobenzene as the photoswitch.²² Here we report the reversible and controlled isothermal photoswitching from the highly ordered smectic to isotropic phase by trans to cis photoisomerization of the hyperbranched polymers. Thin films of the sample between cover glasses were first heated to the isotropic state and slowly cooled to the LC phase where they were exposed to irradiation from a DYMAX Blue Wave 75 light source (output power: 19 W/cm²) while holding the temperature constant. The irradiation resulted in instantaneous (< 2 sec) disruption of the smectic LC ordering due to the trans to cis molecular rearrangement. Upon removal of the irradiation source, the smectic LC phase reappeared immediately since high temperature favors the thermal cis to trans back isomerization. The samples were exposed to UV irradiation at different temperatures in the LC phase after cooling from the isotropic melt. Figure 5.13 shows the isothermal photoswitching of HB-polymer **HB-**

T3S5TEG at 3 different temperatures in the LC phase upon cooling from the isotropic phase around 150 °C.

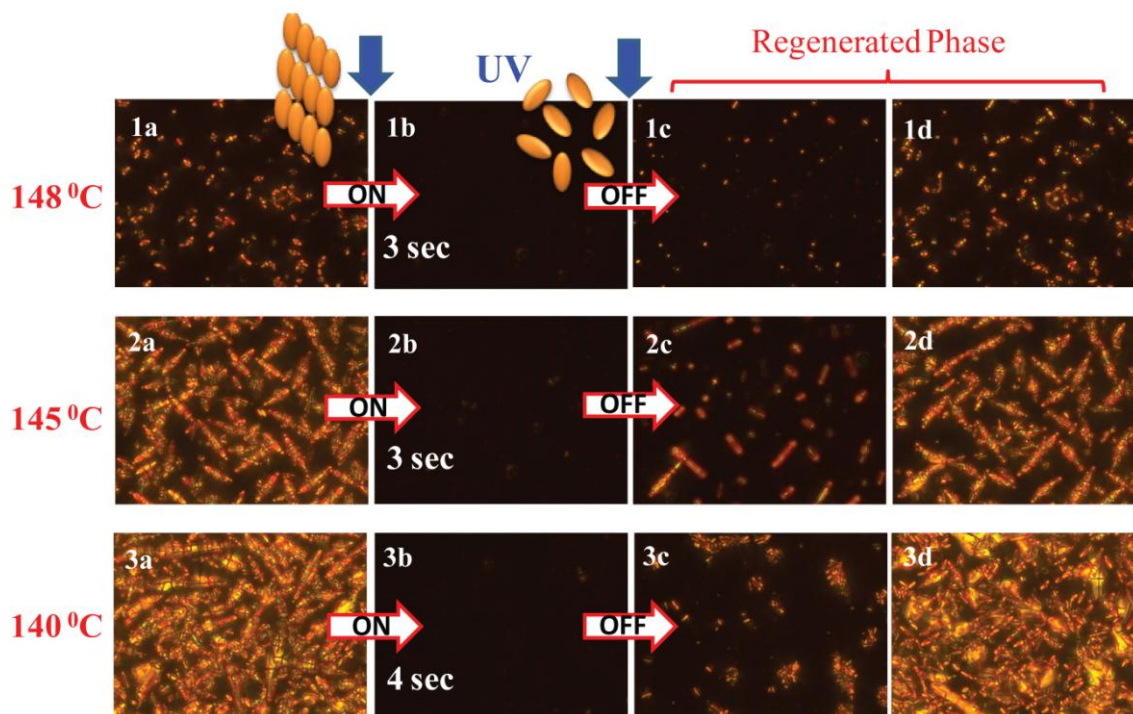


Figure 5.13 Polarized optical microscope images (40 X magnification) depicting the photoinduced isothermal switching behavior of HB polymers **HB-T3S5TEG** at various temperatures upon cooling from isotropic phase at 150 °C. a) LC phase before UV irradiation (b) isotropic state obtained upon UV irradiation (c, d) regeneration of LC ordering upon removal of light source.

Similarly, Figure 5.14 shows the isothermal photoswitching of HB-polymer **HB-T3S10TEG** at 3 different temperatures in the LC phase upon cooling from the isotropic phase around 161 °C. The hyperbranched polymers however were more sluggish compared to the small molecules to undergo disruption of the LC phase upon UV exposure. Even at temperatures closer to the isotropization, when the LC phases were just being formed, more than 2 sec exposure was required to observe complete disruption of the LC ordering. This could be due to the difficulty in bringing about the trans to cis isomerization of the azomoiety which were part of the polymer backbone.

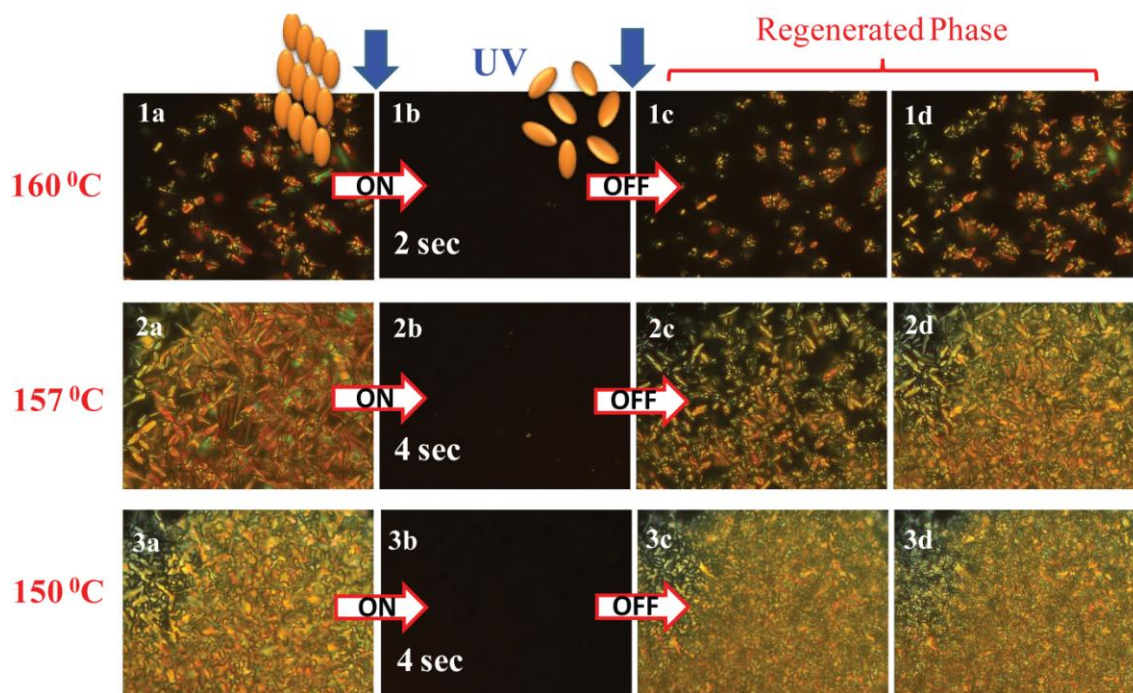


Figure 5.14 Polarized optical microscope images (40 X magnification) depicting the photoinduced isothermal switching behavior of HB polymers **HB-T3S10TEG** at various temperatures upon cooling from isotropic phase at 161 °C. a) LC phase before UV irradiation (b) isotropic state obtained upon UV irradiation (c, d) regeneration of LC ordering upon removal of light source.

Compared to doped systems where small amounts of azo chromophores are doped into inert LC matrix to bring about photoswitchability, these multipod molecules as well as their hyperbranched polymers where the azo chromophores also acted as the LC mesogens inevitably exhibited faster switching response due to the much higher content of the photoactive units.

5.4.4 Photoswitching in spin coated thin films

The solid state absorption spectra were recorded for thin spin-coated film from CHCl_3 solution. The absorption spectra in solution of azo systems in general are characterized by three absorption peaks: a low energy transition around 430-440 nm assigned to the $n-\pi^*$ transition, a transition in the UV region around 350-360 nm assigned for the $\pi-\pi^*$ transition for trans azobenzene (for cis azobenzene the $\pi-\pi^*$

band occurs around 280 nm) and a third energy transition at 230-240 nm to the π - π^* transition of phenyl rings. The spin-coated film samples showed a blue shift in the π - π^* transition for trans azobenzene absorption peak maxima and was more broadened compared to the solution state indicating an excitonic interaction of the aromatic chromophores forming H-aggregates.²³ This behaviour suggested high aggregating tendency of these branched structures in the solid state. Spin coated films (from chloroform) of the HB polymers were subjected to UV irradiation from a DYMAX Blue Wave 75 light source with a 360 nm Oriel bandpass filter and setup photograph is shown Figure 5.15.

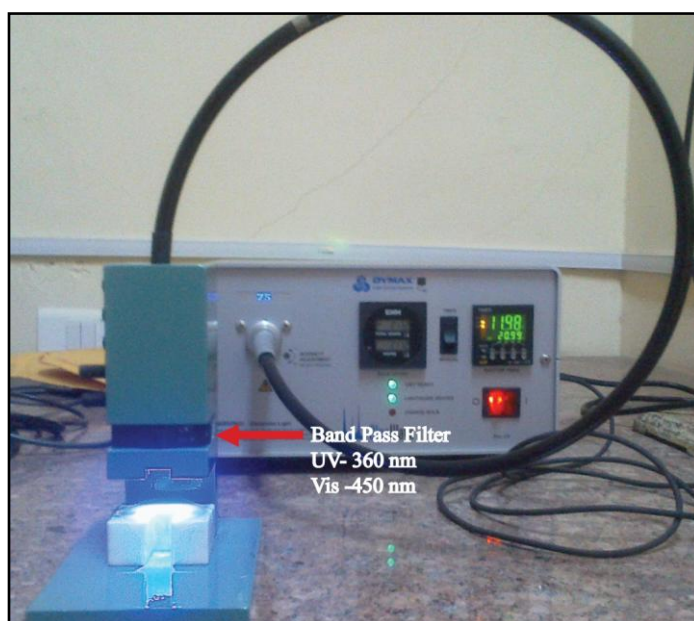


Figure 5.15 Photograph of photoisomerization setup (360 nm Oriel bandpass filter was used for the UV and 450 nm for the visible light).

The comparison of the UV spectra of spin coated films of **HB-T3S5TEG** before and after UV irradiation was shown Figure 5.16a. The dotted line in the figure corresponds to the spectra recorded in CHCl_3 . It can be seen from the figure that compared to the solution spectra, a blue shift of 30 – 35 nm was observed in the spin coated film indicating aggregation in the solid state. UV-Vis absorption spectra of spin coated thin films of the azo HB polymers. Black spectra: as spin-coated film, Red spectra: after UV irradiation, blue spectra: relaxation at room temperature for 24 hrs and dotted spectra: solution state in CHCl_3 solvent.

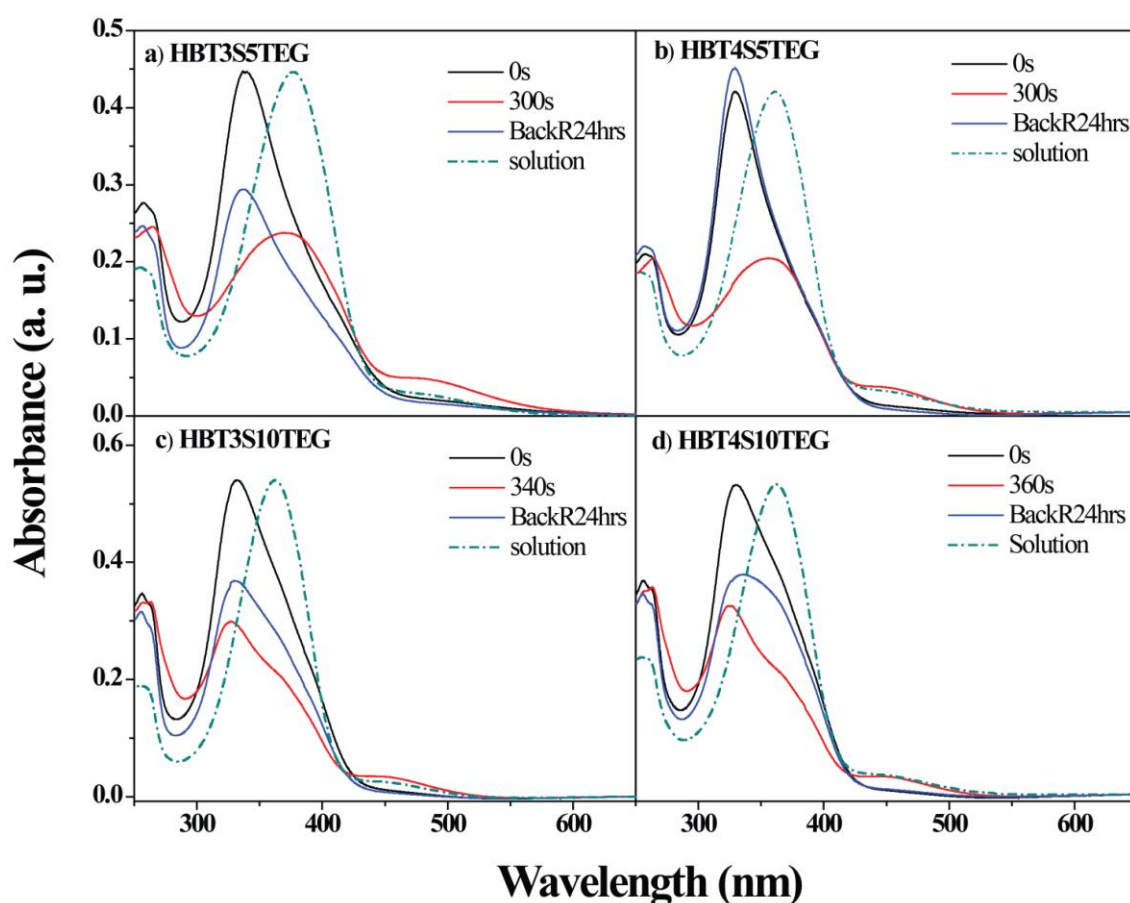


Figure 5.16 UV-Vis absorption spectra of spin coated thin films of the azo HB polymers. Black spectra: as spin-coated film, Red spectra: after UV irradiation, blue spectra: relaxation at room temperature for 24 hrs and dotted spectra: solution state in CHCl_3 solvent.

Upon irradiation for 300 seconds, a red shift of peak maximum to 360 nm along with a reduction in intensity of the π - π^* transition for trans azobenzene and a small increase in intensity of the 430-440 nm transition corresponding to cis isomer was observed. The green spectra corresponded to the spectra recorded after the sample was allowed to relax to the trans state at room temperature in the dark. The absorption wavelength maxima had shifted back to the aggregated blue shifted value indicating the conversion of the non-aggregated cis isomer to the H aggregated trans isomer. A similar observation was seen for the HB polymer having pentyl spacer – **HB-T4S5TEG** (Figure 5.16b). However, in the case of the HB polymers with longer

spacer segment, a slightly different tendency was observed after irradiation. For instance, Figure 5.16c compares the absorption spectra of **HB-T3S10TEG** before and after being subjected to UV irradiation. No red shift to non-aggregated form was observed even though an increase in intensity of the 430-440 nm transition corresponding to cis isomer was observed. After 24 hours, the spectra still remained aggregated and the peak maxima remained blue shifted with respect to that of the same sample recorded in solution in chloroform. For the tetraped hyperbranched polymer with decyl spacer i.e **HB-T4S10TEG** (Figure 5.16d) also the observation was similar to that observed for **HB-T3S10TEG**. These experiments suggested a clear spacer-length dependency in the solid state with reluctance to return to the non aggregated form even after UV irradiation as the spacer length increased. The photoinduced trans/cis isomer concentration in thin polymer film was calculated by using UV-visible absorption spectroscopy. The thin film of HBPs showed aggregated intense absorption peak at 327 nm due to π - π^* transition of trans isomer and weak absorption band at 450 nm corresponding to n - π^* transition. The photoinduced cis/trans isomer fraction was calculated using following equation (1).²⁴

$$Y = \frac{1 - A / A_{\text{dark}}}{1 - \epsilon_{\text{cis}} / \epsilon_{\text{trans}}}$$

Where, A_{dark} = Absorption in dark before irradiation from only trans isomer, at wavelength λ , A = Absorption after UV irradiation, at wavelength λ and ϵ_{cis} , ϵ_{trans} = molar absorption coefficients of cis and trans isomers respectively, as λ ($\epsilon_{\text{cis}} / \epsilon_{\text{trans}}$ for typical azobenzene molecule 0.050).²⁴

The lowest extent of cis isomerization was observed for **HB-T4S10TEG** with only 39 % formation of cis isomers whereas for the others it was ~ 45-52 %.

5.5 Summary

Azo tri and tetrapod molecules were used as B₃ and B₄ type monomers with TEG diol as A₂ comonomer for the synthesis of photoresponsive hyperbranched polymers (HBPs). These multipod monomers were polymerized using melt polycondensation route. Significant differences were observed in the LC properties of these polymers were observed compared to the starting multipod monomers. Most of polymers showed LC to glassy phase transition and this LC glassy phase was stable up to room temperature (25 °C). In case of these polymers, lamellar organization was observed even in the as-solvent precipitated powder, which indicated higher extent of microsegregation.

These hyperbranched polymers showed fast reversible isothermal photoswitching from Smectic-Isotropic (S-I) upon UV irradiation in LC state. The photoswitching behavior in thin film of hyperbranched azo polymers was analyzed with UV-Vis absorption spectroscopy, the influence of varying spacer length on the isomerization property was observed with reluctance to return to the non aggregated form even after UV irradiation as the spacer length increased. Overall, the multipod monomer design containing azo moiety is a simple and robust one enabling melt polymerization without degradation of the azo chromophore for the synthesis of liquid crystalline hyperbranched polymers.

5.6 References

- (1) (a) Voit, B. I.; Lederer, A. *Chem. Rev.* **2009**, *109*, 5924-5973 (b) Zhou, Y.; Huang, W.; Liu, J.; Zhu, X.; Yan, D. *Adv. Mater.* **2010**, *22*, 4567-4590 (c) Yan, D.; Chao, G.; Holger, F. *Hyperbranched Polymers: Synthesis, Properties, and Applications*, 2011.
- (2) Hafiz, H. R.; Nakanishi, F. *Nanotechnology* **2003**, *14*, 649-654.
- (3) Ikeda, T.; Tsutsumi, O. *Science* **1995**, *268*, 1873-1875.
- (4) Abrakhi, S.; Peralta, S.; Fichet, O.; Teyssié, D.; Cantin, S. *Langmuir* **2013**, *29*, 9499-9509.
- (5) Mativetsky, J. M.; Pace, G.; Elbing, M.; Rampi, M. A.; Mayor, M.; Samori, P. *J. Am. Chem. Soc.* **2008**, *130*, 9192-9193.
- (6) Joussetme, B.; Blanchard, P.; Gallego-Planas, N.; Delaunay, J.; Allain, M.; Richomme, P.; Levillain, E.; Roncali, J. *J. Am. Chem. Soc.* **2003**, *125*, 2888-2889.
- (7) Wang, G.; Cheng, H.; Wang, X. *Chem. Lett.* **2002**, *31*, 78-79.
- (8) Marcos, M.; Martin-Rapun, R.; Omenat, A.; Serrano, J. L. *Chem. Rev.* **2007**, *36*, 1889-1901.
- (9) Pandey, S.; Mishra, S. P.; Kolli, B.; Kanai, T.; Samui, A. B. *J. Polym. Sci., Part A: Polym. Chem.* **2012**, *50*, 2659-2668.
- (10) Sato, M.; Kobayashi, Y.; Shimizu, T.; Yamaguchi, I. *Polym. Chem.* **2010**, *1*, 891-898.
- (11) (a) Barberá, J.; Marcos, M.; Serrano, J. L. *Chem. Eur. J.* **1999**, *5*, 1834-1840 (b) Cai, L.; Lu, Y. *Polym. Int.* **2009**, *58*, 640-647 (c) Baars, M. W. P. L.; Söntjens, S. H. M.; Fischer, H. M.; Peerlings, H. W. I.; Meijer, E. W. *Chem. Eur. J.* **1998**, *4*, 2456-2466.
- (12) Jikei, M.; Chon, S.-H.; Kakimoto, M.-a.; Kawauchi, S.; Imase, T.; Watanebe, J. *Macromolecules* **1999**, *32*, 2061-2064.

- (13) Flory, P. *Principles of Polymer Chemistry*; Cornell University Press, Ithaca, NY, 1953.
- (14) Flory, P. J. *Chem. Rev.* **1946**, *39*, 137-197.
- (15) (a) Zhang, B.; Wang, Z. *Chem. Mater.* **2010**, *22*, 2780-2789 (b) Choi, J.-Y.; Tan, L.-S.; Baek, J.-B. *Macromolecules* **2006**, *39*, 9057-9063.
- (16) Unal, S.; Long, T. E. *Macromolecules* **2006**, *39*, 2788-2793.
- (17) (a) Kim, Y. H.; Webster, O. W. *Macromolecules* **1992**, *25*, 5561-5572 (b) Weimer, M. W.; Fréchet, J. M. J.; Gitsov, I. *J. Polym. Sci., Part A: Polym. Chem.* **1998**, *36*, 955-970 (c) Muchtar, Z.; Schappacher, M.; Deffieux, A. *Macromolecules* **2001**, *34*, 7595-7600.
- (18) (a) Shanmugam, T.; Sivakumar, C.; Nasar, A. S. *J. Polym. Sci., Part A: Polym. Chem.* **2008**, *46*, 5414-5430 (b) Scarpaci, A.; Blart, E.; Montembault, V. r.; Fontaine, L.; Rodriguez, V.; Odobel, F. *ACS Appl. Mater. Interfaces* **2009**, *1*, 1799-1806 (c) Li, Z.; Qin, A.; Lam, J. W. Y.; Dong, Y.; Dong, Y.; Ye, C.; Williams, I. D.; Tang, B. Z. *Macromolecules* **2006**, *39*, 1436-1442 (d) Chen, X.; Zhang, Y.; Liu, B.; Zhang, J.; Wang, H.; Zhang, W.; Chen, Q.; Pei, S.; Jiang, Z. *J. Mater. Chem.* **2008**, *18*, 5019-5026 (e) Rao, V. S.; Samui, A. B. *J. Polym. Sci., Part A: Polym. Chem.* **2011**, *49*, 1319-1330.
- (19) Wen, G.-H.; Zhang, B.; Xie, H.-L.; Liu, X.; Zhong, G.-Q.; Zhang, H.-L.; Chen, E.-Q. *Macromolecules* **2013**, *46*, 5249-5259.
- (20) Ichimura, K. *Chem. Rev.* **2000**, *100*, 1847-1874.
- (21) Garcia-Amoros, J.; Szymczyk, A.; Velasco, D. *Phys. Chem. Chem. Phys.* **2009**, *11*, 4244-4250.
- (22) Zhang, S.; Liu, S.; Zhang, Y.; Deng, Y. *Chem. Asian j.* **2012**, *7*, 2004-2007.
- (23) (a) Kasha, M.; Rawls, H. R.; Ashraf El-Bayoumi, M. *Pure Appl. Chem.* **1965**, *11*, 371-392 (b) Tejedor, R. M.; Millaruelo, M.; Oriol, L.; Serrano, J. L.; Alcala, R.; Rodriguez, F. J.; Villacampa, B. *J. Mater. Chem.* **2006**, *16*, 1674-1680 (c) Zebger, I.;

Rutloh, M.; Hoffmann, U.; Stumpe, J.; Siesler, H. W.; Hvilsted, S. *J. Phys. Chem. A* **2002**, *106*, 3454-3462 (d) del Barrio, J.; Tejedor, R. M.; Chinelatto, L. S.; Sánchez, C.; Piñol, M.; Oriol, L. *Chem. Mater.* **2009**, *22*, 1714-1723.

(24) Victor, J. G.; Torkelson, J. M. *Macromolecules* **1987**, *20*, 2241-2250.

CHAPTER 6

Conclusions

This chapter comprises the overall outcome based on the work reported in the thesis. Novel monomer design incorporated with photoresponsive azobenzene moiety was found to be versatile for the synthesis of liquid crystalline polymeric architectures such as main chain LC polymers, hyperbranched LC polymers etc. via solvent-free melt polycondensation approach. The segmented LC azo polyesters containing oligoethylene oxide served as ion conducting media for the lithium ion transport which may find application as solid polymer electrolyte for lithium-ion battery. Thermal and optical modulation of ionic conductivity was observed in these main chain LC polymers. Multipod molecules were efficiently used as multifunctional monomers for the synthesis of azo hyperbranched polymers (HBPs) using melt polycondensation. These multipod molecules as well as HB polymers exhibited reversible fast photoswitching response in LC phase due to trans to cis photoisomerization of azobenzene chromophore. These photoresponsive LC materials could be used in advanced optics and photonics application.

The thesis entitled “**Photoresponsive Liquid Crystalline Azobenzene Polyesters: Design, Synthesis and Self Organization Study**” explores novel design of monomers incorporated with photoresponsive azobenzene moiety which could be directly used in melt polycondensation polymerization for the synthesis of a variety of liquid crystalline polymeric architectures. A range of azo LC polymers such as main chain LCPs, hyperbranched LCPs etc. were prepared using solvent free melt polymerization. The photoresponsive property of azo chromophore has a great impact on LC properties. For instance, one can achieve photochemical phase transitions, photoinduced alignment and photo-triggered molecular cooperative motions upon photoirradiation with suitable light source. Liquid crystalline polymers containing azobenzene holds intriguing properties, due to which they can modulate various physical performances like birefringence, refractive index, modulus viscosity, conductivity, electric and magnetic susceptibility that make them suitable materials for photonic application.

In this aspect, the fine tuning of mesophase and phase transition in main chain LC azo polyesters was demonstrated using using novel twin azobenzene design having the structure azobenzene-spacer-azobenzene, where the spacer was oligooxyethylene of varying length. Two homologous series of twin azobenzene, one with phenylazo (**PnP**) and another with naphthylazo (**NpnNp**) chromophore were developed as monomers. The mesophase behavior was investigated using differential scanning calorimetry (DSC), polarized light microscopy (PLM) combined with variable temperature X-ray diffraction (VTXRD). The **PnP** series of azo twin exhibited smectic LC phase for $n > 3$ central oligooxyethylene units. On the other hand, **NpnNp** series showed spherulitic phases only for the shortest member – **Np2Np**. One non LC short spacer (**P2P**) and one LC long spacer (**P6P**) were incorporated in main chain polyester backbone composed of completely aliphatic sebacate and di or tetraethylene glycol. The investigation of LC behavior of the two series of twin molecules and their copolymers thus showed that the LC properties could be fine tuned both by the chromophore as well as the spacer. Although twin molecules showed smectic LC phases, their incorporation in to copolymer at low incorporation exhibited mostly nematic phase. More importantly in case of random copolymers mesogenicity is a

complex phenomenon, both the “rigid” and the “flexible” spacer would be expected to have almost equal contribution in deciding the final outcome.

Using similar twin azobenzene monomers, segmented main chain azobenzene oligo(ethylene oxide) polyesters were developed. The fine tuning of mesophase and phase transition temperature were demonstrated in these polymers, which were synthesized using twin azobenzene ester as AA type monomer and polymerized with DEG, TEG and HEG via melt polycondensation polymerization. The mesophase characteristics were investigated using differential scanning calorimetry (DSC), polarized light microscopy (PLM) combined with variable temperature X-ray diffraction analysis (VT-XRD). All polymers exhibited smectic mesophases and most of the polymers retained higher order smectic mesophase at RT. These main chain LC polyesters incorporated with photoresponsive azobenzene moiety as well as the oligo(ethylene oxide) segments that support ionic conduction served as excellent thermo as well as photoresponsive ion conducting material upon complexation with Li-alkali salt. Room temperature ionic conductivity was observed in the range of 10^{-5} S cm^{-1} in case of polymer/0.3 Li complex and further the conductivity could be improved to 10^{-4} S cm^{-1} above 65 °C. The temperature dependant ionic conductivity revealed that glass transition had more influence on ionic conductivity compared to ordered liquid crystalline phase transitions. The azobenzene chromophore can act as photoresponsive handle i.e. it can do optical modulation of ionic conductivity. Reversible switching in ionic conductivity was observed upon alternate UV and visible light irradiation at room temperature. An increase in ionic conductivity was observed with UV light irradiation whereas a reduction in ionic conductivity observed upon visible light irradiation. Overall, the design of azo main polyesters addressed the issue of PEO segment crystallization by LC organization additionally providing photoinduced ion-conductive switching.

Going one step further multipod molecules integrated with photoresponsive azobenzene unit were designed. The multipod structures exhibited various liquid crystalline phases based on their ability to undergo nanosegregation of chemically and physically different building blocks in the condensed matter. The triped and tertaped molecule design had a basic structural component composed of a phloroglucinol core connected to three or four azobenzene units via a pentyl or decyl alkyl spacer

segment. These multipod molecules were structurally characterized using $^1\text{H-NMR}$, $^{13}\text{C-NMR}$ and MALDI-TOF spectrometry techniques. The tripod and tetrapod molecules showed smectic liquid crystalline phases. More significantly, wide LC window was observed compared to their conventional calamitic model compounds. Large differences were observed in their mesophase property for instance tripods with five or ten alkyl spacer showed SmA LC organization whereas tetrapods showed higher ordered LC phases. Interestingly, fast and reversible isothermal photoswitching from ordered smectic to isotropic phase was observed in the LC state.

Hyperbranched polymers (HBPs) have distinctive features such as high solubility, lower viscosity, lower crystallinity etc. due to its branched architecture. Recently, it is observed that hyperbranched polymers containing azobenzene chromophore were promising structures for the preparation of LC materials having faster switching response due to their lower viscosity in LC phase. This necessitates versatile HB monomer designs, which are easy to synthesize. With this intent a strategy of azo multipods as monomer precursors was adopted for the synthesis of azo hyperbranched polymers. Azobenzene incorporated tripod (B_3 type) and tetrapod (B_4 type) architectures, underwent melt polycondensation to form liquid crystalline hyperbranched polymers. Most of the polymers showed LC behavior, which was retained as LC glass at room temperature. These HB polymers showed fast reversible isothermal photoswitching from Smectic-Isotropic (S-I) upon UV irradiation in the LC state.

In short the present thesis work is focused on novel monomer design incorporated with photoresponsive azobenzene handle for the preparation of variety of azo LC polymeric architecture. Twin azobenzene based monomer approach was very appealing, as it enabled melt polycondensation as a route for the synthesis of segmented azo LC polyester. Structure-property relationship study on unique design of tri and tetrapod architecture containing azobenzene helped to fine tune the LC properties. These multipod structures carrying terminal methyl carboxylic acid ester moiety facilitated solvent free melt polymerization for the synthesis of azo hyperbranched polyesters. The multipod molecules as well as HB-polymers showed fast reversible isothermal photoswitching in the LC state. Overall, these polymers with inbuilt photoresponsive handle enabled the modulation of numerous physical

properties of the materials in addition to the thermoplastic polyester backbone abiding in processability.

List of research publications:

1. “Twin liquid crystals and segmented thermotropic polyesters containing azobenzene - effect of spacer length on LC properties”

Chinmay G. Nardele, S. K. Asha* *J. Polym. Sci., Part A: Polym. Chem.* **2012**, 50 (14), 2770-2785. **[Highlighted as cover page].**

Original Article

Twin liquid crystals and segmented thermotropic polyesters containing azobenzene—effect of spacer length on LC properties

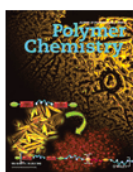
Chinmay G. Nardele, S. K. Asha*

Article first published online: 5 APR 2012

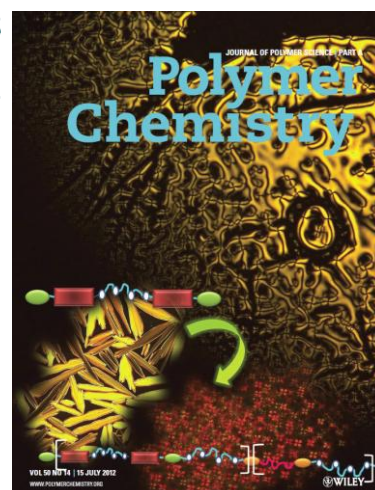
DOI: 10.1002/pola.26062

Copyright © 2012 Wiley Periodicals, Inc.

Issue



Journal of Polymer Science
Part A: Polymer Chemistry
Volume 50, Issue 14, pages
2770–2785, 15 July 2012



2. “Photoresponsive Smectic Liquid Crystalline Multipods and Hyperbranched Azo Polymers”

Chinmay G. Nardele, S. K. Asha* *J. Phys. Chem. B* **2014**, 118 (6), 1670-1684.

3. “Ionic Conductivity Probed in Main Chain Liquid Crystalline Azobenzene Polyesters.”

Chinmay G. Nardele, Vishal M. Dhavale, Kurungot Sreekumar, S. K. Asha*
J. Polym. Sci., Part A: Polym. Chem. **2014**, (Just accepted manuscript).

Symposia Attended/ Poster Presentations:

1. Poster entitled “**Spacer length Dependence on Liquid Crystal Properties of Novel Azobenzene Twin Chromophores**” was presented in the conference *FAPS-Macro 2010*, at Indian Institute of Technology, Delhi, INDIA.

-
2. Poster entitled “**Main Chain Liquid Crystalline polymer scaffolds containing azobenzene**” was represented in The International Conference *Poly Tech-2012*, arranged at Bharati Vidyapeeth University, Pune, Maharashtra, INDIA.
 3. Poster entitled “**Synthesis of Azobenzene incorporated Liquid Crystalline Co-Polyesters by Melt Polycondensation and their Characterization**” was represented in *National Science Day 2012* arranged at CSIR-National Chemical Laboratory, Pune, Maharashtra, INDIA. **[Selected for the best poster award]**.
 4. Participation in "*ACS on campus*" meeting held at CSIR- National Chemical Laboratory, Pune, Maharashtra, INDIA on October 10th, 2012.
 5. Poster entitled “**Star Shaped Liquid Crystalline Azobenzene: Monomers to polymers**” was represented in the conference *Macro-2013* at Indian Institute of Sciences, Bangalore, Karnataka, INDIA.

Erratum